EFFECT OF LIQUID FLOW PATTERNS ON DISTILLATION TRAYS

A THESIS SUBMITTED

BY

CHRISTOPHER JOHN HINE B.Eng.

A candidate for the degree of

Doctor of Philosophy

DEPARTMENT OF CHEMICAL ENGINEERING

AND

APPLIED CHEMISTRY

ASTON UNIVERSITY

OCTOBER 1990

ASTON UNIVERSITY

EFFECT OF LIQUID FLOW PATTERNS ON DISTILLATION TRAYS

A THESIS SUBMITTED BY

CHRISTOPHER JOHN HINE B.Eng.

A candidate for the degree of Doctor of Philosophy

October 1990

Abstract

The thesis describes experimental work on sieve trays in an air-water simulator, 2.44 m in diameter. The liquid flow pattern, for flowrates similar to those used in commercial scale distillation, was observed experimentally by water cooling experiments, in which the temperature of the water is measured at over 100 positions over the tray area. The water is cooled by the rising air which is forced through the tray. A heat and mass transfer analogy is drawn whereby the water temperature is mapped to liquid concentration in mass transfer, and the water temperature profiles reveal how liquid channelling may reduce the tray efficiency.

The first experiment was to observe the flow of water only over an unperforated tray. With the exception of very low weir loads, the flow separated at the ends of the inlet downcomer. This caused liquid to flow straight across the tray between the downcomers and large circulating regions to be formed in the side regions of the tray. The effect of the air crossflow on the flow pattern was then observed on a sieve tray of 10% free area with 1 mm diameter holes (such as is used in cryogenic distillation).

The flow patterns developed on the tray were similar to those produced with water only on the unperforated tray, but at low weir loads the air crossflow prevented separation of the water flow and the associated circulating regions. At higher weir loads, liquid channelling down the centre of the tray and circulation in the side regions occurred. The percentage of the tray occupied by circulating liquid depended upon the velocity of the liquid entering the tray, which was set by the weir load and size of the gap under the inlet downcomer.

The water cooling experiments showed that the temperature of the water in a circulating region is much lower than in other parts of the tray, indicating that the driving force for heat transfer is reduced. In a column section where trays (and circulating areas) are mounted on top of each other, the circulating regions will cause air (or vapour) passing through them to have a reduced change in temperature or concentration leading a loss in tray efficiency.

Keywords: DISTILLATION, SIEVE TRAYS, FLOW PATTERNS, SCALE-UP, PEFORMANCE, HEAT AND MASS TRANSFER.

Acknowledgements

I would like to express my gratitude to the following,

My supervisor, Prof. K. E. Porter, for his guidance and stimulating ideas through the course of my research.

Dr. Q. H. Ali for his assistance with the construction of the air-water simulator.

The excellent workshop technicians, Pete Green, Ian Murkett, Bill Curtis, Cal Geens and Maurizio Santoro for their practical help and assistance.

Mr. J. T. Lavin for his help and commercial expertise.

BOC Cryoplants Ltd. for their sponsorship and training.

The Science and Engineering Research Council (SERC) for their financial support.

My friends and family for their support and encouragement.

And finally to Lyn for her interminable patience.

Table Of Contents

List Of Figures

List Of Tables

Nomenclature

Symbols defined locally are not included here.

A	Active area of tray	$[m^2]$
A_b	Active area of tray	$[m^2]$
C_{air}	Specific heat capacity of air	[kJ/kg K]
C_{wat}	Specific heat of water vapout	[kJ/kg K]
Cp	Specific heat capacity	[kJ/kg K]
CF	Capacity factor	[m/s]
D	Tray diameter	[m]
De	Eddy diffusion coefficient	$[m^2/s]$
De_w	Eddy diffusion coefficient in w direction	$[m^2/s]$
De_z	Eddy diffusion coefficient in z direction	$[m^2/s]$
E_{og}	Murphree point efficiency	[-]
E_{mv}	Murphree tray efficiency, based on liquid phase	[-]
E_{mv}	Murphree tray efficiency, based on vapour phase	[-]
G	Air mass flowrate	[kg/s]
h_{DT}	Dry tray pressure Drop	[m of H_2O]
h_{WT}	Wet tray pressure Drop	[m of H_2O]
h_w	Height of outlet weir	[m]
h_{cl}	Height of clear liquid	[m of H_2O]
h_R	Residual pressure Drop	[m of H_2O]
H_{in}	Average inlet enthalpy	[kJ/kg]
H_{out}	Average outlet enthalpy of air	[kJ/kg]
H_2	Average outlet enthalpy of air	[kJ/kg]
H_1	Average inlet enthalpy of air	[kJ/kg]
H^*_{Tout}	Enthalpy of air in equilibrium with water at temperature T_{out}.	[kJ/kg]
H^*_{Ti}	Enthalpy of air in equilibrium with water at temperature T_i.	[kJ/kg]
H_{2i}	Outlet enthalpy of air from position i on a tray	[kJ/kg]
$Hum_{(Tdb,Twb)}$	Humidity of air at given wet and dry bulb conditions	[-]

L	Liquid mass flowrate	[kg/s]
m	Gradient of equilibrium line	[-]
n	Line normal to column wall	[-]
Pe	Peclet Number	[-]
Q_G	Vapour volumetric flowrate	[m^3/s]
Q_L	Liquid volumetric flowrate	[m^3/s]
t	Time	[s]
T_{in}	Average inlet water temperature to tray	[K]
T_{out}	Average outlet water temperature from tray	[K]
T_{db}	Air dry bulb temperature	[K]
T_{wb}	Air wet bulb temperature	[K]
T_r	Reduced temperature driving force	[-]
T_i	Temperature of water at position i on a tray	[K]
u_h	Tray hole velocity	[m/s]
U_s	Superficial column velocity	[m/s]
V_w	Liquid velocity in w direction	[m/s]
V_z	Liquid velocity in z direction	[m/s]
w'	Coordinate perpendicular to z' direction	
w	Dimensionless coordinate parallel to flow path length	
W	Weir length	[m]
x	Liquid concentration	[kmol/kg]
X	Dimensionless liquid concentration	[-]
X_+	Dimensionless liquid concentration, just above a zero length coordinate	[-]
y_n	Composition of vapour leaving stage n	[kmol/kg]
y_{n-1}	Composition of vapour leaving stage n-1	[kmol/kg]
y_n^*	Composition of vapour in equilibrium with liquid composition x_n	[kmol/kg]
$\underline{x}_n$	Composition of liquid leaving stage n	[kmol/kg]
$\bar{y}_n$	Average composition of vapour leaving stage n	[kmol/kg]
$\bar{y}_{n-1}$	Average composition of vapour leaving stage n-1	[kmol/kg]
y_n^*	Composition of vapour in equilibrium with liquid composition x_n	[kmol/kg]
$\bar{x}_{n+1}$	Average composition of liquid leaving stage n+1	[kmol/kg]
$\bar{x}_n$	Average composition of liquid leaving stage n	[kmol/kg]
x_n^*	Composition of liquid in equilibrium with vapour composition y_n	[kmol/kg]

z'	Coordinate parallel to flow path length	
z	Dimensionless coordinate perpendicular to z' direction	
Z	Flow Path Length	[m]
α	Relative volatility of a binary mixture	[-]
ΔT	Temperature difference	[K]
ρ_l	Liquid density	[kg/m^3]
ρ_A	Air density	[kg/m^3]
ρ_g	Vapour density	[kg/m^3]
ρ_f	Froth density	[-
λ	Ratio of gradient of equilibrium line to operating line (mG/L)	[-]
ζ	Orifice coefficient	[-]
λ	Latent heat of water	[kJ/kg]

CHAPTER 1

1. INTRODUCTION

Distillation is the most widely used separation process, despite its intensive use of energy. In 1976, it was estimated that distillation accounted for 3% of the world energy demand (Mix et al., 1980). Due to the high operating costs associated with distillation, any incremental improvements in efficiency, however small, lead to significant financial savings.

In order to keep distillation competitive in the fluid separation field, both capital and operating costs must be kept to a minimum. Capital costs can be reduced by making the contacting devices, be they trays or packings, as efficient as possible and operating costs can be reduced by the better integration of distillation equipment into the whole process. In the words of Rush (1980),

> ".....perhaps the greatest energy reduction we can accomplish in the immediate future is to operate our existing distillation equipment more efficiently. We need to run our distillation systems 'leaner and harder'."

If designs are to be made tighter to reduce both capital and operating costs, then the degree of risk associated with the column not performing as to the design specification must increase. To reduce this risk requires a thorough understanding of the distillation process and on distillation trays this means understanding the liquid flow patterns. The long term objective for distillation tray research must therefore be to develop the appropriate theories of two-phase flow, such that for any tray design and fluid system the flow pattern may be predicted. Before this can be accomplished though, more knowledge is required of the behaviour of the biphase crossing the tray and thus a major objective of this work is to start a comprehensive experimental investigation of the many different tray phenomena which may be expected to determine the liquid flow pattern.

The importance of liquid flow patterns on distillation trays was recognised as far back as the 1930^{s} (Kirschbaum, 1934), when it was discovered that the assumption of completely mixed liquid on a tray was erroneous, even though the tray was of a small diameter

compared to today's standards.

Since this period, many theoretical models have been proposed (Lewis, 1936; Kirschbaum, 1948; Gautreaux and O'Connell, 1955; Diener, 1967; Porter et al., 1972; Bell and Solari, 1974; Yu et al., 1990), which attempt to account for the flow and mass transfer interactions over distillation trays. The models are based on the concepts of well mixed pools of liquid with liquid flow between them or the plug flow of liquid with backmixing. Prior to the 1970s, one-dimensional models seemed to be accepted as adequate for the modelling of distillation trays, however, two-dimensional modelling became necessary as the diameter of columns increased and the existence of non-uniform liquid flow became apparent.

In order to solve the two-dimensional models, an input of the froth velocity over the tray area was required. Hypothetical models of the liquid flow pattern, based on limited experimental observation, have been used for numerical solution of the equations. The solutions obtained by assuming hypothetical liquid flow patterns have highlighted the importance of the effect of the liquid flow pattern on mass transfer.

A full scientific investigation into the flow phenomena on distillation trays has never been carried out. On the other hand, the number of variables in tray design can be very large.

The flow of froth on a distillation tray can more generally be described as open channel two phase flow, and there must always be considerable uncertainty in tray design until it can be shown just how close the hypothetical liquid flow patterns are to reality.

By performing a scientific study, starting from the case of water-only flow, the objective of this work is to obtain experimental observations and data, so as to provide a more secure basis for comparing theoretical models, which may be developed in the future.

After a brief literature review, chosen for evidence of the existence and effect of the liquid flow pattern on tray and column performance, an outline of the approach to the research programme is reported. There the four experimental procedures, used to investigate open channel two phase flow, are introduced, before the construction of the new 2.44 m diameter air-water simulator and experimental techniques are described in more detail. At the end of the experimental sections, a discussion is presented where the results from all the experimental procedures are brought together before the stating of the main conclusions.

CHAPTER 2

2. LITERATURE REVIEW

The origins of distillation date back several hundred years, to the small scale production of crude liquors by ancient civilisations, but the development of distillation as a scientific technology has only been around for about 70 years, coinciding with the establishment of the petrochemical industry. Problems associated with the scale of operation and the difficulty of extensively testing real columns has led to a negligible amount of test data being published in all this time. Rather, distillation technology has developed by the means of theoretical models, which are used to correlate existing experience with safety factors, usually by the incorporation of an efficiency. This essentially empirical nature of distillation was reviewed by Porter and Jenkins (1979).

This literature review is intended to put the research presented in this thesis into perspective and to explain why it was carried out. Thus, the structure of this chapter is broken down into the following headings,

(i) Theoretical models of distillation tray efficiency.

(ii) Hypothetical liquid flow patterns over a distillation tray.

(iii) Flow control devices for distillation trays.

(iv) The techniques used for the experimental investigation of liquid flow patterns on distillation trays.

2.1 Modelling of Tray Efficiency

Distillation column design based on the flowrates and vapour-liquid equilibrium data assumes that the column consists of a series of equilibrium stages, the vapour and liquid leaving each stage in equilibrium with each other. In reality, equilibrium stages are replaced by column hardware such as crossflow contact trays (bubble-cap, valve and sieve), and usually a fractional approach to equilibrium is achieved. The number of actual

trays is related to the number of calculated theoretical trays by the tray efficiency. This review discusses the tray efficiency.

2.1.1 Definitions of Point and Tray Efficiencies

At any particular point on a tray the mass transfer between the liquid and the vapour entering and leaving that point relative to the equilibrium state is defined as the point efficiency (Murphree, 1925), which is given by,

$$E_{og} = \frac{y_n - y_{n-1}}{y_n^* - y_{n-1}} \qquad (2.1)$$

where y_n and y_{n-1} are the compositions of the vapour leaving and entering the point respectively and y_n^* is the composition of the vapour in equilibrium with the liquid at the point x_n.

For a single ideal tray the vapour leaving is assumed to be in equilibrium with the liquid leaving. The Murphree tray efficiency is defined as the ratio of the actual change in composition to that which would occur assuming equilibrium. Thus, the Murphree tray efficiency in terms of the vapour phase is defined as

$$E_{mv} = \frac{\bar{y}_n - \bar{y}_{n-1}}{y_n^* - \bar{y}_{n-1}} \qquad (2.2)$$

where $\bar{y}_n$ and $\bar{y}_{n-1}$ are the average compositions of the vapour leaving and entering the tray respectively and y_n^* is the composition of the vapour in equilibrium with the liquid, x_n, actually leaving the tray. In terms of the liquid phase, the Murphree tray efficiency can be represented as

$$E_{ml} = \frac{\bar{x}_n - \bar{x}_{n+1}}{x_n^* - \bar{x}_{n+1}} \qquad (2.3)$$

where $\bar{x}_{n+1}$ and $\bar{x}_n$ are the average compositions of the liquid entering and leaving the tray respectively and x_n^* is the composition of the liquid that would be in equilibrium with the average composition y_n of the vapour stream actually leaving the tray.

If the gradient of the operating line is constant and the equilibrium line is also straight over the composition range involved such that

$$y_n^* = m\bar{x}_n + b \tag{2.4}$$

and $$\bar{y}_n = mx^*_n + b \tag{2.5}$$

then it can be shown that

$$E_{mv} = \frac{E_{ml}}{E_{ml} + \lambda(1 - E_{ml})} \tag{2.6}$$

where λ is the ratio of the slope of the equilibrium line to the slope of the operating line.

2.1.2 Theoretical Tray Models

Tray efficiency concepts have been proposed and used as bases for the development of tray models. The following tray models are reviewed below,

(i) Completely mixed tray.

(ii) Plug flow tray.

(iii) Tray modelled by mixed pools.

(iv) Backmixing imposed on the plug flow of liquid.

(v) Multi region tray model with backmixing.

Completely Mixed Tray

Up to the 1920S it was customary to believe that the action of the rising vapour passing through the froth on a distillation tray was sufficient to mix completely the froth on the tray. On a completely-mixed tray, the liquid composition at any point is equal to the outlet composition of the liquid, and if the assumption is made that the inlet vapour composition is completely mixed also, then the vapour leaving all points of the tray must also be equal. These conditions of a completely mixed tray lead to the tray efficiency being equal to the point efficiency, i.e.

$$E_{mv} = E_{og} \tag{2.7}$$

Kirschbaum (1934), however, found considerable liquid concentration gradients across a tray of only a few inches in diameter, even at high superficial vapour velocities. This

observation was to lead Kirschbaum and others to develop hypothetical models for the way in which the liquid crossed an operating tray.

Plug Flow Tray

Lewis (1936) proposed that the liquid crossed the tray in a plug flow fashion across a rectangular tray and developed equations to account for this. Three analyses were carried out, but it must be noted that the analyses were all performed for a tray within a section of trays. He continues by making the following assumptions:

(i) No mixing of liquid across the tray.

(ii) Rectangular liquid flow path, no segmental regions.

(iii) Constant liquid and vapour flowrates.

(iv) Constant point efficiency.

Lewis Case 1

Lewis Case 1 describes the tray efficiency where the vapour entering the tray of interest is completely mixed and the direction of liquid flow is of no consequence. The result obtained is:

$$E_{mv} = \frac{1}{\lambda}\left[\exp\left(\lambda E_{og}\right) - 1\right] \qquad (2.8)$$

Lewis Case 2

Lewis Case 2 describes the tray efficiency where no vapour mixing occurs and the liquid flows in the same direction on successive trays, giving:

$$E_{mv} = \frac{\alpha - 1}{\lambda - 1} \qquad (2.9)$$

where $$\lambda = \left[\frac{1}{E_{og}} - \frac{1}{\alpha - 1}\right] \ln \alpha \qquad (2.10)$$

Here α is the relative volatility.

Lewis Case 3

Lewis Case 3 describes the tray efficiency where again no vapour mixing occurs but the liquid flows in alternate directions on successive trays, giving the result:

$$E_{mv} = \frac{\alpha - 1}{\lambda - 1} \tag{2.11}$$

where, if $\alpha < 1$,

$$\lambda = \left[\frac{\alpha^2 - (1 - E_{og})^2}{E_{og}^2(1 + \alpha)(1 - \alpha)}\right]^{0.5} \cos^{-1}\left[1 - \frac{(1 - \alpha)(\alpha - 1 + E_{og})}{\alpha(2 - E_{og})}\right] \tag{2.12}$$

and, if $\alpha > 1$,

$$\lambda = \left[\frac{\alpha^2 - (1 - E_{og})^2}{E_{og}^2(\alpha + 1)(\alpha - 1)}\right]^{0.5} \cosh^{-1}\left[1 - \frac{(1 - \alpha)(\alpha - 1 + E_{og})}{\alpha(2 - E_{og})}\right] \tag{2.13}$$

The main contribution of Lewis was to show the difference between parallel flow of liquid, where the liquid flow on successive trays is in the same direction, and non-parallel flow liquid flow, where the liquid flows in different directions on successive trays.

Series of Mixed Pools

Kirschbaum (1948), working at the same time as Lewis, divided the liquid on the tray into a number of well mixed pools which were in series. The liquid moved from pool to pool changing composition as it crossed the tray. This idea of a series of mixed pools was extended by Gautreaux and O'Connell (1955) who derived an expression for the tray efficiency. The main difficulty in using this technique is determining the number of mixed pools. Bruin and Freije (1974) later proposed a two-dimensional model using the same series of mixed pools approach.

Backmixing Imposed on Plug Flow

Gerster et al. (1955 and 1958), working on the AIChE research program, was the first worker to use an eddy diffusion model to represent the liquid mixing on a tray, which was carried out for a one-dimensional, rectangular tray. The eddy diffusion model

assumes that the rate of mixing of a component is proportional to the local concentration gradient of that component. Gerster's method was the basis for the well documented AIChE method of estimating tray efficiency (AIChE, 1958).

In the AIChE method the mass transfer is modelled on a twin resistance concept, one resistance in the liquid phase and the other in the gas phase. The method involves fixing a tray design and calculating, or fixing, the operating and system variables. The following empirical equations give a guide to the efficiency calculation procedure. The initial required parameters are:

Q_l	liquid flowrate	[gpm]
Q_v	vapour flowrate	[ft^3/s]
ρ_l and ρ_v	liquid and vapour densities	[lb/ft^3]
λ	slope of the equilibrium line divided by the slope of the operating line	[-]
h_w	weir height	[in]
W	average width of liquid flow	[in]
A	active area	[ft^2]
D_l	liquid molar diffusivity	[ft^2/hr]
d_c	bubble cap diameter	[in]
Δ	liquid gradient across tray	[in liquid]

Step 1: Calculate the superficial gas velocity, U_s [ft/s],

$$U_s = \frac{Q_v}{A} \tag{2.14}$$

Step 2: Calculate the F-factor, F $[lb/ft\ s^2]^{0.5}$,

$$F = U_s(\rho_g)^{0.5} \tag{2.15}$$

Step 3: Calculate the height of clear liquid on the tray, h_{cl} [in liquid],

$$h_{cl} = \frac{103 + 11.8h_w - 40.5F + 1.25\frac{Q_l}{W}}{\rho_l} \tag{2.16}$$

Step 4: Calculate the average liquid contact time on the tray, θ_l [s],

$$\theta_l = \frac{37.4 h_{cl} A}{Q_l} \tag{2.17}$$

Step 5: Calculate the resistance to mass transfer in the liquid phase, N_l [-],

$$N_l = 103 (D_l)^{0.5} (0.26F + 0.15) \theta_l \tag{2.18}$$

Step 6: Calculate the resistance to mass transfer in the gas phase, N_g [-],

$$N_g = \left[\frac{\rho_g D_g}{\mu_g}\right]^{0.5} (0.776 + 0.116 h_w - 0.290F + 0.0217\frac{Q_l}{W} + 0.200\Delta) \tag{2.19}$$

Step 7: The calculated vapour and liquid resistances are combined to obtain the overall resistance to mass transfer, N_{og} [-],

$$\frac{1}{N_{og}} = \frac{1}{N_g} + \frac{\lambda}{N_l} \tag{2.20}$$

Step 8: The point efficiency, E_{og} [-], is calculated from the overall mass transfer resistance,

$$E_{og} = 1 - \exp(-0.434 N_{og}) \tag{2.21}$$

Step 9: The eddy diffusivity coefficient, D_e [ft^2/s], is calculated,

$$D_e = \left[1 + 0.044(d_c - 3)\right]^2 \left[0.0124 + 0.015 h_w + 0.017 U_s + 0.0025\frac{Q_l}{W}\right]^2 \tag{2.22}$$

Step 10: The Peclet number, Pe [-], is calculated,

$$Pe = \frac{Z_l^2}{D_e \theta_l} \tag{2.23}$$

Step 11: The enhancement of the Murphree point efficiency, E_{mv}/E_{og}, or the Murphree tray efficiency, E_{og}, can be found graphically knowing the values of λE_{og} and Pe. See AIChE (1958).

Multi-Region Tray with Backmixing

Several other eddy diffusional models have been proposed for the prediction of tray efficiencies (Porter et al., 1972; Bell and Solari, 1974; Biddulph, 1975; Sohlo and Kouri 1982; Yu et al., 1990), some of which allow for eddy diffusion in two directions on the tray. The basis of all of these models is a material balance over an element of froth. The differences occur when assumptions are relaxed and different boundary conditions are used.

Below, the example of the Porter and Lockett (1972) eddy diffusion tray model is derived,

Assumptions of the model:

(i) Constant point efficiency over the tray.

(ii) Linear equilibrium relationship over the concentration range.

(iii) Entering streams are perfectly mixed, both flows and compositions.

(iv) Liquid is totally mixed throughout the froth depth.

(v) Bulk liquid flow occurs only in the z direction.

(vi) Eddy diffusivity, De, is equal in all directions.

(vii) Liquid channels between the two weirs and is stagnant at the side regions.

The coordinate system:

The coordinate system used for the circular plate is shown in Figure 2.1. Due to symmetry about the centre of the flow path length, all calculations should be restricted to the half plate such that $0 \leq w \leq (W/2)$.

The governing equation for the model is derived from reference to Figure 2.2,

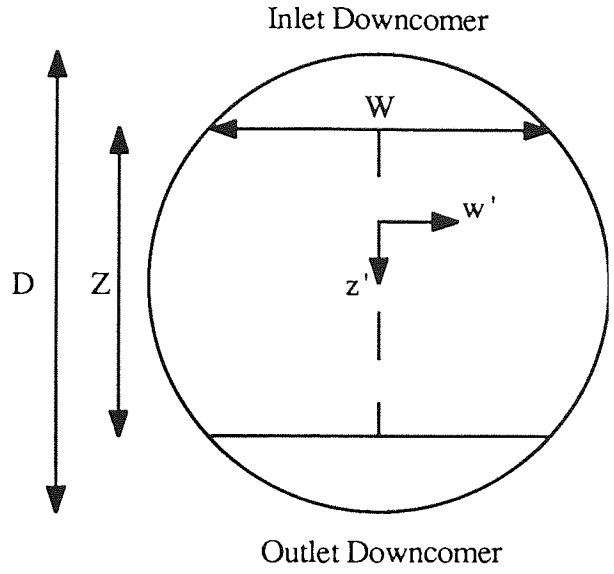

Fig. 2.1 Coordinate System for the Mathematical Tray Model.

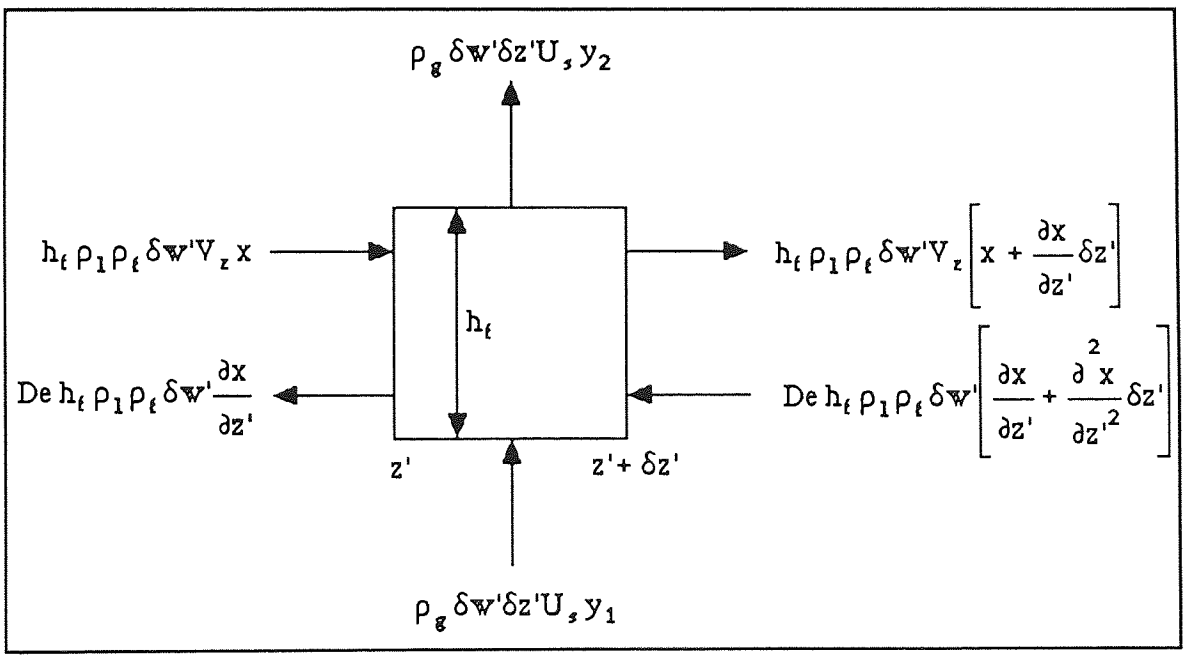

Fig. 2.2 Material Balance over an Element of Froth, z direction shown only.

Material is transferred into and out of the volume of froth by the following mechanisms,

(i) Bulk movement of liquid across the plate, z direction only.

(ii) Random "back-mixing" of liquid as a result of the vapour passing through it.

(iii) Mass transfer from the liquid to the vapour.

A material balance over the elemental volume leads to the following relationship for the main flow region,

$$De\left[\frac{\partial^2 x}{\partial z'^2} + \frac{\partial^2 x}{\partial w'^2}\right] - V_z \frac{\partial x}{\partial z'} + \frac{\rho_g U_s}{h_f \rho_l \rho_f}(y_1 - y_2) = 0 \qquad (2.24)$$

And a similar relationship in the stagnant region, where $V_z = 0$,

$$De\left[\frac{\partial^2 x}{\partial z'^2} + \frac{\partial^2 x}{\partial w'^2}\right] + \frac{\rho_g U_s}{h_f \rho_l \rho_f}(y_1 - y_2) = 0 \qquad (2.25)$$

Using the the following definitions,

$$E_{og} = \frac{y_1 - y_2}{y_1 - y^*} = \frac{y_1 - y_2}{m(x_e^* - x)} \qquad (2.26)$$

$$Pe = \frac{D V_z}{h_f \rho_f \rho_l W De} \qquad (2.27)$$

$$\lambda = \frac{m G}{L} \qquad (2.28)$$

and dimensionless quantities,

$$z = \frac{z'}{D} \quad , \quad w = \frac{w'}{D} \quad \text{and} \quad X = \frac{(x_e^* - x)}{(x_e^* - x_1)} \qquad (2.29)$$

equations 2.24 and 2.25 are transformed into the dimensionless forms,

$$\frac{1}{Pe}\left[\frac{\partial^2 X}{\partial z^2}+\frac{\partial^2 X}{\partial w^2}\right]-\frac{\partial X}{\partial z}-\left[E_{og}\lambda\frac{W D}{A}\right]X = 0 \qquad (2.30)$$

and

$$\frac{1}{Pe}\left[\frac{\partial^2 X}{\partial z^2}+\frac{\partial^2 X}{\partial w^2}\right]-\left[E_{og}\lambda\frac{W D}{A}\right]X = 0 \qquad (2.31)$$

The method of solution is to transform equations 2.30 and 2.31 into finite difference equations and then for the solution to proceed numerically. The eventual solution is a function of the dimensionless groups λ, E_{og}, Pe and DW/A. The first three groups are primarily concerned with the system being separated, whereas the fourth term is a measure of the size of the stagnant region.

Boundary Conditions:

(i) By symmetry along the centreline

$$\text{at} \quad w = 0 \quad \text{for} \quad 0 \le z \le \frac{Z}{D} \quad , \quad \frac{\partial X}{\partial w} = 0 \qquad (2.32)$$

(ii) At the liquid inlet (Danckwerts, 1953; Wehner and Wilhelm, 1956)

$$\text{at} \quad z = 0 \quad \text{for} \quad 0 \le w \le \frac{W}{2D} \quad , \quad X_+ = 1 + \frac{1}{Pe}\frac{\partial X}{\partial z} \qquad (2.33)$$

(iii) At the liquid outlet

$$\text{at} \quad z = \frac{z}{D} \quad \text{for} \quad 0 \le w \le \frac{W}{2D} \quad , \quad \frac{\partial X}{\partial z} = 0 \qquad (2.34)$$

(iv) At the impermeable column wall

$$\frac{\partial X}{\partial n} = 0 \qquad (2.35)$$

Porter et al. (1972) calculated that volatile material could only penetrate the stagnant regions, by random liquid mixing, a limited distance before being removed by the rising vapour. They estimated that the width of the mixing zone was approximately 0.3 m to 0.5 m, and that up to 1.5 m diameter columns, the mixing was sufficient to overcome the liquid channelling, but at diameters in excess of 1.5 m, regions where no replenishment of fresh volatile material occurred, the section efficiency was reduced by vapour bypassing (vapour passing through the liquid without any significant change in composition).

Other Tray Models

Bell and Solari (1974) produced a model where no diffusion was present at all. They quoted that operating Peclet numbers in the range 20 to 35 are sufficiently high that little error is introduced by setting them equal to infinity. The general equation developed is

$$q.\nabla x_n - \lambda E_{og}(x_{n+1}^{*} - x_n) = 0 \qquad (2.36)$$

where the vector q represents the liquid velocity distribution normalised by the average liquid velocity. Equation 2.36 was then solved numerically for the following liquid velocity distributions,

Inverted Parabolic $$q(\xi) = 3(1 - q_s)(1 - \xi)^2 + q_s \qquad (2.37)$$

Linear $$q(\xi) = 2(1 - q_s)(1 - \xi) + q_s \qquad (2.38)$$

Parabolic $$q(\xi) = \frac{3}{2}(1 - q_s)(1 - \xi^2) + q_s \qquad (2.39)$$

Each of the velocity distributions is given as a function of the transverse position, ξ, and also allows for a non-zero slip velocity, q_s, at the wall. Kouri and Sohlo (1985) solved for a similar inverted parabolic liquid velocity distribution, but their model also allowed for diffusion in terms of the Peclet number.

Biddulph (1975) developed the model of Gerster et al. (1958), by allowing for changes in the bulk liquid flow in the z-direction. However liquid mixing was still limited to the z-direction.

Sohlo and Kouri (1982) presented a model very similar to that of Porter et al. (1972), but which allowed for non-equal eddy diffusional coefficients in the transverse and

longitudinal directions. However when the equation was solved equal values of the diffusion coefficient were assumed along with simple non-uniform velocity profiles, based on the measurements of Bell (1972) and Sohlo and Kinnunen (1977). These were

Turbulent $$v = 1.2\,(1.0 - w^5) \tag{2.40}$$

Parabolic $$v = 1.5\,(1.0 - w) \tag{2.41}$$

Severe channelling $$v = 2.14 + 1.47w - 19.9w^2 + 29.83w^3 - 13.47w^4 \tag{2.42}$$

where, w is the dimensionless coordinate perpendicular to the flow direction and v is the liquid velocity at the coordinate. The main conclusion was that the most obvious way of overcoming the adverse effect of the non-ideal liquid velocity profile was the improvement of the liquid velocity profile itself.

Yu et al. (1990) have proposed one of the most complex two-dimensional mathematical tray models, which allows for the possibility that the eddy diffusion coefficient varies with position on the tray. The model is generated using an elemental volume of froth approach, as shown in Figure 2.2, but the velocity, eddy diffusion coefficient and the liquid concentration all change with position, both in the z and w directions. The proposed equation is

$$\frac{\partial x}{\partial t} = \frac{\partial}{\partial w}\left(De_w \frac{\partial x}{\partial w}\right) + \frac{\partial}{\partial z}\left(De_z \frac{\partial x}{\partial z}\right) - V_z \frac{\partial x}{\partial z} - V_w \frac{\partial x}{\partial w} \tag{2.43}$$

Note that the mass transfer is expressed in the form of an accumulation term. The authors then make the assumption that over a small area of tray the eddy diffusion coefficient remains constant, this simplifies the modelling equation to,

$$\frac{\partial x}{\partial t} = De_w \frac{\partial^2 x}{\partial w^2} + De_z \frac{\partial^2 x}{\partial z^2} - V_z \frac{\partial x}{\partial z} - V_w \frac{\partial x}{\partial w} \tag{2.44}$$

The authors then proceed to solve numerically the modelling equation with ten cells, covering a half tray. The reported results indicate forward flow in the centre of the tray with slowly circulating flow towards the side of the tray, the behaviour shows close agreement with the residence time distribution as determined by Yu from his salt tracer experiments. No tray efficiencies have yet been reported from this flow model.

2.1.3 Conclusions On Tray Models

In the two-dimensional eddy diffusion model of Porter et al. (1972), lateral mixing was introduced to take account of variations in the liquid flow across the width of the tray. This concept was generated at the start of a very intensive period of research into the liquid flow pattern on distillation trays in the early 1970s. Column diameters were increasing and reports of scale-up failures were being published (Weiler et al., 1971 and 1973). The next section deals with some of the hypothetical flow patterns that were proposed in this research period.

2.2 Hypothetical Flow Patterns on Trays

Through experimental investigation of the liquid flow pattern on circular distillation trays, several hypothetical liquid flow patterns have been proposed. These hypothetical liquid flow patterns have then been used as input parameters to mathematical tray models, which can then determine the effect of a given flow pattern on tray efficiency.

Three hypothetical flow patterns are described:

(i) The stagnant regions model.

(ii) The retrograde flow model.

(iii) The composite flow model.

2.2.1 Stagnant Regions Model

The stagnant regions model was proposed by Porter et al. (1972) and is presented in Figure 2.3.

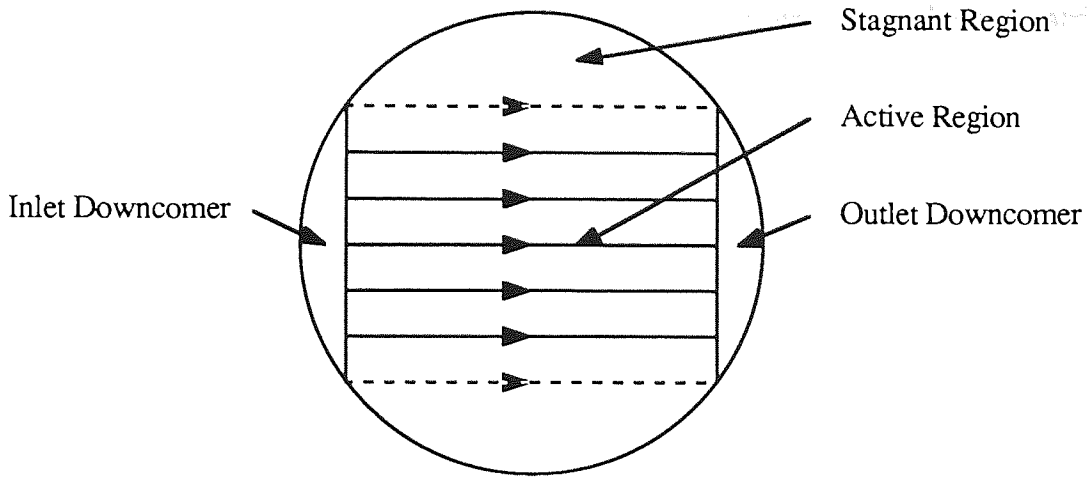

Fig. 2.3 Hypothetical Flow Pattern: Stagnant Regions Model.

This model of the liquid flow pattern came about by the experimental observation of the way in which water flowed across a 1.2 m diameter tray section, which was inserted in a water flume. The water entered the tray section and flowed straight across to the outlet of the section with a uniform bulk velocity. The water at the sides of the tray was separated from the liquid in the centre of the tray and was described as slowly circulating or stagnant. This flow pattern was observed to be independent of the water flowrate and the weir condition.

2.2.2 Retrograde Flow Model

The retrograde flow model was proposed by Bell (1972b) and is presented in Figure 2.4.

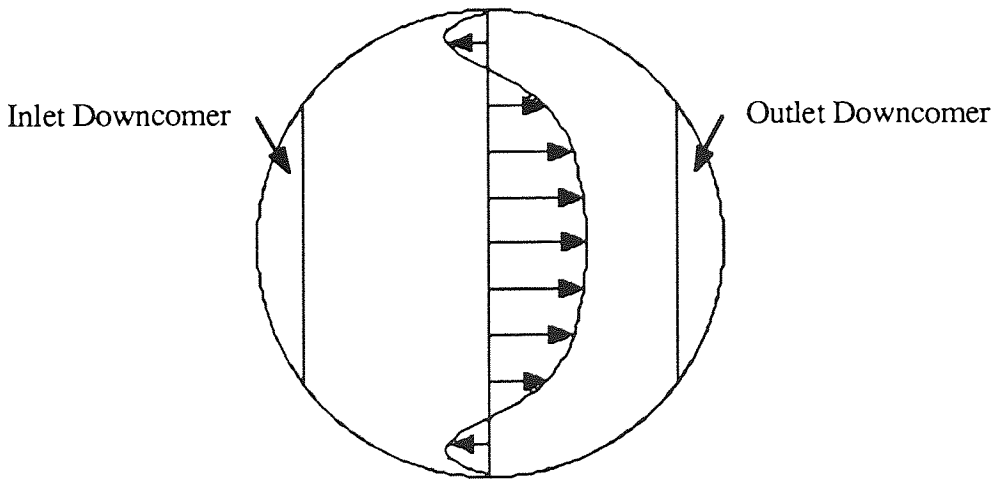

Fig. 2.4 Hypothetical Flow Pattern: Retrograde Flow Model.

This model was based upon the experimental findings of a fibre-optic technique, carried out on an a 2.44 m diameter air-water test tray. Although data were not gathered adjacent to the tray wall, extrapolated data revealed the presence of closed lines of constant residence time. The explanation of the closed isolines was for reverse or retrograde flow to be occurring at the sides of the tray, with high speed flow down the centre of the tray between the two weirs. This proposal of retrograde flow at the sides of the tray was confirmed by a pulse of dye injected along the transverse centreline of the tray. The dye was detected near to the inlet weir at the sides of the tray and, as expected, at the outlet weir. However, a second peak of dye was detected near to the inlet weir at the sides of the tray confirming the presence of retrograde flow as compared to eddy diffusional effects.

2.2.3 Composite Model

The composite flow model proposed by Yu et al. (1982, 1986) is the most complex of the hypothetical models, see Figure 2.5. The flow model was based upon experimental observations on 2.00 m and 2.44 m diameter air-water test trays.

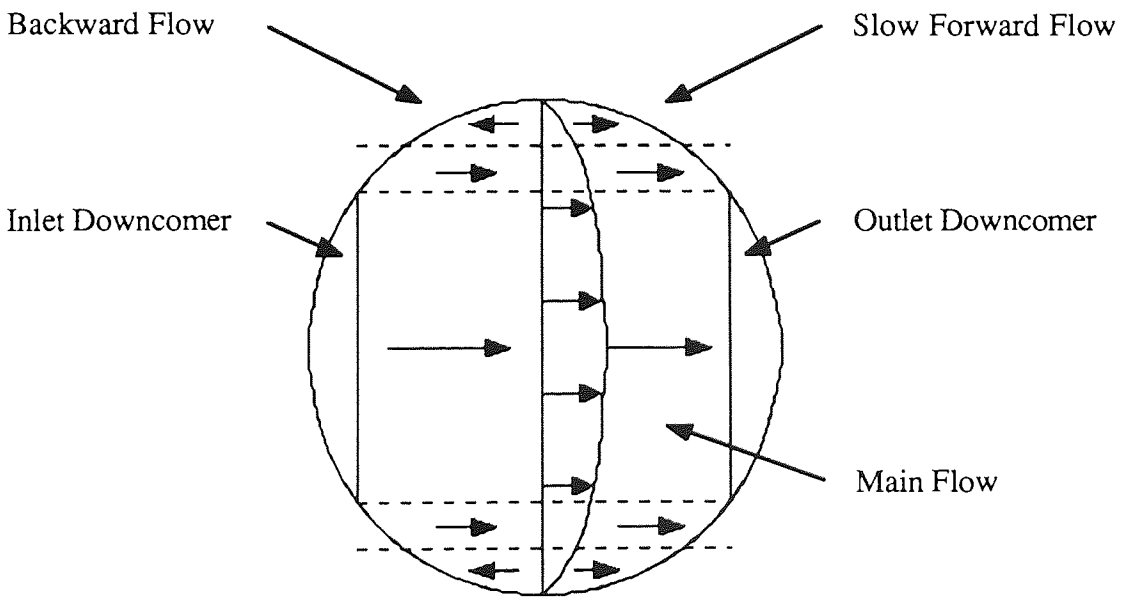

Fig. 2.5 Hypothetical Flow Pattern: Composite Flow Model.

Three regions are described over the tray. A main flow region exists between the inlet and outlet weirs, on which a non-uniform velocity distribution is superimposed. At the side of the tray two regions exist, one a slowly forward flow region positioned towards the outlet

weir and the other a backward flow region positioned towards the inlet weir.

2.2.4 Conclusion on Hypothetical Flow Patterns

From the open literature, the hypothetical models of the liquid flow patterns on distillation trays are in agreement with some form of liquid channelling between the two downcomers. However, between the channelling liquid and the sides of the column exist regions which could be stagnant, circulating or slowly moving forward. It is anticipated that the flow condition of the side regions is very much a function of tray design and the operating conditions. Sohlo and Kouri (1982) pointed out that the most obvious way of overcoming the adverse effect of the non-ideal liquid velocity profile was the improvement of the liquid velocity profile itself. The next section deals with devices that improve the liquid flow pattern over distillation trays.

2.3 Flow Control Devices for Trays

Liquid channelling was thought to be the major contributor to the fall-off in tray efficiency as column diameters increased. This fact was reported by Smith and Delnicki (1973) when a large diameter column failed to achieve separation The series of papers by Porter et al. (1972; Lockett et al., 1973; Lim et al., 1974) predicted that the width of the mixing zone was approximately 0.3 m to 0.5 m, and that on trays above 1.50 m diameter, the liquid channelling would be detrimental to tray efficiency. Research was carried out into how the liquid flow pattern could be controlled or with a view to restoring the expected tray efficiency.

Since this period many tray and downcomer developments to control the liquid flow have been invented and patented with a view to eliminating the flow non-uniformities, each claiming that the tray efficiency is improved due to the more uniform liquid flow. These include,

(i) The directional slotted sieve plate.

(ii) The FRI downcomer.

(iii) The step flow downcomer.

(iv) Inclined counter-current contact tray.

(v) Winged downcomer.

(vi) BOC Tray.

2.3.1 The Directional Slotted Sieve Plate

The use of slots to overcome the non-uniform liquid flow on sieve trays was developed by Union Carbide as patented by Williams and Yendall (1963 and 1968), Matsch (1973) and Kirkpatrick and Weiler (1978). Directional slots are punched into a sieve plate through which the vapour preferentially passes, imparting some horizontal momentum to the liquid in the direction that the slot faces. A typical design of slot is shown in Figure 2.6. The slot density and alignment are controlled over the tray area so that a more uniform liquid flow can be achieved. Weiler et al. (1971 and 1973) have tested the slotted trays and found the liquid flow to be near to uniform.

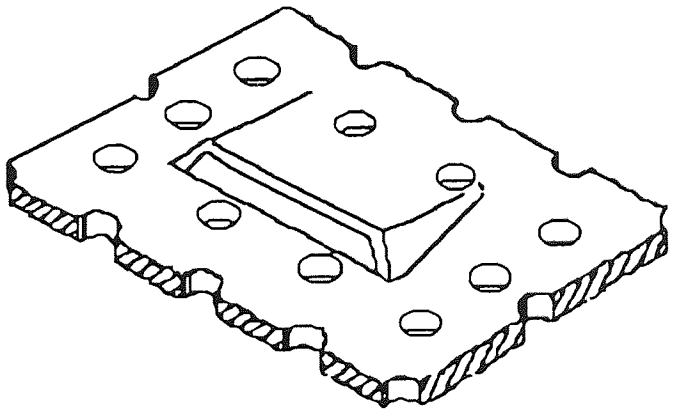

Fig. 2.6 Single Slot as used on Sieve Trays.

2.3.2 The FRI Downcomer

Fractionation Research Incorporated (FRI) have patented modifications to the inlet downcomer and the outlet weir (Keller, 1973). The modification at the inlet was that the downcomer clearance could be independently varied along the length of the inlet weir. This was accommodated by the downcomer apron being made from numerous vertical strips of metal. The technique seemed to increase the gap size at the ends of the inlet weir and to decrease the gap at the centre of the downcomer. The draw-back of this modification would seem that the inlet arrangement was tuned for a particular liquid flowrate and that the performance would deteriorate for non-design flowrates.

The modifications to the outlet weir consisted of notches in the outlet weir to allow the preferential flow of liquid off the tray at certain positions along its length.

2.3.3 The Step Flow Downcomer

The Step Flow Downcomer is a modification to the inlet downcomer of a tray (Porter, 1973). The top of the downcomer is, in general, of a conventional arrangement as it is meant to fit the outlet downcomer of the tray immediately above. The bottom part is half a cylindrical tube with the circular part facing the active area of the tray. If, as is held by several authors, flow non-uniformities originate from the uneven momentum flux of the liquid issuing from a straight downcomer, then liquid redistribution forced by the shape of the downcomer is expected to make the liquid flow more even.

2.3.4 Inclined Counter-Current Contact Tray

Monovyan and Gaivanskii (1980) reported that the non-uniformity of the liquid flow pattern can be eliminated by the slanting of the tray deck towards the downcomer leaving the tray. However, the use of an inclined tray of this sort, reduces the residence time of the liquid in the bubbling zone. This disadvantage does not exist with the inclined counter-current trays, as the design combines the principles of a slanting tray deck and opposing directions of the movement of the gas and liquid phases. Figure 2.7 presents a sketch of the inclined tray arrangement.

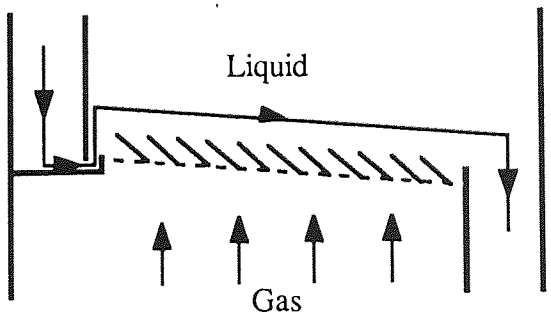

Fig. 2.7 Sketch of Inclined Counter-Current Contact Tray.

2.3.5 Winged Downcomer

The BOC Group have patented a downcomer development whereby the length of the inlet weir is greatly increased (Lavin, 1986), see Figure 2.8.

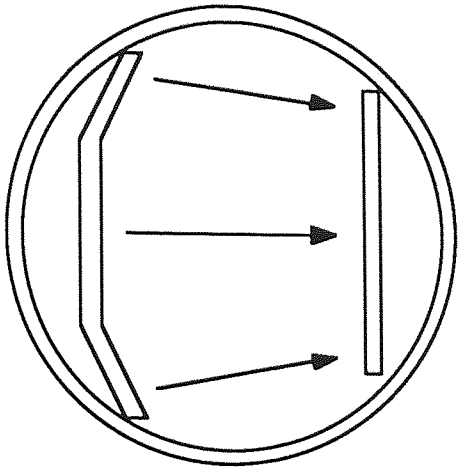

Fig. 2.8 Winged Downcomer.

The winged downcomer design seems to serve two purposes. The effective weir length to diameter ratio is much increased serving to minimise the size of any stagnant regions, and, the flow path length from all positions along the inlet weir seems to be much more uniform. Lavin (1986) also suggests that the hole density over the active tray should be varied to compensate for the different froth velocities in different parts of the tray. He indicates that the hole density should be greater in the centre of the tray than at the sides, and that this could lead to a more constant operating line (L/G ratio) over the tray.

2.3.6 BOC Tray

The BOC Group have patented a new type of contact tray, Biddulph et al. (1990), which is formed from two sheets of expanded metal, one with fine slots and the other a coarse grid. The fine sheet of expanded metal serves to support the biphase, but additionally the fine slots are directed away from the inlet weir which causes a change in the direction of the entering vapour, thus the vapour aids the liquid in its passage from the inlet to the outlet weir. The second coarse grid is attached on top of the lower sheet of expanded metal and serves to maintain a uniform liquid hold-up on the tray by way of an intermediate weir effect.

2.3.7 Conclusion on Flow Control Devices

Many flow control devices already exist and more are currently being invented, the most recent of them in 1990 (Biddulph et al. 1990). This suggests that commercial research and development into distillation hardware is still a very active field, and due to the number of new flow control devices invented, the liquid flow pattern must be of great importance to optimum tray performance.

Flow control devices seem to be concerned with the modification of the liquid flow at the inlet downcomer and by using directed gas flow further down the tray. There appears to be no scientific understanding of why a non-uniform liquid flow pattern should appear; neither in terms of a theoretical analysis, such has been done for the separation of open channel water flow into an expanding section, or as a scientificly designed series of experiments which identify the important causes in terms of tray design and flowrates.

In the next section several experimental procedures are described for the investigation of the liquid flow pattern on distillation trays.

2.4 Experimental Techniques for Determining Liquid Flow Patterns on Trays

Various experimental techniques have been used over the years to investigate the flow patterns developed over distillation trays, which are described below.

2.4.1 Coloured Dye and Camera

The coloured dye and camera technique of using coloured dye to reveal flow non-uniformities has been used by many researchers (Weiler et al., 1971, 1973; Aleksandrov and Vybronov, 1971; Porter et al., 1972; Solari et al., 1982), and the possibility exists for the recorded raw data to be transformed into a residence time distribution. Essentially two versions of the technique are used.

(i) To demonstrate the presence of non-uniform flow over the tray area, dye is continuously injected onto the tray until the biphase is completely coloured. The dye injection is then stopped and the removal of dye by clear liquid entering the tray is monitored and recorded using an overhead video camera. The areas where the dye remains longest are areas of increased residence time. One disadvantage of this version is that it consumes a large volume of liquid, the coloured liquid having to be drained.

(ii) This version is generally favoured to obtain the raw data for residence time distributions and is more sparing in the amount of water consumed. A pulse of dye is injected along a line perpendicular to the flow path length and its movement is monitored using an overhead video camera. Weiler et al. (1971, 1973) favoured the pulse to be introduced just after the inlet weir, whereas Porter et al. (1972) and Solari et al (1982) introduced the pulse along the central transverse line.

Weiler et al. (1971 and 1973) proposed that the distance travelled by the mid-point of the dye band, at various times, was a measure of the bulk liquid flow and that the widening of the dye band with time was a measure of the localised mixing or eddy diffusivity.

2.4.2 Floating Balls and Camera

The use of floating balls and a camera is another illustrative technique to show the presence of non-uniform flow. Porter et al. (1972), Lim et al. (1974) and Lockett and Safekourdi (1976) filmed the movement of table tennis balls around a wooden tray section through which water only flowed. Sohlo and Kinnunen (1977) attempted to measure froth velocities by timing the motion of cork balls on a sieve tray.

2.4.3 Coloured Dye Injection and Sampling

Aleksandrov and Vybronov (1971) used a technique whereby a pulse of coloured dye, of a known concentration, was injected parallel and near to the inlet weir and liquid samples were taken from three points along the outlet weir at discreet time intervals. The samples were mixed together and the dye concentration was determined using a photocolorimeter. A response curve was then constructed for the dye leaving the tray.

2.4.4 Fibre-Optic Technique

The fibre-optic technique is based on the use of fibre-optic probes to detect the presence of a fluorescent tracer which has a very rapid activation and decay time (Bell, 1972a,b). The technique involves injecting a pulse of fluorescent dye at a point or points on a crossflow contact tray and monitoring its progress across the tray using an array of fibre optic probes, which are strategically placed over the tray area. As the dye passes the tip of a probe, it is activated, fluoresces and a portion of the fluorescence is detected by the secondary part of the probe, which passes it to a photomultiplier tube.

The data was collected by an on-line computer, the time taken to sample and analyse the twenty-five points was about thirty seconds (Solari and Bell, 1986). Processing of the data involved finding the mean residence time of the dye as it passed the probes, which led to a measure of the residence time distribution over the tray, and finding the variance of the dye residence at each probe, which gave a measure of the localised mixing when compared to adjacent probes. The technique has the advantage that it can be used in real columns where normally the potential hazards are great.

2.4.5 Salt Tracer and Electrodes

In a series of research papers, Yu et al. (1982, 1986 and 1990) used a similar system to the fibre optic technique, but sodium chloride was used as the tracer material, detected by electrical conductivity probes. The tracer was introduced onto the crossflow tray along the length of the inlet downcomer. An array of conductivity probes, fifteen on a moveable truss, measured the change of electrical conductivity with time of the flowing liquid, the data being stored on a personal computer. The sampling time of each probe was 0.033 seconds and so the authors claimed that the measurements were essentially taken simultaneously.

2.4.6 Water-Cooling Technique

In the water-cooling technique the effect of the liquid flow pattern on mass transfer is investigated by drawing an analogy between heat and mass transfer. Hot water is fed onto the crossflow test tray and is cooled by the passing of rising air. The progress of the heat transfer is monitored by an array of temperature measuring devices and lines of constant temperature are constructed. The regions of lower temperatures are those where the water has an extended residence time.

Stichlmair et al. (1973 and 1987) first used the technique to show the effect of tray out-of-levelness and blockages of the inlet and outlet downcomers. The generated lines of constant temperature were interpreted as lines of constant residence time. Porter et al. (1982) further developed the technique to enable the calculation of a Murphree-based thermal tray efficiency, work repeated by his co-workers (Enjugu, 1986; Ani, 1988; Porter et al. 1987).

2.4.7 Direct Froth Velocity Measurement

The direct froth velocity measurement technique, developed by Bultitude (1989), makes a direct assessment of the local point froth velocity. The method is very simple and relies on the fact that the momentum of the froth introduces a strain into a flat titanium probe which is installed in the froth. A network of strain gauges on the probe converts the strain into an electrical signal, the magnitude of which is dependant upon the froth velocity. A calibration is required for the conversion of the electrical signal into the froth velocity.

2.5 Conclusion on the Literature Review

Sufficient practical experience and theoretical analysis exist to demonstrate the importance of the liquid flow pattern in determining tray and column efficiency. In general, a non-uniform flow of liquid frequently occurs over operating distillation trays and this reduces the tray and column efficiency. However, no scientific experimental work has been done which seeks to discover the causes of non-uniform liquid flow. With the exception of Enjugu (1986) and Ani (1988), little or no work provides reliable data on the effect of the liquid flow pattern on mass transfer. The next section explains the approach to designing the experiments described in this thesis.

CHAPTER 3

3. APPROACH TO THE PROBLEM

The understanding of the fluid dynamics of a horizontal two-phase flow, with a free upper surface and a crossflow of vapour through the liquid, is very limited. This type of flow is very specific to distillation, but there have been few previous experimental observation into how and why it occurs. On the other hand much work exists into the flow of water in open channels. Workers have experimentally observed and characterised the flow of water through varying flow sections and transitions, for example in rivers and converging and diverging channels

Thus the approach taken to observe the liquid flow pattern on crossflow distillation trays, was to first study the flow of water only over an unperforated tray set between an inlet and outlet downcomer, and then to repeat the studies with a perforated tray through which air is forced. This way any observed differences between the two flow patterns could be attributed to the crossflow of air.

For the experimental programme, it was decided that after the water only experiments, the perforated tray would consist of a 10% free area sieve tray with 1 mm diameter holes. This sieve was chosen for three main reasons,

(i) A 10% free area sieve tray is typical of sieve trays used in commercial columns.

(ii) In a progression from "zero hole diameter sieve", 1 mm diameter holes are the smallest used in practice.

(iii) The 1 mm diameter holes enable the tray to operate in one regime only, the bubbly region, and the study would not be complicated by the phenomena of changing operating regimes on the tray.

The research plan was drawn up with the following objectives in mind,

Construction of a new 2.44 m diameter air-water simulator with a facility for water cooling.

The air-water simulator had to be of a significant diameter, so that the flow phenomena observed would be representative of real distillation trays. On operating trays the froth height can reach up to 300 mm and so the tray diameter must be sufficiently larger so as to prevent wall effects from dominating the flow behaviour. The eventual choice of 2.44 m diameter for the simulator was in keeping with the average size of commercial trays at 2.0 to 2.5 m in diameter. The heating facility was required to enable water cooling experiments to be carried out, see below.

Observation of the movement of a dye tracer for water-only flow across a distillation tray section.

This study would provide a base, to which all experimentally observed flow patterns could be compared. A broad range of water flowrates were investigated, for various settings of the gap under the inlet downcomer and the height of the outlet weir.

Observation of the direction of liquid flow for a perforated sieve tray being operated with air-water contacting, using a new experimental technique of directional flow pointers.

The "directional flow pointers" were thin aluminium sheets, with a directional indicator, loosely hinged to a vertical rod and supported clear of the tray floor such that they could freely rotate to align with the flow direction. Similar ranges of flowrate to the water only studies were investigated, along with several different values of air velocity.

Measurement of the variation in clear liquid height over the tray, and the uniformity of flow over the outlet weir.

These measurements were made by water manometer and by flow into compartments along the outlet weir, from which the flow was determined by means of a calibrated orifice. An attempt was made to relate any changes in these measurements directly to the flow pattern.

Experiments on the operating tray using the water cooling technique

In the cooling of water by air, an analogy between heat and mass transfer can be made. Relating this to distillation, the water temperature is analogous to liquid concentration and the air enthalpy is analogous to vapour concentration. Thus by measuring the water temperature at over 100 positions on the tray, the effect of the flow pattern on mass transfer can be determined.

More complete descriptions of the above objectives and their experimental results can be found in the relevant chapters. Thus through this research programme, it is hoped to obtain a comprehensive set of experimental observations and data concerning two-phase open channel flow on a commercial size distillation tray.

CHAPTER 4

4. DESIGN AND CONSTRUCTION OF 2.44 METRE DIAMETER COLUMN

4.1 Introduction

Prior to the start of the project to design and construct a 2.44 m diameter simulator, with a water heating facility, the Aston Research Programme had operated a similar 1.22 m diameter column. The services for this smaller column are supplied from a central source, but the rig still occupies 16 m^2 of floor space. The new 2.44 m diameter simulator was envisaged to be self-contained on its own site, and so a 100 m^2 area was made available for the siting of the new simulator and all the ancillary equipment.

This chapter is presented in an order not too dissimilar to the way in which the 2.44 m diameter simulator was designed and constructed. The test column was initially designed to test a sieve tray with 1 mm diameter holes, but the design was to be flexible enough to accommodate other trays and weir configurations.

4.2 Choice of Process

The floor space of 100 m^2 seemed more than adequate for the process equipment and did not put any major constraints on the design.

The heart of the process is the air-water simulator, to this must be added an air circuit, a water circuit and some form of heating for the water. The only real decision concerned the method of heating the water, for which several systems were considered using electricity, gas, steam and combinations of the three. The eventual process design chosen was that presented in Figure 4.1, using standard chemical process drawing symbols (Austin, 1975), and a photograph of the constructed test facility is contained in Figure 4.2.

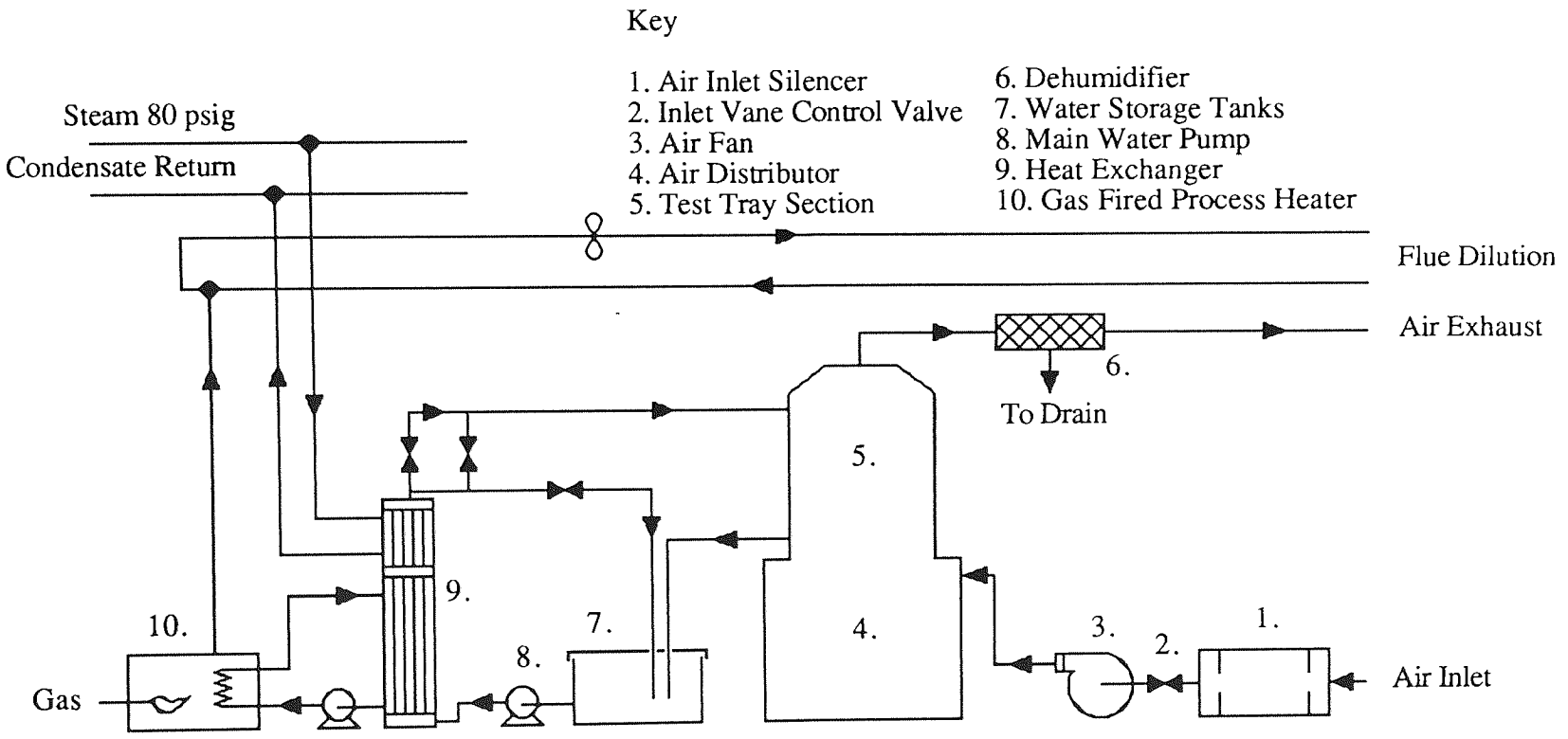

Fig. 4.1 Process Flowsheet of Air-Water Simulator with Water Heating Facility.

Fig. 4.2 Photograph of the 2.44 m Diameter Test Facility.

4.2.1 The 2.44 Metre Diameter Simulator

A new 2.44 m diameter air-water simulator was designed to be constructed in the pilot plant. The base of the new simulator was to incorporate a gas distributor, which would provide uniform air to the test tray. The middle section, as well as containing the test tray, was to include a liquid distributor to ensure that the water also entered the test tray evenly. The two phases were to contact on the test tray, and the humid air to leave the column from the top section.

4.2.2 The Air Circuit

Unsaturated ambient air is drawn into the system, at floor level, through a protective grill in the outside wall of the pilot plant. The air passes through a silencer and vane control valve to the inlet of the fan. The exiting air from the fan flows through a short section of ducting to the flow measuring device, and then into the simulator. Saturated warm air leaves the simulator through the column top and passes through a demister, where excess water is removed from the air stream before it exhausts from the pilot plant at approximately eight metres above ground level.

4.2.3 The Water Circuit

Water is contained in a holding tank at ground level, from which it is pumped through a double heat exchanger. The first exchanger heats the water by counter-current contact with hot water, the hot water being supplied in a closed cycle from gas-fired process heaters. The water immediately flows into the second heat exchanger where it is further heated by condensing steam, from the departmental generator. The warm water leaving the double heat exchanger passes through one of two flowmeters, after which it is piped directly to the inlet downcomer of the simulator.After flowing across the test tray, the cool water leaves over the outlet weir and flows out through the downcomer, back to the sump tanks. A water make-up, not shown, is incorporated to account for evaporative losses.

4.2.4 The Heating Circuits

Gas-Fired Process Heaters

Gas fired process heaters are used to create hot water in a closed loop system. The exhaust gases from the heaters are ducted from the pilot plant using a flue-dilution system. The hot water in the closed loop system is pumped from the gas-fired heaters to

the first stage of the double heat exchanger.

Steam

Steam is generated in the department and is condensed in the second stage of the double heat exchanger. The condensate is returned to the departmental generator.

4.3 Air, Water and Heating Flows

The process flowsheet having been accepted, the design centred on the simulator itself and the throughputs of air, water and heat in the system. A flexible approach was taken towards the design of the air-water simulator, with the aim of accommodating envisaged experimental procedures easily. The flows of air, water and heat through the process were based on maximum expected flowrates.

4.3.1 Maximum Air and Water Flows

As has been discussed earlier, tray flooding curves can be used to determine which regime of operation a tray is performing in. The curves, for a particular geometry and tray, consist of a jet flooding curve and a weeping line, which relate to maximum throughput and minimum throughput respectively. Figure 4.3 presents a tray flooding curve which was used to determine the maximum flowrates of the air and water.

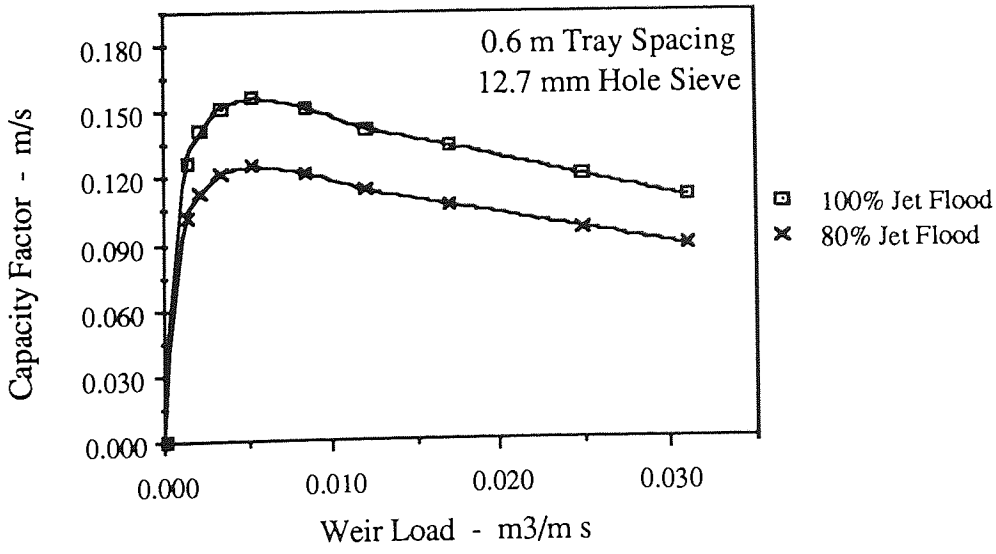

Fig. 4.3 Tray Flooding Curve - 12.7 mm hole sieve, 8% free area and 0.6 m tray spacing.

The capacity factor, Cf, is defined as,

$$Cf = \frac{Q_G}{A_b}\sqrt{\frac{\rho_G}{\rho_L - \rho_G}} \qquad (4.1)$$

The maximum value of the capacity factor, Cf, from the 80% jet flooding curve is 0.12 m/s. Using equation 4.1 and given that D=2.44 m, W=1.50 m, A_b=4.189 m^2, ρ_L=1000 kg/m^3 and ρ_G=1.22 kg/m^3, the maximum air flowrate, $Q_{G(max)}$, is 14.38 m^3/s.

Similarly, the maximum value of the weir load, (Q_L/W), is 0.03 m^3/m s. Using equation 4.2 and given the same conditions, the maximum water flow, $Q_{L(max)}$, is 0.045 m^3/s.

$$Q_L = \left[\frac{Q_L}{W}\right] W \qquad (4.2)$$

In order to specify the duty for a fan, not only has the air throughput to be specified, but the pressure drop against which the flow must move must also be specified. This is usually called the system pressure drop, and is estimated by the addition of individual pressure resistances around the system. It was anticipated that the wet-tray pressure drop would be the major component of the system pressure drop and so this had to be calculated.

4.3.2 Maximum Tray Pressure Drop - 80% Flood

The maximum wet tray pressure drop is itself an addition of three component pressure drops,

$$h_{WT} = h_{DT} + h_{cl} + h_R \qquad (4.3)$$

Dry tray pressure drop - the pressure resistance caused by the air passing through the perforated tray.

Height of clear liquid - the resistance caused by the height of froth on the tray, expressed in terms of clear liquid.

Residual pressure drop - pressure resistance due to gas-liquid momentum transfer processes.

The maximum possible flows, of air and water are 14.38 m^3/s and 0.03 m^3/m s.

Dry Tray Pressure Drop

The usual practice is to represent the dry tray pressure drop, h_{DT}, by an orifice-type equation,

$$h_{DT} = \frac{\zeta \rho_G u_h^2}{2 g \rho_L} \qquad (4.4)$$

Many correlations exist in the literature for the orifice coefficient, ζ. The major influences on ζ are the free area of the tray, ϕ, and the tray thickness to hole diameter ratio, (t/d_h). Using the orifice coefficient correlation, due to Stichlmair and Mersmann (1978), it is observed that the maximum value of ζ is 2.6. Substituting this value into equation 4.4, along with a value of 10% for ϕ, gives a maximum dry tray pressure drop of 0.19m of H_2O.

Height Of Clear Liquid

The air, once onto the tray deck, must pass through the froth on the plate and therefore pressure energy is lost, due to this equivalent height of clear liquid, h_{cl}. Many workers have proposed semi-analytical equations to correlate the height of clear liquid, a recent paper by Bennet et al. (1983), proposes the following correlation, based upon the equation of Francis (1883).

$$h_{cl} = \alpha_e \left[h_w + C \left(\frac{Q_L}{W \alpha_e} \right)^{0.67} \right] \qquad (4.5)$$

where $$\alpha_e = \exp\left[-12.55\,(Cf)^{0.91}\right] \qquad (4.6)$$

and $$C = 0.50 + 0.438 \exp\left[-137.8\, h_w\right] \qquad (4.7)$$

It is known that as the superficial vapour velocity increases, the height of clear liquid decreases and so a maximum height of clear liquid must theoretically occur when the capacity factor, Cf, takes a value of zero (See equation 4.1). Equation 4.6 would give the value of α_e as 1.0, if Cf took the theoretical value of zero, and assuming a 0.075 m outlet weir the calculated height of clear liquid would be 0.17 m of H_2O.

Residual Pressure Drop

The residual pressure drop, h_R, is calculated by the difference between the other pressure drop terms. This term accounts for many small factors such as excess pressure to overcome surface tension effects, pressure energy lost due to gas-liquid and gas-gas momentum transfers just above the tray deck and again the effect of tray thickness to hole diameter ratio. The effect is small compared to the h_{DT} and h_{cl}, and so a value of 0.03 m of H_2O was assigned for h_R.

The Wet Tray Pressure Drop

The maximum wet tray pressure drop envisaged, from the addition of the previously explained pressure drop components due to equation 4.3, was 0.37 m of H_2O.

4.3.3 The Air Fan and the Water Pump

The final specification for the air fan was to deliver 14.38 m^3/s against a pressure head of 0.51 m of H_2O. The extra pressure capacity was to take account of the system pressure drop, terms of which include for the inlet silencer, the air flow meter, the air distributor and other losses due to flow contractions and expansions. A number 48 "Mistral Backward Inclined" fan made by the Halifax Fan Manufacturing Co. Ltd. was purchased along with a 150 HP electric motor.

The final specification of the water pump was to deliver 5.5×10^{-2} m^3/s against a head of 12.75 m of H_2O. The head value takes into consideration the vertical height of rise, the friction due to expansions, contractions and fittings and the head loss due to the water passage through the double heat exchanger - see Section 4.3.5. The chosen pump was an in-line centrifugal pump manufactured by Myson Pumps and Motors Ltd. with a 15 kW electric motor.

4.3.4 Heating Requirement and Equipment

The water-cooling process involves the removal of heat from liquid water. In order to operate at steady state, heat must be supplied at an equivalent rate to that at which heat is being removed, as the water flows in a closed-loop cycle. The column is to be used to investigate a wide range of operating conditions, ranging from low- to high- water loading and low- to high- air throughput. Thus the design heat load would vary between a small temperature drop across the tray with a large water flowrate and a large temperature drop across the tray with a low water flowrate, for a constant air throughput. It was

obvious that heat removal will be at its greatest when the air rate is at its highest level, but a priori it can not be determined which liquid rate, high or low, will result in the greatest heat loss.

From experimental data, obtained on the 1.22 m water cooling simulator by Ani (1988), the maximum amount of heat removed occurs at high liquid loadings. The results show that for an inlet temperature of around 40 °C the temperature drop across the tray is approximately 3 °C. For the maximum liquid loading on the 1.22 m diameter column the heat removed for a 3 °C temperature drop would be given by equation 4.8,

$$\text{Heat Removed} = Q_{L(max)} \rho_L Cp \Delta T \qquad (4.8)$$

As, C_p, the specific heat of water, is equal to 4.2 kJ/kg K,the heat removed is 284 kW. However for the same position on a tray flooding curve, a 2.44 m diameter tray has twice the liquid loading and four times the vapour throughput as a geometrically similar 1.22 m diameter tray. Thus the heat removed will be four times that calculated for the 1.22 m diameter column at 1134 kW.

The heat load was designed with a capacity of 1.2 MW.

Steam Supply

The departmental steam generator was capable of raising 2000 lb/h of steam at 120 psig, which is equivalent to 528 kW, as the supply line was limited to 80 psig, and a corresponding temperature of 162 °C. It was proposed to utilise all this steam when the maximum heating requirement was necessary, but during normal use the steam would only be used as a final top-up of heat. The steam provided a high grade heat source which was hoped would provide a good fast response for control purposes. A 100 mm steam line was laid from the generator to the double heat exchanger next to the simulator, with a suitable condensate return line.

Gas-Fired Process Heaters

The varying heat load of the simulator necessitated a flexible supply of source heat, and so two smaller gas-fired process heaters were purchased as opposed to one large heater. After discussions with various suppliers, the nominal rating of each burner was chosen as 500 kW. However, when burner efficiency and heat transfer efficiency within the process heater, are taken into account the actual efficiency of a process heater is only 80%, thus making 400 kW available.

This maximum efficiency occurred for an 11 °C temperature difference between the inlet and return water pipes,with the return pipe having a temperature of 82 °C. This allowed for the flowrate of water to each process heater to be calculated at 8.66×10^{-3} m/s. So the flowrate of primary heating water through the water-water exchanger would be twice this value at 1.73×10^{-3} m/s. The only other information required was the hydraulic resistance of a process heater, 0.26 m of H_2O, which was to enable the sizing of the small circulation pump.

The flue gases from the process heaters had to be removed from the building and passed to a tall stack or could be diluted with fresh, ambient air and disposed of just above ground level. The second option was chosen and a suitable system installed.

Double Heat Exchanger

The double heat exchanger fulfilled the role of transferring heat from the process heaters and the steam line to the main water circuit. The design conditions of flow and temperature for the steam and primary heating water circuit were known, however in the main water circuit the flow, and therefore the temperature, was likely to vary. All the information was forwarded to a heat exchange equipment supplier, who finalised the design and manufactured the double heat exchanger.

The calculated areas for heat transfer were 10.22 m^2 for the lower water-water exchanger and 3.37 m^2 for the upper condensing steam-water exchanger. The hydraulic resistance on the shell side of the water-water exchanger was 2.79 m of H_2O, and the resistance through the tubes of both sections was 3.21 m of H_2O. Also the tubes on the main water circuit side were coated with aluminium bronze, to prevent corrosion from the warm highly oxygenated water.

4.4 The Simulator Column

4.4.1 Introduction

The 2.44 m diameter column was designed and constructed in three separate sections. The base of the column consists of the air inlet and air distribution system, the middle section contains the test tray with supports and downcomer arrangements and the top section directs the air to the exhaust ducting. Figure 4.4 presents a schematic diagram of the simulator.

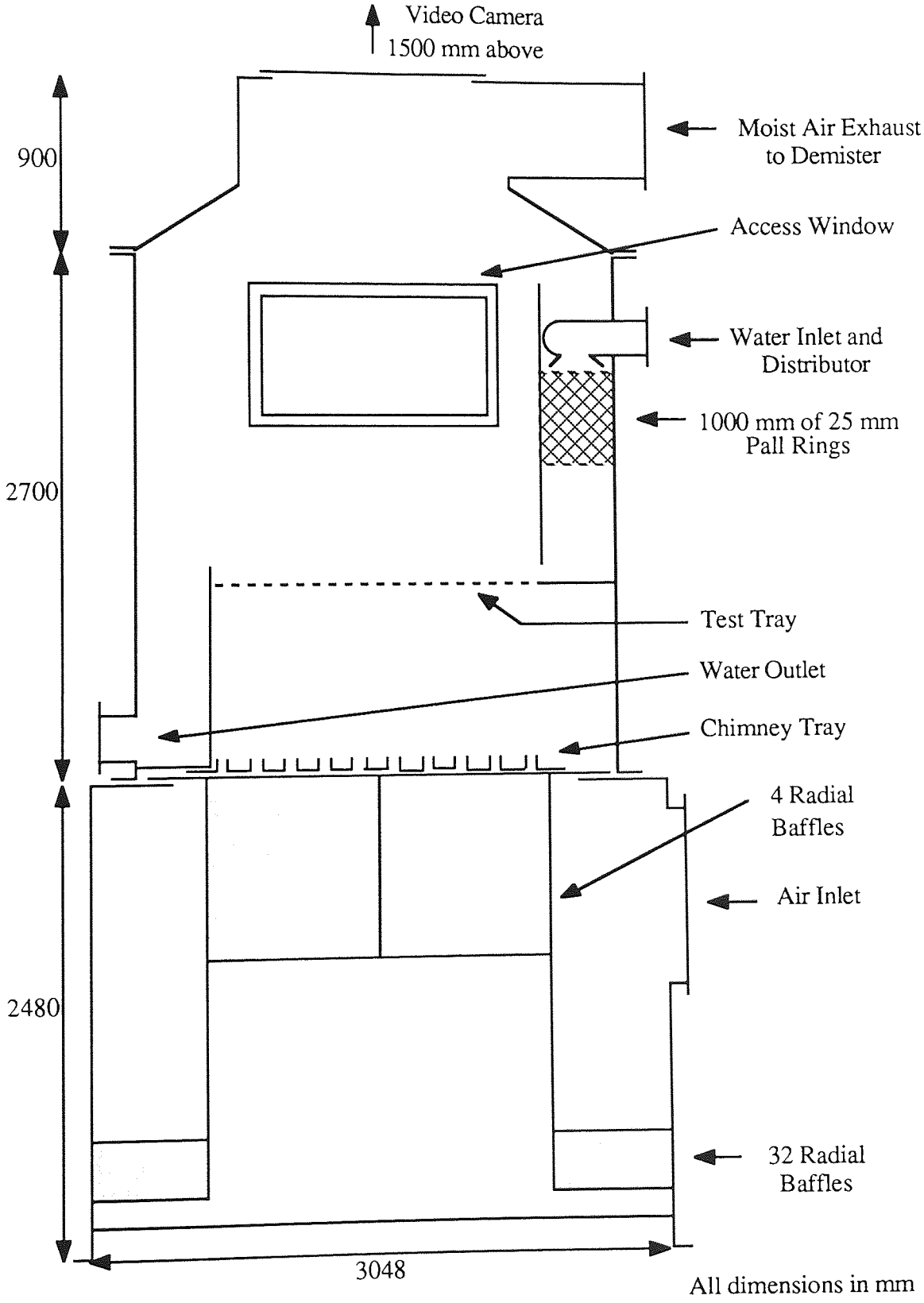

Fig. 4.4 Schematic Diagram Of The 2.44 m Diameter Simulator.

4.4.2 The Air Distributor

Air enters the 3.048 m diameter gas distributor tangentially from a 0.978 x 0.622 m^2 section of ducting, after passing through a flowmeter. The air swirls inside an annulus, between the outer and inner shells, until it reaches the 32 radial baffles, which are 0.3 m deep. The radial baffles remove most of the tangential swirl and cause a downward vertical flow of air to the base of the distributor. The air escapes from the annulus under the inner shell into the central body of the distributor where four more radial baffles, 0.978 m deep, continue to remove any remaining swirl. The distributor was designed using design methods based on the work of Ali (1985).

The shells of the distributor were constructed of mild steel, 0.005 m thick, and the baffles being non-weight bearing were fabricated of thinner steel.

Ideally the distributor works on a dry basis, to prevent the air inside picking up any moisture and thereby changing its properties. To achieve this, a chimney tray with 128 risers was placed between the test tray and the air exit from the distributor, and the collected water removed. An additional advantage of the chimney tray is that the air distribution can also be determined by means of the measuring the flow of air from each riser. The base was coated internally with an epoxy resin to prevent corrosion should any water happen to enter the base.

4.4.3 The Test Column

The 2.44 m diameter test section is mounted directly on to the distributor. The air travels about a metre before encountering the tray support on which the test trays are mounted. The tray support structure is integral and connects to the outlet downcomer. After the air leaves the test tray it flows up and into the exhaust ducting. Water enters the side of the column and must also be uniformly distributed across the inlet downcomer, so the arrangement which proved successful on the 1.22 m column, as described by Audu (1986), is used, where a sparge pipe directs water over a one-metre deep bed of Pall Rings, which itself is supported on a 10% free area tray.

The test section needed to be resistant to corrosion and ideally transparent. Due to the size aluminium was the chosen material of construction with observation windows and access holes. The column was designed and BOC Cryoplants Ltd. prepared drawings and dealt with the manufacture.

4.4.4 The Exhaust Section

The top section of the column served as an interface between the test section and the air exhaust ducting. The cross section is reduced from 2.44 m to 1.50 m and the exhaust air leaves from the side. The reducing section contains four observation windows and the top plate can be removed to perform video studies. The construction material is a heavy gauge galvanised steel.

4.5 Specification of Measuring Instruments by Error Analysis

4.5.1 Introduction

One advantage of using the water-cooling technique to investigate the liquid-flow pattern on a tray is that the measured temperatures can be processed to calculate the tray and point efficiencies. The error associated with the efficiency value is itself determined by the accuracy of the instruments used to measure the variables.

An error analysis method is used to determine the effect of assumed errors in the measured variables on the calculated efficiency values. Knowing the sensitivity of the efficiency to each of the measured variables, the specification of the measuring instruments can then be determined.

4.5.2 Basis of Error Analysis

Whenever a value, E, is quoted there should always be an associated error, e, due to the scale not having an infinite number of markings or because there is already a degree of uncertainty about the value. The point in question is how to combine these errors in a calculation. This is probably best explained by example.

Let $y = f(x)$ (4.9)

Suppose x is a measured quantity and y is the quantity calculated from the equation 4.9. If the error in x is δx, the corresponding error in y is δy where,

$$\lim_{\delta x \to 0} \frac{\delta y}{\delta x} = \frac{dy}{dx} \quad \text{or} \quad \frac{\delta y}{\delta x} \approx \frac{dy}{dx} \quad \text{for small } \delta x \tag{4.10}$$

From this definition, clearly the error in y, δy, can be computed. Expanding this idea, the

following relationship appears for some calculated quantity, z, where z is a function of the measured quantities a, b and c.

Thus, $z = g(a,b,c)$ (4.11)

$$\delta z = \frac{\partial z}{\partial a}\,\delta a + \frac{\partial z}{\partial b}\,\delta b + \frac{\partial z}{\partial c}\,\delta c \tag{4.12}$$

The first term is the error in z due to the error in a, the next to the error in b, etc..... This is known as the "Principle of Superposition of Errors", and is referenced in many error analysis books such as that by Taylor (1982). Also, if δa, δb, and δc are independent random errors in the ranges, -a to a, -b to b and -c to c respectively, then the most probable error in z, δz, is given by,

$$[\delta z]^2 = \left[\frac{\partial z}{\partial a}\,\delta a\right]^2 + \left[\frac{\partial z}{\partial b}\,\delta b\right]^2 + \left[\frac{\partial z}{\partial c}\,\delta c\right]^2 \tag{4.13}$$

This is the basis of the error analysis performed in this study.

4.5.3 Equations used and Raw Data

The Equations

The equation used in calculating the Murphree tray efficiency, E_{mv}, based on the vapour phase is defined as

$$E_{mv} = \frac{(H_{out} - H_{in})}{(H^{*}_{Tout} - H_{in})} \tag{4.14}$$

where H_{in} is the enthalpy of the entering air, H_{out} is the average enthalpy of the leaving air and H^{*}_{Tout} is the enthalpy of the air in equilibrium with the average water temperature leaving the tray. The enthalpy values are calculated from the experimental data as follows where

$$H_{out} = \frac{L * Cp}{G}\,(T_{in} - T_{out}) + H_{in} \tag{4.15}$$

$$H_{in} = (C_{air} * T_{db}) + (Hum_{(T_{db},T_{wb})} * ((C_{wat} * T_{db}) + \lambda)) \tag{4.16}$$

$$H^{*}_{Tout} = (C_{air} * T_{out}) + (Hum_{(T_{out},T_{out})} * ((C_{wat} * T_{out}) + \lambda)) \tag{4.17}$$

The above equations are linear with respect to our proposed measured variables, L, G, T_{in}, T_{out}, T_{db}, and T_{wb}. However, a complication arises due to the humidity value, Hum, being a function of pressure, dry bulb temperature and wet bulb temperature. To simplify this complexity it is proposed to calculate the partial derivatives of E_{mv}, with respect to the other variables numerically. Equation 4.18 shows the approximation, appropriate for the dry bulb temperature, T_{db}, which is not too dissimilar from the definition in equation 4.11.

$$\frac{\partial E_{mv}}{\partial T_{db}} \approx \frac{E_{mv}(T_{db}+\delta T_{db}) - E_{mv}(T_{db})}{\delta T_{db}} \quad \text{for small } \delta T_{db} \qquad (4.18)$$

The Raw Data

The original error analysis was performed on data obtained from the 1.2 m diameter test column. However, now that results have been generated from the 2.44 m diameter test column it would seem more appropriate to use them as the raw data for this analysis. The outcome of the analysis will in no way be affected by this slight change in the raw data.

Table 4.1 contains all the raw data necessary to carry out the analysis, including the associated measurement errors. The analyses were carried out for the prescribed errors, the results of which were to determine the accuracy of the bought measuring devices.

Variable To Be Measured	**Value**	**Assumed Error In Measured Value**
L - Water Flowrate	37.5 kg/s	4.0%, 2.0%, 1.0% and 0.5%
G - Air Flowrate	11.41 kg/s	
T_{in} - Water Inlet Temperature	41.93 °C	0.10 °C, 0.05 °C and 0.02 °C
T_{out} - Water Outlet Temperature	35.29 °C	
T_{db} - Inlet Air Dry Bulb Temperature	12.64 °C	1.0 °C and 0.5 °C
T_{wb} - Inlet Air Wet Bulb Temperature	8.50 °C	

Table 4.1 Measured Variables, Values and Associated Errors.

4.5.4 Results of Analysis

The Murphree tray efficiency, E_{mv}, based on the vapour phase for the conditions stated was calculated to be 86.7%. By changing the variables slightly, (i.e. within the error margins), one at a time, and by repeating the calculation the effect of the change on the calculated value of E_{mv} can be observed. Figures 4.5 and 4.6, are "Snowflake Diagrams", which show the sensitivity of the calculated value of E_{mv} to the measured variables. When viewing "Snowflake Diagrams" the greater the magnitude of the gradient, the more sensitive the calculated value is to that particular measured variable.

From Figures 4.5 and 4.6, it can be seen that the effect of accuracy of both the flowrate measurements have an equal, but opposite, affect on the calculated Murphree tray efficiency. The accuracy of the temperature measurements reveal a more varied affect on the tray efficiency. T_{out} has the greatest affect followed by T_{in}, then T_{wb} and finally T_{db}. It would seem that the dry bulb temperature of the inlet air has virtually no affect on the calculated tray efficiency, as the partial derivative of E_{mv} with respect to T_{db} tends towards zero.

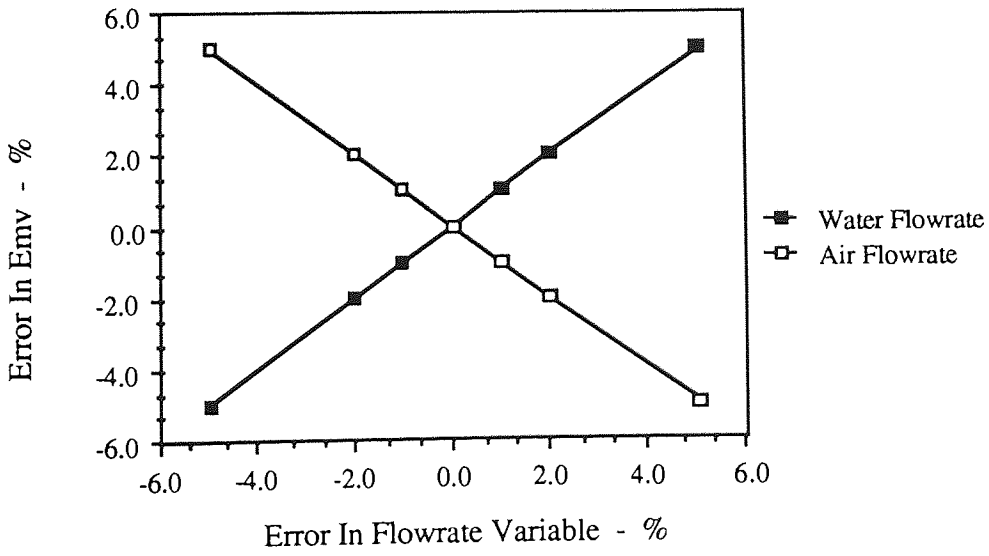

Fig. 4.5 Sensitivity of E_{mv} to Changes in Flowrate Variables.

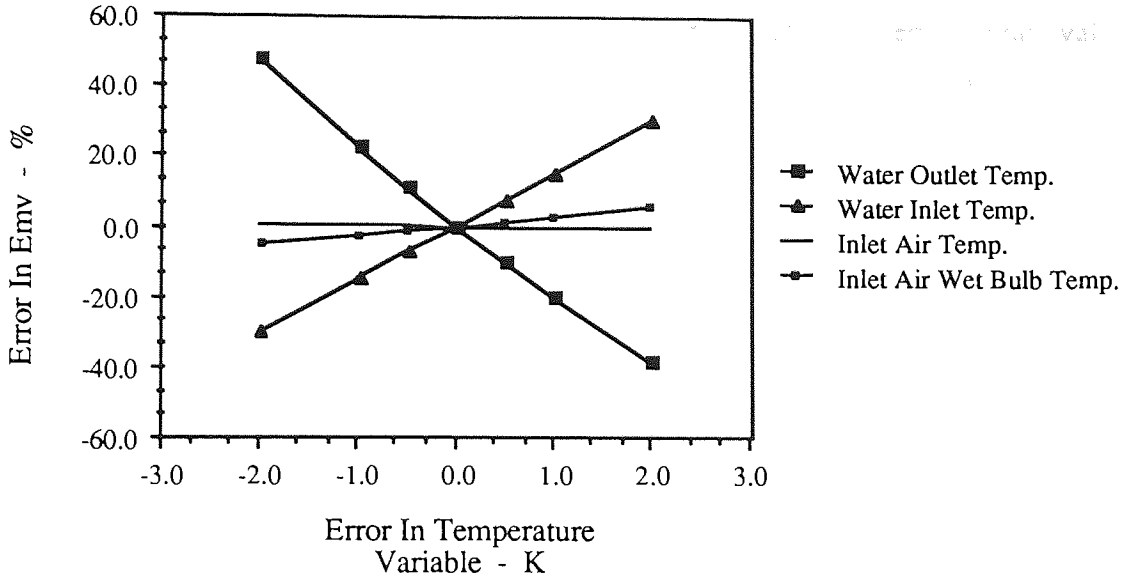

Fig. 4.6 Sensitivity of E_{mv} to Changes in Temperature Variables.

Table 4.2 utilises the partial derivatives along with given accuracies or errors to show the effect on the calculated tray efficiency.

Measured Variable	**Error**	**Error**	**Error**	**Error**
Water Flowrate	4.0%	2.0%	1.0%	0.5%
Air Flowrate	4.0%	2.0%	1.0%	1.0%
Inlet And Outlet Water Temperatures	0.1°C	0.05°C	0.02°C	0.02°C
Inlet Air Wet And Dry Bulb Temperatures	1.0°C	1.0°C	0.5°C	0.5°C
Murphree Tray Efficiency - 0.867	± 0.0573 Or ± 6.6%	± 0.0328 Or ± 3.8%	± 0.0161 Or ± 1.9%	± 0.0142 Or ± 1.6%

Table 4.2 Accuracy of Murphree Tray Efficiency for Given Variable Errors.

As is expected, the error in the Murphree tray efficiency decreases as the accuracy of the measured variables increases. To accept too large an associated error in the tray efficiency

would reduce the value of any published results, whereas to go for a very accurate value of the tray efficiency would prove prohibitive in capital expenditure, so a compromise must be reached.

4.5.5 Accuracy of Measurement Equipment

The conclusion of this error analysis is the following specification for flow and temperature measurements:

Liquid Flowrate	0.5%
Air Flowrate	2.0%
Water Temperatures	0.02 °C
Air Temperatures	0.5 °C

This specification leads to the accuracy in the Murphree tray efficiency of 2.1%, which would seem acceptable. It must be remembered though that this calculation assumes steady state operation, so if there are any variations in the measured variables with time then these must be taken account of in any final errors analysis.

4.6 Measurement Equipment

Now that the accuracy of flow and temperature measurements have been specified, suitable measuring devices can be chosen.

4.6.1 Air Flowmeter

The options for where to position the air flowmeter were very limited indeed, either just before or just after the fan. Both sections of ducting have a large cross sectional area, 0.978 x 0.622 m^2 and 0.978 m diameter, and thus the number of effective diameters allowable before the measuring device was limited to one and a half. This together with a desired accuracy of 2% in the measured flowrate set a challenge to find a suitable air flow measuring device.

A flowmeter fitting the requirements was designed and purchased from Tekflo Ltd.. The flow grid was supplied with a calibration certificate for our required flow conditions.

A brief outline of the technology used follows. A differential pressure, proportional to the flow in accordance with classical Bernoulli theory, is developed between fifteen impact and static pressure sensors.The impact and static pressure sensors are distributed uniformly, at centres of equal area, over the cross section of the ducting to obtain an acceptable flow characteristic. The pitot sensor array is interconnected to provide a representative average differential pressure. Flow profile irregularities are reduced by the use of shrouds around the pitot sensors and by honeycomb flow straighteners, located upstream of the flow sensors.

For superficial air velocities in the test column of between 0.7 and 3.0 m/s, the corresponding differential pressure generated by the pitot array lies in the range 3.19 to 57.92 mm of H_2O. A mechanical micromanometer, supplied by Perflow Instruments, was used to measure the differential pressure, with an accuracy of better than ±0.005 mm of H_2O.

4.6.2 Water Flowmeter

Again the problem arises of requiring an accurate measurement of flow combined with a limited amount of space for an undisturbed piping run upstream of the measuring device. A decision was made to incorporate two flowmeters into the water circuit, because the range of flowrates was so great. For normal operation and the higher flowrates an electromagnetic flowmeter was used, and for lower flowrates, which account for less than 5% of operation, an orifice plate was used.

The Electromagnetic Flowmeter

An electromagnetic flowmeter has no moving parts and causes no disturbance to the flow of fluid. The system is a compact, volumetric liquid flowrate detector that utilises as the process transducing method the characteristic of a conductive fluid to generate an induced voltage when flowing through a magnetic field. The amplitude of the voltage thus produced is directly proportional to the average flow velocity of the fluid, and is almost independent of all flow patterns.

The meter chosen was a 10 cm unit capable of measuring water flowrates of between 0.009 and 0.090 m^3/s manufactured by Combustion Engineering. The unit was supplied with a certificate of calibration and the accuracy was within the specification of 0.5%.

The orifice plate was used to measure water flowrates of less than 0.009 m^3/s, as the

electromagnetic flowmeter requires a critical velocity of fluid through the sensor. The accuracy of the orifice plate was in the order of 2 to 3%, but as the low flowrates accounted for less than 5% of operation the device was deemed acceptable.

4.6.3 The Humidity Sensor

The type of hygrometer selected measured moisture by means of a moisture sensitive silicon chip sensor. If the water vapour pressure of the atmosphere surrounding the sensor alters, then the number of water molecules held in the pores of the sensor will vary, producing a detectable change, which is then converted to an analogue signal.

Using the supplied factory calibration information the output signal from the hygrometer was converted to the wet bulb temperature of the air sample. The unit required a flowrate of 0.5 lit/min of air to operate successfully and the accuracy of the final temperature was 0.5 ^{o}C.

4.6.4 The Temperature Measuring Devices

Platinum resistance thermometers were chosen as the temperature measuring devices. A full description of the temperature accuracy (including the data-logging controller) is contained in the next chapter.

CHAPTER 5

5. DATA COLLECTION AND PROCESSING

5.1 Temperature Data Collection

As is evident from the previous chapters the technique of water cooling involves the monitoring of the water temperature at various positions over the tray area. In principle, the more temperature measuring devices mounted, the more precise will be the generated pattern of temperatures. In this work over 100 point temperatures were measured and it was desired that these measurements were made simultaneously. In practice this was done by means of a data-logging device, which collected all the temperature data over a short but finite period of time, of the order of one to two seconds.

5.1.1 Temperature Measuring Devices

The choice of temperature measuring devices was between thermocouple technology and resistance thermometry. The desired accuracy of the temperature reading was determined, by the error analysis, to be 0.02 ^{o}C which suggested resistance thermometry would be more suitable. The basic principle of resistance thermometry, is that the resistance of a conductor varies according to its temperature. The reasons for choosing resistance thermometers were as follows.

(i) Measures required in thermocouple technology are not necessary when using resistance thermometers. Copper wires are used to connect the resistance thermometer to the associated instrumentation, and since the calibration is absolute, reference or cold junction correction techniques are not required.

(ii) The freedom from drift, as compared with a thermocouple, makes frequent re-calibration unnecessary.

(iii) The accuracy and long term stability of resistance thermometers are superior to those of thermocouples.

Due to the high accuracy of resistance thermometers, the resistance of the external leadwires must be taken into account, and if the values have an affect on the required

accuracy of the thermometer then the effect should be minimised. To obtain the greatest degree of accuracy from a resistance thermometer four leadwires are necessary in a current/voltage measuring mode. Figure 5.1 shows the typical circuit for the four-wire configuration. The errors due to leadwire resistance can be made negligible by having a very high input impedance amplifier.

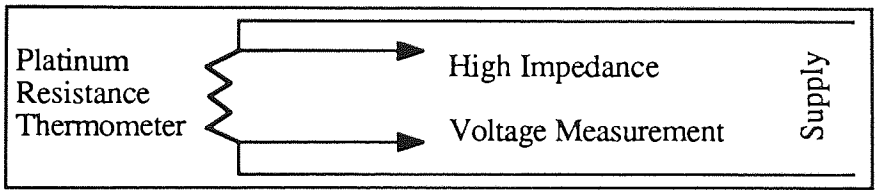

Fig. 5.1 Circuit used for Platinum Resistance Thermometers.

The resistance thermometer was mounted inside the tip of a 300 mm long stainless steel probe, of diameter 3 mm. The four sheathed leadwires, six metres long, were made of copper and sealed in an exterior PVC coating, to provide the final resistance against water.

5.1.2 Mounting of the Platinum Resistance Thermometers

From a preliminary layout it seemed 108 resistance thermometers was suitable for a good, even coverage of the 2.44 m diameter tray. This number of thermometers suggested that they should be mounted from below, due to the multitude of wires leading from the column to the data-logging interface. A simple and cost effective solution for the mounting of the thermometers was found in the form of a rubber grommet. During commissioning, it was noticed that the use of a bare probe resulted in an erroneous temperature, probably due to the cooling effect of the passing air. The problem was overcome by the addition of a shroud, which guaranteed that the probe was surrounded by water only. Water entered the shroud from the top and was allowed to circulate about the tip of the probe, where the platinum resistor is contained, before exiting from the shroud to the biphase through the circulation outlet. Figure 5.2 shows how the probe, supported by the grommet, is held in the water phase.

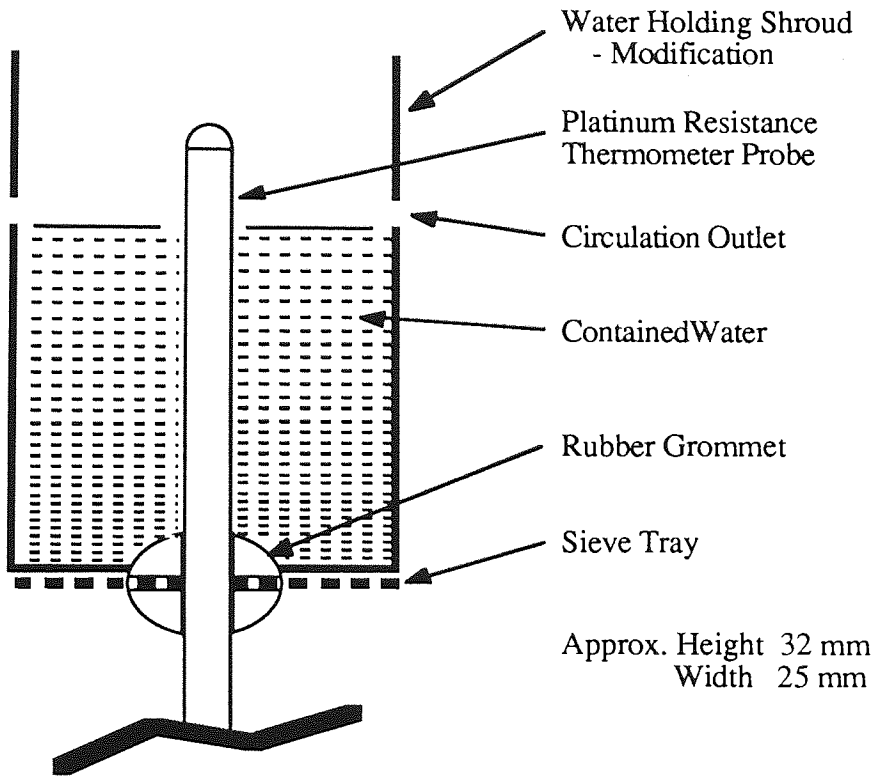

Fig. 5.2 Thermometer Mounting Technique Using Rubber Grommet.

5.1.3 Data Logging Electronics

The water-cooling technique is essentially a steady-state technique of investigating flow patterns on an air-water simulator tray. Despite taking care to maintain all the flowrates and heat inputs at constant values throughout the tests, it is likely that some drift in temperature will occur because of the scale of operation. Thus it was necessary to consider a data-logging interface suitable for operation in both steady and unsteady modes.

When studying transient changes a "snap-shot" view of the water temperatures on the tray has to be taken. However, a finite period of time must pass during the collection of the temperature data, and so this time must be minimised to make the data collection as simultaneous as possible. Taking into account the rate of change of the water temperature at a particular point, and that operation was likely to be near steady-state, one to two seconds seemed an appropriate period over which to collect the temperature data.

A MICROLINK data logging interface, supplied by Biodata Ltd., was purchased, courtesy of BOC Cryoplants Ltd., for controlling the temperature probes. The unit is designed to allow flexible interchange of data between instrumentation and computers that

have an ability to act as controllers of an IEEE-488 bus. An Opus (PC V) personal computer, with a 30 Mbyte hard disk, was used to control the interface.

The MICROLINK consists of a mainframe unit with eighteen available slots for different modules. The eighteen modules were made up of a **High Speed Clock**, an **A-D Converter** and sixteen **RTD8H** modules. Each RTD8H is an analogue input module and has the capacity to accept eight four-wire resistance thermometers, or channels as they are commonly referred to.

High Speed Clock

The high speed clock module allows the interface to be used for rapid data acquisition at equally spaced time intervals between channels. As the aim is to collect all the temperature data simultaneously, a burst mode of the clock module controls the multiplexing and analogue to digital conversion which enables the data collection to occur as quickly as possible, with a constant delay between each channel. The smallest delay was one micro-second, but the settling time for the current in each resistance thermometer was just under a milli-second, so the basic clock unit was set to one milli-second. The time to scan all the 120 potential channels, sixteen RTD8Hs each with eight channels, was 1.2 seconds, which seemed reasonable.

A-D Converter

The A-D Converter is a twelve-bit analogue to digital converter, which means that any measured value after conversion has a resolution of 2^{-12} of the full-scale range. The analogue signal from the RTD8H input module selected, is converted by the a-d converter and the result can be sent over the IEEE-488 bus.

RTD8H

The RTD8H is an analogue input module accepting either sixteen two-wire or eight four-wire resistance thermometers. The module has two range settings, a wide range covering -200 ^{o}C through 900 ^{o}C and a reduced range covering -10^{o}C through 55^{o}C. The reduced range when combined with the twelve-bit converter gave a temperature resolution of better than 0.02 ^{o}C.

5.1.4 Calibration of Resistance Thermometers

The resistance thermometer leads were all of slightly differing lengths and a similar variation was expected in the length of the platinum resistors. When all the thermometers were connected to the interface and computer, the measured temperatures varied within one degree, even though all the probes were in the same temperature environment, and so some calibration or standardisation of the measured temperatures was required.

An insulated water bath with a variable heating source was set up and all the thermometer probe tips were immersed into the centre of the bath. Space was allowed between the probe tips for the free movement of water, which was circulated by a submerged pump. A platinum standard thermometer was selected and this was also placed at the centre of the bath. The standardisation was done at the following bath temperatures to 0 °C, 15 °C, 25 °C, 35 °C and 50 °C. At each calibration temperature steady-state was achieved on all the thermometers, including the standard thermometer, and temperature readings were recorded to provide a calibration point. Between the calibration points linear interpolation is used to determine the actual temperatures from the measured temperatures.

5.1.5 Collected Temperature Data

Program

A Fortran 77 program was developed to drive the data logging interface and is listed in Appendix 1. Input parameters, such as the basic clock unit and the range of the RTD8Hs, are sent to the data-logger, over the IEEE-488 bus. Some supplied driver software was included with the system, and calls to these routines are made from within the main program. Once steady-state has been achieved on the tray, twenty complete scans of the thermometers are taken, the measured values corrected using the calibration points and if steady state has been maintained during the data collection the conditions, data and averaged data are recorded in a data file on the personal computer.

The control used to determine whether steady-state had been achieved was manual. The criterion used was that one inlet temperature and the outlet downcomer temperature were monitored during the run and if either varied more than 0.1 °C then the run was considered void.

Temperature Positions on the Tray

Figure 5.3 shows the positioning of the 108 resistance thermometers over the tray area. The aim was to get an even coverage and this has been achieved using a square pitch configuration, with a length of 200 mm. The thermometers measuring the temperature of the inlet water, as it enters the tray, are positioned 50 mm to the rear of the straight chordal inlet downcomer.

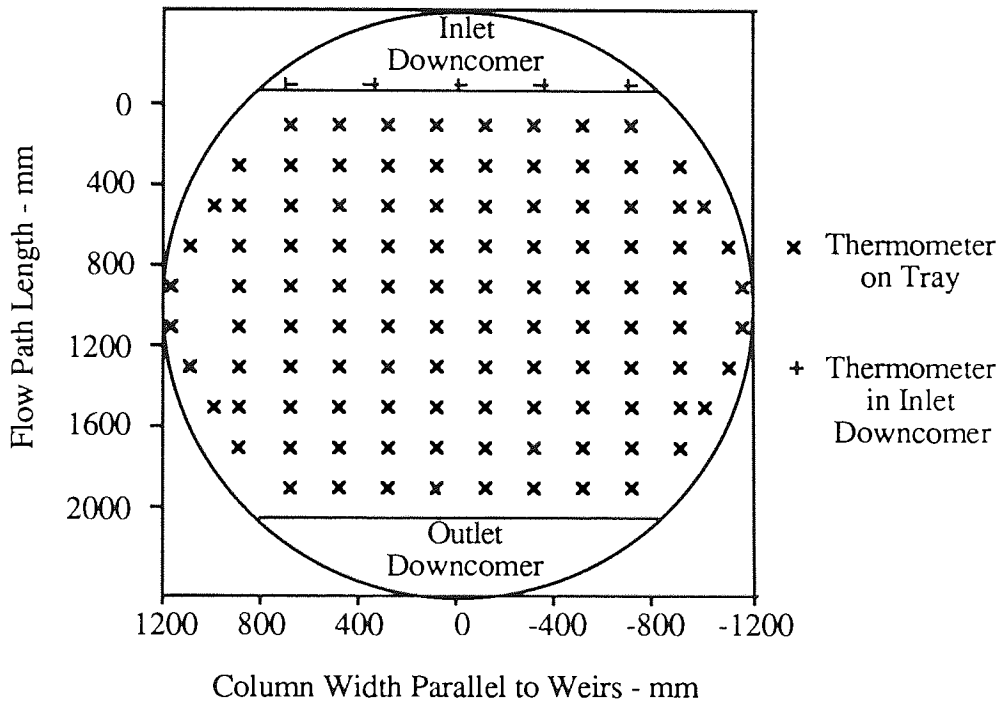

Fig. 5.3 Positions of Thermometers on Test Tray.

Collected Temperature Data

The collected temperature data, from a particular run, are software screened, calibrated, averaged and then stored in a data file. The software screening consists of searching the collected data for rogue data and if found the value in error is made void, by replacement with a default value. Figure 5.4 shows the actual calibrated and averaged temperature data collected from a run and a description of the temperature data file follows.

```
AIR VELOCITY (m/s)      1.5
WEIR LOAD (cm3/cm.s)    100.
DEW POINT (deg c)        8.5

COLUMN DIAMETER (m)     2.440
WEIR LENGTH (m)         1.500
FREE AREA (%)           10.0
OUTLET WEIR HEIGHT (m)   .020
INLET WEIR GAP (m)       .020
```

				99.99	45.25	45.04	45.35	45.33		
		43.90	43.01	36.28	43.15	43.29	42.25	43.28	43.08	
	37.64	42.30	42.75	42.24	42.94	42.64	41.29	41.35	40.05	32.49
34.69	36.64	41.92	41.59	40.83	41.40	40.70	39.89	40.63	40.27	34.19	32.96
31.52	36.63	41.06	39.79	39.64	40.20	39.68	37.82	38.48	38.87	35.84	32.07
30.01	35.73	39.37	38.64	38.28	38.57	37.64	35.90	35.84	37.93	35.44	31.17
30.73	35.21	37.64	37.30	37.39	37.92	36.10	34.31	35.04	36.73	35.17	32.00
30.83	34.35	36.91	36.27	35.46	36.60	35.10	33.39	33.96	35.34	33.72	31.53
30.77	31.47	35.35	34.98	34.95	35.61	99.99	31.58	33.28	33.67	31.47	31.10
	29.72	32.60	34.09	33.64	34.65	32.78	31.14	33.05	31.81	30.68	
		30.68	32.92	32.93	33.62	32.92	30.52	31.43	29.76		
						32.42					
15.47		13.43		12.21							

Fig. 5.4 Example of Collected Temperature Data.

The first eight lines of the file contain the physical geometry of the tray tested (as the only hole size that has been tested is 1 mm this should automatically be assumed), along with the physical flowrates of air and water and the inlet air wet bulb temperature.

The first row of numerals encountered are the inlet water temperature measurements, in ^{o}C, taken just before the water enters onto the tray. The temperature 99.99 ^{o}C is a default temperature and indicates that the measuring device was either defective or giving an erroneous reading.

The next section of multiple temperature value lines show the water temperature measurements over the tray area. The positions of these point values are as found in Figure 5.3.

The single temperature value on line twenty is the water outlet temperature taken at the bottom of the outlet downcomer. The reason for the measurement to be taken at the bottom is to allow for a thorough mixing of all the water streams leaving the active tray at slightly differing temperatures.

The final three temperatures are inlet air dry bulb temperatures.

5.2 Temperature Surface and Contour Processing

The temperature data generated using the water-cooling technique are not easy to interpret due to the large amount of presented data. Although temperatures were measured at known positions over the tray area, it is only possible to determine temperatures at intermediate points by some "theoretical" method. However once intermediary temperature values can be calculated, from the original temperature data, two- or three-dimensional displays can be constructed making interpretation of the collected temperature data much simpler.

5.2.1 The Software Routines

Several software packages are available that can handle the processing and display of general three-dimensional graphics. A recent survey by the Inter University Software Committee's (IUSC) Information Graphics Working Party (IGWP, 1988) concluded that of the graphics software available, the UNIRAS suite of routines was the most powerful; the packages were evaluated over many challenges including interpolation and

presentation of data. The UNIRAS routines were mounted on a mainframe computer and so the temperature data files were uploaded, from the personal computer, to be processed.

5.2.2 Interpolation or Pre-Processing of Data

All mapping display routines use gridded representations of surfaces as these are much more adaptable to picture processing. Since many practical situations only allow the collection of irregularly spaced data, some method of pre-processing of the data must be undertaken to produce regular gridded data. The routine selected interpolates from a set of irregularly distributed data points to a regular grid of points, with the objective of fitting a smooth surface between the control, or measured, point values.

The routine considers the control point values to be accurate samples and the surface must pass through these points. The gridding operation is performed using the following operations,

1. Interpolation of data to grid node locations with weighted average interpolation.
2. Computation of surface slopes using quadratic interpolation.
3. Final smoothing of surface by distance weighting method.

Weighted Average Interpolation

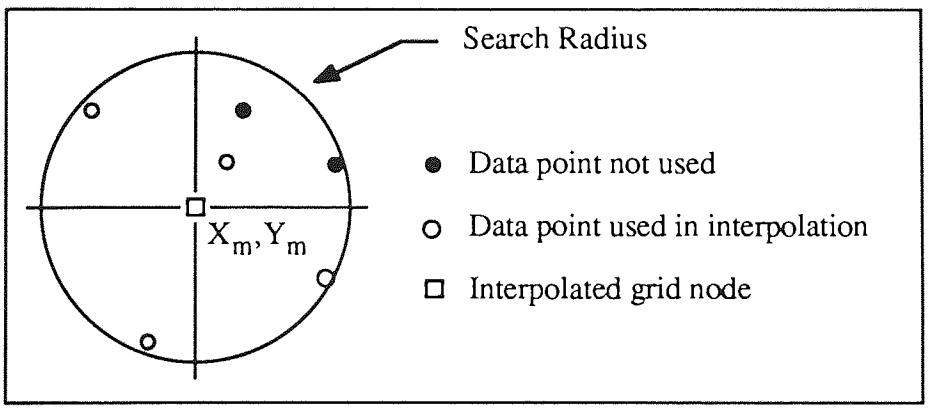

Fig. 5.5 The Weighted Average Interpolation and the Data Points Selected.

The closest data point in each quadrant is selected. If a data point is found in one or more of the quadrants a weighted average interpolation is performed. The distance from the grid node to the closest data point, RAD1, is saved for the next quadratic interpolation step.

The first step in the weighted average interpolation is to calculate the squared differences from the grid node to the data points found,

$$D_i = \left[\frac{X_i - X_0}{DX}\right]^2 + \left[\frac{Y_i - Y_0}{DY}\right]^2 \quad \text{for } i = 1,\ldots,N \tag{5.1}$$

where N is the number of data points, (X_0,Y_0) are the coordinates of the grid node, (X_i,Y_i) for i = 1,...,N are the coordinates of the data points and DX and DY are the grid spacings in the respective X and Y directions.

In the second step the routine computes a weighted average value, ZEST, for each grid node.

$$ZEST_{X_0Y_0} = \frac{\Sigma\,(W_i Z_i)}{\Sigma\, W_i} \tag{5.2}$$

where $W_i = 1/D_i$ for i = 1, ..., N and Z_i for i = 1, ..., N are the height values of the data points.

Quadratic Interpolation

The quality of the surface fit is improved by the quadratic interpolation. At each grid node the slope components are calculated from the closest data point (RAD1, calculated from the previous step) and those found RADQ*RAD1 units further away, where RADQ is factor equal to 1.25. Quadratic interpolations are performed for the slope components. This process tends to continue surface slopes, which are supported by data points, into void data areas, see Figure 5.6.

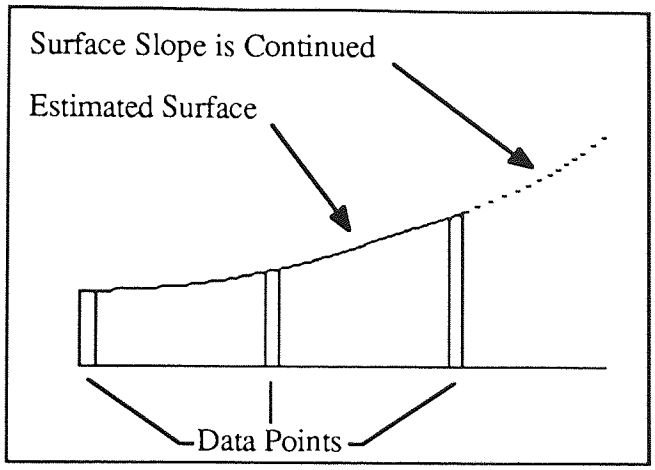

Fig. 5.6 The Surface Slope is Continued into Void Data.

If RAD1 is the distance to the closest data point, then RAD2 is RADQ*RAD1 units away from the grid node. By letting Z_1 and Z_2 be the average values of data points at grid distance RAD1 and RAD2 from the grid node, $Z_{x,y}$, is the estimated value at the grid node (X,Y).

$$Z_{int} = \frac{RAD2^2 Z_1 - RAD1^2 Z_2}{RAD2^2 - RAD1^2} \tag{5.3}$$

$$Z_{x,y}^{new} = Z_{x,y}^{old} + (Z_{int} - Z_{x,y}^{old}) \times SFACT \tag{5.4}$$

where SFACT is a relaxation factor of default value 0.15. The value of $Z_{x,y}$ is iterated eight times for every grid point, and $Z_{x,y}$ will thus change slightly for each loop, thereby obtaining a smooth surface.

The quadratic interpolation includes the effect of slope in interpolating a value at the grid point. Without the quadratic interpolation the interpolated surface would have zero gradient at every grid point.

Distance Weighting Method

The final step, a smoothing operation, is performed by a two-dimensional filter applied to the grid. The filter is designed to reduce the curvature in areas of sparse data while maintaining the quality of the interpolated results around the input data points. If high levels of smoothing are required then the accuracy of the data points are slightly reduced. Due to this affect the distance weighting method for final smoothing of the surface was not used.

5.2.3 Graphical Representation Of Data

The data has now been transformed into a regular gridded data set, which can be displayed in a number of formats, each highlighting different aspects of the data.

For the presentation of the temperature data, two formats were thought appropriate, one a two-dimensional temperature contour plot and the other a three-dimensional surface temperature plot. Figures 5.7 and 5.8 present the two different styles using the temperature data contained in Figure 5.4. The Fortran 77 coding used to generate the temperature contours and surface is contained in Appendix 2.

The three-dimensional plot clearly shows temperature changes over the tray area at the cost of not knowing precise point temperatures, whereas the two-dimensional contour plot gives a better knowledge of point temperatures at the expense of temperature gradient clarity, but the temperature gradients on the contour plot are demonstrated by the space between adjacent isotherms, as the isolines represent equal temperature increments.

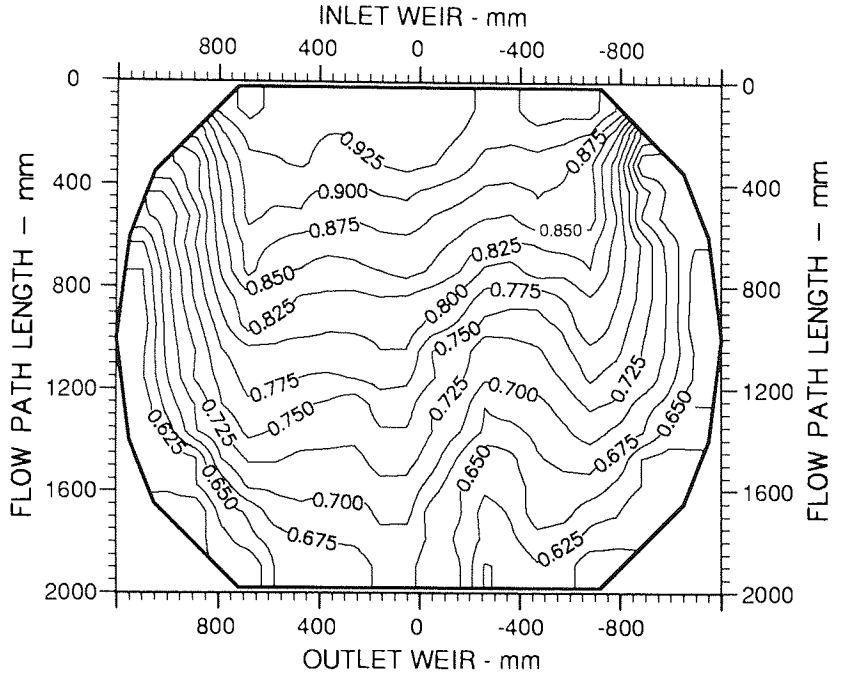

Fig. 5.7 Two-Dimensional Temperature Contour Plot.

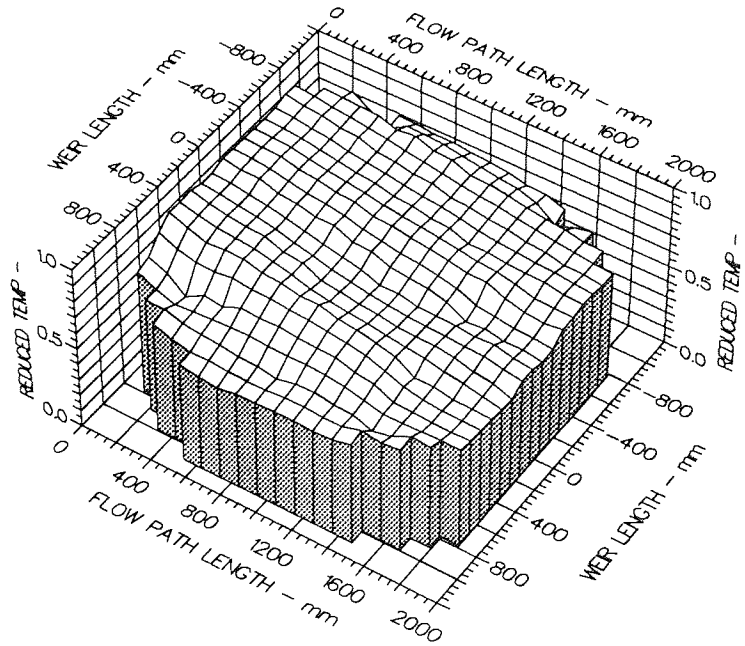

Fig. 5.8 Three-Dimensional Surface Temperature Plot.

5.3 Commissioning

The 2.44 m diameter air-water simulator was commissioned in stages during the construction period. The equipment was evaluated for performance, and procedures for the safe operation of the facility were written.

5.3.1 Water-Cooling Experimental Procedure

The procedure for the safe operation of the test facility while carrying out water cooling experiments is presented for start-up, normal operation and shut-down.

Start-Up

1. Switch on the main electricity isolator and open the manual gas valves to the process heaters.
2. Start the circulation pump, in the primary heating circuit, and the flue dilution fan.
3. Start the main water pump and circulate the water through the double heat exchanger and back to the water holding tanks.
4. Switch on the electrical supply to the gas shut-off valve.
5. Start one or both of the process heaters.
6. Open steam valve.
7. When the water, in the holding tanks, approaches 40 ^{o}C start the air fan and set the desired air flowrate.
8. Once the water reaches 45 ^{o}C, set the desired water flowrate to the test column, then make any small adjustments to the air flowrate.
9. Manual control of the steam and process heaters until an equilibrium is reached.
10. After about tem minutes of steady operation, initiate temperature data collection.

Normal Operation

11. Set new flowrates of air and water, going back to instruction 8.

Shut-Down

12. After the last temperature data collection, close the steam valve and switch off the process heaters, leaving the simulator in operation.

13. Switch off all electrical equipment apart from the two water pumps. and close the manual gas valves.

14. When the bulk water temperature in the holding tanks has reached about 20 °C and both sections of the heat exchanger are cool, the water pumps can be stopped.

15. Five minutes after stopping the water pumps the air fan can be closed down.

The commissioning period highlighted that the tray support structure was out of level and that the temperature probes, measuring the water temperature, were being influenced by the passing air.

5.3.2 Levelness of Tray

The first tests to be performed on the newly-constructed column concerned the flow of water only. A dye tracer was injected along the inlet weir and its progress was followed as it passed from the inlet to the outlet of the tray. The initial results showed that the water had a tendency to flow to the outer left quadrant of the tray. The cause of the flow distortion was thought to be either the liquid distribution system or the tray levelness itself.

On investigating the back-up in the inlet downcomer, the level, although not constant, was symmetrical about the centreline of the tray and so the liquid distribution system was discounted as the cause of the flow non-uniformity. The tray itself was then tested for levelness using an engineering level, a normal spirit level being unsuitable for the task. The level detected that the left half of the tray was lower than the right by about 5 mm, and that the tray support structure was slightly twisted. Spacers were placed under the left half of the tray until the transverse level, across the 2.44 m diameter, was within one or 2 mm. The spacers corrected the non-uniformity of the water flow, to provide a better symmetry about the tray centreline.

5.3.3 Temperature Probe Modification

The temperature data collection system operated satisfactorily and the temperatures collected were symmetrical about the centreline of the tray. However, when the temperature data was processed some of the calculated point efficiencies were in excess of unity. The calculation involved the use of measured flowrates along with the measured temperature values, and so the error had to be traced. The identified source of the error were the temperatures measured over the tray area. The air passing through the water was having a cooling effect on the bare temperature probes thus reducing the measured temperatures. As the probes were to measure the water-only temperature, and not the biphase temperature, a modification was made to them, consisting of a shroud surrounding each temperature measuring probe, which guarantees that the water-only temperature was "seen" by the probe, see Figure 5.2.

CHAPTER 6

6. WATER-ONLY STUDIES

6.1 Introduction

The air-water mixture on a sieve tray is extremely chaotic and the flow pattern over the tray area is complex due to the geometry of even a simple tray. To simplify the situation, water-only studies were conducted, in which the two-phase interaction was eliminated, thereby revealing the effect of the tray geometry only on the developed flow pattern. Also, by studying the flow of water only, base cases were generated to which the flow of biphase could be compared, and the effect of the air flow determined.

The objectives of the water-only studies were to determine what flow patterns were developed over the tray area and also to determine the effect, on the flow pattern, of changes in the water flowrate, inlet gap and outlet weir.

6.2 Experimental Procedure

Different water flow regimes were created over the tray geometry by varying the water flowrate, inlet gap and outlet weir. After steady state was achieved, a pulse of dye (potassium permanganate solution) was released along the length of the inlet weir using a solenoid-controlled injection system. The progress of the dye, as it crossed the tray from the inlet weir to the outlet weir, was monitored by a video camera mounted 4.5 m above the tray.

The water-only test tray had the same geometry as that of a simple sieve tray with straight chordal weirs. The diameter of the tray section was 2.44 m and the weir lengths were 1.50 m, giving a weir length to diameter ratio of about 60%. The water flow was controlled onto the tray area by virtue of a gap under the inlet downcomer face and off it by the presence of an outlet weir. The study was performed for inlet gaps of 10, 20 and 50 mm and outlet weirs of 0, 10, 20 and 50 mm. The water flowrate, expressed as a weir loading, was varied between 2.5×10^{-3} and 3.0×10^{-2} m^3/m s.

6.3 Results and Discussion

Many dye tracer runs were videoed and studied, the results are presented in such a way as to show the individual effects of changing the water flowrate, inlet gap and outlet weir. The exact conditions at which changes occur are discussed later due to the inter-dependence of the three parameters being investigated.

6.3.1 Effect of the Water Flowrate

Changes in the water flowrate caused different flow patterns to develop over the tray area. At the low water flowrate, 2.5×10^{-3} m^3/m s, virtually all the flow was in the forward direction, confined only by the physical walls of the tray, but at comparatively higher water flowrates the bulk flow separated from the physical walls of the tray and reverse flow was observed. The forward flowing water was confined by new flow boundaries, with circulating regions filling the areas between the new flow boundaries and the tray walls.

The circulating regions emanated from the edges of the inlet downcomer and gradually increased in size with increasing water flowrate to a maximum when the circulating region extended from the edge of the inlet downcomer to the edge of the outlet weir. Figures 6.1 and 6.2 each present a series of still photographs taken from the video recording of the water-only dye tracer studies. The weir arrangement for each of the figures is the same with a 10 mm inlet gap and a 10 mm outlet weir, but the water weir load is changed, 5.0×10^{-3} m^3/m s in Figure 6.1 and 1.0×10^{-2} m^3/m s in Figure 6.2.

Together these figures show that a change in the water flowrate, keeping the inlet gap and outlet weir constant, can have a dramatic effect on the developed flow pattern. The flow boundaries can be determined from the video recordings, and Figures 6.3a to 6.3d present a sequence of the flow patterns as the water flowrate is increased. The percentage of the total tray area taken up by the circulating regions is also expressed below each figure.

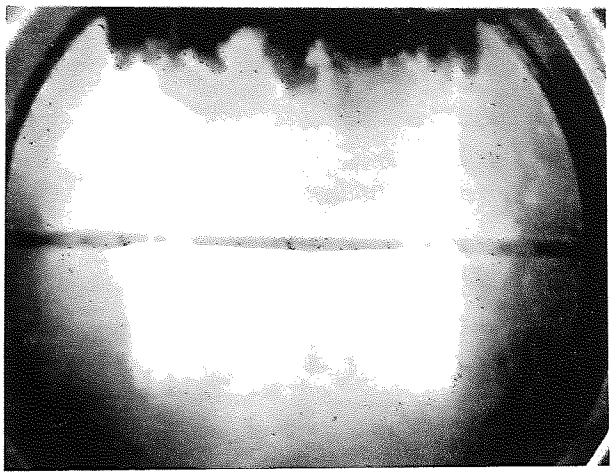

1 Second

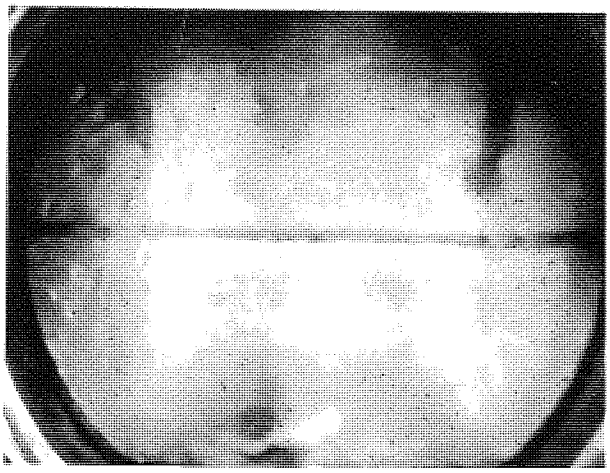

2 Seconds

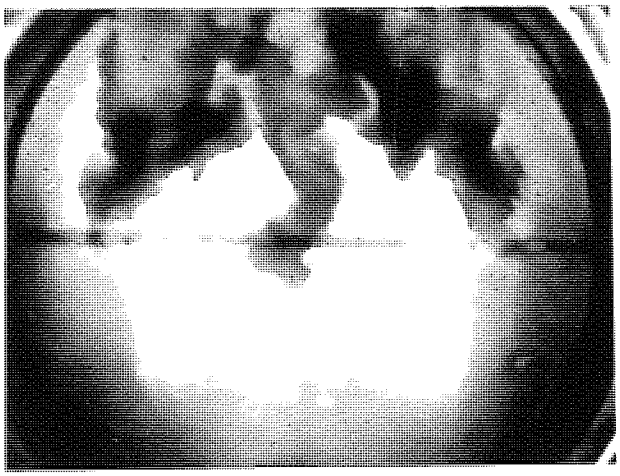

4 Seconds

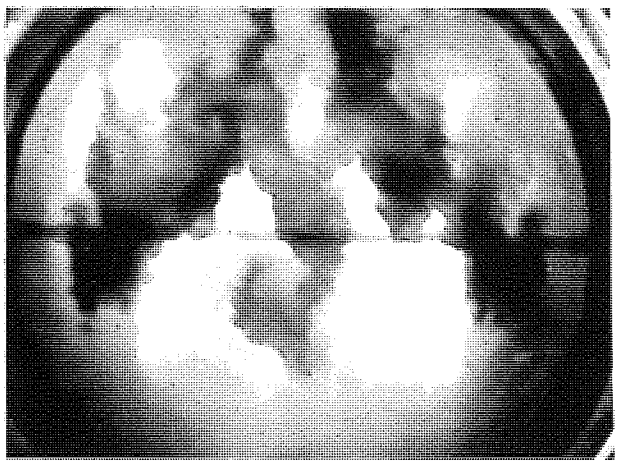

6 Seconds

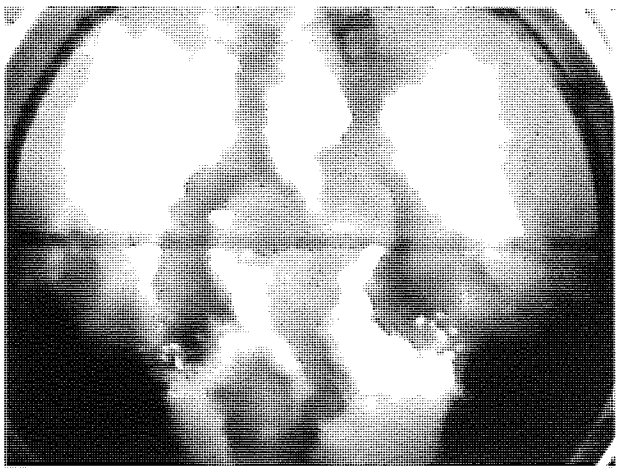

10 Seconds

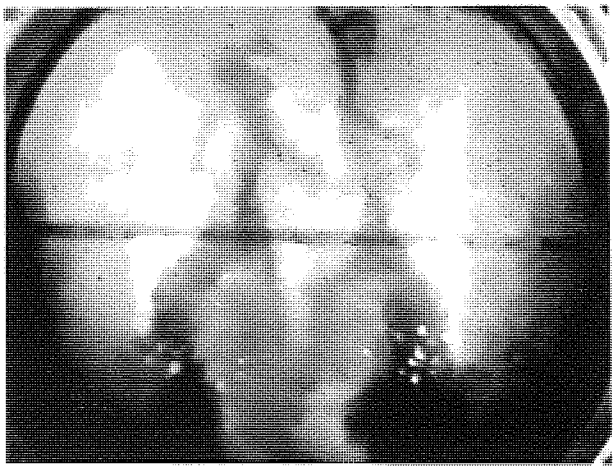

14 Seconds

Fig. 6.1 Dye Traces for Water Flume Weir Loading of 50 cm^3/cm s.

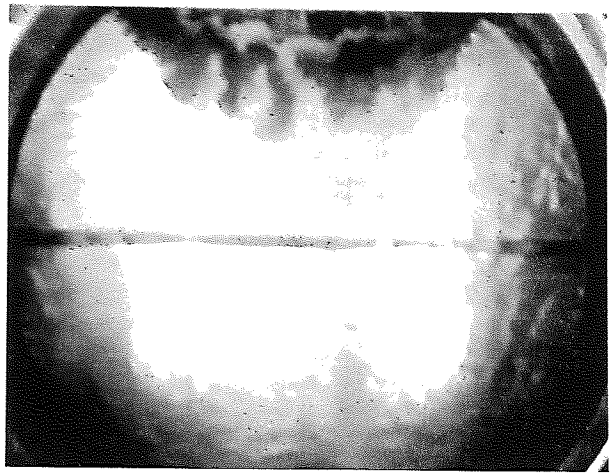

1 Second

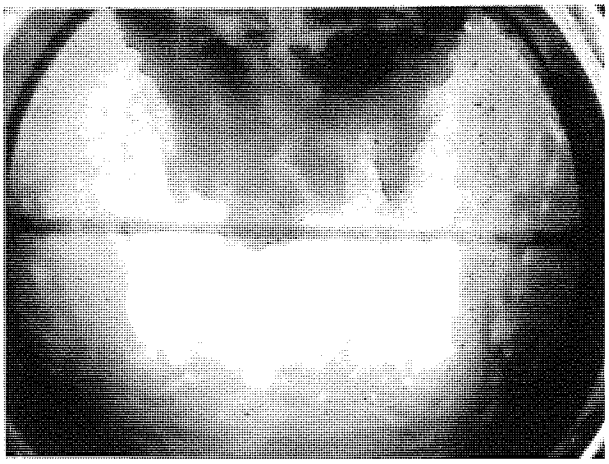

2 Seconds

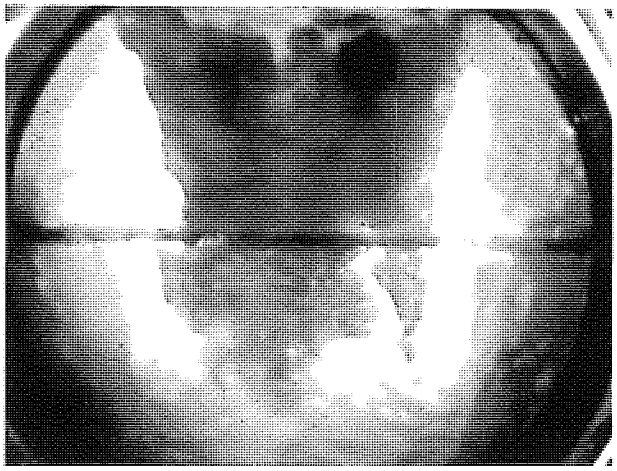

3 Seconds

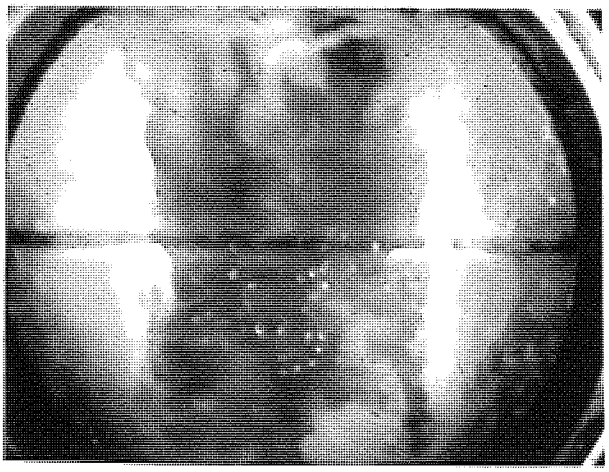

4 Seconds

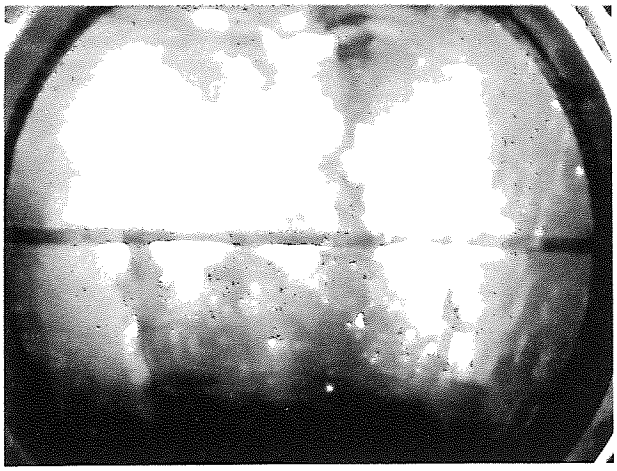

6 Seconds

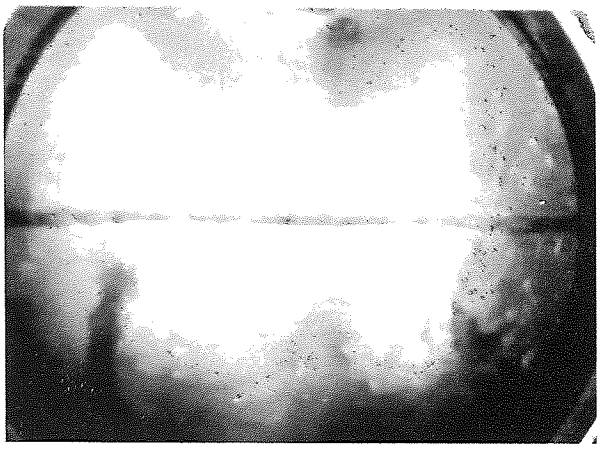

8 Seconds

Fig. 6.2 Dye Traces for Water Flume Weir Loading of 100 cm^3/cm s.

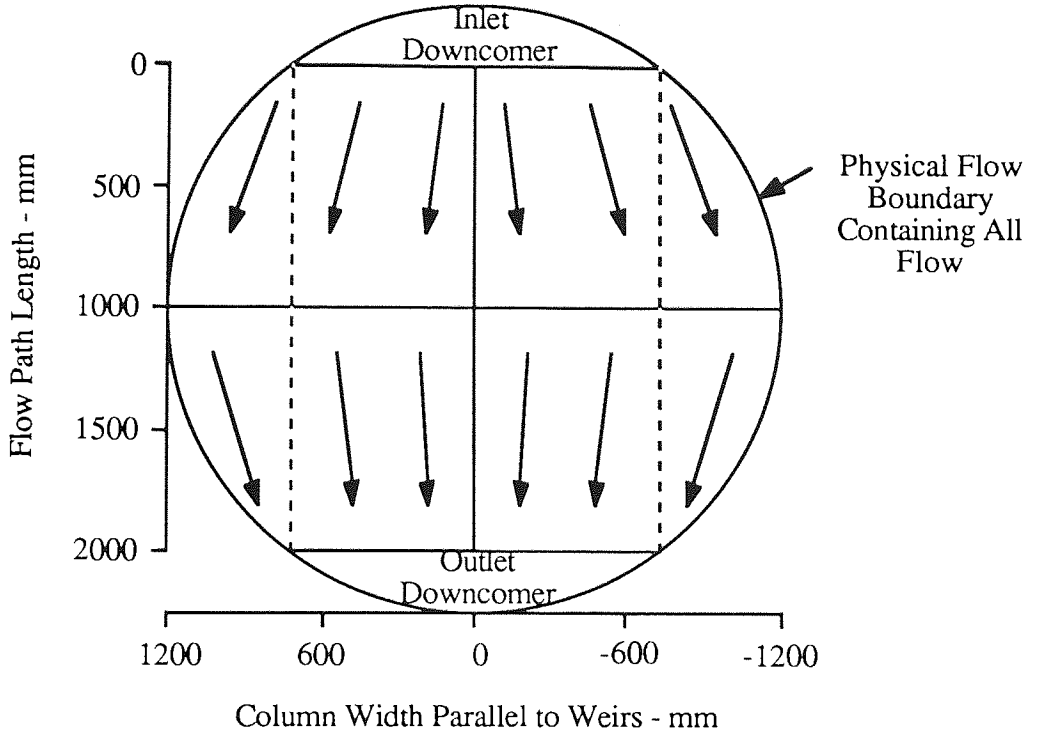

Fig. 6.3a Water-Only Flow Pattern - 0% Circulation.

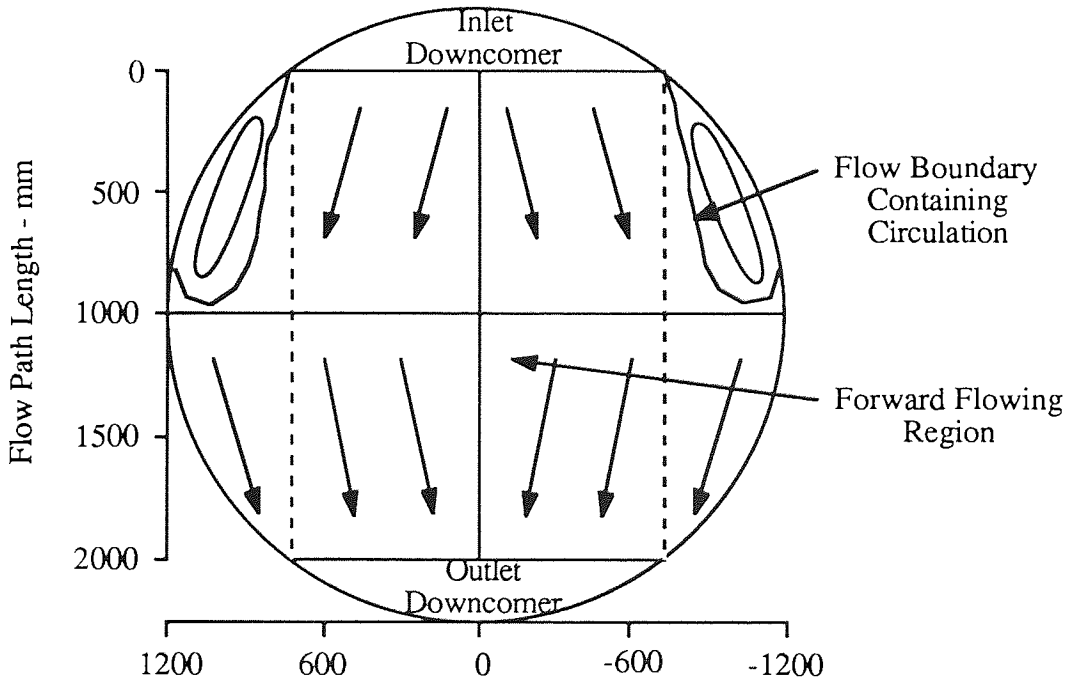

Fig. 6.3b Water-Only Flow Pattern - 10% Circulation.

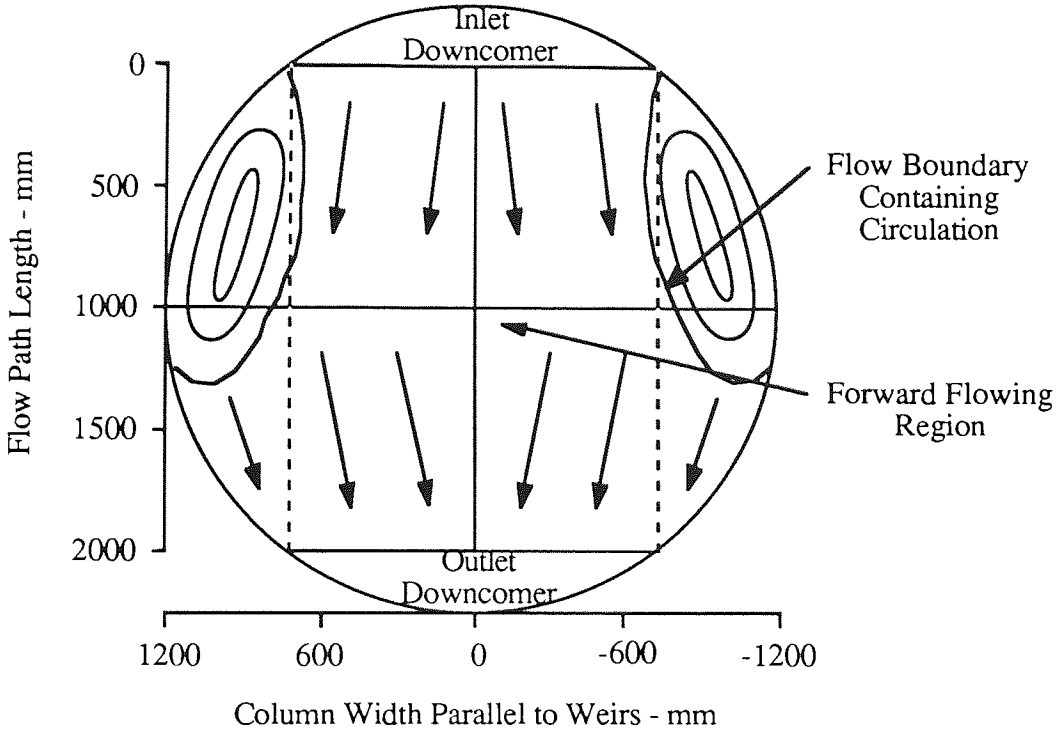

Fig. 6.3c Water-Only Flow Pattern - 20% Circulation.

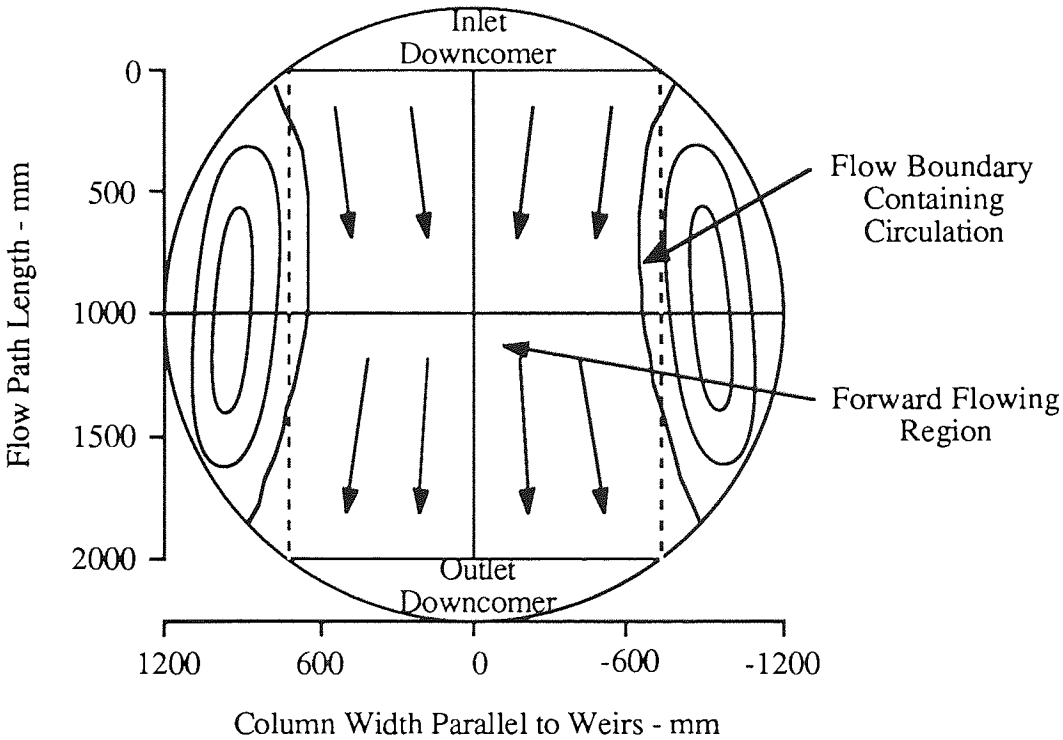

Fig. 6.3d Water-Only Flow Pattern - 30% Circulation.

0% Circulation

The 0% circulation flow pattern is presented in Figure 6.3a. The water surface was very calm and no disturbances were visible. The water, on entering the tray, spread out to take up the full chordal width throughout its journey in the inlet half of the tray. The leading edge of the dye pulse shows that the forward component of the water velocity in both halves of the tray was the same, but dye streaks, similar to those in Figure 6.1, indicate that there is some variation in this speed, randomly distributed across the flow width.

In the outlet half of the tray the water flow contracted with the tray geometry and flowed over the outlet weir. The speed of the flow at the outlet weir seemed to be greater at the edges of the weir than in the centre, but no noticeable difference in the crest over the weir was observed. Dye streaks, connected to the outlet weir stretched into the inlet half of the tray between the weirs. No reverse flow was exhibited.

10% Circulation

The 10% circulation flow pattern is presented in Figure 6.3b, the still photographs in Figure 6.1 revealing a similar sized circulation. The water surface contained some surface disturbances, but generally the flow was calm. The water, on entering the tray from the inlet gap moved in a forward direction only and did not immediately spread out to take up the tray width in the inlet half of the tray. When the leading edge of the dye pulse reached the centre of the tray, the dye started to spread to the sides to take up the tray width. Reverse flow was then observed in the inlet half of the tray adjacent to the tray walls. The flow area occupied by the circulating region was of the order of 10% of the total tray area.

The flow in the outlet half of the tray was similar to that of the 0% circulation flow pattern.

20% Circulation

The 20% circulation flow pattern is presented in Figure 6.3c. The water surface contained even more disturbances, but the flow could still be described as calm. The water flowed straight across towards the outlet chordal weir, without penetrating the the side zones at all. In the outlet half of the tray a mixing zone was observed where all the water streams entering were thoroughly combined. This zone occupied the area bounded by the outlet weir, the tray walls and a chord 0.5 m from, and parallel to, the outlet weir and was probably caused by the constriction of flow around the outlet weir. The forward flowing

dye entered the mixing zone and visually the dye concentration in the zone became uniform; the dye stalling before spreading out over the tray width and leaving the mixing zone. The exit flows from the mixing zone were streams over the outlet weir and reverse flow adjacent to the tray walls. The reverse flow carried water from the thoroughly mixed zone back to the edge of the inlet weir.

The crest of liquid over the outlet weir was non-uniform with a build up of water at the sides of the weir. The area occupied by the circulating zones was about 20% of the total tray area, and the dye was visible in the circulating regions for several revolutions, showing that the flow boundaries between the centre and side regions were a well formed feature of the flow pattern.

30% Circulation

The 30% circulation flow pattern is presented in Figure 6.3d, the still photographs in Figure 6.2 revealing a similarly sized circulation. The water flowed straight across towards the outlet chordal weir, without penetrating the the side zones at all, but the mixing zone adjacent to the outlet weir was reduced in size, by a bounding chord 0.3 m from, and parallel to, the outlet weir. The circulating regions were both large in size and strong in effect, the dye being visible in the circulating regions for about six complete revolutions showing that the flow boundaries between the centre and size regions were a strong feature of the flow pattern. The size of the circulating regions was 30% of the total tray area, and thus they expanded into the centre portion of the tray causing a *vena contracta* -type effect on the bulk forward flowing water.

6.3.2 Effect of the Inlet Gap

When the inlet gap was set at 10 mm, all the four aforementioned flow pattern stages were observed. On increasing the inlet gap to 20 mm, and subsequently to 50 mm, the flow patterns with circulations of 10% and 20% were replaced by an alternative flow pattern where the circulating regions were not adjacent to the tray walls. The alternative flow pattern is presented in Figure 6.4.

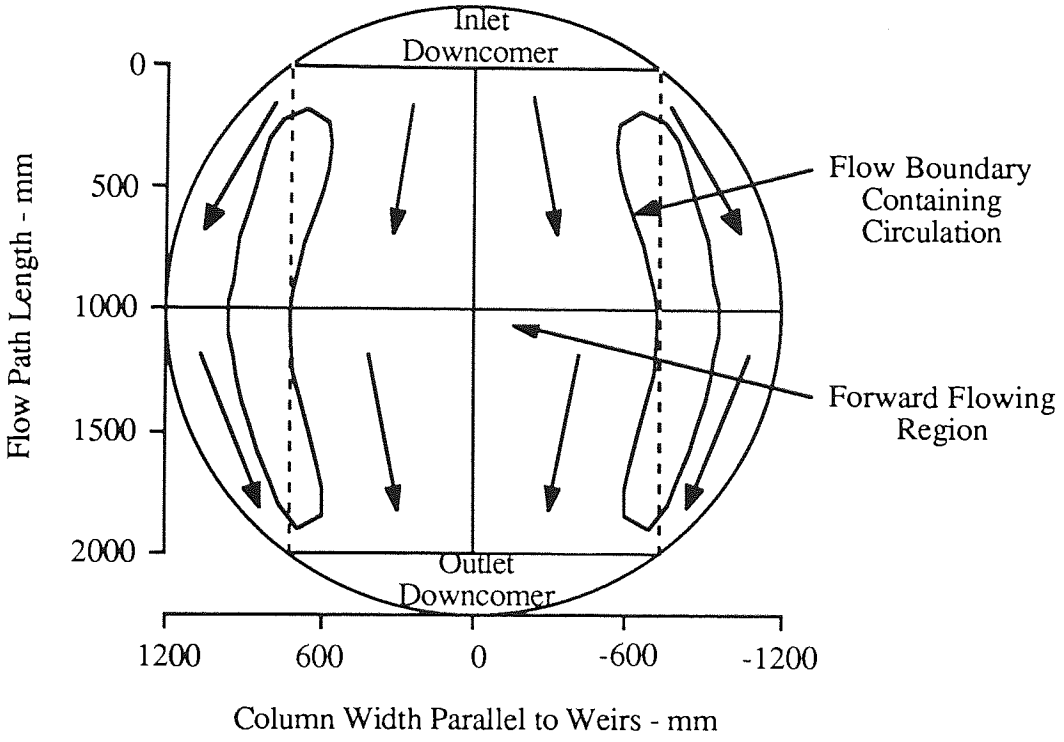

Fig. 6.4 Alternative Water-Only Flow Pattern - 10% and 20% Circulations.

Alternative 10% and 20% Circulations

The alternative circulation flow pattern, although looking very different from the 10% and 20% circulation flow patterns, was formed in a similar way. The change in flow pattern was due to two water streams, one at either side of the inlet weir, which flowed around the tray walls. These new flows prevented any circulation regions from attaching to the tray walls, and in effect caused the circulating regions to find a more stable position. The size of the circulation regions did change with increasing flowrate, but only in the width dimension. The area occupied by these alternative circulating regions was in the order of 10% to 20% of the total tray area.

6.3.3 Effect of the Outlet Weir

The outlet weir did have an effect on the flow pattern which caused the developed circulating regions to become fuller with increasing outlet weir. Figures 6.5a to 6.5c show the effect of increasing the outlet weir height on the flow pattern, while keeping the flowrate of water at 5.0×10^{-3} m^3/m s and the inlet gap at 10 mm.

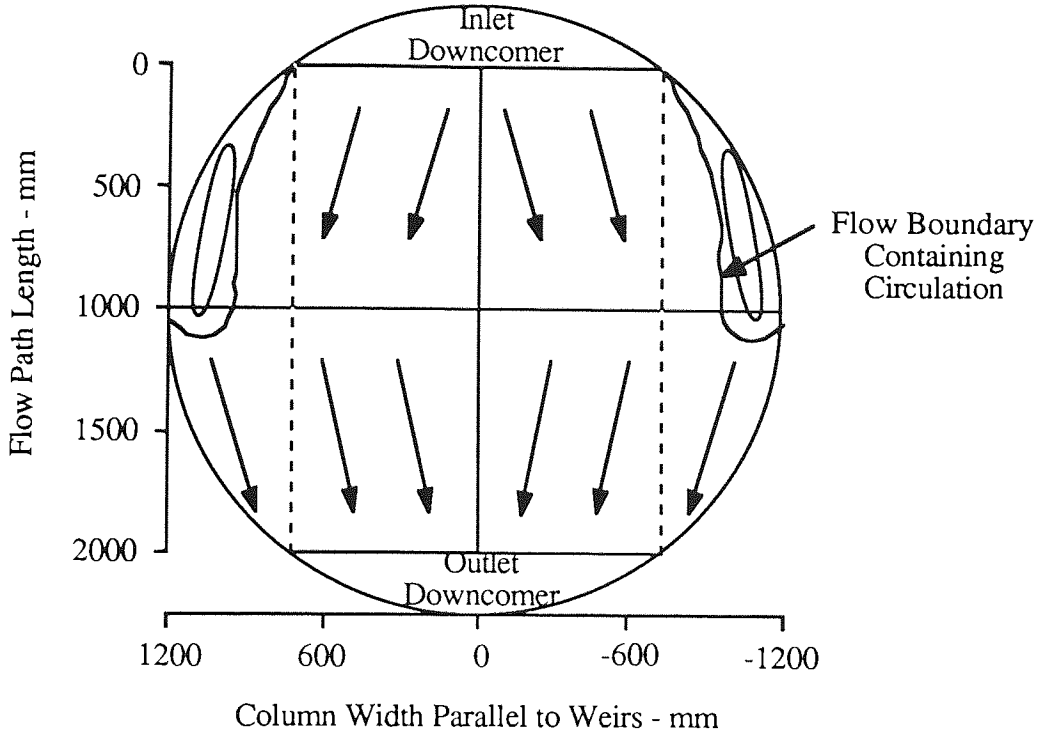

Fig. 6.5a Water-Only Flow Pattern for 10 mm Outlet Weir.

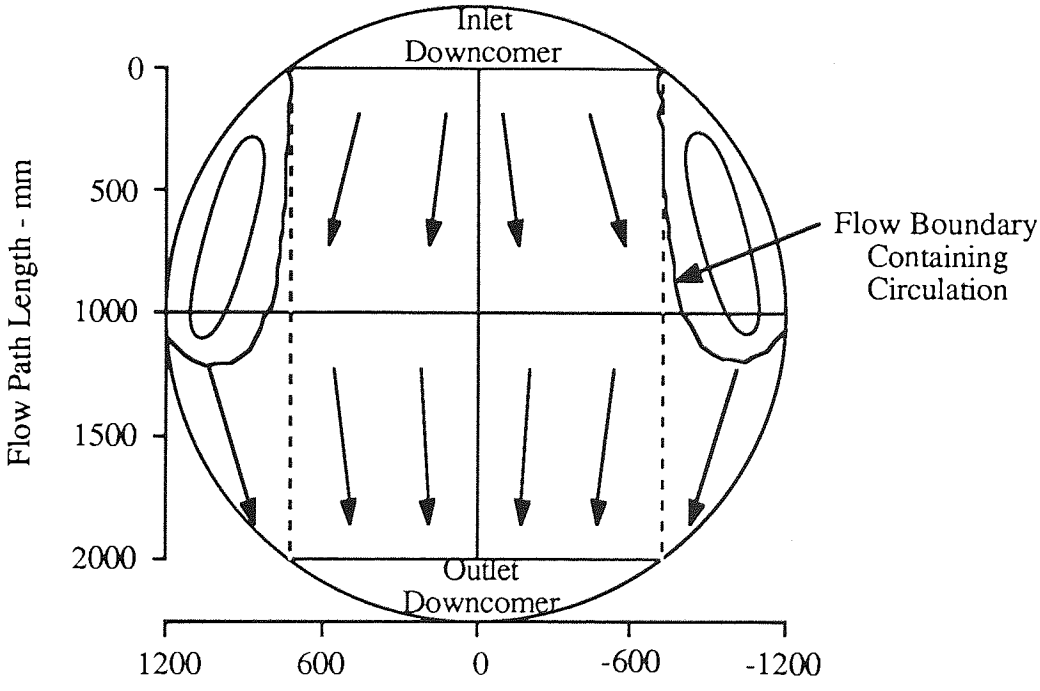

Fig. 6.5b Water-Only Flow Pattern for 20 mm Outlet Weir.

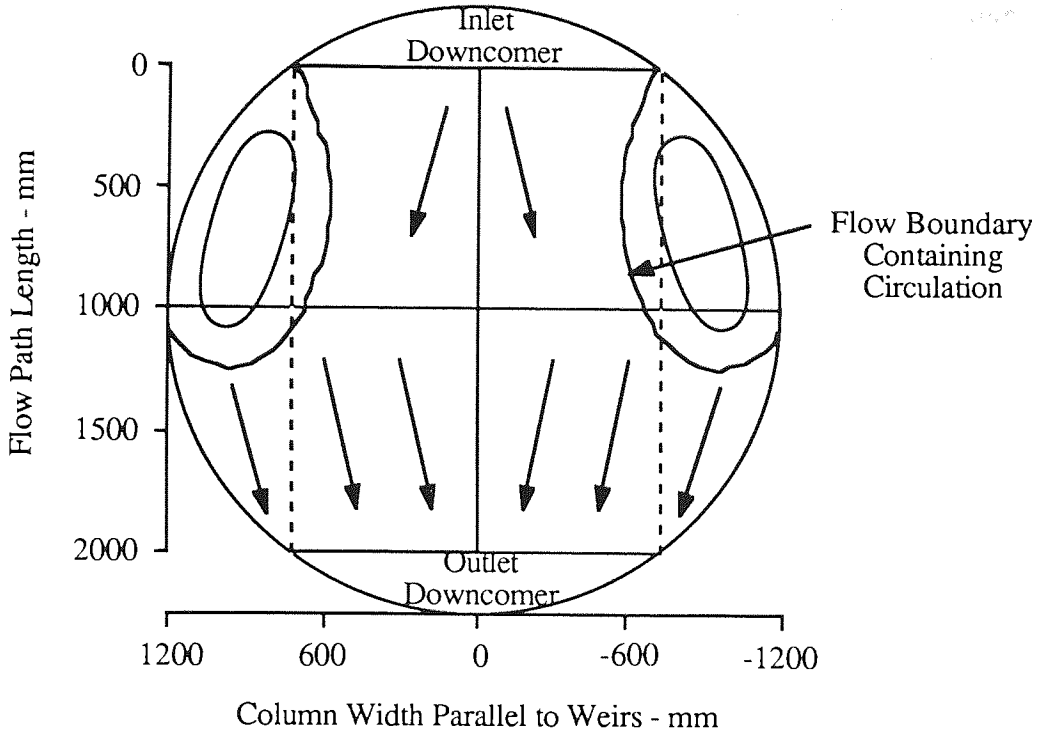

Fig. 6.5c Water-Only Flow Pattern for 50 mm Outlet Weir.

6.3.4 Effect of the Weir Loading on the Degree of Circulation

The results discussed above refer to circulation regions adjacent to the tray walls, and that these zones are large or small depending on the water flowrate, inlet gap and outlet weir. The measure of the percentage of the tray area circulating was found for several discrete values of the water weir load and is presented in Figure 6.6.

Figure 6.6 shows the approximate size of the observed circulation zones against the water weir load for all the combinations of inlet gap (10, 20 and 50 mm) and outlet weir (0, 10, 20 and 50 mm). Due to the figure being constructed from discrete values for the water weir loading, the critical weir load at which the circulation is initiated is not known precisely, but its value is known to lie between 0.0 and 2.5×10^{-3} m^3/m s.

From Figure 6.6, it can be seen that the range of weir loads at which a particular tray area is circulating is narrow at 2.5×10^{-3} m^3/m s. The maximum degree of circulation is approximately 30% of the tray area, and any further increase in the water flowrate only serves to define the flow boundary better and to increase the rotational velocity of the formed eddy. Similarly the segmental side regions of a 60% weir to diameter ratio tray, expressed as a percentage of the tray area also approximates to 30% (31.8% to be

precise). This limiting case of 30% of the tray area circulating would seem to agree with the Stagnant Regions Model proposed by Porter et al. (1972), which was also based on observations of water-only flow. The phenomena responsible for these circulations or eddies is that of flow separation, which is well documented in the open literature (Chow, 1959; Henderson, 1956; French, 1986).

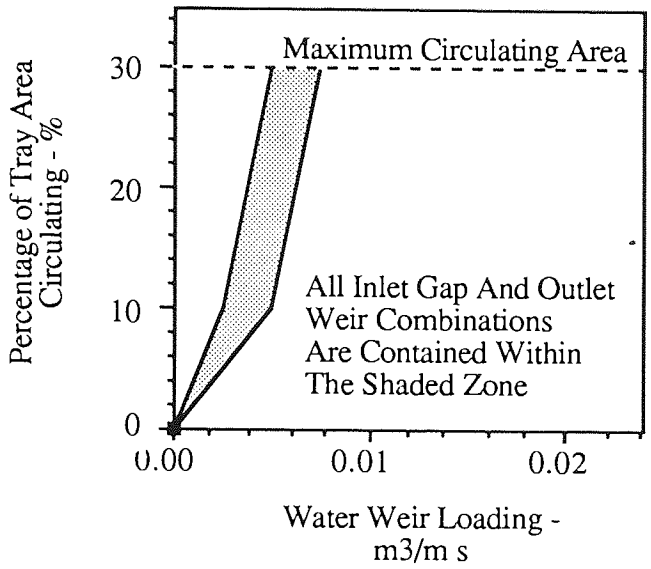

Fig. 6.6 Degree of Circulation for Water Only.

6.3.5 Separation of Flow

When surfaces or flow boundaries change greatly over a short distance, such as in a rapidly diverging channel, the pressure of the fluid varies in the direction of flow and the behaviour of the fluid may be greatly affected, see Figure 6.7.

As the fluid flows along the flat surface the pressure gradient in the x-direction is, as expected, negative and the net pressure force on an element in the boundary layer is in the forward direction. Such a pressure gradient is said to be favourable and it counteracts to some extent the "slowing down" effect of the boundary on the fluid. However, as the physical flow boundary moves away from the direction of flow, the velocity must decrease. (The Bernoulli equation requires that as the velocity term decreases the pressure term must increase accordingly, if all the other terms constant are kept constant.) Thus the net pressure force on an element in the boundary layer opposes the forward flow. Although the pressure gradient has practically the same value throughout the cross-section of the boundary layer, its most significant effect is on the fluid closest to the physical

flow boundary. This is because the fluid there has less momentum and so when its momentum is reduced still more by the adverse pressure gradient, the fluid near the physical flow boundary is soon brought to a standstill. The velocity gradient at the physical flow boundary is then zero, which becomes the point of separation.

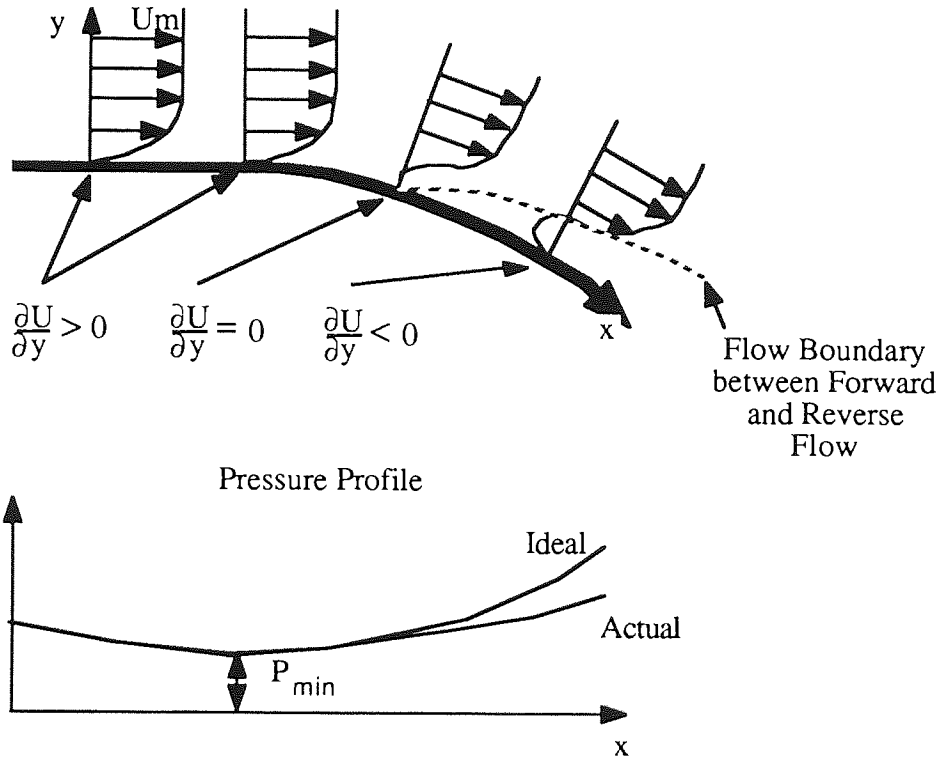

Fig. 6.7 Onset of Separation.

Separation is caused by the reduction of the velocity in the boundary layer, combined with an adverse pressure gradient; and it can only take place when an adverse pressure gradient exists. The line of zero velocity dividing the forward and reverse flows leaves the physical flow boundary at the separation point, and is known as the separation streamline. The result of the reverse flow is the formation of an eddy in which energy is dissipated leaving the pressure downstream similar to that at the point of separation. Separation having occurred, the fluid flow is guided by the separation streamline or flow boundary as opposed to the physical flow boundary.

6.3.6 General Discussion

From the discussion in the previous paragraph, it appears that circulation zones can only exist if an adverse pressure gradient exists. The pressure gradient is caused as a result of the difference between the water velocity through the inlet gap and the water immediately

on the tray area. If the hold-up on the tray is large, the flow cross-section is greater than that of the inlet gap multiplied by the weir length and so the entering water must slow down thereby causing an adverse pressure gradient and the possibility of separation. Therefore any factor which increases the depth of water, or flow, on the tray has a chance of causing separation. From the arguments set out above, the likelihood of separation should be enhanced by:

(i) Increasing the the water flowrate.

(ii) Increasing the outlet weir.

(iii) Decreasing the inlet gap.

However as shown in Figure 6.6, these last two effects are hardly noticeable as circulation occurred for all settings of the inlet gap and outlet weir.

CHAPTER 7

7. A NEW EXPERIMENTAL TECHNIQUE TO DETERMINE THE FLOW DIRECTION OF A BUBBLY MIXTURE ON A SIEVE TRAY

7.1 Introduction

The original objective of flow pattern investigation on distillation trays was to determine experimentally the liquid velocity profile over the tray area. Once the liquid velocity profile is known, the relationship between the point efficiency and tray efficiency can be determined.

Many workers have carried out such an investigation into the liquid flow pattern, the results being presented in the form of residence time distributions, lines of constant concentration and lines of constant temperature, depending on the technique employed. What many of the authors fail to do is to separate the effects of the liquid velocity and the intense mixing on the tray. The froth velocity has seldom been addressed alone, but a recent thesis by Bultitude (1989) goes some way to making such a direct measurement.

Of the experimental techniques described in the literature review, the coloured dye and camera must be the most visual method of viewing the flow interactions on a sieve tray. However difficulties arise due to the clarity of the dye in the two-phase mixture and so another investigative method is necessary to overcome this.

7.2 A Technique Using Flow Pointers

A new technique of using directional flow pointers has been devised for investigating the liquid flow direction of a bubbly mixture on a sieve tray. This new method is based on the same principle as a weather vane, and leads to observation of the directional vector of the biphase flow at a single point on the tray. Several flow pointers are sited over the tray area, and are allowed to move freely with the flow into stable positions. The position that each pointer stabilises in, is the direction of liquid flow at the fulcrum of the respective

flow pointer. As the flow pointers are viewed from above an indicator has to be incorporated into the design so that the pointer direction can be seen and the patterns produced by them recorded.

7.2.1 The Design of a Flow Pointer

The nature of a flow pointer is very simple and thus the design could also be kept simple, as shown in Figure 7.1.

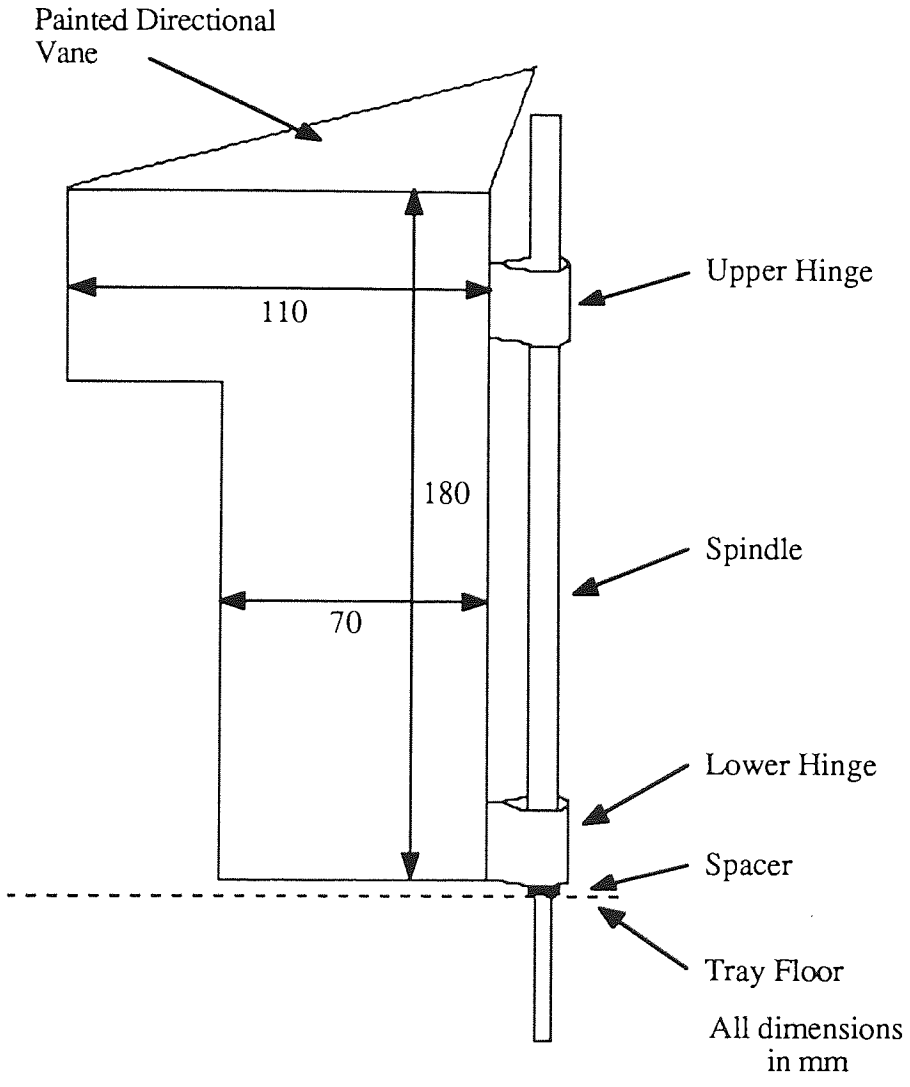

Fig. 7.1 Sketch of a Flow Pointer.

A thin aluminium sheet was cut to form the flow pointer, the top being turned over to provide the flow indicator. The hinges for the pointer were simply a loop of the aluminium sheet wrapped around an aluminium bar, the fitting was very loose allowing

free rotational movement. Under the bottom hinge a spacer provided enough lift for the pointer to avoid making contact with the tray should any tray deflection occurr. The friction between the spacer and the pointer was minimal and was easily overcome by the passage of biphase; this was mainly due to the small weight of the aluminium pointer, about 60g. The main body of the pointer was cut away to allow a more precise direction of flow to be assigned to the fulcrum or spindle.

7.3 Experimental Procedure

Thirty-two flow pointers were positioned over the 2.44 m diameter sieve tray as shown in Figure 7.2. The tray geometry was not changed from that of the tray used for the water-only studies with the exception that a sieve plate replaced the unperforated aluminium sheet. The sieve plate was made from 1 mm aluminium sheet, punched with sharp faced holes, 1 mm in diameter, to provide a 10% free area.

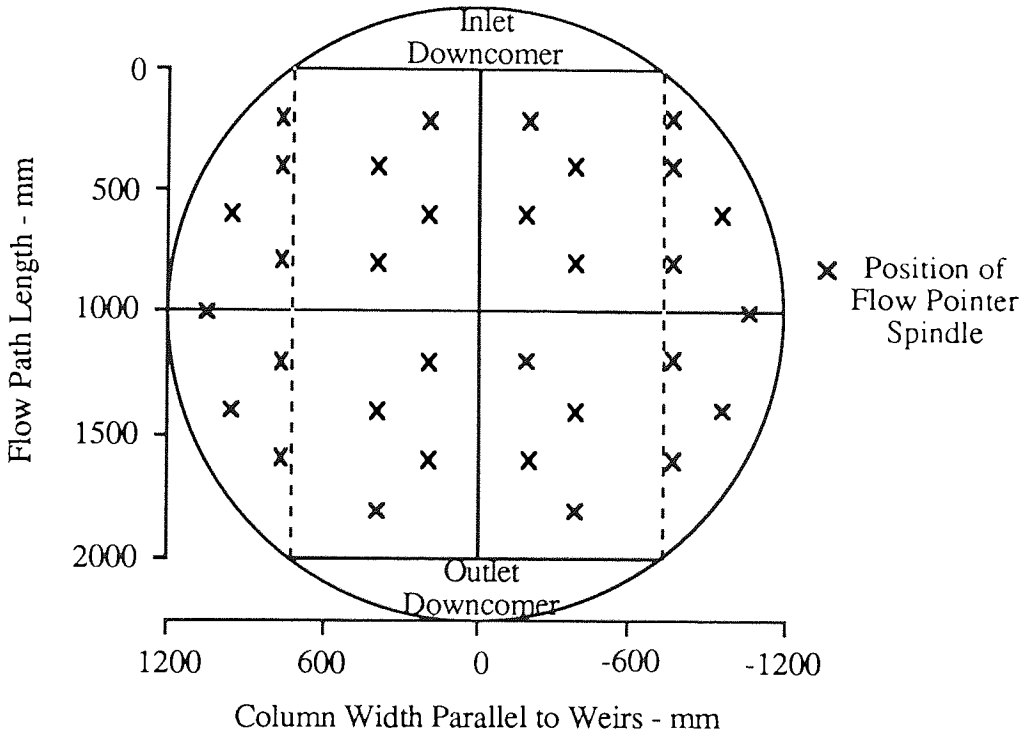

Fig. 7.2 Positions of the Flow Pointers over the Tray Area.

The direction of the flow pointers were monitored and recorded for various combinations of inlet gap, outlet weir, air flowrate and water flowrate, using both the overhead video

camera and visual observation. The inlet gap and outlet weir were set and then the water flowrate was slowly increased for different air flowrates. Whenever a change in the direction of the flow pointers occurred, the water flowrate was noted along with the associated changes.

The study was performed for inlet gaps of 10, 20 and 50 mm and outlet weirs of 0, 10, 20 and 50 mm. Three values of air flowrate were used, 1.0, 1.5 and 2.0 m/s (given in terms of the superficial air velocity), while the water flowrate was varied between 2.5×10^{-3} and 3.0×10^{-2} m^3/m s.

7.4 Results and Discussion

The flow pointers were successful in that they do reveal the direction of the liquid flow, and they are also responsive to changes in the flow direction, due to changes in the liquid flowrate. However, although the flow pointer indicators were clearly visible to the naked eye, the video camera had difficulty "seeing through" the mist of water droplets illuminated between the tray and the camera lens. Figures 7.3a and 7.3b show photographs of the flow pointers, taken from the video monitor, for typically the lowest and highest water flowrates respectively. Although the photographs are not clear, it can be discerned that the flow pointer directions for the two cases are changed, especially at the sides of the inlet half of the tray.

Due to the video camera not being able to see through the mist of water droplets, illuminated between the tray and the camera lens,the directions of the flow pointers were recorded manually, through the observation windows at the top of the column. The results are presented in such a way as to show the individual effects of changing the water flowrate, the inlet gap, the outlet weir and the air flowrate. The exact conditions at which the effects occur are discussed later due to the interdependence of the parameters studied.

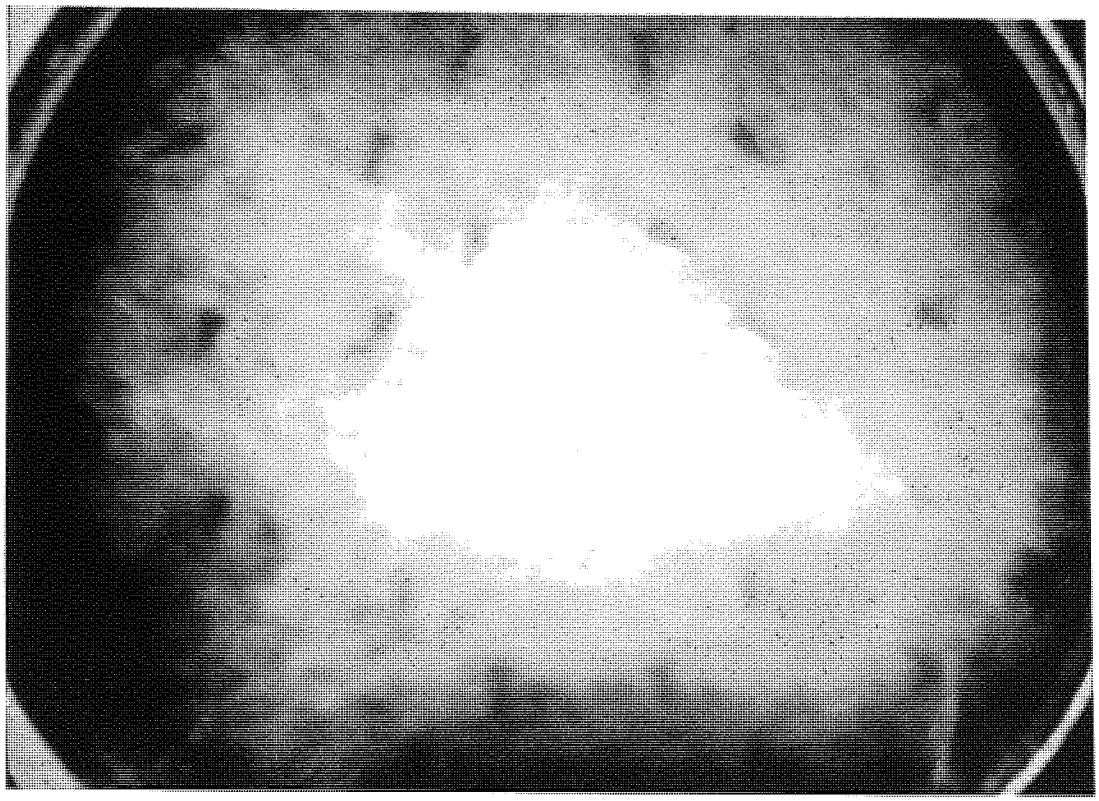

Fig. 7.3a Photograph of Flow Pointers at a Comparatively Low Water Flowrate.

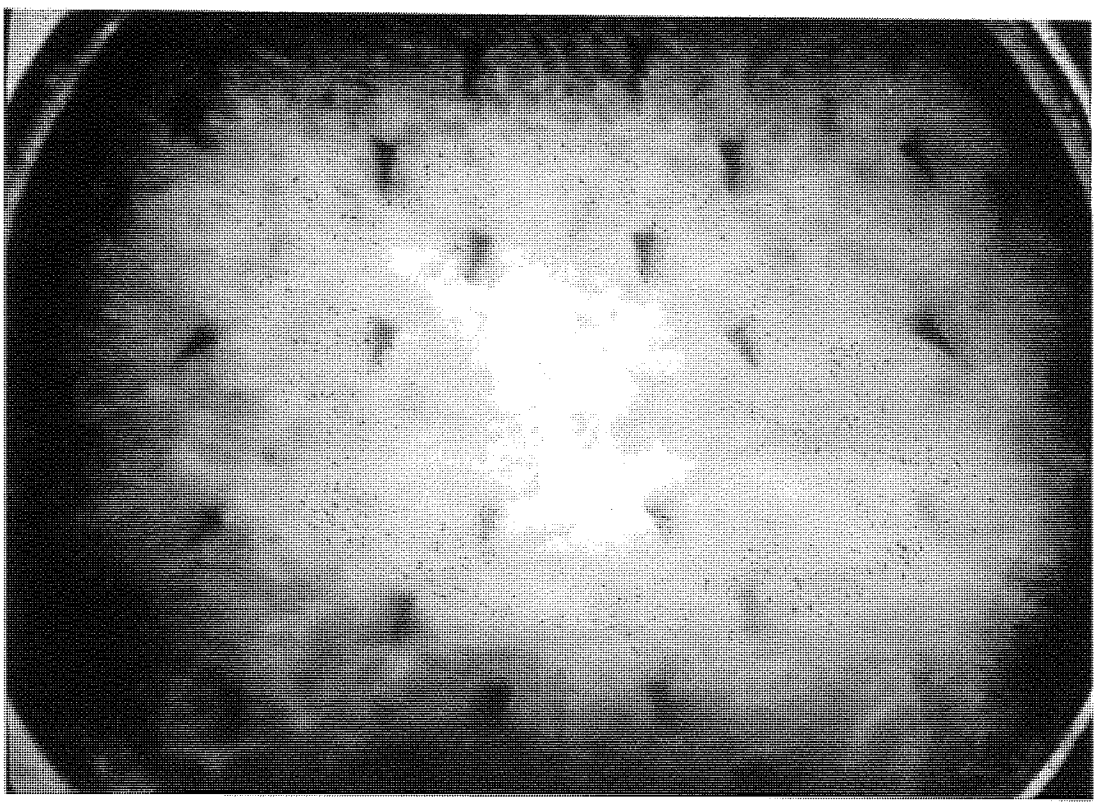

Fig. 7.3b Photograph of Flow Pointers at a Comparatively High Water Flowrate.

7.4.1 Effect of Water Flowrate

At the low water flowrate of 2.5×10^{-3} m^3/m s, non of the flow pointers indicated any signs of reverse flow. The water on entering the tray was aerated, and the biphase flowed so as to fill the tray area, with an underlying forward-only flow direction. As the water flowrate was increased the flow pointers in the side zones of the tray indicated changes in the biphase flow direction, which became more apparent at higher water flowrates. At certain water flowrates some flow pointers continually rotated whereas others indicated reverse flow and the presence of circulating regions. The circulating regions, determined from the recorded flow pointer directions, emanated from the edges of the inlet downcomer and gradually increased in size, with increasing water flowrate.

Figures 7.4a to 7.4d present a sequence of recorded flow pointer directions as the water flowrate is increased. By looking at the flow pointer directions over the tray, it is possible to make an estimate of the area occupied by the circulating regions, which is expressed below each figure.

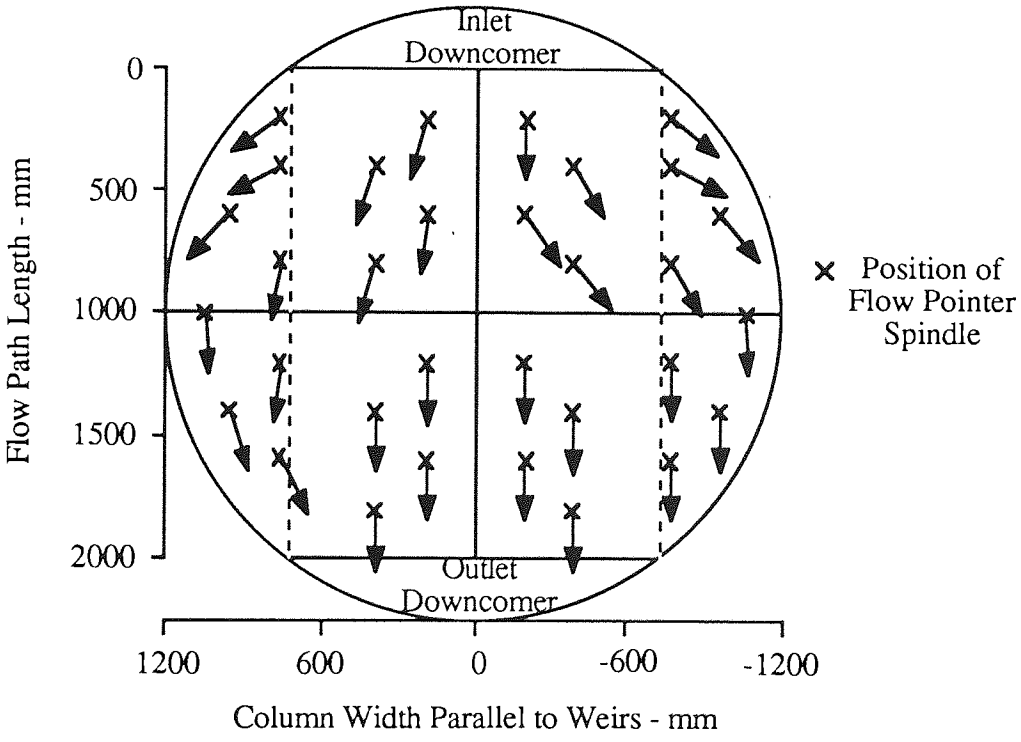

Fig. 7.4a Flow Pointer Directions - 0% Circulation.

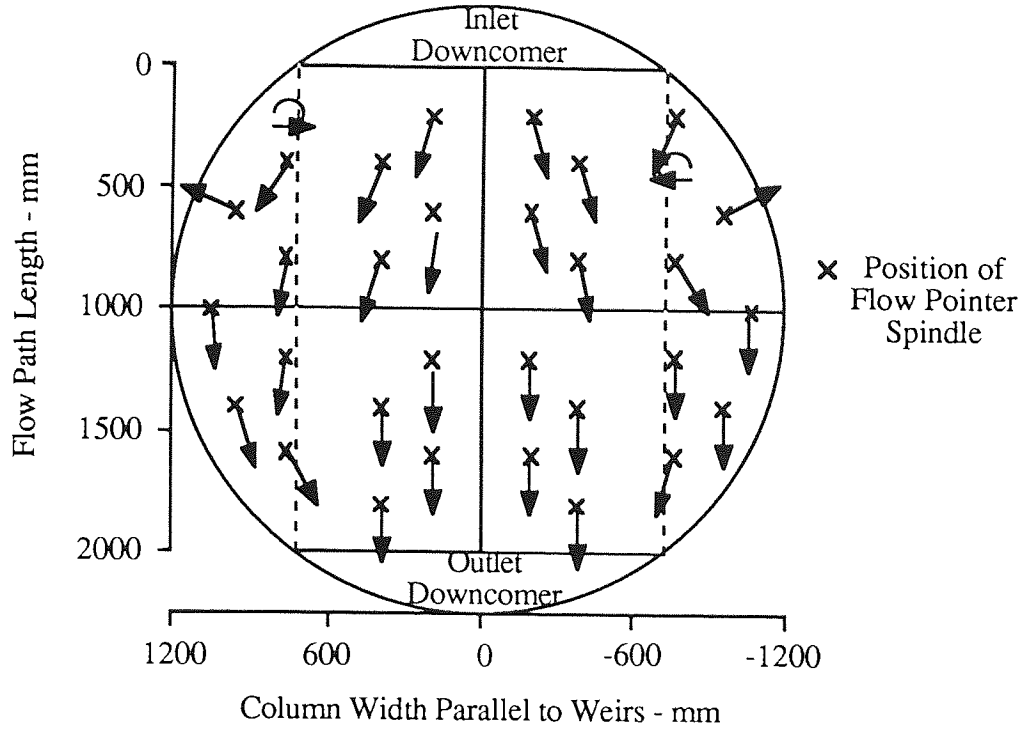

Fig. 7.4b Flow Pointer Directions - 10% Circulation.

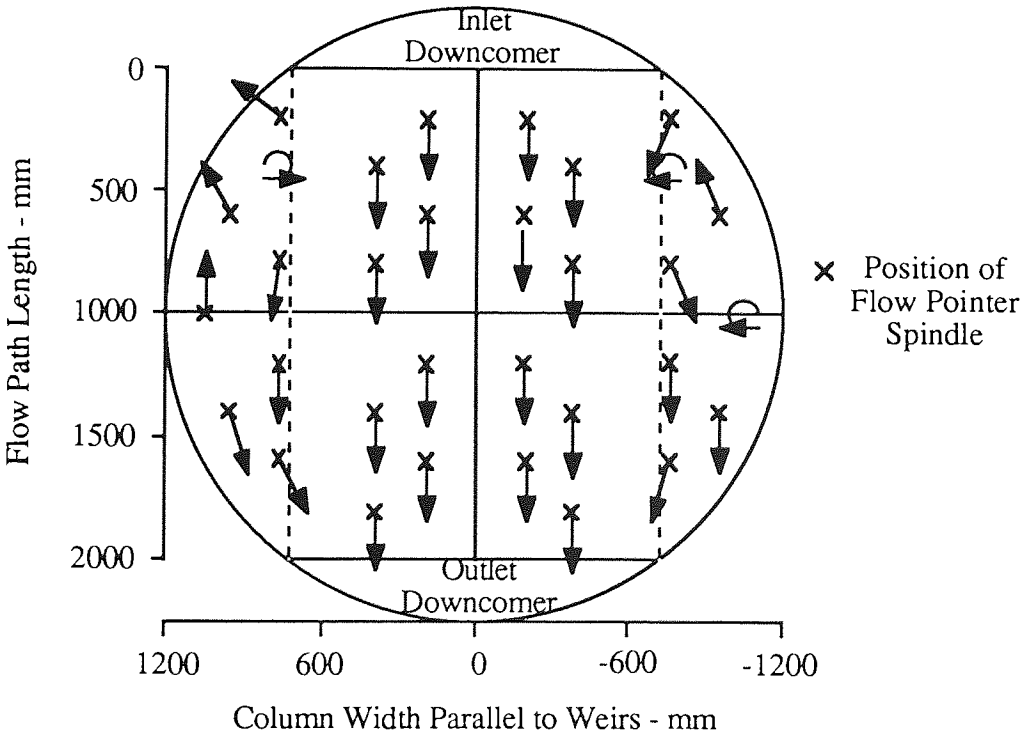

Fig. 7.4c Flow Pointer Directions - 20% Circulation.

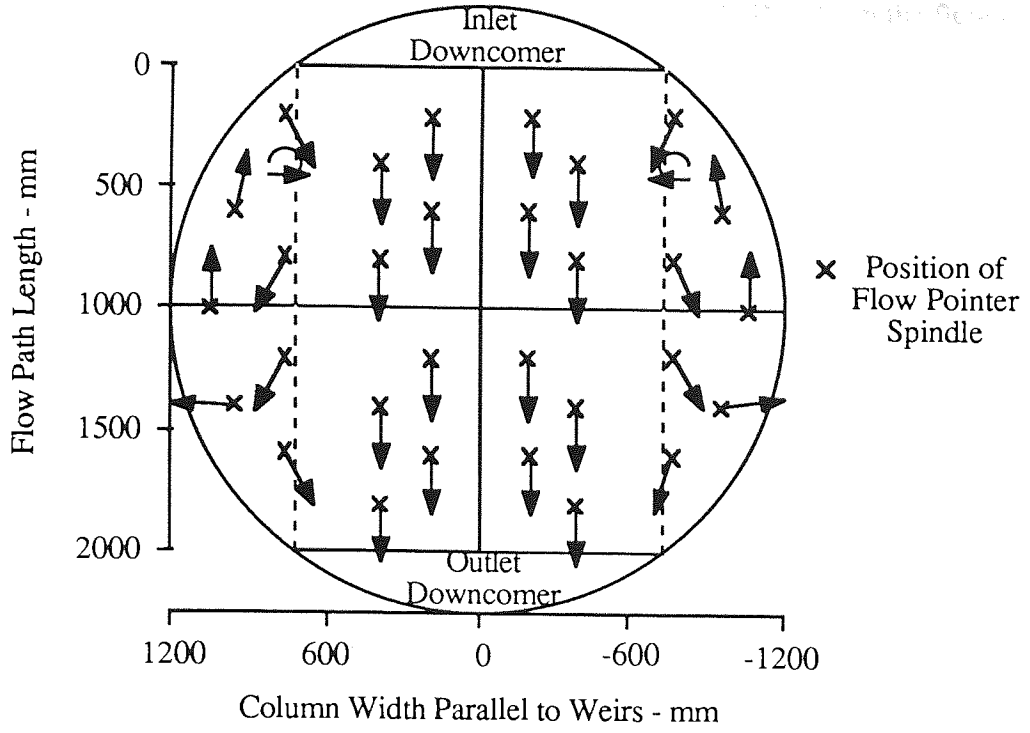

Fig. 7.4d Flow Pointer Directions - 30% Circulation.

0% Circulation

The 0% circulation flow pointer directions are presented in Figure 7.4a. Once the flow pointers were steady, showing dominant flow directions, it was noticed that none of the flow pointers indicated reverse flow. However, flow pointers adjacent to the tray walls did have a tendency to point normally towards the tray walls at times. This behaviour was put down to the fact of the support ring, and the effect it had on the local biphase characteristics. The support ring was 50 mm wide and supported the outer edge of the sieve tray.

Slight deviations in symmetry about the flow centreline were observed, more noticeably in the inlet half of the tray where the biphase was expanding to take up the flow width. This was accounted for by the low biphase velocities in the horizontal direction, and that the effectiveness of the flow pointers will reduce with lower biphase velocities. Note that the flow pointers can not disappear, even for zero velocity. Having mentioned this the recorded flow pointer directions seem a good representation of the flow when compared with dye tracer studies in the biphase, which can not be presented due to the difficulty of seeing through the spray above the tray.

No obvious circulating regions were visible from the flow itself or from the flow pointer directions.

10% Circulation

The 10% circulation flow pointer directions are presented in Figure 7.4b. From a visual observation of the flow pointers, an emergence of two circulation regions, either side of the inlet weir, was demonstrated. The flow pointers affected by the biphase flow pattern are the first three pointers in the side zones of the tray. The figure gives a true representation of the positions of the flow pointers, but the slowly-rotating flow pointers clearly can not be represented in a still figure. The flow pointers do show the presence of reverse flow and by considering an imaginary flow separation streamline an estimation of the circulating region was made as 10% of the tray active area.

Rotating Flow Pointers

Figures 7.4b, 7.4c and 7.4d show at least one flow pointer that rotated in one direction only. The explanation for this observation is presented in Figure 7.5.

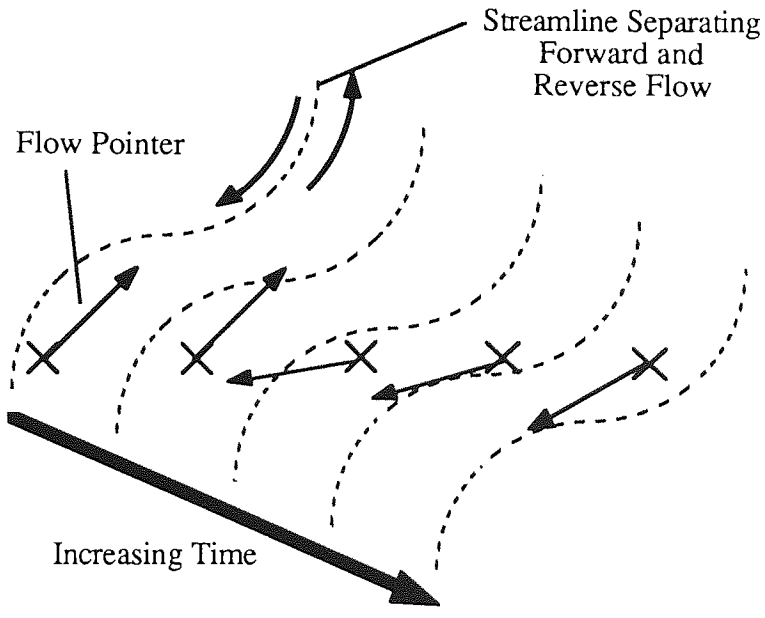

Fig. 7.5 Schematic Diagram of Rotating Flow Pointer.

From a distance the separation streamline, dividing forward and reverse flows, seems stationary, however on closer investigation this velocity interface is wavering randomly.

It is this non-steady property of the flow boundary which enables a flow pointer to rotate continually. The pre-requisite for a flow pointer to be able to rotate continually is that it must be sited in close proximity to the flow boundary.

Refer to Figure 7.5, the flow pointer is totally surrounded by one direction of flow only. Due to the random fluctuations of the velocity interface, the tip of the flow pointer manages to breech the interface, and enter the opposite flowing fluid. After this has occurred a pressure balance over the flow pointer determines its position, invariably resulting in the flow pointer turning until it is pointing in the opposite direction. Thereafter the process repeats itself continually.

One method of inhibiting this rotational problem with the flow pointers would be to reduce the length of the flow pointer, from the spindle to the tip. This would lead to a more precise location of the indicated flow direction and mean that a flow boundary would have to be even nearer to the flow pointer to cause the rotating effect. The disadvantage to this is that more fluctuations in the flow direction could be picked up by the flow pointer, thereby making the determination of the direction more difficult. Having mentioned these design factors, the flow pointers used did work satisfactorily and the underlying flow direction was easily determined.

20% Circulation

The 20% circulation flow pointer directions are presented in Figure 7.4c. Five flow pointers are now affected by the biphase flow pattern, with the two circulating regions extending into the second half of the tray, demonstrated by the rotating flow pointer at the join of the inlet and outlet halves of the tray. The flow pointers in the central region of the tray indicate that the bulk water flow travels in a straight direction between the inlet and outlet downcomers. Around the sides of the tray, the reverse flow could be distinguished from the bulk forward-flowing water, and the estimated size of the circulating region was 20% of the active tray area.

30% Circulation

The 30% circulation flow pointer directions are presented in Figure 7.4d. The only change occurring between Figures 7.4c and 7.4d is that the size of the circulating regions have increased to an estimated 30% of the active area. Visually the reverse flow is very strong throughout the whole of the side regions and this effect is very clearly shown by the direction of all the flow pointers in the side regions.

7.4.2 Effect of Inlet Gap

When the inlet gap was set at 10 mm, the above series of flow pointer directions were all observed, the 30% circulation being achieved at a water flowrate of 1.2×10^{-2} m^3/m s. On increasing the inlet gap to 20 mm, again all the flow pointer directions up to a 30% circulation were observed but the water flowrate at which the 30% circulation was formed had increased to 2.0×10^{-2} m^3/m s. By increasing the inlet gap further to 50 mm, only the flow pointer directions up to a 20% circulation were observed. The water flowrate was increased to 3.0×10^{-2} m^3/m s but the recorded flow pointer positions did not reveal a 30% circulation. The 20% circulation based on the flow pointer directions was achieved at a water flowrate of 2.3×10^{-2} m^3/m s.

The general trend observed was that an increase in the inlet gap, keeping all the other parameters constant, delayed the onset of separation, and slowed down growth of the circulating regions with increasing water flowrate.

7.4.3 Effect of Outlet Weir

The outlet weir was varied from 0 mm through to 50 mm. Visually the height of the froth on the tray increased with increasing outlet weir, but no evidence was found to show that this parameter had an effect on flow pointers.

7.4.4 Effect of Air Flowrate

The superficial air velocity had values of 1.0, 1.5 and 2.0 m/s, varying in total by a factor of two. The positions of the flow pointers did not change for different settings of the air flowrate and so it was concluded that this parameter had no effect on the flow direction.

7.4.5 Effect of The Weir Loading and the Inlet Gap on the Degree of Circulation

Figure 7.6 shows the approximate size of the circulating regions, determined from the flow pointers, against the water flowrate for all the combinations of inlet gap (10, 20 and 50 mm), outlet weir (0, 10, 20 and 50 mm) and air superficial velocity (1.0, 1.5, and 2.0 m/s).

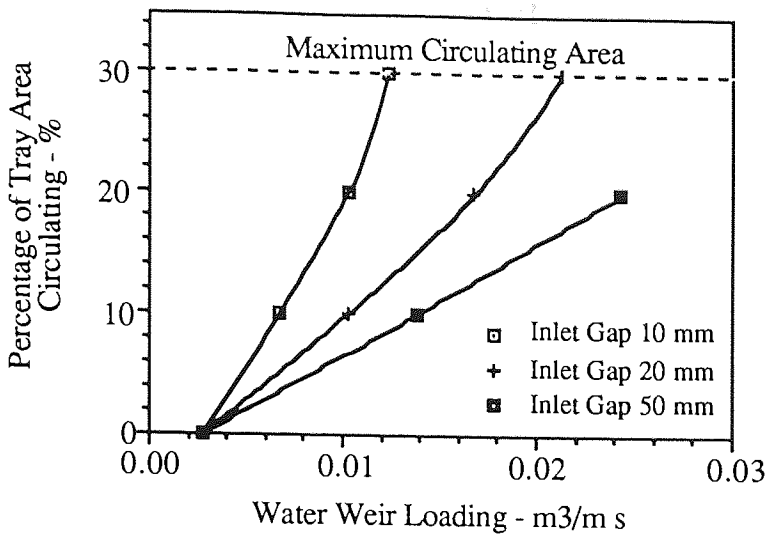

Fig. 7.6 Degree of Circulation for Biphase.

As has been mentioned earlier, the outlet weir and air flowrate, for the values investigated, did not have any noticeable effect on the developed flow pattern, as determined by the flow pointers, and thus no reference is made to these parameters in Figure 7.6.

At the lowest water weir load of 2.5×10^{-3} m^3/m s no regions of circulation were observed for any setting of the inlet gap. At weir loads above 2.5×10^{-3} m^3/m s the flow pointers indicate that circulation is present at the side regions of the tray, the degree of circulation being dependant upon the inlet gap. The 10 mm inlet gap generated the largest degree of circulation for a fixed water weir load, whereas the 50 mm inlet gap generated the smallest degree of circulation. It was also noted that the rate of increase of the circulation area against the water weir load was much greater for the 10 mm inlet gap than for the 50 mm inlet gap. Attempts were made to correlate the entering water velocity or momentum to the circulating area with no success.

As with the water-only studies the maximun degree of circulation, from the flow pointers, was 30%, further increases in the water flowrate serving only to strengthen the rotational velocity of the formed circulation

CHAPTER 8

8. MEASUREMENT OF OPERATING VARIABLES OVER THE SIEVE TRAY

8.1 Introduction

The previous chapters have shown that the liquid flow direction, over an operating sieve tray, is far from uniform. It was anticipated that the flow pattern would therefore affect the depth of the froth over the tray area and also the flow of liquid leaving the tray over the outlet weir. This chapter concerns the measurement of the height of clear liquid over the tray area along with the liquid flow over the outlet weir.

8.2 Measurement of Clear Liquid Hold-up

The flow pattern can be considered to be made up of three components:

(i) Flow direction.

(ii) Flow velocity.

(iii) Flow depth.

Each of the components combine to give the overall flow pattern. It is important then, while investigating the flow pattern, to give some thought to the flow depth over the tray area. Text books assume all the flow to be in a uniform direction and that the froth height decreases from the liquid inlet to the liquid outlet of the tray. As the liquid flow has already been found to be non-uniform then the assumption of decreasing froth height from the liquid inlet to the liquid outlet must be investigated.

The froth height is a difficult parameter to measure, due to the mobile froth surface. However the pressure drop through the froth, which is proportional to the froth height, can be determined by the measurement of the effective froth height or the liquid hold-up. The liquid hold-up on a tray is defined as the height of the clear liquid on the tray when

the vapour supply is cut off to eliminate the foaming vapour and liquid droplets above it.

8.2.1 Measurement Technique

One standard method of measuring the clear liquid height on an air-water test tray is to connect a manometer, filled with water, to a pressure tapping mounted flush on the tray floor, see Figure 8.1.

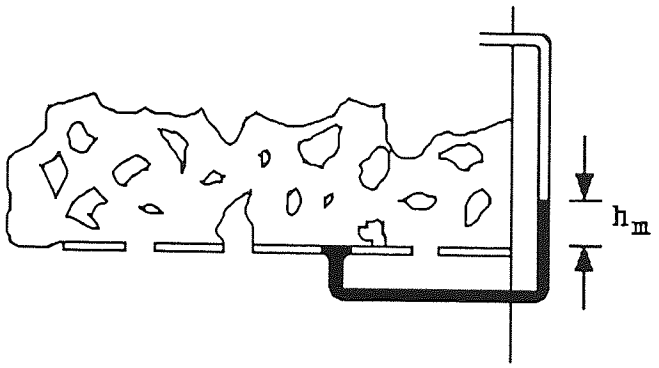

Fig. 8.1 Arrangement for Measuring Clear Liquid Hold-Up.

Lockett (1986) points out that corrections to the measured value must be made to account for capillary rise and gas momentum. These corrections were overcome by relating all the manometer readings to a datum level, which was generated by operation with air flow but no liquid hold-up. Then the datum level was subtracted from the actual reading with liquid hold-up, the gas momentum term dropped out of the equation. Also this technique allowed account to be taken of tray deflection, which is more significant on large diameter trays.

8.2.2 Experimental Procedure

Thirty-two pressure tappings were positioned over the 2.44 m diameter sieve tray as shown in Figure 8.2. PVC tubing connecting the sample points to manometers were filled with water and the lines were cleared of air bubbles by purging them with water under pressure prior to any tests being conducted.

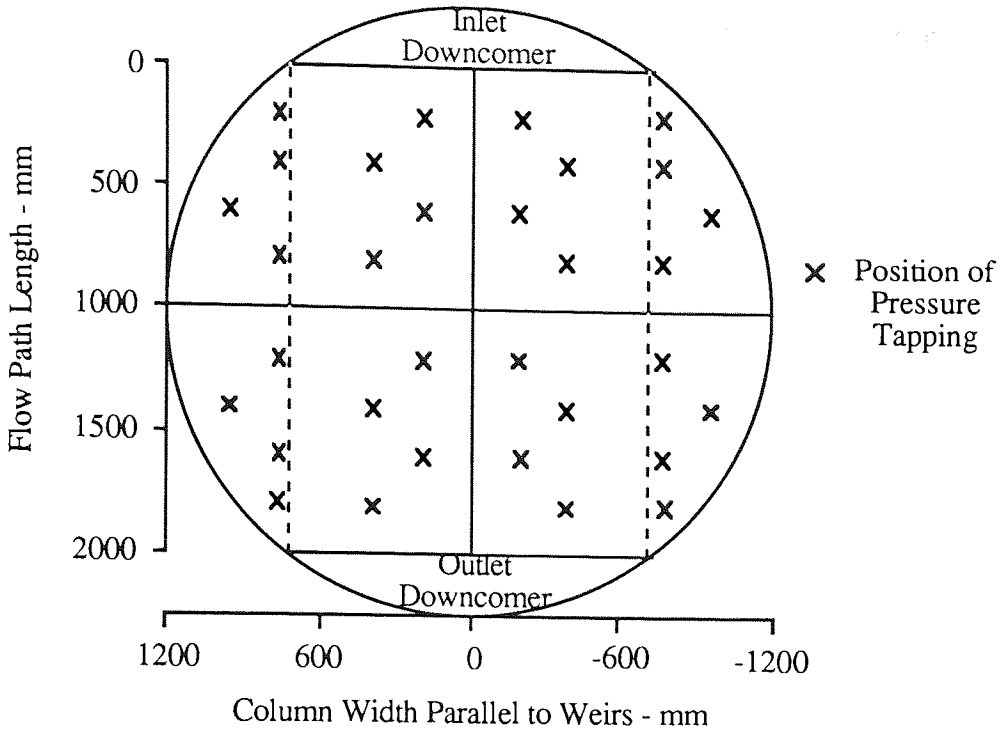

Fig. 8.2 Positions of the Pressure Tappings over the Tray Area.

For a particular air flowrate the datum manometer levels were recorded without any water flowrate, and thus zero liquid hold-up. The water flowrate was then set and after a period to allow for steady state to be achieved all the manometer levels were recorded. The water hold-up was then calculated by subtracting the datum manometer levels from the actual levels.

The geometry of the sieve tray was the same as that previously described, a 2.44 m diameter sieve tray with 1.50 m straight chordal weirs, 1 mm diameter holes and 10% free area. The inlet gap was fixed at 10 mm and the outlet weir was also fixed at 10 mm. Superficial air velocities of 0.7, 0.9, 1.2 and 1.5 m/s, and water flowrates of 2.5, 3.5, 5.5, 7.5 and 11.0×10^{-3} m^3/m s were used for the water hold-up investigation.

8.2.3 Results and Discussion

Measurements of the liquid hold-up indicated a significant variation over the area of the operating tray. Continuous surfaces of the liquid hold-up are presented in Figures 8.3a-e, 8.4a-e and 8.5a-e for superficial air velocities of 0.7, 0.9 and 1.2 m/s respectively (presented at the end of the section), and mean liquid hold-up values, along with their standard deviations, are presented in Table 8.1. The actual point liquid hold-up data are contained in Appendix 2.

Air Superficial Velocity (m/s)	Water Loading ($cm^3/cm\ s$)	Mean Liquid Hold-Up (mm)	Standard Deviation (mm)
0.7	25	21.7	6.64
	35	24.4	7.51
	55	26.4	7.94
	75	29.0	6.89
	110	32.8	7.67
0.9	25	22.7	5.17
	35	24.5	5.29
	55	26.2	6.00
	75	28.5	6.19
	110	30.3	6.65
1.2	25	13.8	2.17
	35	15.8	2.38
	55	16.9	2.42
	75	18.4	3.18
	110	20.8	4.19
1.5	25	12.0	1.63
	35	13.5	2.28
	55	14.7	2.24
	75	14.8	2.68
	110	16.9	3.48

Table 8.1 Mean Height of Clear Liquid for Stated Conditions of Flow.

From Table 8.1, the trend of the mean liquid hold-up seems to increase with increasing water flowrate and to decrease with increasing air flowrate. These trends are in keeping with the results of previous workers (Bennet et al., 1983; Stichlmair, 1978; Hofhuis and Zuiderweg, 1979). However this work gives a measure of the possible variation in the liquid hold-up in terms of the standard deviation of thirty-two point measurements, if an average liquid hold-up value is assumed.

Superficial Air Velocities 0.7 and 0.9 m/s

At the lower superficial air velocities, 0.7 and 0.9 m/s, significant variations in the clear liquid height were measured, see Figures 8.3a-e and 8.4a-e, and the standard deviations in Table 8.1. The figures reveal that the liquid hold-up in the side zones of the circular tray is much greater than the liquid hold-up in the central flow region. This variation in the liquid hold-up measurement can be explained by visual observation of the operating tray. At the low air flowrates, non-bubbling areas of clear liquid were observed over the tray area. The central region of the tray was constantly bubbling, whereas in the side zones, and nearer to the inlet downcomer, only sporadic bubbling occurred, which lasted for typically 5 to 10 seconds. Although clear liquid was observed on the "active" tray, no significant weeping occurred beneath these regions,which was put down to a combination of the small hole size, 1 mm diameter holes, and the high surface tension of water.

Another noticeable observation is that the clear liquid hold-up almost always decreases with distance from the inlet downcomer. The exception from this occurs at the high liquid weir loading of 1.1×10^{-2} m^3/m s, where low clear liquid hold-ups are measured just after the inlet weir, see Figures 8.3e and 8.4e. In these cases the liquid seemed to jet from the inlet gap and did not become fully aerated until about 200 mm from the inlet weir.

Superficial Air Velocities 1.2 and 1.5 m/s

At the superficial air velocities of 1.2 and 1.5 m/s, the variation in the measured clear liquid heights was very much reduced, see Figures 8.5a-e and the standard deviations in Table 8.1. Also, no "dead" zones or non-bubbling zones were observed over the operating tray, which was put down to the fact that normal (for distillation) superficial air velocity conditions were prevailing with all the tray "active".

The clear liquid hold-up still decreases with distance fron the inlet weir although at a much reduced hold-up gradient and the exception from this still occurs at the high liquid weir loading of 1.1×10^{-2} m^3/m s. Due to the low liquid hold-up associated with higher superficial air velocities, significant differences were not detected in the liquid hold-up despite the flow pointers indicating that large circulating regions exist at the higher liquid weir loads. From this, the conclusion is made that the technique used for measuring the liquid hold-up is not sensitive enough for the small differences around circulating regions.

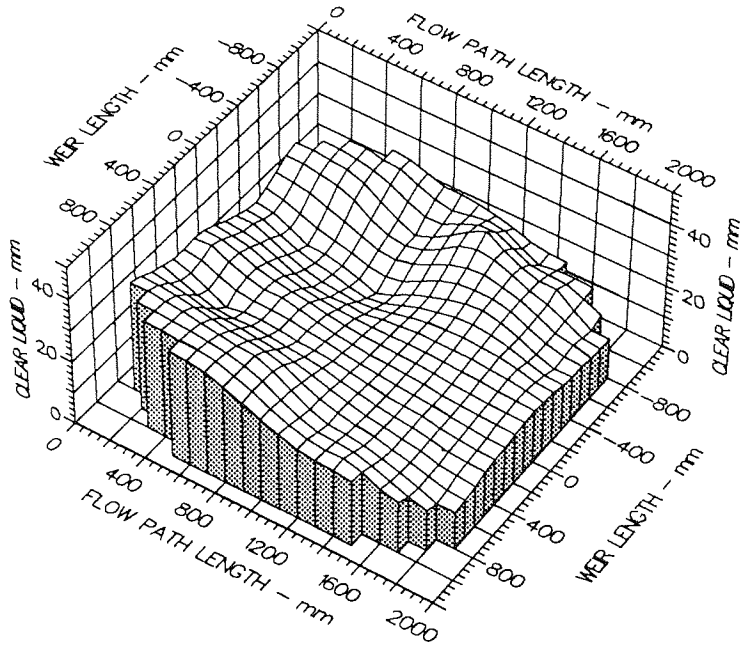

Fig. 8.3a Surface of Clear Liquid Hold-Up - Superficial Air Velocity 0.7 m/s.

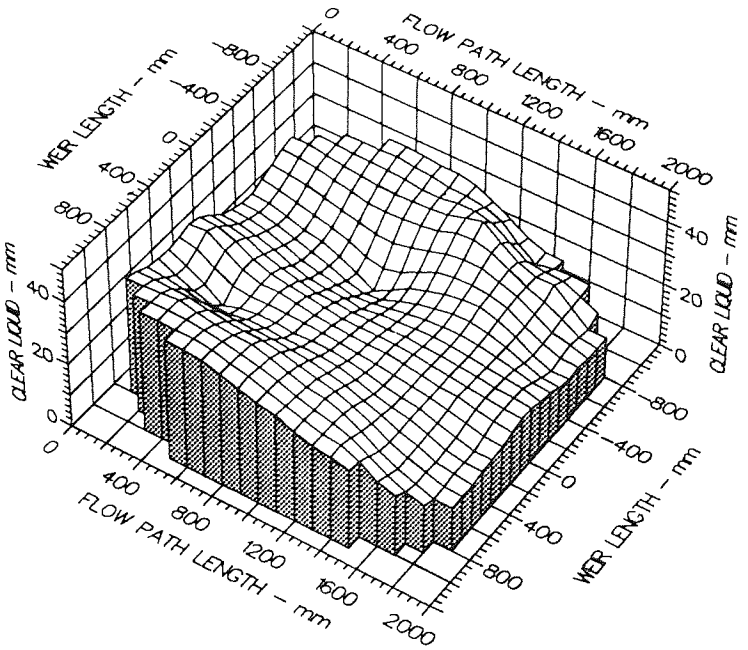

Fig. 8.3b Surface of Clear Liquid Hold-Up - Superficial Air Velocity 0.7 m/s.

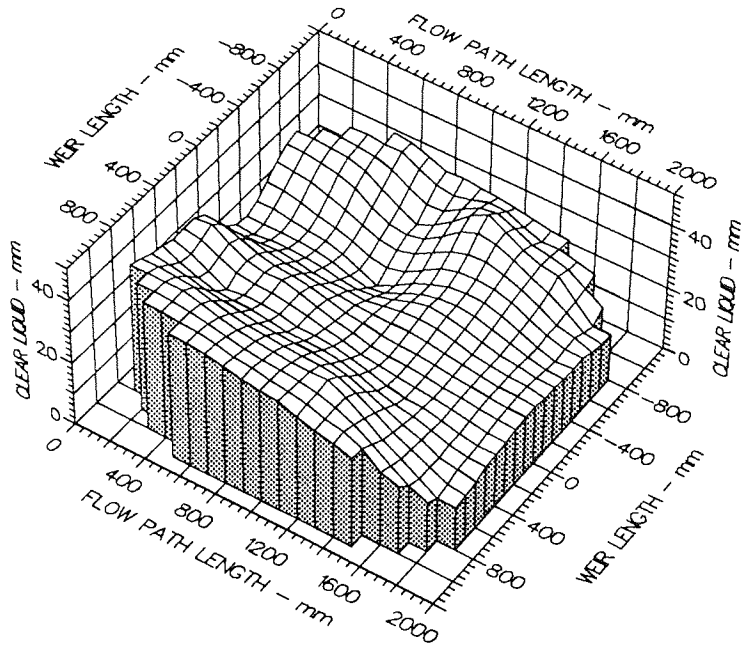

Fig. 8.3c Surface of Clear Liquid Hold-Up - Superficial Air Velocity 0.7 m/s.

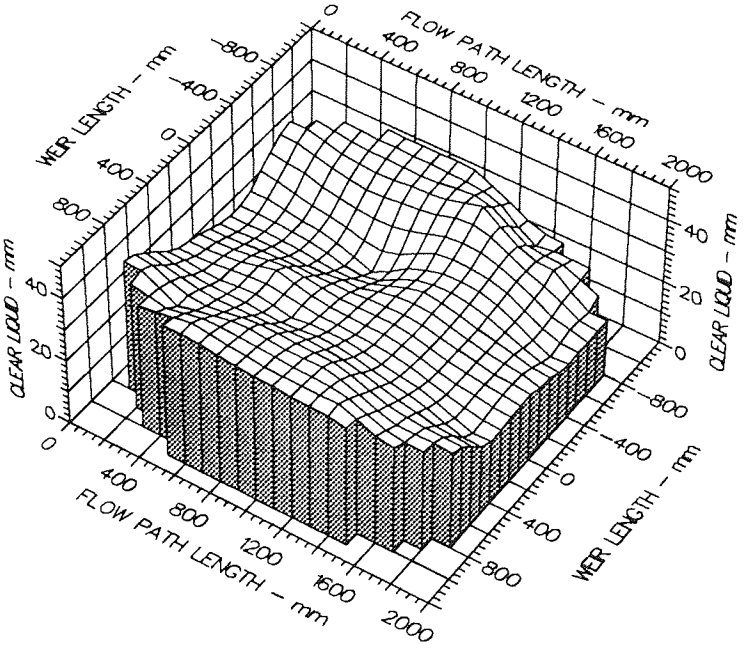

Fig. 8.3d Surface of Clear Liquid Hold-Up - Superficial Air Velocity 0.7 m/s.

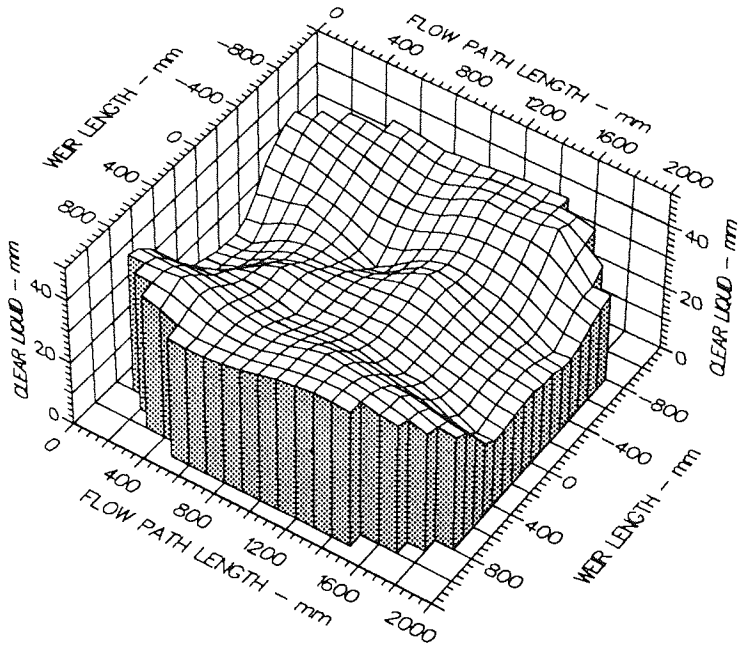

Fig. 8.3e Surface of Clear Liquid Hold-Up - Superficial Air Velocity 0.7 m/s.

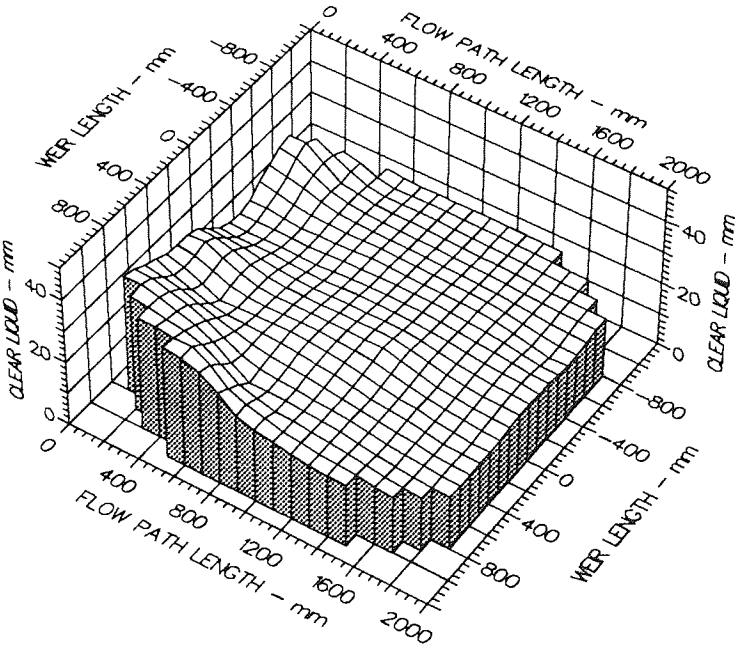

Fig. 8.4a Surface of Clear Liquid Hold-Up - Superficial Air Velocity 0.9 m/s.

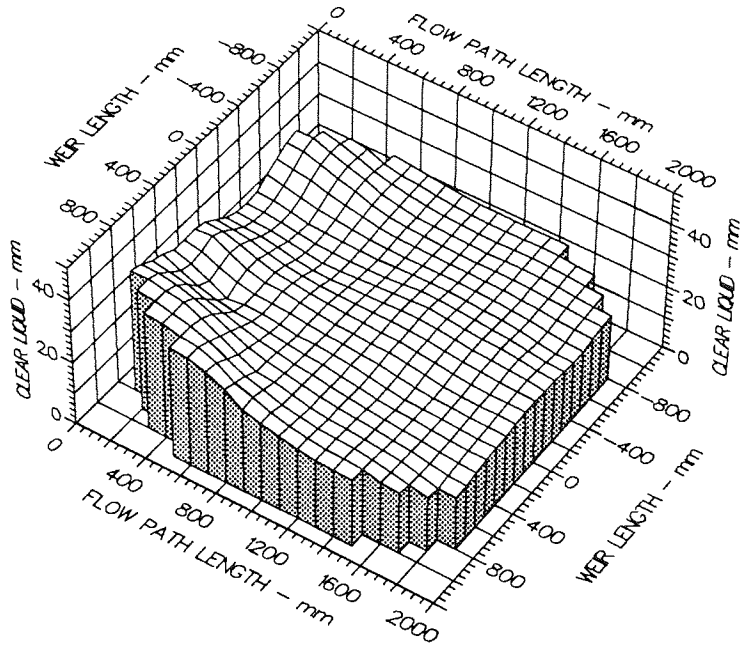

Fig. 8.4b Surface of Clear Liquid Hold-Up - Superficial Air Velocity 0.9 m/s.

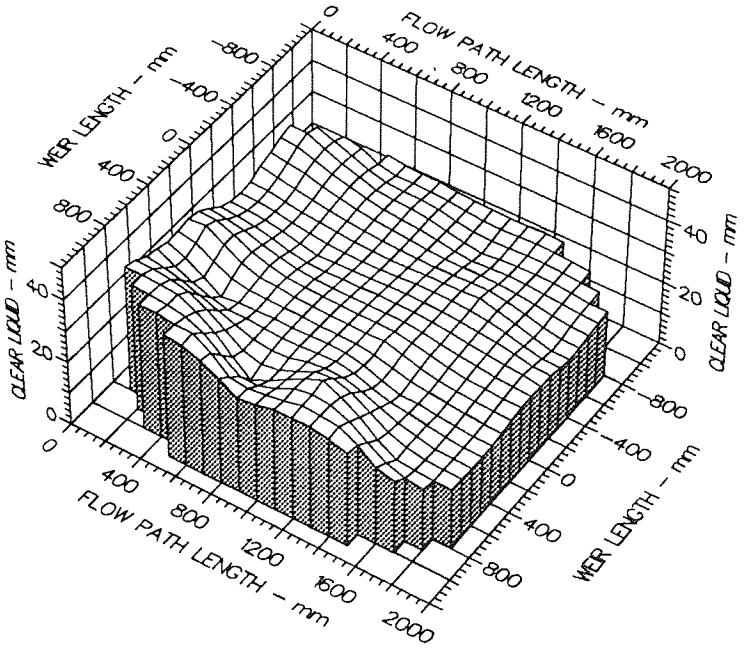

Fig. 8.4c Surface of Clear Liquid Hold-Up - Superficial Air Velocity 0.9 m/s.

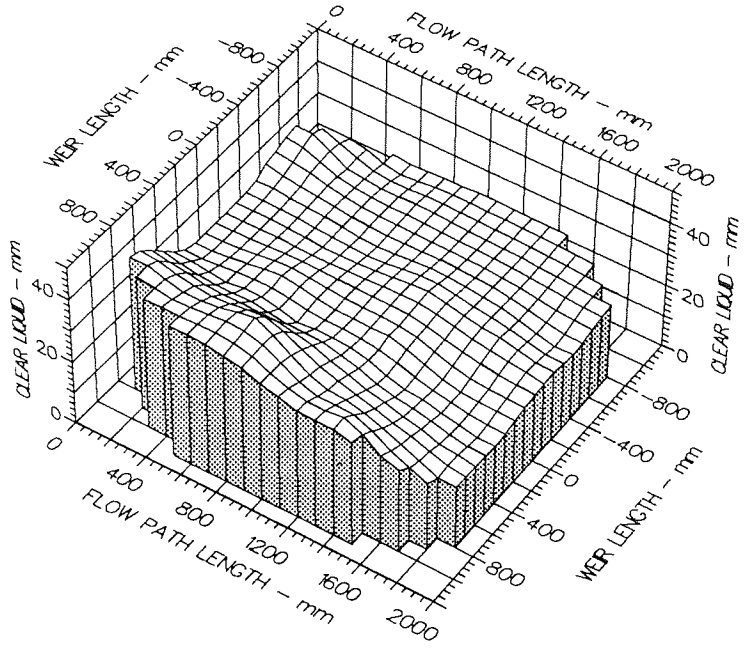

Fig. 8.4d Surface of Clear Liquid Hold-Up - Superficial Air Velocity 0.9 m/s.

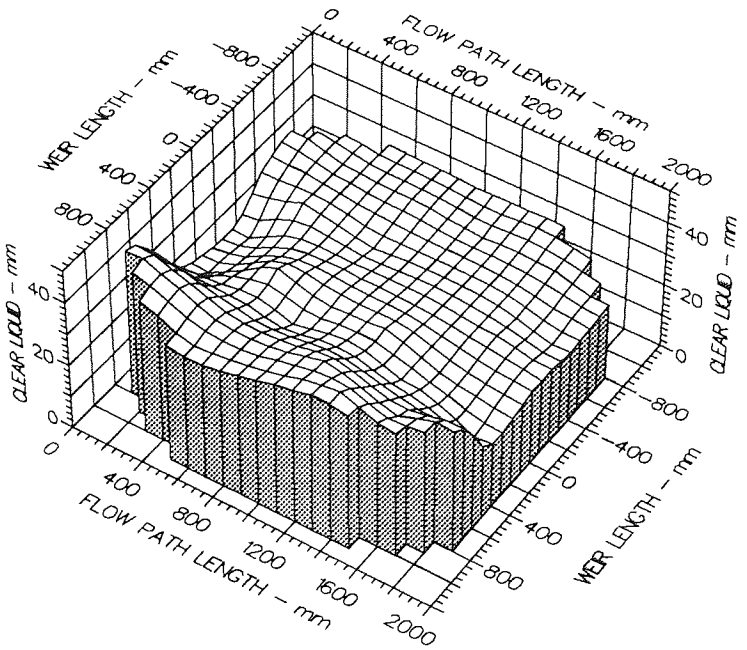

Fig. 8.4e Surface of Clear Liquid Hold-Up - Superficial Air Velocity 0.9 m/s.

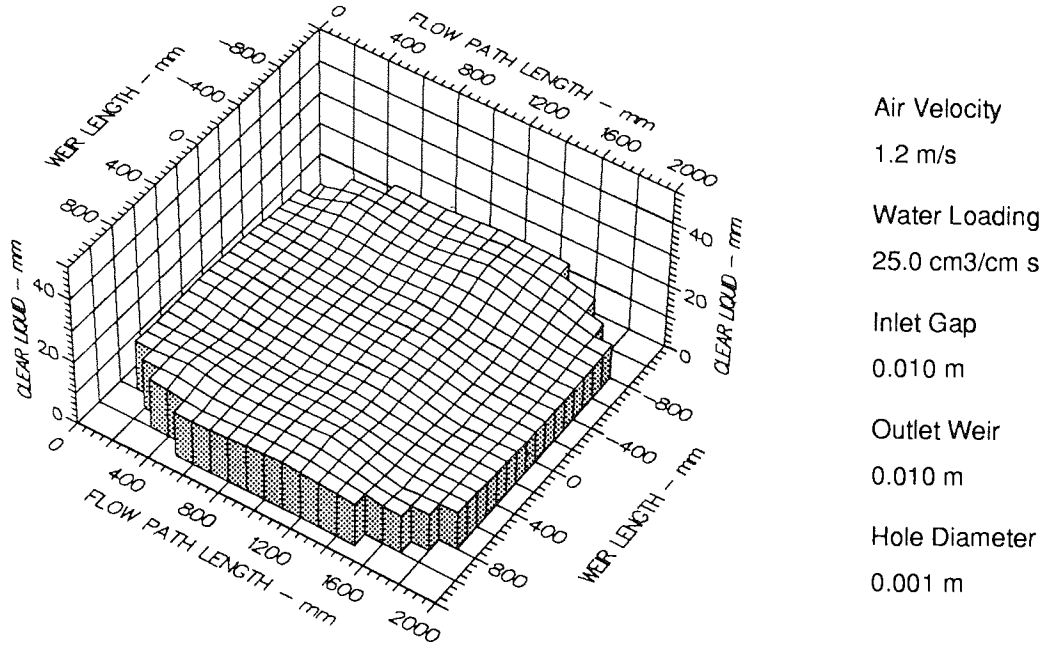

Fig. 8.5a Surface of Clear Liquid Hold-Up - Superficial Air Velocity 1.2 m/s.

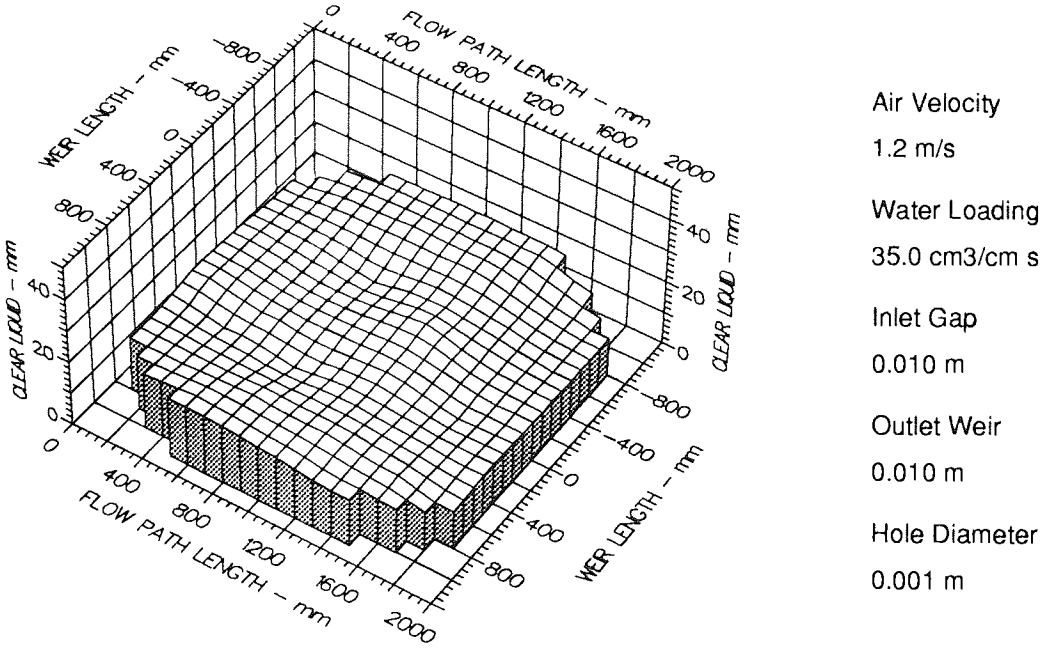

Fig. 8.5b Surface of Clear Liquid Hold-Up - Superficial Air Velocity 1.2 m/s.

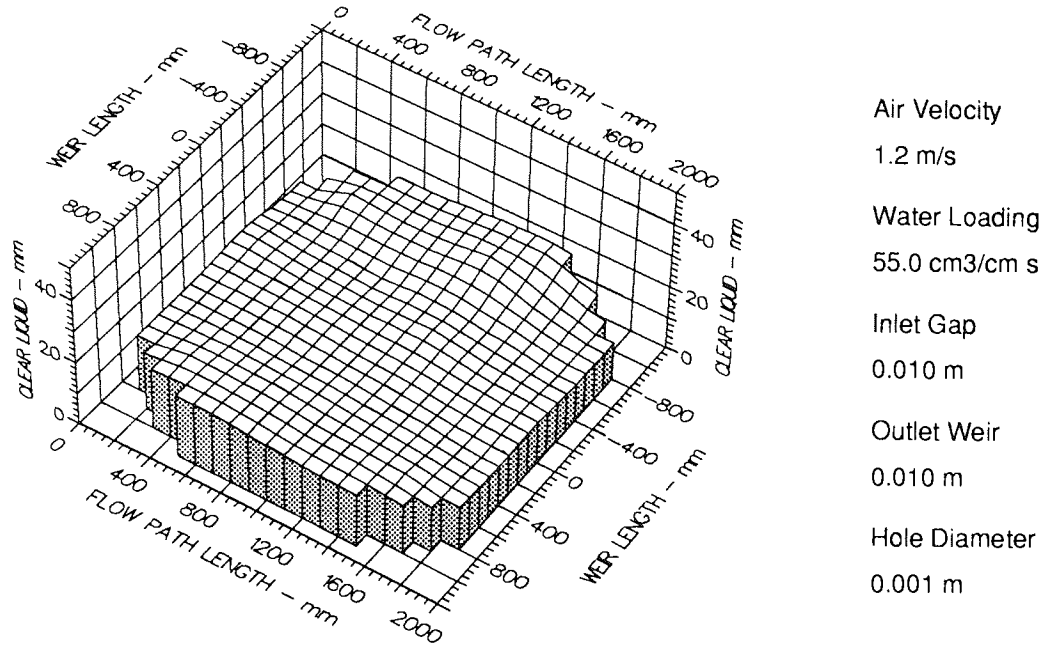

Fig. 8.5c Surface of Clear Liquid Hold-Up - Superficial Air Velocity 1.2 m/s.

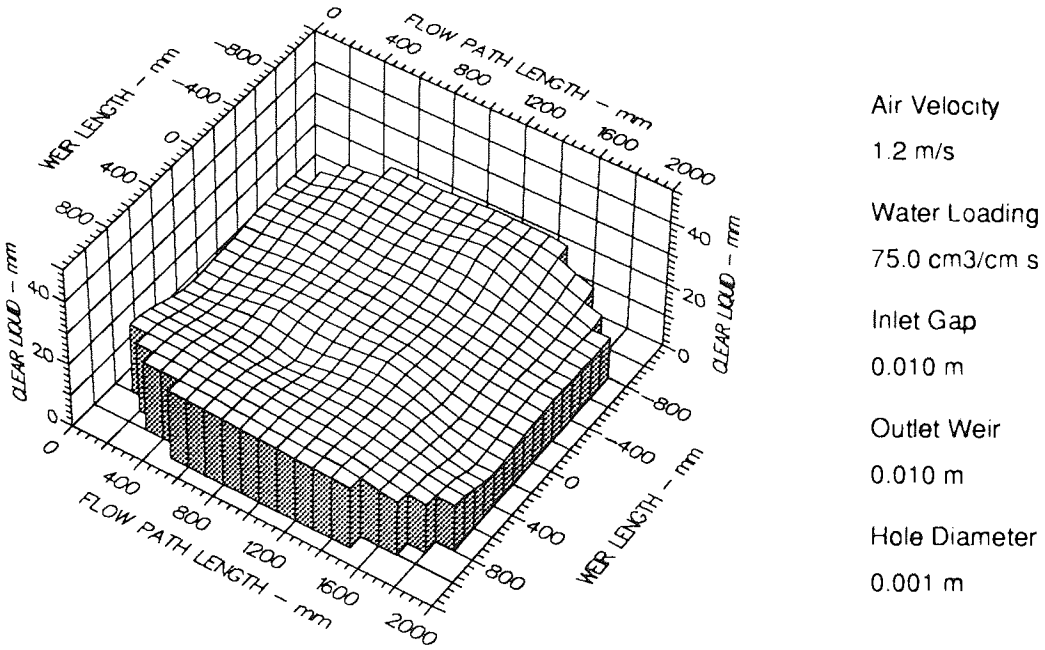

Fig. 8.5d Surface of Clear Liquid Hold-Up - Superficial Air Velocity 1.2 m/s.

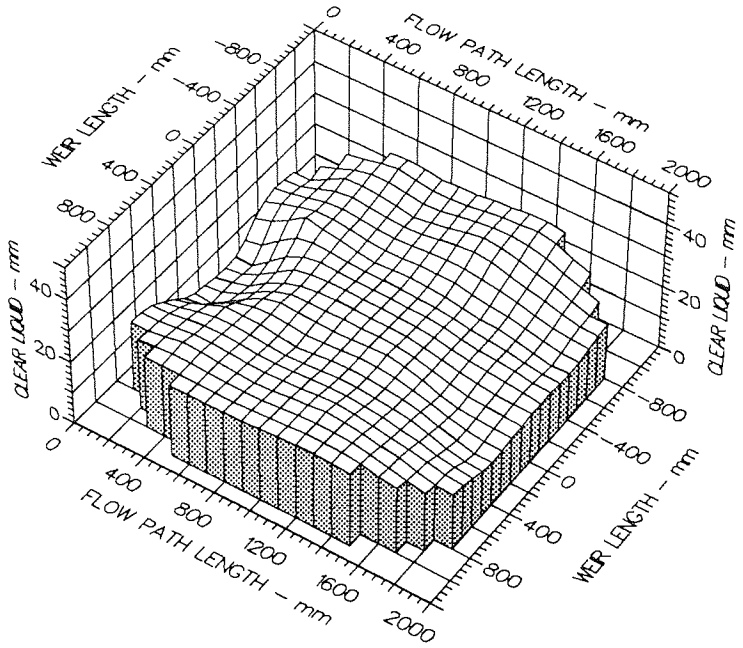

Fig. 8.5e Surface of Clear Liquid Hold-Up - Superficial Air Velocity 1.2 m/s.

8.3 Measurement of Liquid Flow over the Outlet Weir

The previous work has shown the existence of non-uniform flow over the tray and sometimes there appeared to be a significant variation in liquid head along the outlet weir. These observations provided the starting point for the work described below in which the uniformity or variation of the liquid flow over the outlet weir is measured.

8.3.1 Measurement Technique

A liquid collection box was designed and fitted into the outlet downcomer, such that the liquid leaving the tray entered one of eight compartments within the collection box. Thus, the length of the outlet weir was divided into eight equal lengths. Each compartment had an orifice at the base which provided a resistance to the leaving liquid. The result of the resistance to flow was the development of a liquid head within each compartment. At steady state, the head of liquid above the orifice in each compartment was representative of the liquid flow into the compartment. A water manometer connected to the base of the compartment was used to measure the developed head of liquid, from which the compartmental flow was determined using the generated calibration.

Calibration: Liquid Head Against Flow

The orifice in each compartment was 38 mm in diameter, but as the weir flow measuring device contained varying shapes of collection compartment, due to the column curvature, it was considered necessary to calibrate each different compartment for the liquid head against flow relationship.

Liquid at a known flowrate was passed through each compartment shape and the head of liquid in the compartment was recorded. The calibration of liquid flowrate against the recorded liquid height was constructed, see Figure 8.6, and was used to determine the actual liquid flowrate in each compartment during the experiment. Note that the liquid flowrate is expressed in terms of a weir loading, i.e. $cm^3/cm\ s$.

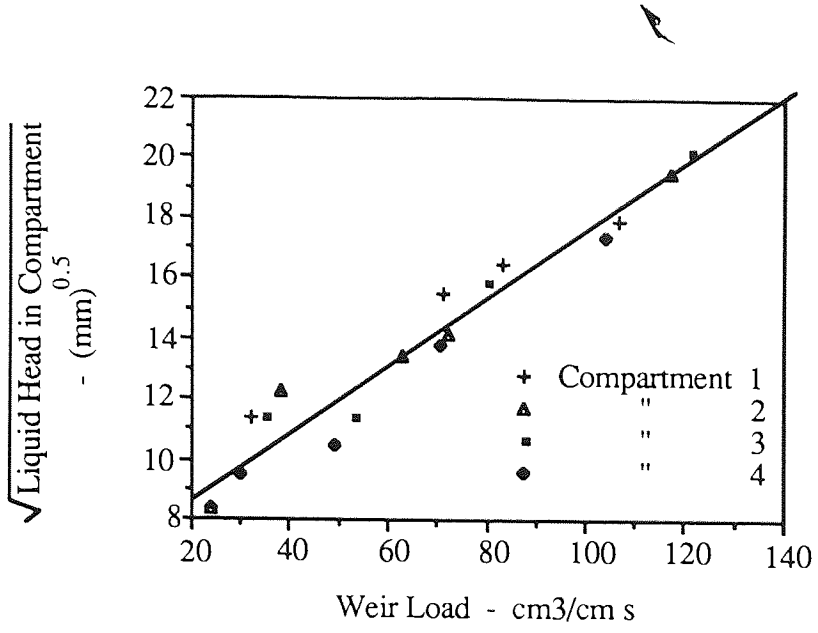

Fig. 8.6 Compartment Calibration for Flow over the Outlet Weir.

The liquid head increased with increasing flow through the compartments, however the differing compartmental shapes seemed to have little bearing on the calibration curve. At low weir loadings, below 2.0×10^{-3} m^3/m s, the data became extremely scattered and so experimental operation was limited to compartmental weir loadings of above 2.0×10^{-3} m^3/m s.

8.3.2 Experimental Procedure

The tray geometry was the same as that used for the height of clear liquid measurements. The inlet gap and outlet weir were each set at 10 mm, and the same flow conditions were used as for the height of clear liquid measurements. Note that the 10 mm inlet gap gives the largest variation of flow patterns, over the tray area, for increasing water weir load.

8.3.3 Results and Discussion

The recorded depths of liquid in the compartments for each of the flow conditions are contained in Appendix 3. The derived variations in weir loading from the data in Appendix 3 are presented graphically in Figures 8.7 to 8.10. Each of the Figures, 8.7 to 8.10, presents the flow of water over the outlet weir for a different superficial air velocity, at several values of the water weir load expressed as the mean weir load.

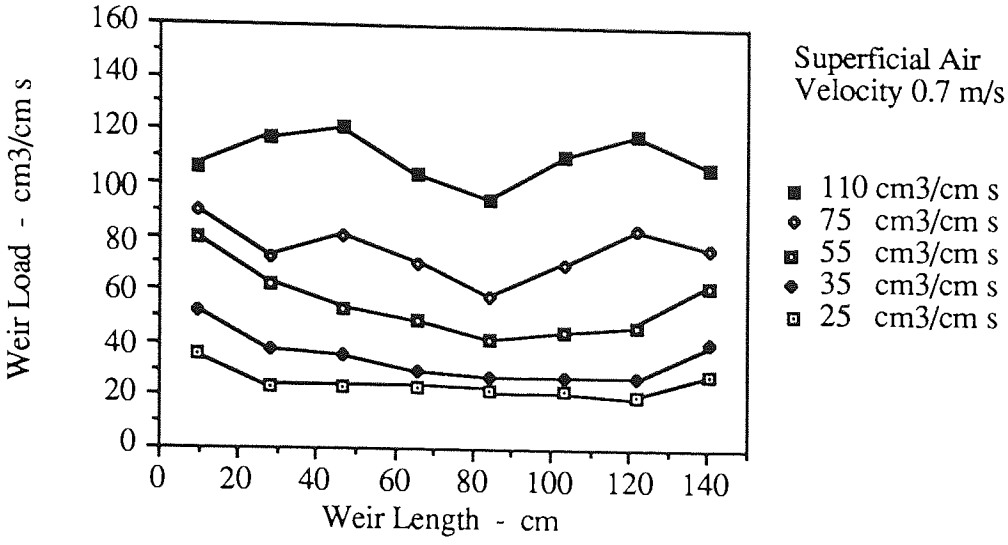

Fig. 8.7 Weir Load over Outlet Weir - Superficial Air Velocity 0.7 m/s.

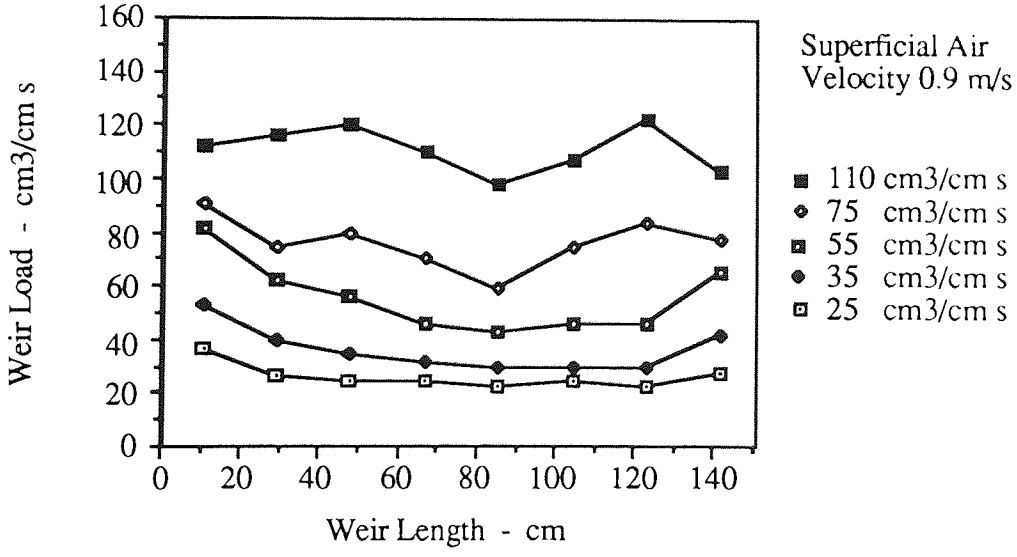

Fig. 8.8 Weir Load over Outlet Weir - Superficial Air Velocity 0.9 m/s.

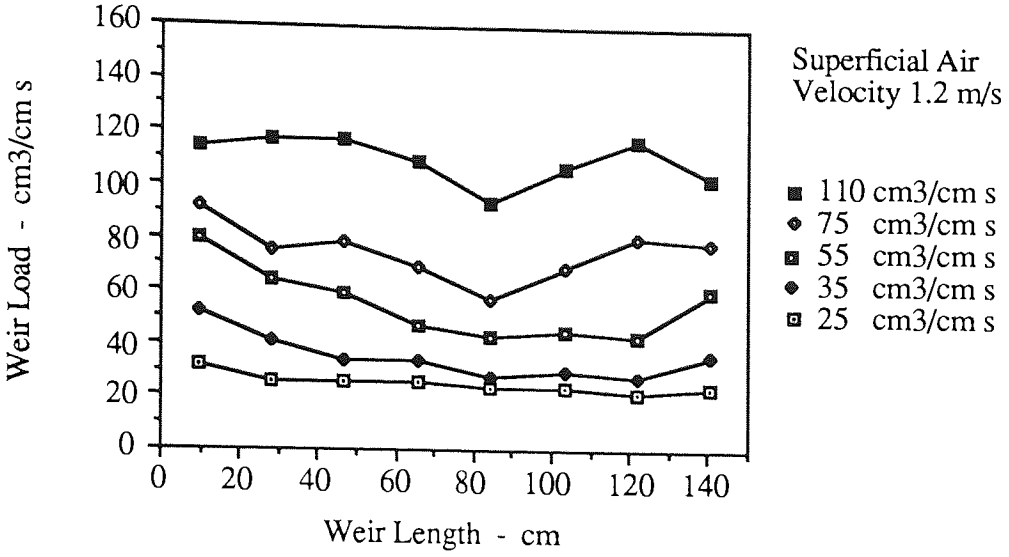

Fig. 8.9 Weir Load over Outlet Weir - Superficial Air Velocity 1.2 m/s.

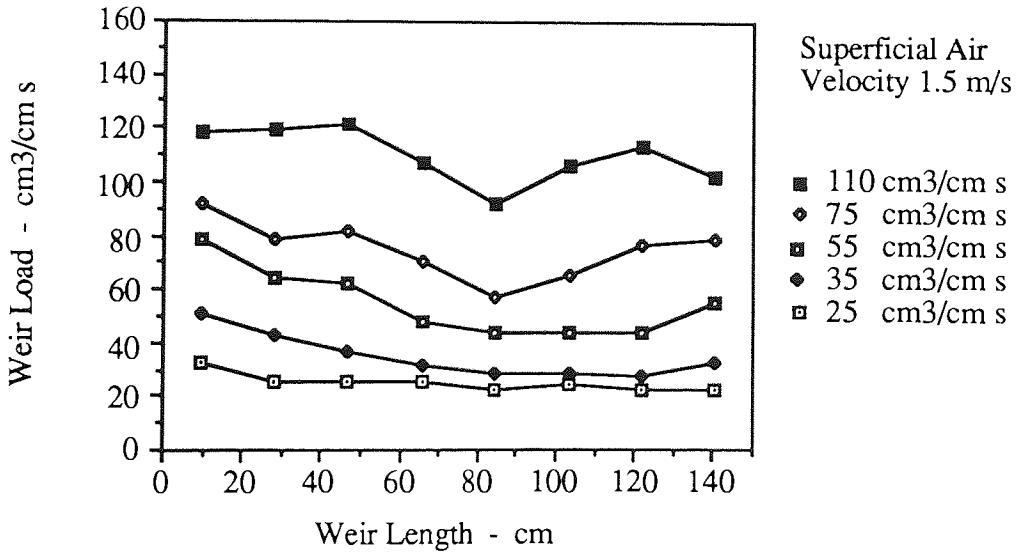

Fig. 8.10 Weir Load over Outlet Weir - Superficial Air Velocity 1.5 m/s.

The first comment is that all the figures look remarkably similar showing that the superficial air velocity has little effect on the water flow over the outlet weir for the investigated values.

At the low inlet weir load, 2.5×10^{-3} m^3/m s, the flow over the outlet weir is mainly uniform with a slightly greater flow per unit length at the edges of the outlet weir. This trend is continued for both the inlet weir loadings of 3.5 and 5.5×10^{-3} m^3/m s. However in these two cases the outlet flow is weighted to one side of the weir and is not as symmetrical as expected. The reason for this non-symmetry could be put down to one of a number of causes including poor liquid inlet condition, poor air flow through the tray, non-level outlet weir or out-of-levelness of the sieve tray. The most likely cause of the unsymmetrical flow over the outlet weir would be the levelness of the sieve tray itself.

At the high inlet weir loads of 7.5 and 11.0×10^{-3} m^3/m s the variation of the weir load measured over the outlet weir took on a different shape or form. Maximum weir loadings occurred at two points positioned at approximately one quarter and three quarters along the outlet weir. At these flow conditions the flow pointer experiment shows that near to 30% of the tray area is circulating, and that the circulating zones stretch from the edge of the inlet weir to the edge of the outlet weir. If the flow at the edge of the outlet weir is circulating, and at an obviously lower forward velocity than the main flow region, then the weir load at the edges of the outlet weir should be expected to be somewhat lower, thus pushing in the position of maximum outlet weir load from the edge of the weir. Also at the edges of the outlet weir some degree of choking was observed with an associated build-up of liquid, which was not apparent at the lower inlet weir loads.

This chapter has described the measured variations in the liquid hold-up over the tray area and the non-uniformity of the liquid flow over the outlet weir, the next chapter details how the effect of the liquid flow pattern on mass transfer was investigated.

CHAPTER 9

9. THE INVESTIGATION OF DISTILLATION TRAY FLOW PATTERNS BY THE USE OF THE WATER COOLING TECHNIQUE.

9.1 Introduction

The previous sections have clearly demonstrated that different liquid flow patterns are formed on distillation trays, depending on the operating conditions. In particular at high liquid flow rates, circulating regions are formed at the sides of the tray, while at low liquid flow rates, the liquid is always flowing in the forward direction. No direct measurements of liquid velocity have been made, but it is expected that variations in velocity exist. It is also expected that mass transfer on a tray will depend strongly on the liquid flow patterns. This chapter describes investigations into the effect of the liquid flow pattern on mass transfer by means of the water-cooling technique.

9.2 The Water-Cooling Technique

The water-cooling technique allows the effect of the liquid flow pattern on the mass transfer process to be investigated, using the model distillation system of air and water. Hot water is fed on to the crossflow test tray and is cooled by the passage of the rising air, evaporating a small fraction of the water. The progress of the heat transfer is observed by an array of temperature measuring devices placed over the active tray, which measure the water temperatures. The recorded temperature data are processed and lines of constant temperature are generated, which are presented in the form of two-dimensional temperature profiles over the tray area.

The flowrates used in the experimental programme were designed to enable temperature profiles to be generated for a matrix of superficial air velocities and water weir loadings. Also, throughout the programme different combinations of inlet gap and outlet weir were used with the air and water flowrates to gain a thorough understanding of the effects of each parameter.

9.3 Experimental Procedure

The inlet gap and outlet weir were configured as required and the experimental procedure carried out as described in Chapter 5, Section 5.4.2. During the water cooling process the water temperatures on the tray were continuously monitored and displayed on a personal computer. When initiated, the temperature data collection software carried out twenty complete scans of all the platinum resistance thermometers, at the end of which the option of recording the collected data was available. The criteria for accepting the collected data was that none of the inlet or outlet resistance thermometers varied by more than 0.1°C.

All the experiments were carried out in the previously described 2.44 m diameter air-water simulator. Table 9.1 contains the sieve tray design specification along with the experimental flowrates of air and water.

Column	Diameter	2.440 m
	Weir Length	1.500 m
	Flow Path Length	1.925 m
Tray	Material	Aluminium
	Free Area	10%
	Hole Size	1 mm
	Thickness	1 mm
	Edge of Hole	Sharp
Areas	Downcomer Area	0.243 m^2
	Active Area	4.189 m^2
	Free Area	0.419 m^2
Experimental Variables	Inlet Gap	10, 20 and 50 mm
	Outlet Weir	0, 10, 20 and 50 mm
	Superficial Air Velocity	1.0, 1.5 and 2.0 m/s
	Water Weir Load	25, 50, 100, 150, 200 and 250 $cm^3/cm\ s$

Table 9.1 Tray Design Specification and Experimental Variables.

9.4 Results And Discussion

The manual control over the heat supply allowed for the inlet water temperature to be held constant during a particular experiment, but it was not possible in the time available to set the inlet water temperature at exactly the same particular value for each experiment. Also the inlet air condition, i.e. dry and wet bulb temperatures, varied from day to day. To enable the data from all the experiments to be compared on a like basis, a reduced temperature was calculated and plotted. The reduced temperature, T_r, at a particular point is defined as

$$T_r = \frac{T - T_{wb}}{T_{in} - T_{wb}} \qquad (9.1)$$

where T is the measured water temperature at the given point, T_{in} is the water inlet temperature to the tray and T_{wb} is the wet bulb temperature of the entering air. By definition the entering air wet bulb temperature is the minimum temperature that can be exhibited by a simple air-water system. The water entering the tray has a reduced temperature, T_r, equal to 1.0, and the water leaving the tray has a reduced temperature lying between 1.0 and 0.0.

The complete set of temperature data for each experimental condition can be found in Appendix 5. In discussing the effects of the individual study parameters, reduced temperature profiles are referred to, which are contained in Figures 9.1 to 9.8 at the end of the chapter. Each Figure shows a different combination of inlet gap and outlet weir, and contains up to six different water weir loadings.

The general rule for the temperature profile Figures is that the inlet gap, outlet weir and superficial air velocity all remain constant in each Figure. The Figure subscript "a-f" indicates the relative water weir loading, "a" representing a low weir load and "f" representing a high weir load. The actual values of the water weir load associated with subscripts "a-f" are shown in Table 9.2.

Figure Subscript	Water Weir Loading (cm^3/cm s)
a	25
b	50
c	100
d	150
e	200
f	250

Table 9.2 Figure Subscripts and their Relationship to Water Weir Loading.

At the low water weir loadings of 25 and 50 cm^3/cm s, for all the Figures, the reduced temperature profiles reveal a degree of non-symmetry on the operating tray. This non-symmetry was probably due to very slight out-of-levelness, which shows that the technique is sensitive to levelness at low flowrates. The non-symmetry also makes a judgement on one temperature profile difficult, however if the particular temperature profile is seen as one of a series of profiles, a view beneath the non-symmetry can be obtained. For clarity, the discussion of the results will be concentrated on the left hand side of the tray and remarks concerning the non-symmetry will be included after the effect of each study parameter has been identified.

9.4.1 Effect of the Water Flowrate

Figures 9.1a-d are reduced temperature profiles for the test tray operating with an inlet gap of 10 mm, an outlet weir of 20 mm and a superficial air velocity of 1.5 m/s.

At the water weir loading of 25 cm^3/cm s, Figure 9.1a, the lines of constant reduced temperature enter the tray parallel to the inlet downcomer, satisfying the condition that at the inlet gap the reduced temperature, T_r, is equal to unity. Midway through the inlet half of the tray the temperature profiles have taken on a slight U-shape with the temperature, actual or reduced, at the sides of the tray slightly cooler than in the main flow region between the chordal weirs.

As the temperature profiles move into the outlet half of the tray, the reduced isotherm values become smaller, but of more significance is that the temperature difference between the edge and the centre of the tray has become greater, leading to more pronounced U-shaped profiles. The isotherm at the edge of the outlet weir, $T_r = 0.400$, connects with the column wall midway through the outlet half of the tray, or 350 mm from the outlet weir.

The reduced temperature is always decreasing in the direction of the outlet weir, and so the region bounded by the reduced isotherm, $T_r = 0.400$, and the column wall is classed as a stagnation zone rather than an area of circulating biphase. The difference between these two terms will become more apparent at the higher water weir loadings.

On increasing the water weir loading to 50 cm^3/cm s, Figure 9.1b, the overall temperature profile shapes are similar to those in Figure 9.1a for the weir loading of 25 cm^3/cm s. The profile shapes indicate that a better degree of symmetry exists for this higher weir loading. The isotherm at the edge of the outlet weir, in this case where $T_r = 0.450$, connects with the column wall 750 mm from the outlet weir, showing that the stagnation zone has increased in size.

As the water weir load is increased to 100 cm^3/cm s, Figure 9.1c, the overall temperature profile changes significantly from the aforementioned slight U-shaped temperature profiles to severe U-shaped profiles. Each reduced isotherm is initiated at the edge of the inlet downcomer and travels directly towards the corresponding edge of the outlet weir before moving transversely across the tray to meet its other end. This shape of profile suggests that plug flow is occurring in the main flow region between the chordal downcomers, due to the transverse reduced isotherms in this region. The width of the main flow region at the centre of the tray is comparable to the length of the inlet downcomer at 1500 mm.

As a consequence of all these isotherms being initiated at the edge of the inlet downcomer and travelling directly towards the edge of the outlet weir, a steep temperature gradient is observed between the main flow region where the temperatures are relatively high and the cooler side regions. The reduced isotherm which ends at the edge of the outlet weir, $T_r = 0.625$, virtually connects the edges of both the inlet and outlet weirs, and within the area bounded by this isotherm and the column wall, even more cooler isotherms can be seen! The water at the side of the tray is cooler than the average water temperature as it flows over the outlet weir. In this experiment, the lowest value of the reduced temperature at the side of the tray is $T_r = 0.550$, whereas the average reduced temperature of the water leaving the tray is $T_r = 0.637$.

At the lower weir loadings of 25 and 50 cm^3/cm s, stagnation zones were positioned in the outlet half of the tray adjacent to the column walls. However the phenomenon observed at the water weir loading of 100 cm^3/cm s is more significant in the way that it affects the overall temperature profile. This temperature pattern has occurred because

water jetting from the inlet gap has caused flow separation to occur near to the edge of the inlet weir, and associated with this flow separation is reverse flow at the sides of the tray.

If the hypothesis is taken in which the water flows out of the inlet gap, around the edge of the tray and over the outlet weir, then the temperature of the water would always be decreasing with distance travelled. Looking at Figure 9.1c, the water temperature decreases rapidly near to the edge of the inlet weir and reaches a minimum temperature 350 mm from the inlet weir. From this minimum temperature, the temperature of the water would have to increase as it continued its journey to the outlet weir. Obviously this is an impossible phenomenon and so the hypothesis that the water flows forward around the sides of the tray is incorrect.

The only feasible explanation why a minimum water temperature is measured at the side of an operating tray is that reverse flow or circulating flow are encountered in the side regions of the tray.

On increasing the water weir load even further to 150 cm^3/cm s, Figure 9.1d, the developed temperature profile is somewhat similar to Figure 9.1c. The change due to the increased weir load is that the circulating region at the side of the tray has increased in size, squeezing the width of the main flow region to 1350 mm at the centre of the tray, compared to the inlet downcomer length of 1500 mm. Also the overall temperature profile can now be described as symmetrical in comparison to the temperature profiles at the low weir loadings.

The temperature profiles generated by increasing the water weir load reveal that the weir load has a major influence on the developed flow pattern over the tray area. At the low weir loads, up to 50 cm^3/cm s, temperature profiles are only slightly U-shaped, showing only a slight deviation from plug flow, but at higher weir loads, 100 cm^3/cm s, the temperature profiles are severely U-shaped indicating the presence of flow separation and circulation on the tray. Again, it is worth pointing out that these results were collected with an inlet gap of 10 mm, an outlet weir of 20 mm and a superficial air velocity of 1.5 m/s. However, a glance over Figures 9.2a-f through to 9.8a-f confirms the effect of an increasing weir load.

9.4.2 Effect of the Inlet Gap

The effect of changing the inlet gap, on the generated reduced temperature profiles, is shown by the comparison of Figures 9.1a-d, 9.2a-f and 9.3a-f. Each of Figures 9.1, 9.2 and 9.3 contain temperature profiles for various water weir loadings, the test tray having

been configured with inlet gaps of 10, 20 and 50 mm respectively. For each of the temperature profiles presented, the outlet weir was fixed at 20 mm and the operating superficial air velocity was set at 1.5 m/s.

At the water weir load of 25 cm^3/cm s, Figures 9.1a, 9.2a and 9.3a, the inlet gap has little effect on the developed reduced temperature profiles, the difference between them being that on increasing the inlet gap a slight flattening of the U-shaped temperature profiles is observed. This flattening of the reduced temperature profiles is most apparent in the outlet right quarter of the tray where a non-symmetrical effect or a cool "finger" is seen emanating from the outlet weir. As the inlet gap is increased from 10 to 20 to 50 mm, the "finger" although not disappearing becomes less pronounced.

At the increased water weir load of 50 cm^3/cm s, Figures 9.1b, 9.2b and 9.3b, the overall temperature profiles are very much similar to those for the lower water weir load of 25 cm^3/cm s. However, the cool "finger" has become much smaller for each of the inlet conditions. This has resulted in the "finger" disappearing for the inlet gap of 50 mm.

At the water weir load of 100 cm^3/cm s combined with the 10 mm inlet gap, Figure 9.1c reveals the phenomena of flow separation and biphase circulation at the sides of the tray as described in Section 9.4.1. On increasing the inlet gap to 20 mm and then to 50 mm, Figures 9.2c and 9.3c, again severe U-shaped temperature profiles are exhibited, however in both cases the reduced temperature always falls in the direction of the outlet weir. Stagnation regions are visible at the sides of the tray towards the outlet weir, but no closed isotherms can be seen in the inlet half of the tray.

At 150 cm^3/cm s both Figures 9.1d and 9.2d are showing signs of biphase circulation at the sides of the tray, where closed isotherms are seen. The width of the main flow regions are 1350 and 1500 mm for the 10 and 20 mm inlet gaps respectively. The temperature profile for the inlet gap of 50 mm does not reveal any closed isotherms near to the inlet downcomer, but again the temperature profiles are severely U-shaped. The stagnation zones that were positioned near to the outlet weir have increased in size and stretch back, along the column wall, into the inlet half of tray by about 350 mm.

The water weir load of 150 cm^3/cm s was the maximum weir load used in conjunction with the inlet gap of 10 mm. Weir loads of 200 and 250 cm^3/cm s were investigated with the larger inlet gaps of 20 and 50 mm. The generated reduced temperature profiles for these high weir loading conditions can be found in Figures 9.2e-f and 9.3e-f.

The temperature profiles generated by increasing the inlet gap do reveal an influence on

the developed flow pattern over the tray area. At low weir loads, up to 50 cm^3/cm s, temperature profiles are only slightly affected by the changed inlet condition, but at higher weir loads of 100 cm^3/cm s and above, the temperature profiles show that the width of the main flow region can be maintained by using a larger inlet gap, whereas if a small inlet gap is used closed circulations are developed at the side regions of the tray.

These results were based on the test tray having been configured with a 20 mm outlet weir and being operated with a superficial air velocity of 1.5 m/s.

9.4.3 Effect of the Outlet Weir

The effect of changing the outlet weir, on the generated reduced temperature profiles, is shown by the comparison of Figures 9.4a-f, 9.5a-f, 9.2a-f and 9.6a-f. The figures contain temperature profiles for various water weir loadings, the test tray having been configured with outlet weirs of 0, 10, 20 and 50 mm respectively. Note that the Figure numbers are out of arithmetic sequence.

At the water weir load of 25 cm^3/cm s, Figures 9.4a, 9.5a, 9.2a and 9.6a, the outlet weir has little if any effect on the temperature profiles in the inlet half of the tray. In the outlet half of the tray, the non-symmetrical profiles reveal that disturbances at the exit of the tray protrude further into the tray with increasing outlet weir height. The "finger" feature, as mentioned earlier, serves to show this effect. With no outlet weir, Figure 9.4a, the "finger"feature can hardly be detected, but as the outlet weir height is raised to 10, 20 and 50 mm, Figures 9.5a, 9.2a and 9.6a, the "finger" becomes more prominent, reaching back 750 mm into the centre of the tray from the outlet weir.

On increasing the water flow to 50 cm^3/cm s, Figures 9.4b, 9.5b, 9.2b and 9.6b, the above trend is confirmed. At this higher weir load the "finger" does not reach quite as far back into the tray, barely 300 mm when the outlet weir is at 50 mm, Figure 9.6b. The stagnation zones can now be observed in the outlet half of the tray adjacent to the tray walls.

Figures 9.4c, 9.5c, 9.2c and 9.6c present reduced temperature profiles for a water weir load of 100 cm^3/cm s. The configuration with no outlet weir, Figure 9.4c, shows the presence of U-shaped profiles over the tray area, where cooler biphase exists at the sides of the tray. On increasing the outlet weir to 50 mm, Figure 9.6c, the temperature profiles become severely U-shaped and closed isotherms can be seen in the inlet half of the tray adjacent to the column wall.

In the outlet half of the tray, an area of increased mixing can be seen to form just in front of the outlet weir. This observation is predominantly noticed when the high outlet weir of 50 mm is used, and again the non-symmetrical feature connected to the outlet weir serves as a demonstration. At 100 cm^3/cm s the increasing outlet weir has caused the "finger" to increase in prominence, but at the high outlet weir of 50 mm the "finger" has smeared and decreased in prominence. This change is due to the increased mixing in the vicinity of the outlet weir, causing warmer water to enter the cooler "finger". The increased mixing could come about by a diffusional effect with water rebounding off the high outlet weir.

Increasing the water weir load further has a marginal change on the overall temperature profiles for all the outlet weirs, although the higher weir loads of 200 and 250 cm^3/cm s do highlight the enhanced mixing associated with the 50 mm outlet weir.

9.4.4 Effect of the Superficial Air Velocity

The effect of changing the superficial air velocity, on the generated reduced temperature profiles, is shown by the comparison of Figures 9.7a-f, 9.2a-f and 9.8a-f. The Figures contain temperature profiles for various water weir loadings, the test tray being operated with superficial air velocities of 1.0, 1.5 and 2.0 m/s respectively. Note that the figure numbers are out of arithmetic sequence.

The interpretation of the reduced temperature profiles, for the effect of the superficial air velocity, proved difficult due to the different number of reduced isotherms generated for each superficial air velocity. The definition of the reduced temperature allows only one fixed value on the tray, that of the inlet water which has a reduced temperature of 1.0. All other values of the reduced temperature lie somewhere between 1.0 and 0.0, and the two-dimensional reduced temperature profiles are plotted using a fixed reduced temperature interval of 0.025. So the limitation of the reduced temperature profiles must be borne in mind when viewing the contour figures.

At the water weir load of 25 cm^3/cm s, Figures 9.7a, 9.2a and 9.8a, the higher superficial air velocities reveal an increased degree of mixing on the tray. The region where this increase in mixing is most apparent is the stagnation zone positioned in the outlet half of the tray adjacent to the column wall. At the superficial air velocity of 1.0 m/s, Figure 9.7a, the stagnation zone consists of three reduced isotherms, namely 0.525, 0.500 and 0.475. On increasing the superficial air velocity to 2.0 m/s, extra isotherms are expected to be created due to the increased mass flow of air, but Figure 9.8a reveals that the number of reduced isotherms has now decreased to two, 0.375 and 0.350. The

explanation for this reduction is that of increased mixing/turbulence associated with the higher superficial air velocity.

Another observed effect is due to a combination of an effective air flow baffle and the superficial air velocity itself. The sieve tray is supported on a structure consisting of angle beams, and at the centre of the column, along the flow path length, one such angle is present as shown in Figure 9.9.

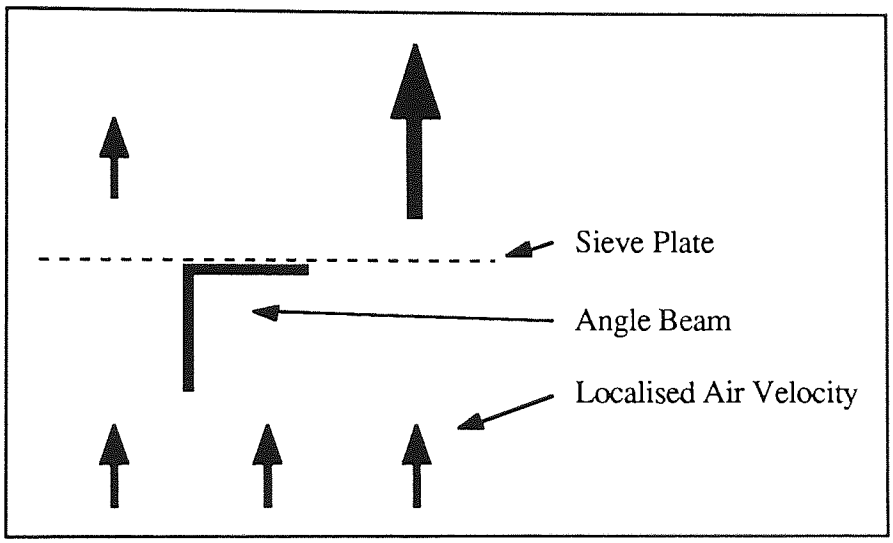

Fig. 9.9 Angle Beam Acting as Air Flow Baffle.

At the low superficial air velocity of 1.0 m/s the effect of the angle acting as a flow baffle is minimal as shown in Figure 9.7a, but at the increased superficial air velocities of 1.5 and 2.0 m/s, Figures 9.2a and 9.8a, the baffling effect becomes very pronounced. This obstruction to the air flow causes a localised high air velocity on the open side of the angle, which shows up as a temperature imbalance over the angle beam.

At 100 cm^3/cm s and even more so at 150 cm^3/cm s the emergence of liquid channelling occurs for the higher superficial air velocities, Figures 9.7d, 9.2d and 9.8d. The increased superficial air velocity seems to prevent the formation of non-forward velocity components. However, previously it was pointed out that associated with higher superficial air velocities was an increased degree of turbulence or mixing. This increase in mixing with increasing air superficial velocity is now dominated by the bulk liquid flow effects, but its presence can still be detected by looking at the separation point near to the edge of the inlet weir. At the superficial air velocity of 1.5 m/s the flow separates at the edge of the inlet weir, Figure 9.2d, whereas when the superficial air velocity is increased

to 2.0 m/s the point of separation has moved 400 mm away from the edge of the inlet weir, Figure 9.8d, and this delay in separation is due to the increased mixing effects.

9.5 Efficiency Calculations

The air-water test tray while operating can be represented by Figure 9.10.

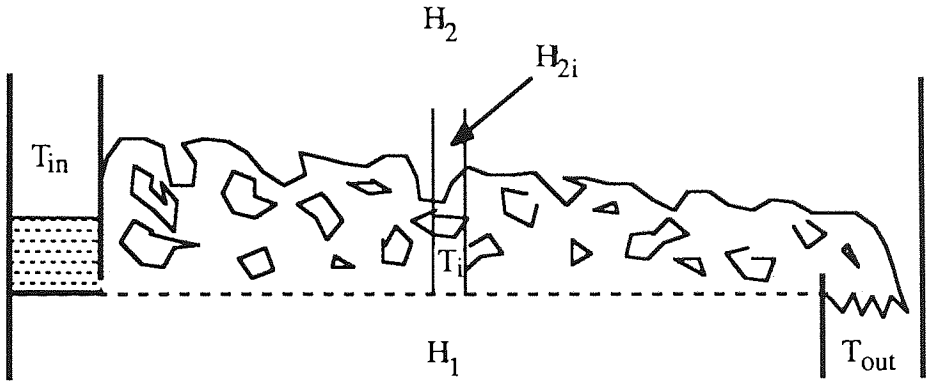

Fig. 9.10 Schematic Diagram of an Operating Tray.

Hot water enters the test tray at a temperature T_{in}, and the average temperature of the water leaving the tray is T_{out}. The air enters the tray from below with a uniform enthalpy of H_1 and after passing through the biphase leaves with an enthalpy of H_2. The Murphree tray efficiency, E_{mv}, based on the enthalpy of the air is defined as:

$$E_{mv} = \frac{H_2 - H_1}{H^*_{Tout} - H_1} \qquad (9.1)$$

where H_{Tout} is the enthalpy of the air in equilibrium with the average temperature of the water leaving the tray. The saturated air enthalpy, in equilibrium with water at a particular temperature, can be calculated from equations given in BS 2520.

The Murphree point efficiency based on the enthalpy of the air is defined as:

$$E_{og} = \frac{H_{2i} - H_1}{H^*_{Ti} - H_1} \qquad (9.2)$$

where T_i is the local water temperature on the tray and H_{Ti} is the enthalpy of the air in

equilibrium with the local water temperature.

Temperature data concerning the water phase is collected during the water cooling process, for fixed operating conditions of air and water flowrates. The overall heat balance

$$G\,(H_{2i} - H_1) = LCp\,(T_{in} - T_{out}) \qquad (9.3)$$

yields the average enthalpy of the leaving air and allows the calculation of the Murphree tray efficiency. The Murphree point efficiency, averaged over the tray area, is then determined using the following relationship which merely averages the air enthalpy leaving above each of the 108 temperature measuring devices.

$$\frac{1}{n}\sum_{i=1}^{n} H_{2i} = H_2 \qquad (9.4)$$

A computer program written in Fortran 77 was used to determine the Murphree point and tray efficiencies and is given in Appendix 6. The efficiencies along with the enhancement ratios are presented in Tables 9.3, 9.4 and 9.5, for inlet gaps of 10, 20 and 50 mm respectively. To supplement the tables, three Figures are presented which show how the point efficiency, tray efficiency and the enhancement ratio vary against the water weir load.

Figure 9.11 shows how the Murphree point efficiency, averaged for each water weir load, varies with the weir load. At the weir loading of 25 $cm^3/cm\ s$ the point efficiency is measured to be 47%, but this value rises up rapidly to 80% as the weir load increases to 100 $cm^3/cm\ s$. Further increases in the weir load lead to a marginal increase in the point efficiency, the maximum measured point efficiency being 83%.

Figure 9.12 shows how the Murphree tray efficiency, averaged for each water weir load, varies with the weir load. The tray efficiency at the weir load of 25 $cm^3/cm\ s$ is measured at 80%. On increasing the weir loading to 50 $cm^3/cm\ s$ the tray efficiency rises to its maximum value of 114% from where the tray efficiency falls off with increasing weir load. An interesting point to note is that the 50 mm inlet gap yields a better tray efficiency than the 20 mm inlet gap, at the flowrates of 100 $cm^3/cm\ s$ and above, whereas the point efficiency values for the two inlet gaps are identical. This suggests that the flow pattern exhibited by the tray with the 50 mm inlet gap is superior, in the respect of tray efficiency, than that exhibited by the tray with the 20 mm inlet gap. This observation leads to Figure 9.13, where the enhancement ratio or the enhancement of point efficiency is plotted against the weir load.

Inlet Gap - 10 mm													
Outlet Weir - mm		0			10			20			50		
Air Velocity - m/s		1.0	1.5	2.0	1.0	1.5	2.0	1.0	1.5	2.0	1.0	1.5	2.0
Water Load - $cm^3/cm\ s$	Efficicency - %												
25	E_{og}	45	44	42	51	48	42	51	50	47	56	58	53
	E_{mv}	75	71	77	91	90	85	86	91	88	93	110	99
	E_{mv} / E_{og}	1.65	1.63	1.82	1.75	1.86	2.01	1.67	1.80	1.89	1.67	1.89	1.86
50	E_{og}	71	71	65	72	68	63	74	74	67	86	87	77
	E_{mv}	109	113	112	114	110	112	113	123	116	137	153	136
	E_{mv} / E_{og}	1.52	1.60	1.72	1.60	1.62	1.78	1.54	1.66	1.73	1.60	1.76	1.76
100	E_{og}	83	83	77	78	76	73	81	83	76	87	93	86
	E_{mv}	102	105	104	99	100	97	102	107	105	114	122	118
	E_{mv} / E_{og}	1.23	1.27	1.34	1.27	1.30	1.34	1.26	1.28	1.38	1.30	1.31	1.37
150	E_{og}	85	84	78	83	78	77	83	84	78	93	96	87
	E_{mv}	89	89	88	90	86	89	89	93	91	110	109	103
	E_{mv} / E_{og}	1.04	1.07	1.12	1.08	1.09	1.15	1.07	1.11	1.17	1.17	1.14	1.18

Table 9.3 Measured Murphree Efficiency Data - 10 mm Inlet Gap.

Inlet Gap - 20 mm													
Outlet Weir - mm		0			10			20			50		
Air Velocity - m/s		1.0	1.5	2.0	1.0	1.5	2.0	1.0	1.5	2.0	1.0	1.5	2.0
Water Load - cm^3/cm s	Efficicency - %												
25	E_{og}	41	42	40	45	43	40	47	51	47	57	56	50
	E_{mv}	66	69	64	77	76	68	79	84	82	96	93	85
	E_{mv} / E_{og}	1.61	1.62	1.60	1.69	1.74	1.68	1.68	1.64	1.75	1.68	1.65	1.70
50	E_{og}	65	65	59	68	67	62	71	76	68	85	83	75
	E_{mv}	100	101	90	107	111	100	110	121	107	132	125	124
	E_{mv} / E_{og}	1.55	1.54	1.52	1.58	1.64	1.60	1.55	1.59	1.57	1.55	1.52	1.67
100	E_{og}	72	77	71	73	80	71	77	82	78	87	88	81
	E_{mv}	94	100	93	97	109	103	98	107	107	113	112	109
	E_{mv} / E_{og}	1.31	1.30	1.33	1.32	1.36	1.44	1.28	1.31	1.37	1.30	1.26	1.35
150	E_{og}	78	80	75	81	81	75	80	86	80	87	91	83
	E_{mv}	93	91	88	98	94	91	94	99	94	104	103	96
	E_{mv} / E_{og}	1.20	1.13	1.17	1.20	1.16	1.21	1.17	1.15	1.18	1.19	1.13	1.16
200	E_{og}	79	83	77	84	82	78	80	88	80	86	91	86
	E_{mv}	88	89	84	93	88	87	87	94	87	98	97	93
	E_{mv} / E_{og}	1.10	1.07	1.09	1.11	1.07	1.12	1.08	1.07	1.09	1.13	1.06	1.08
250	E_{og}	79	84	79	82	83	79	79	87	84	85	93	84
	E_{mv}	80	84	81	84	83	82	79	88	87	89	95	87
	E_{mv} / E_{og}	1.01	1.01	1.03	1.02	1.01	1.04	1.00	1.00	1.03	1.04	1.02	1.03

Table 9.4 Measured Murphree Efficiency Data - 20 mm Inlet Gap.

Inlet Gap - 50 mm													
Outlet Weir - mm		0			10			20			50		
Air Velocity - m/s		1.0	1.5	2.0	1.0	1.5	2.0	1.0	1.5	2.0	1.0	1.5	2.0
Water Load - cm^3/cm s	Efficicency - %												
25	E_{og}	43	45	42	44	41	38	48	48	41	50	53	48
	E_{mv}	65	76	73	70	66	64	80	84	71	80	89	87
	E_{mv} / E_{og}	1.52	1.67	1.74	1.58	1.62	1.68	1.67	1.74	1.71	1.59	1.69	1.80
50	E_{og}	71	69	65	69	65	60	68	69	63	75	79	74
	E_{mv}	105	110	105	111	103	100	110	110	104	112	124	125
	E_{mv} / E_{og}	1.49	1.60	1.61	1.61	1.58	1.66	1.62	1.60	1.66	1.49	1.57	1.70
100	E_{og}	76	84	78	75	79	70	73	82	76	81	88	83
	E_{mv}	100	117	116	101	109	100	99	115	113	107	119	118
	E_{mv} / E_{og}	1.33	1.39	1.48	1.34	1.37	1.43	1.35	1.41	1.50	1.31	1.35	1.43
150	E_{og}	76	88	82	75	78	74	75	83	75	79	93	85
	E_{mv}	95	110	109	93	98	94	91	102	95	94	113	107
	E_{mv} / E_{og}	1.24	1.25	1.33	1.24	1.23	1.27	1.22	1.23	1.26	1.20	1.21	1.26
200	E_{og}	78	94	87	74	83	78	74	85	78	79	92	88
	E_{mv}	93	113	108	88	95	93	87	100	94	90	106	103
	E_{mv} / E_{og}	1.19	1.20	1.24	1.18	1.15	1.19	1.17	1.17	1.20	1.15	1.14	1.17
250	E_{og}	75	96	91	74	86	81	73	85	81	75	91	89
	E_{mv}	85	110	109	84	97	92	82	98	93	82	101	101
	E_{mv} / E_{og}	1.14	1.15	1.19	1.13	1.13	1.14	1.13	1.15	1.15	1.09	1.11	1.13

Table 9.5 Measured Murphree Efficiency Data - 50 mm Inlet Gap.

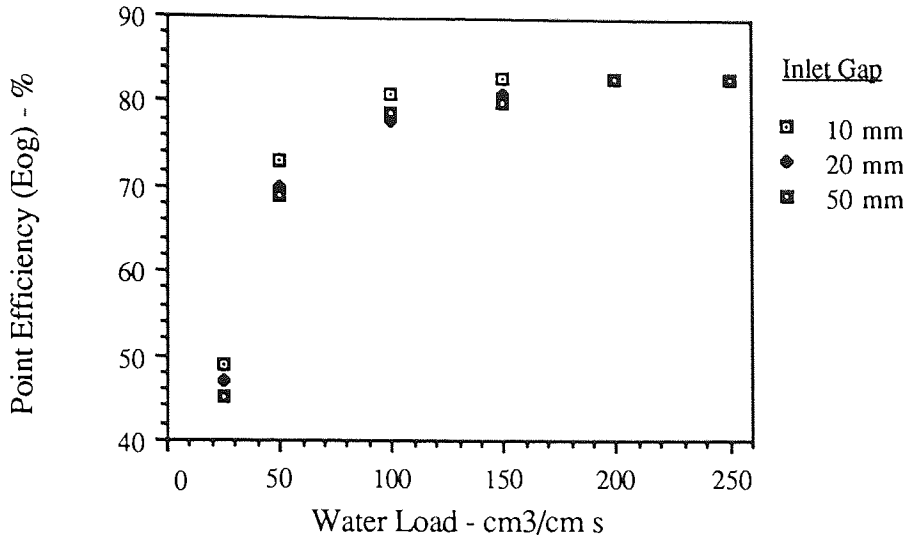

Fig. 9.11 Graph of Measured Point Efficiency against Weir Load.

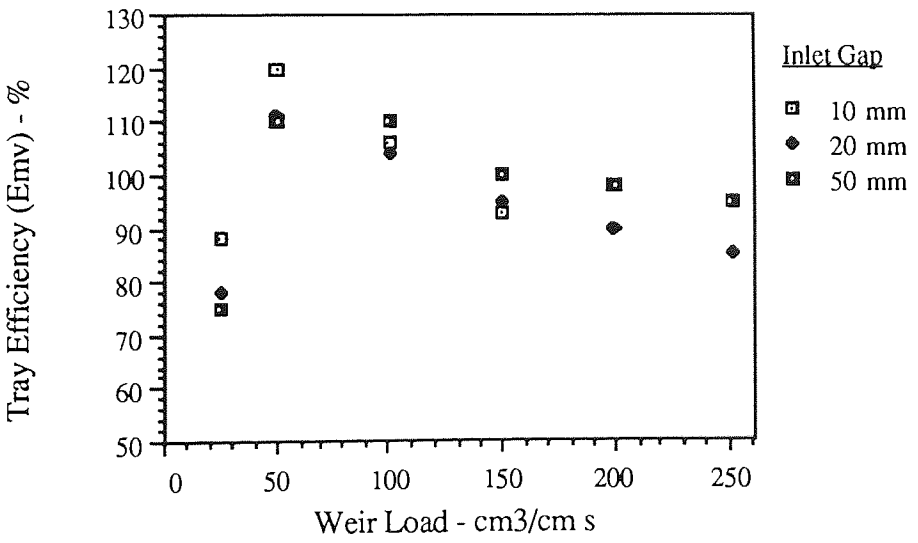

Fig. 9.12 Graph of Measured Tray Efficiency against Weir Load.

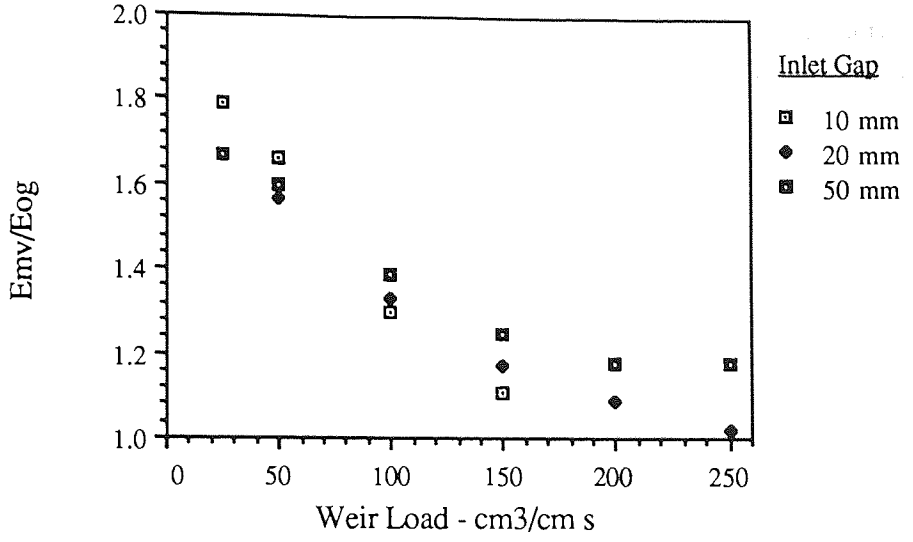

Fig. 9.13 Graph of Measured Enhancement Ratio against Weir Load.

At the low weir load of 25 cm^3/cm s the lowest measured tray efficiency of 80% was recorded, however this low tray efficiency was combined with a low point efficiency of 47%. The result of the low tray efficiency and the even lower point efficiency is a high enhancement factor for the point efficiency of 1.71. Although the tray efficiency rises as the weir load increases from 25 cm^3/cm s, the point efficiency also rises but at a steeper rate and the enhancement factor falls from its maximum value of 1.71 with increasing weir load.

The tray configured with a 10 mm inlet gap gives the greatest point efficiency enhancement factor for weir loads up to 75 cm^3/cm s. Increasing the weir loading above 75 cm^3/cm s and the larger inlet gaps return the greater point efficiency enhancements, with the 50 mm inlet gap performing better than the intermediate 20 mm gap.

9.5.1 Discussion of Efficiency Results

In simple distillation tray models where plug flow of liquid with back-mixing is assumed, the enhancement of the point efficiency, E_{mv}/E_{og}, increases with increasing λ (mG/L). Similarly with the stagnant regions model of Porter and Lockett (1972), E_{mv}/E_{og} depends upon λ

In distillation, an optimum design near to the minimum reflux ratio means that λ, the ratio of the equilibrium line to the operating line, is near to 1.0. Most practical distillation is covered with λ in the range 0.7 to 1.3, even though an optimal designs in vacuum distillation yields a low weir load and in pressure distillation a high weir load. However

when using the water cooling technique to simulate the effect of flow patterns on mass transfer it is not possible to separate the value of λ from the air and water flowrates. Thus at high water flowrates λ values approach 0.5 which are much lower than λ is at low water flowrates which approach 12.0. Nevertheless, it is proposed with some confidence that the efficiency results determined provide a sound basis for the evaluation of any future theoretical models of mass transfer, based on a theoretical description of the real flow pattern.

Before leaving the discussion of tray efficiency, it is important to consider the way in which tray efficiency in a column of single pass trays is seriously reduced by the cumulative effect of vapour passing from one stagnant region to another. Porter and Lockett (1972) discussed the case of single pass trays stacked one above another. They found that for a single tray the estimated reduction in tray efficiency due to liquid channelling was only such to restrict the tray efficiency to a value close to that of the point efficiency, even for trays of 10.0 m in diameter or more, but with ten trays above each other, the column and tray efficiency were predicted to be much less than the point efficiency.

Reference to the temperature profiles in Figures 9.1 to 9.8 show that in the circulating regions the water temperature is reduced even below that leaving the tray. This implies that the enthalpy change of the air passing through the circulating region will be much reduced and a similar form of bypassing may be expected to occur in distillation.

Thus all in all, the water cooling experiments have confirmed that channelling and circulation are the cause of a serious loss of efficiency in distillation columns where they occur.

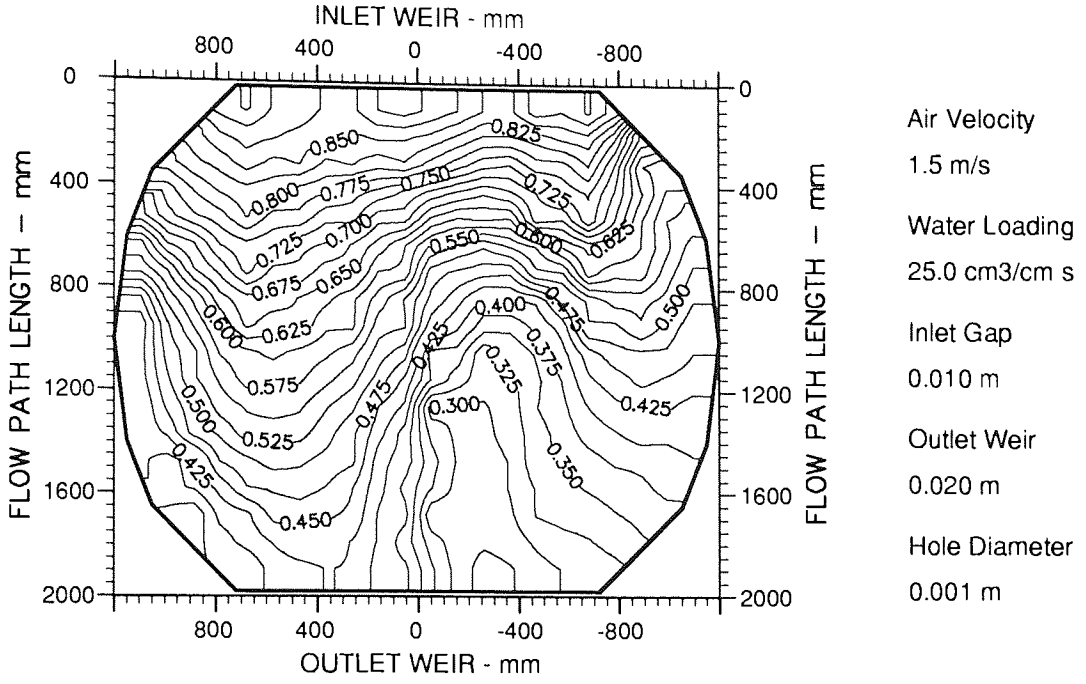

Fig. 9.1a Two-Dimensional Reduced Temperature Contours.

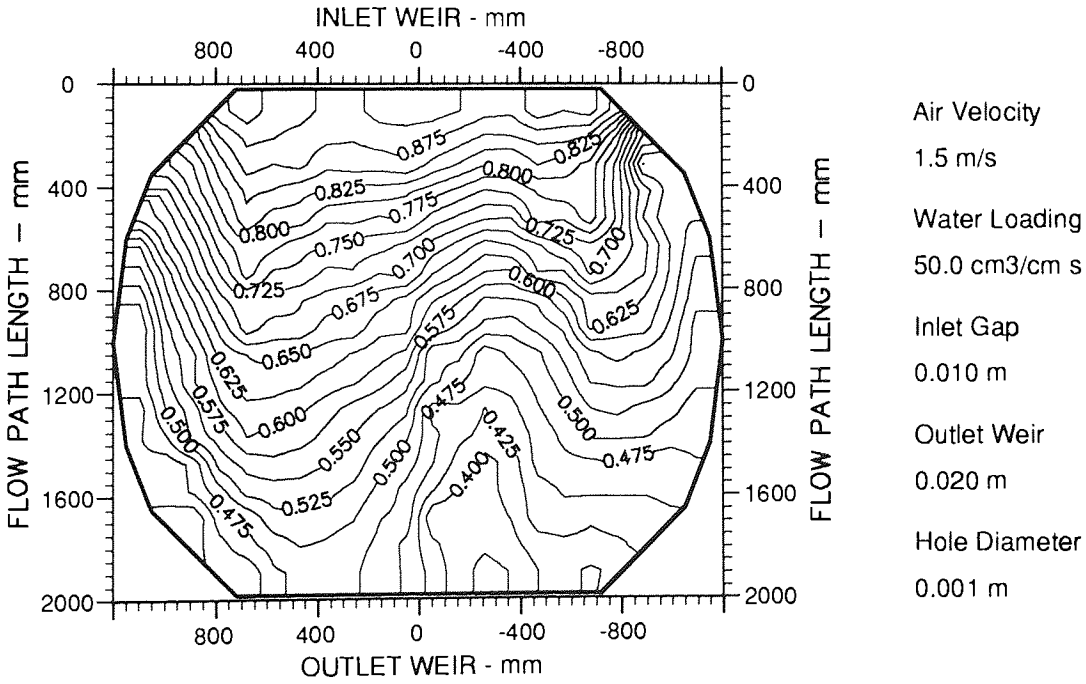

Fig. 9.1b Two-Dimensional Reduced Temperature Contours.

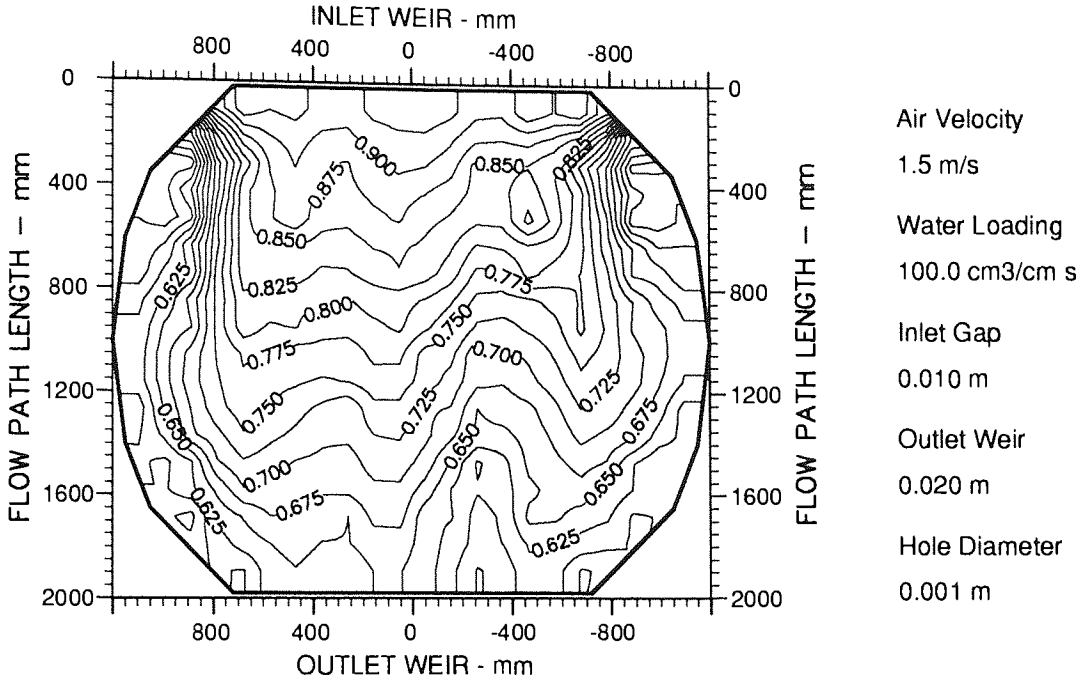

Fig. 9.1c Two-Dimensional Reduced Temperature Contours.

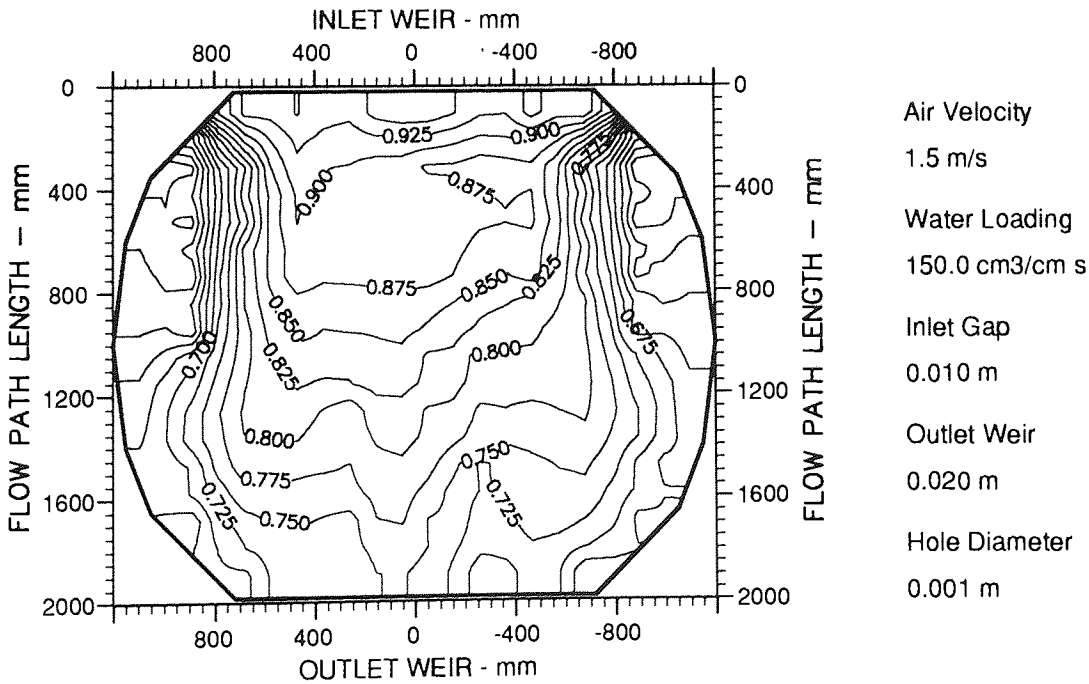

Fig. 9.1d Two-Dimensional Reduced Temperature Contours.

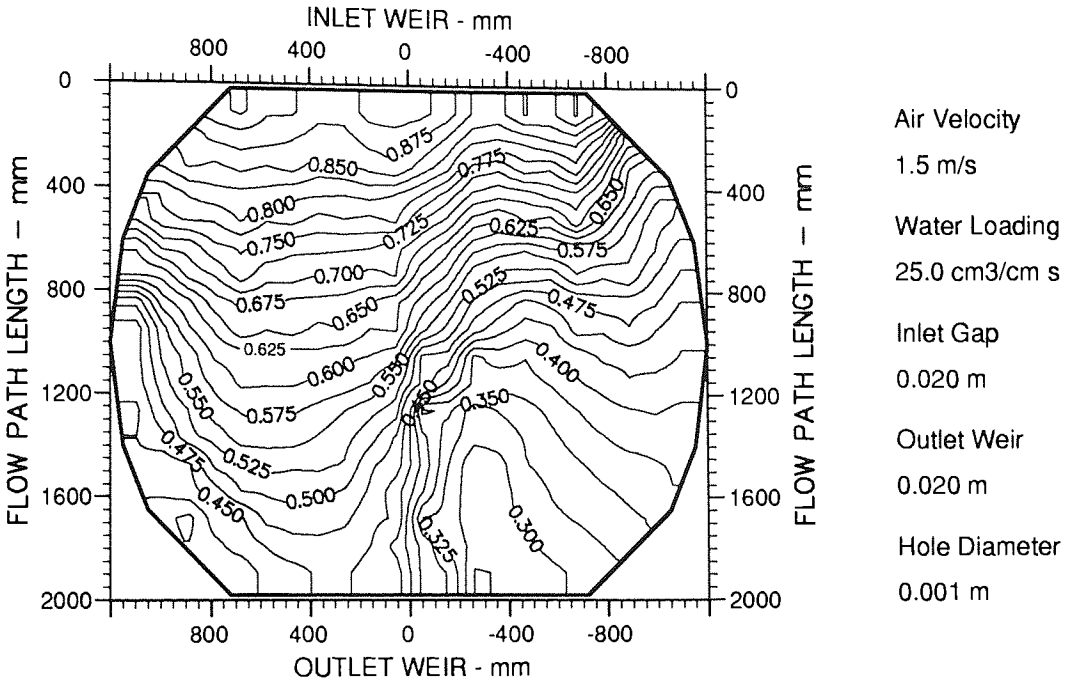

Fig. 9.2a Two-Dimensional Reduced Temperature Contours.

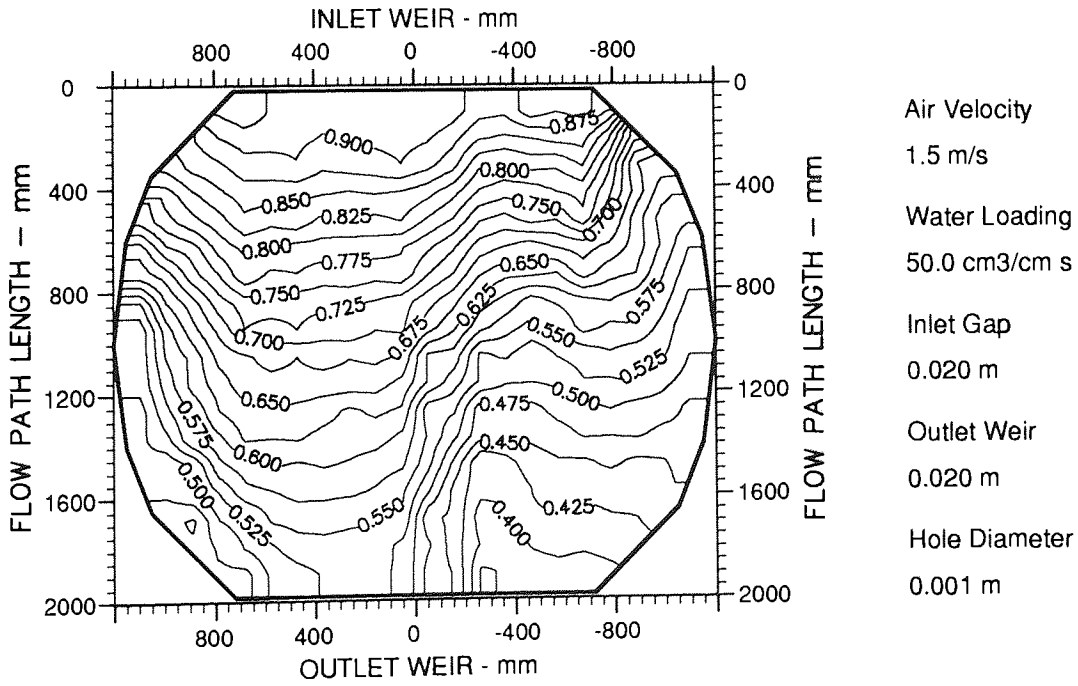

Fig. 9.2b Two-Dimensional Reduced Temperature Contours.

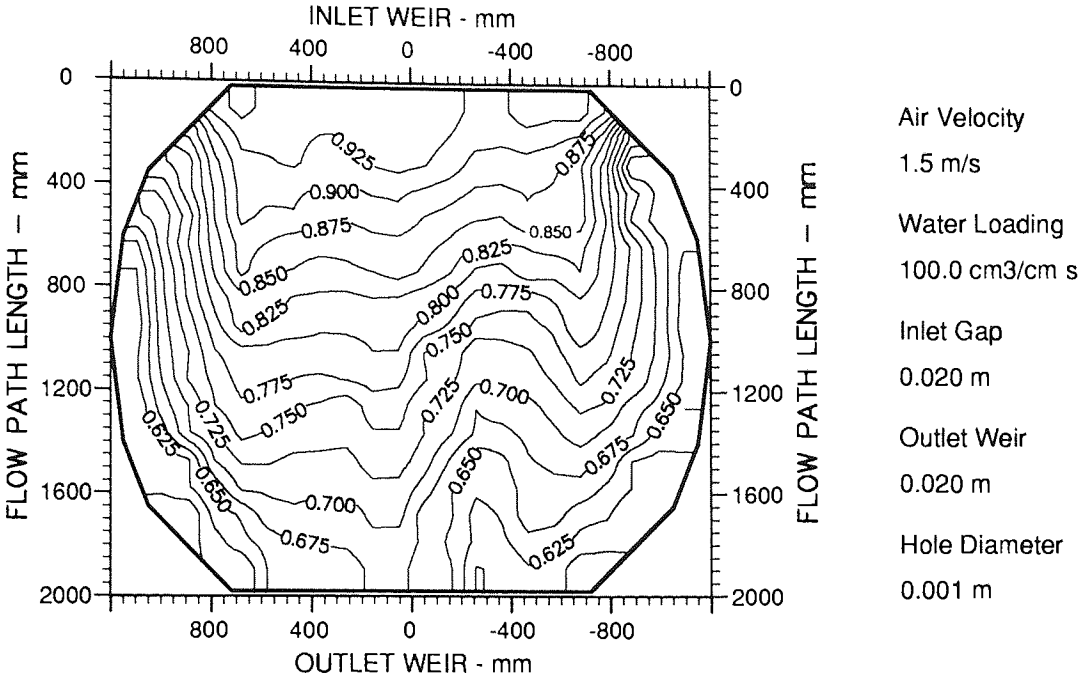

Fig. 9.2c Two-Dimensional Reduced Temperature Contours.

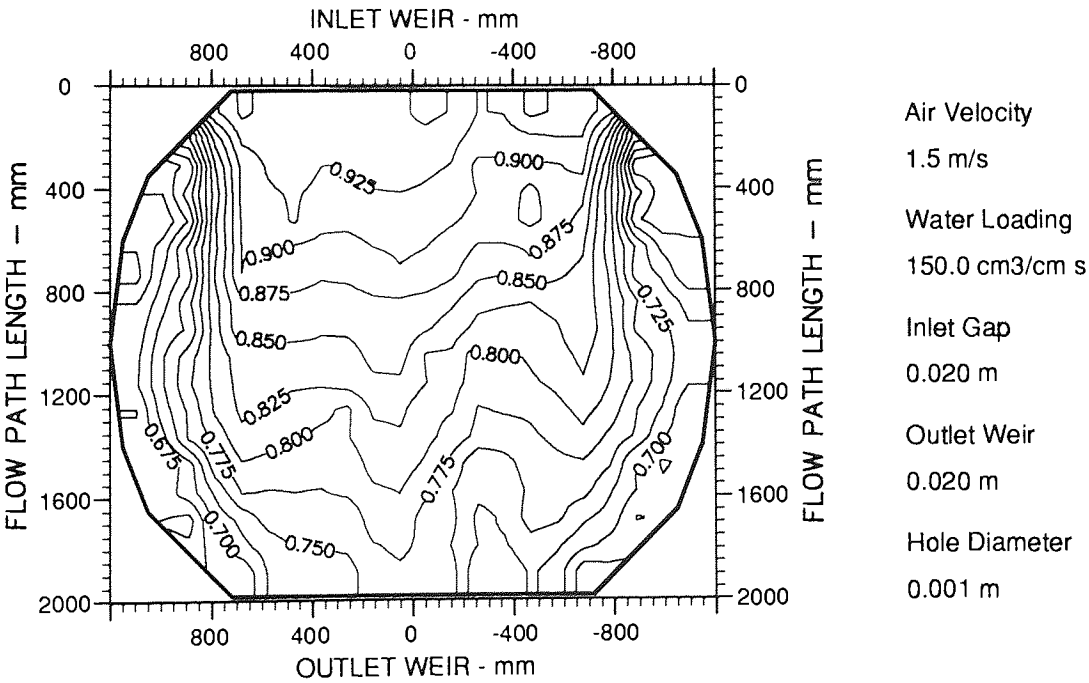

Fig. 9.2d Two-Dimensional Reduced Temperature Contours.

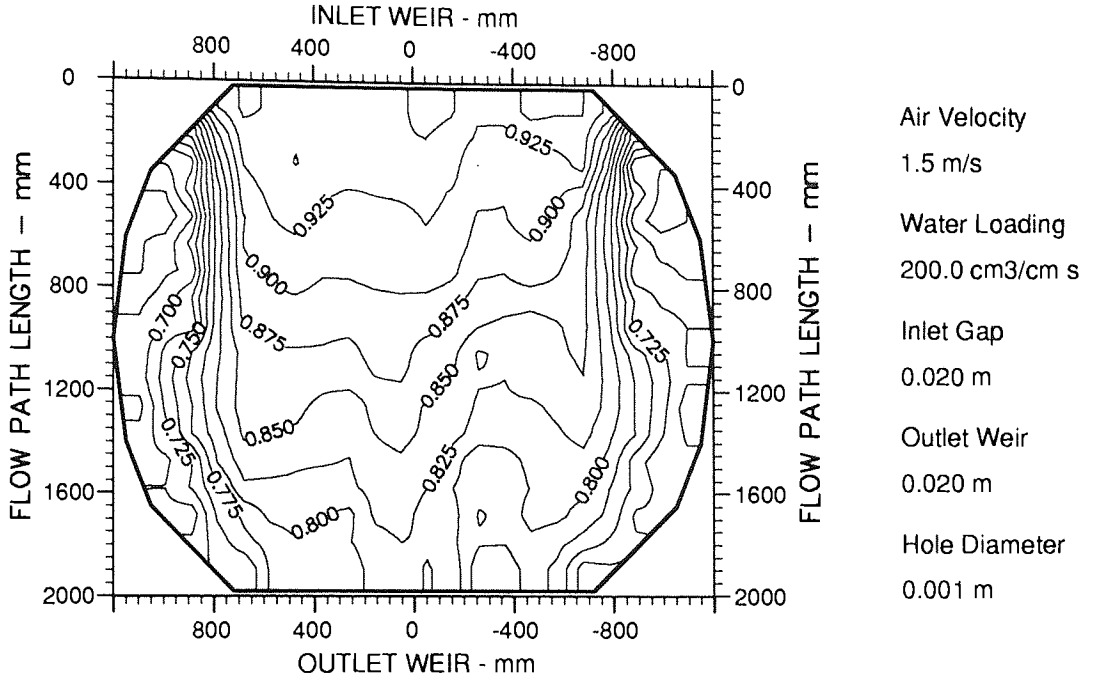

Fig. 9.2e Two-Dimensional Reduced Temperature Contours.

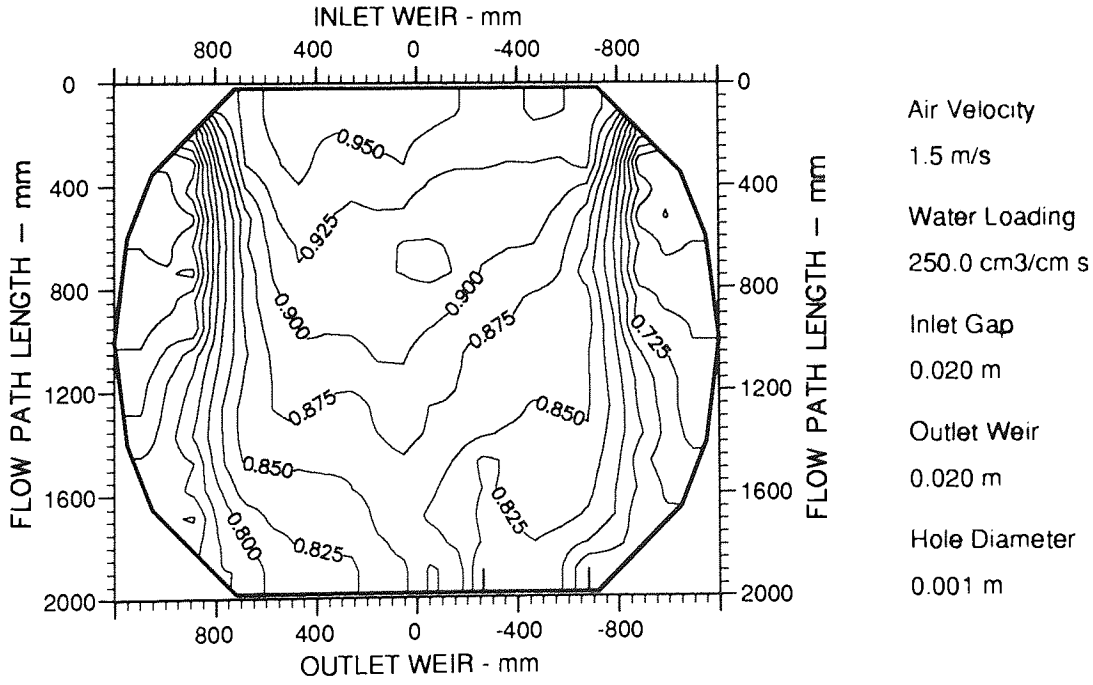

Fig. 9.2f Two-Dimensional Reduced Temperature Contours.

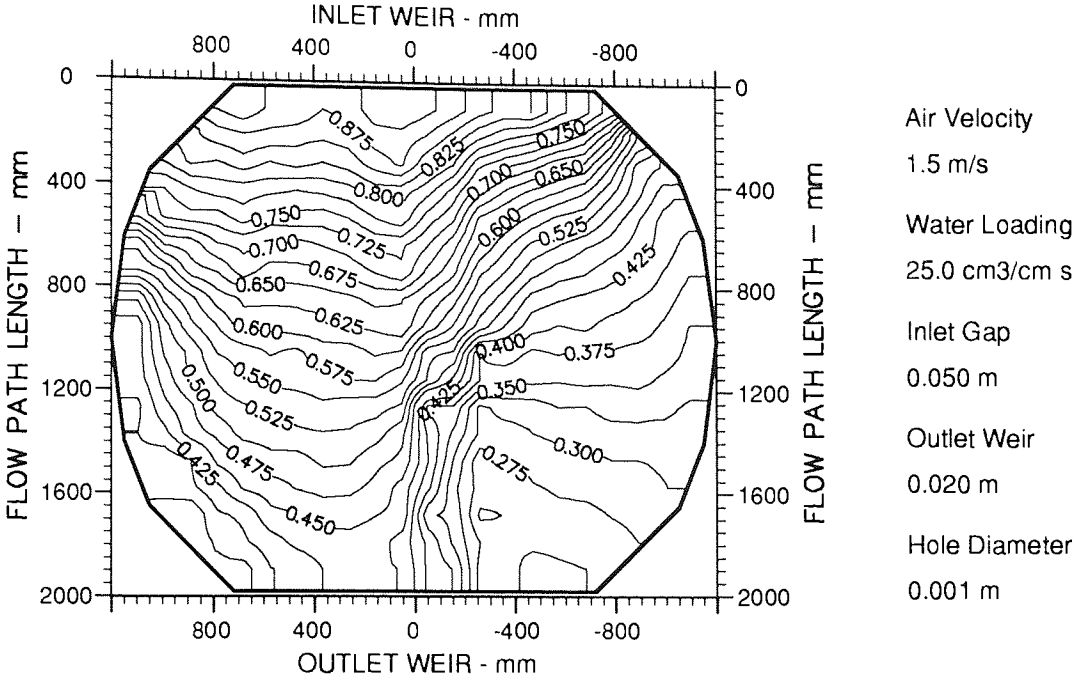

Fig. 9.3a Two-Dimensional Reduced Temperature Contours.

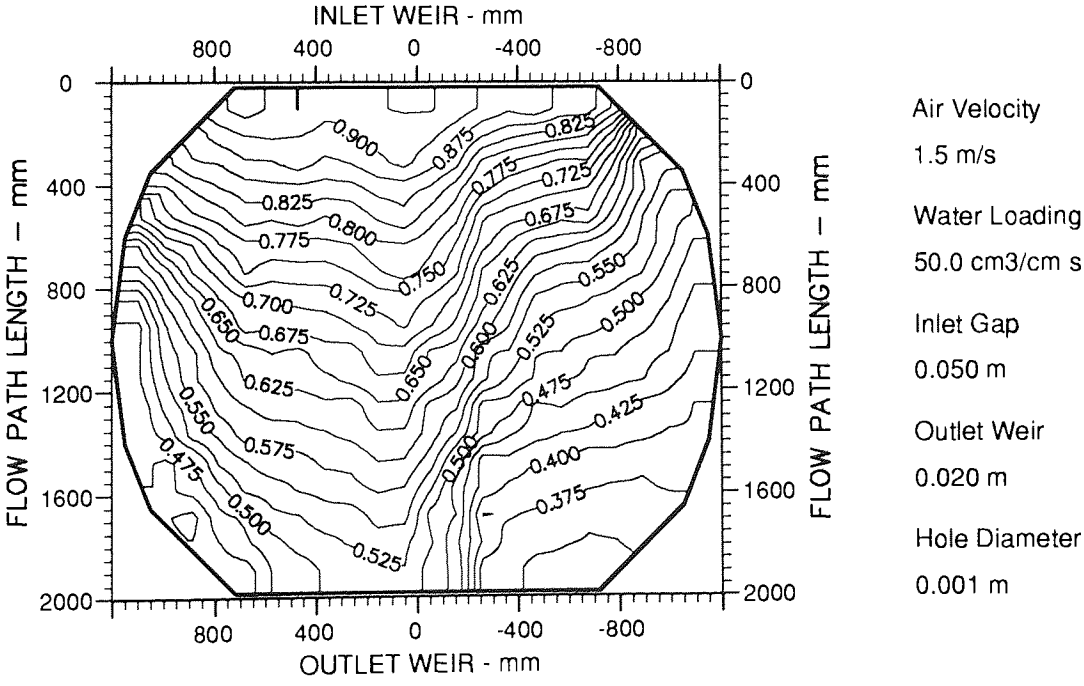

Fig. 9.3b Two-Dimensional Reduced Temperature Contours.

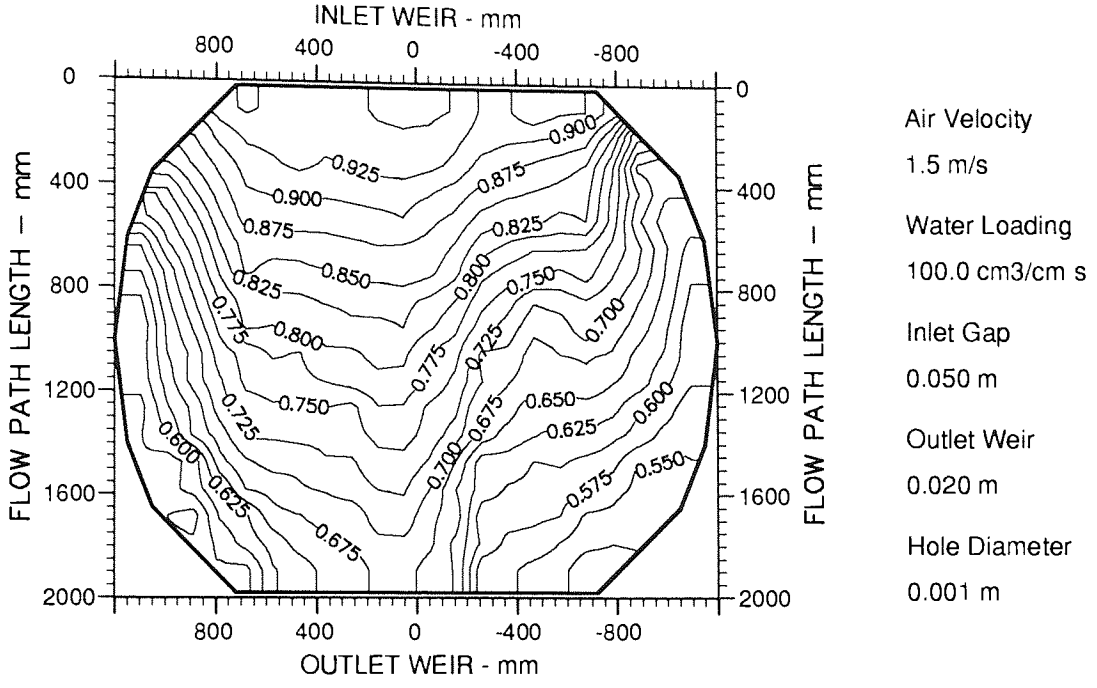

Fig. 9.3c Two-Dimensional Reduced Temperature Contours.

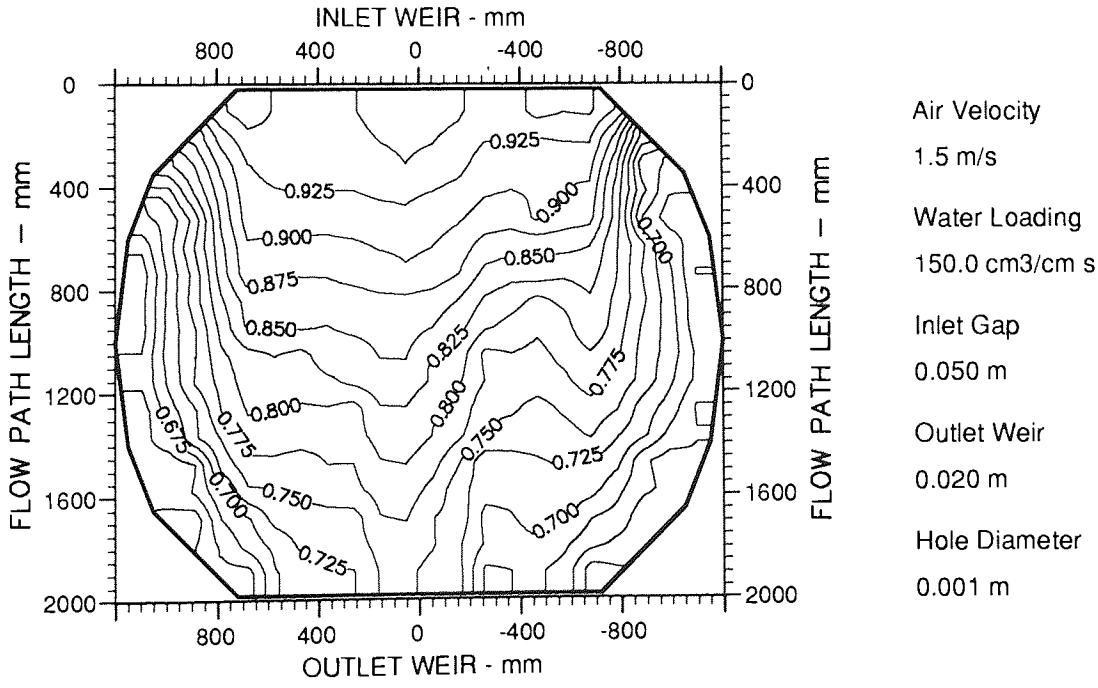

Fig. 9.3d Two-Dimensional Reduced Temperature Contours.

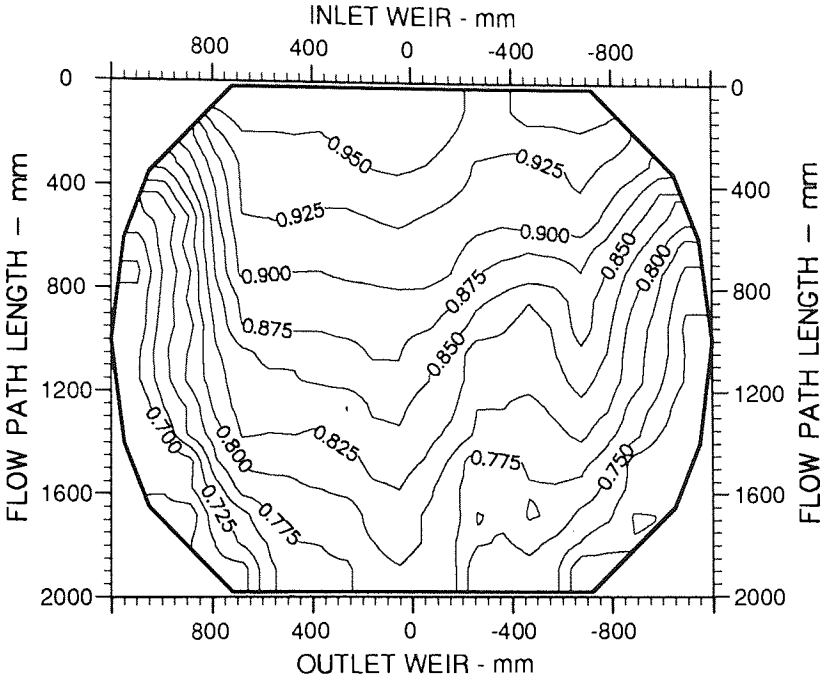

Fig. 9.3e Two-Dimensional Reduced Temperature Contours.

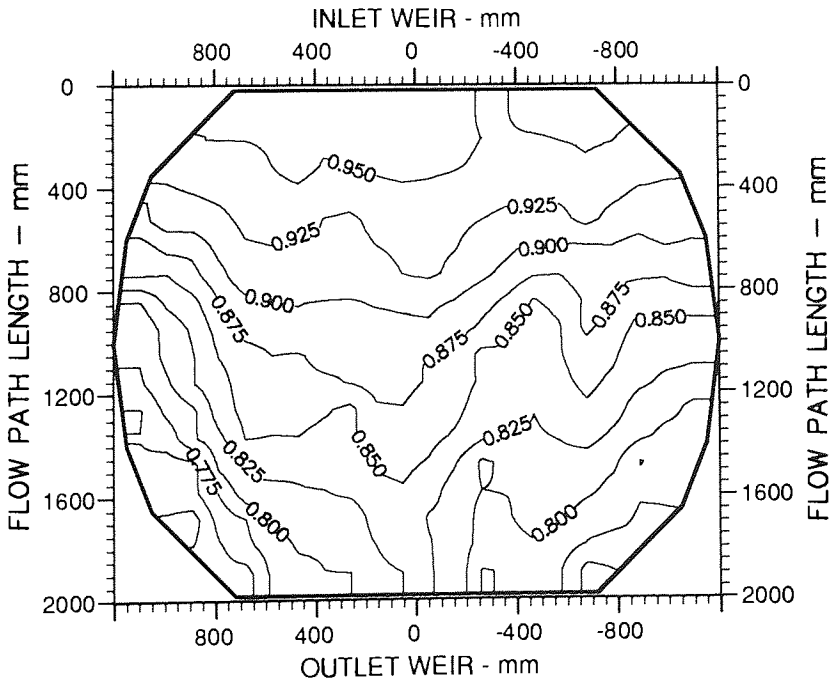

Fig. 9.3f Two-Dimensional Reduced Temperature Contours.

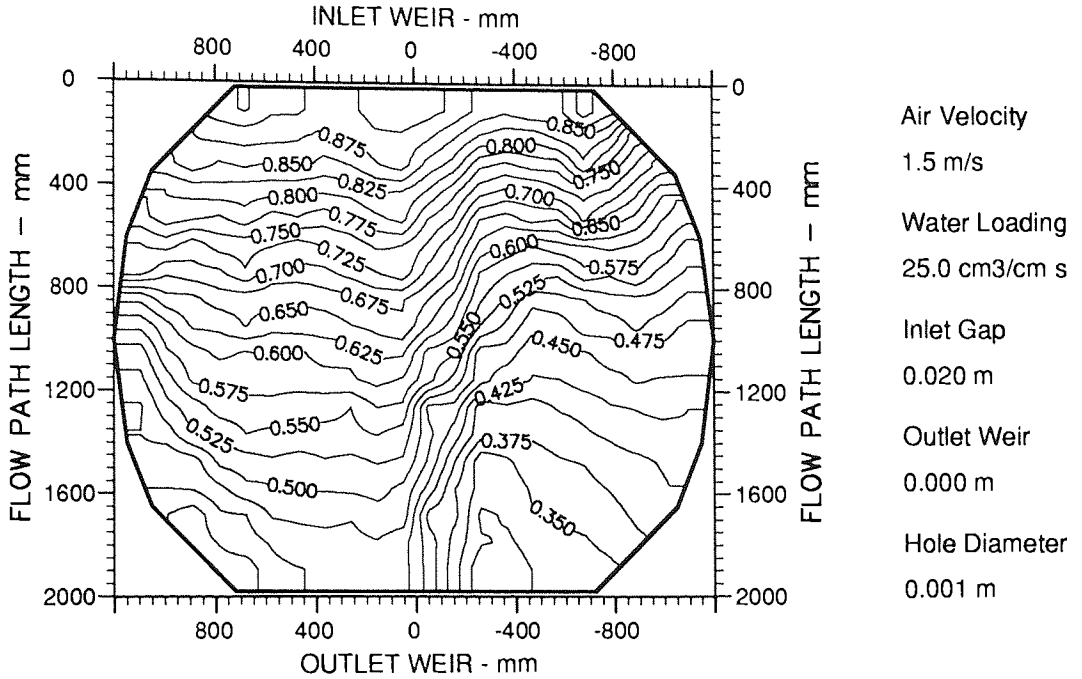

Fig. 9.4a Two-Dimensional Reduced Temperature Contours.

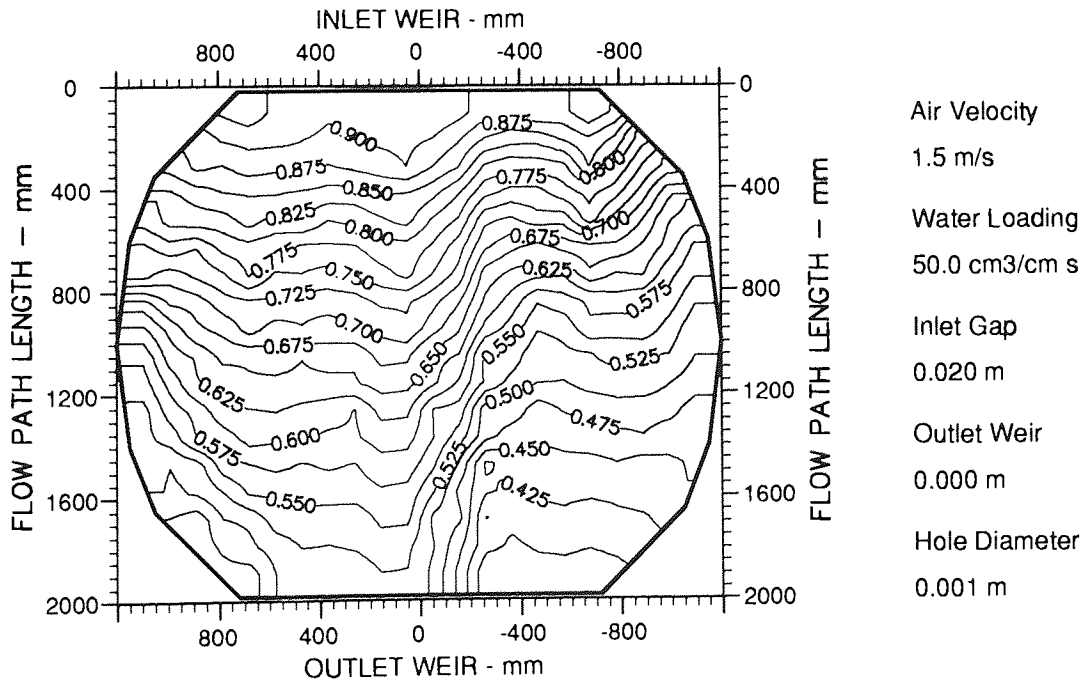

Fig. 9.4b Two-Dimensional Reduced Temperature Contours.

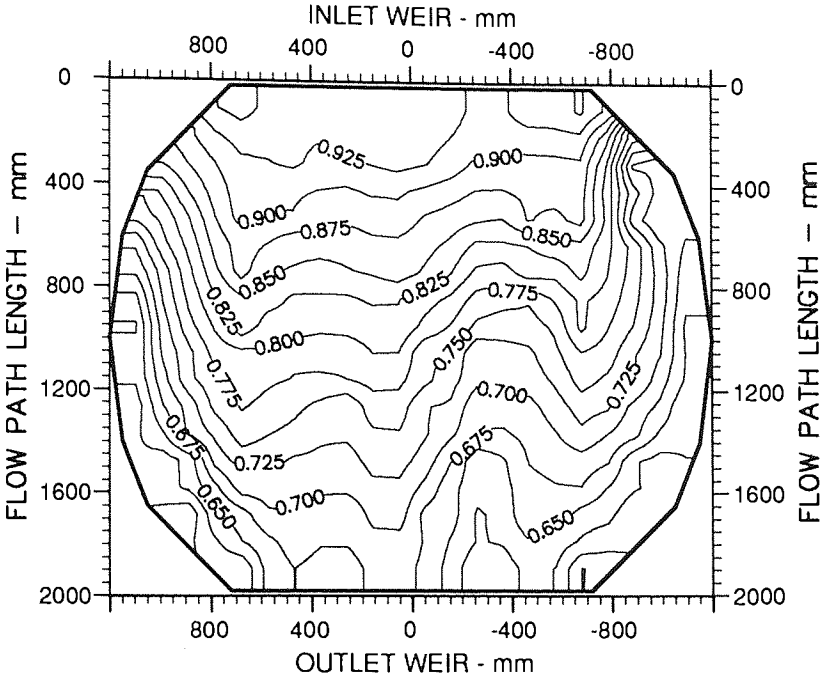

Fig. 9.4c Two-Dimensional Reduced Temperature Contours.

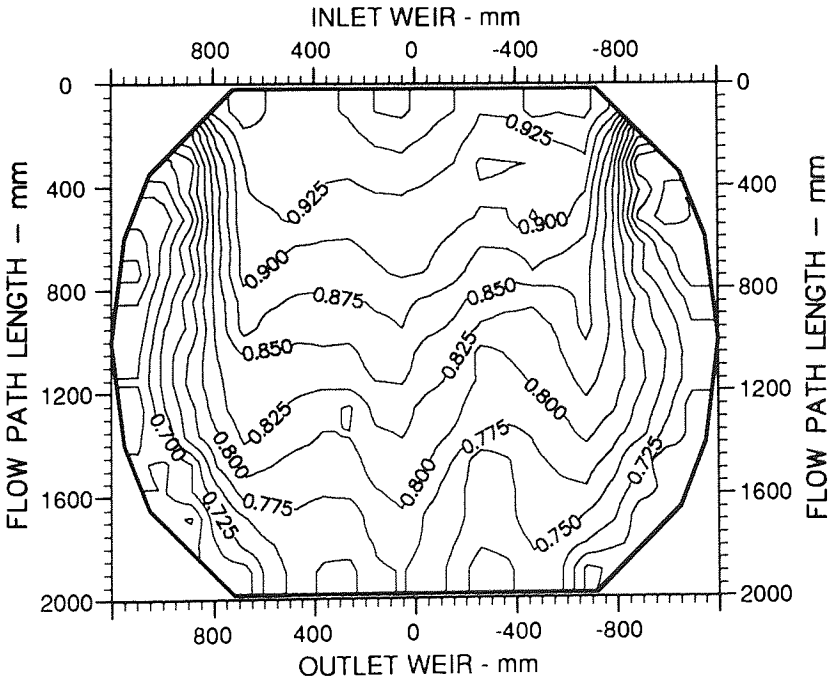

Fig. 9.4d Two-Dimensional Reduced Temperature Contours.

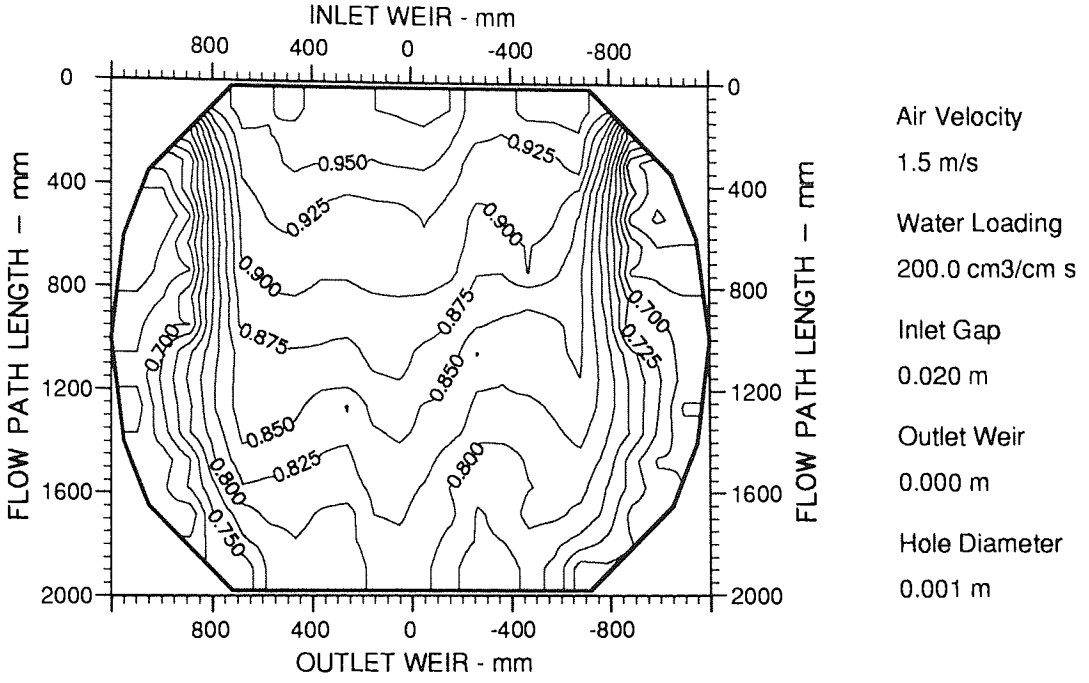

Fig. 9.4e Two-Dimensional Reduced Temperature Contours.

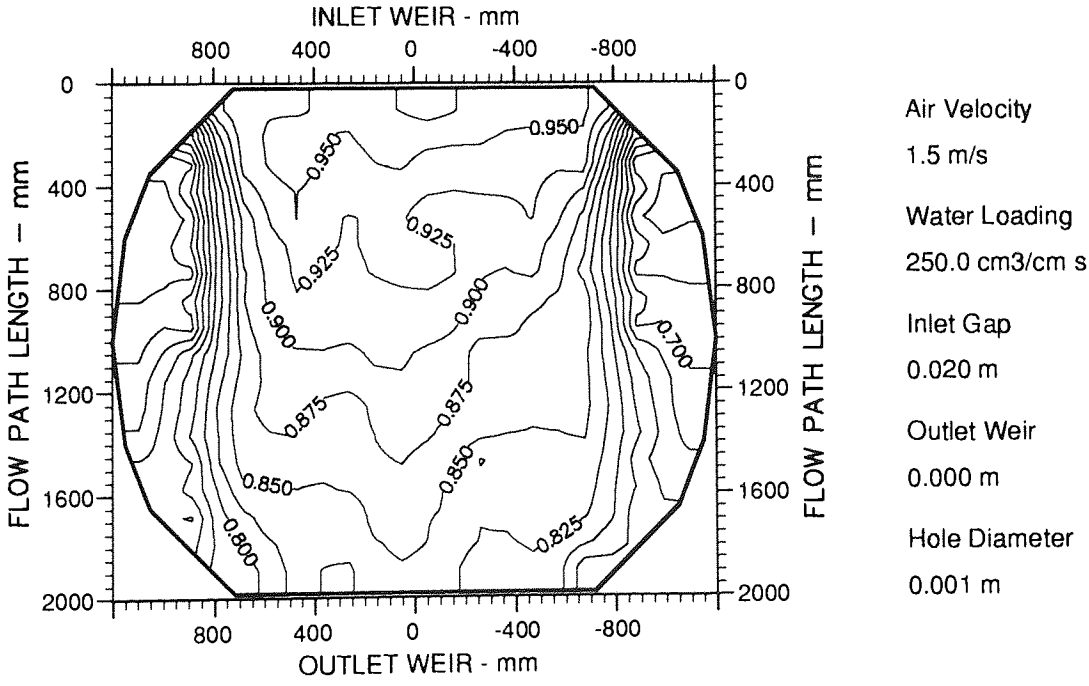

Fig. 9.4f Two-Dimensional Reduced Temperature Contours.

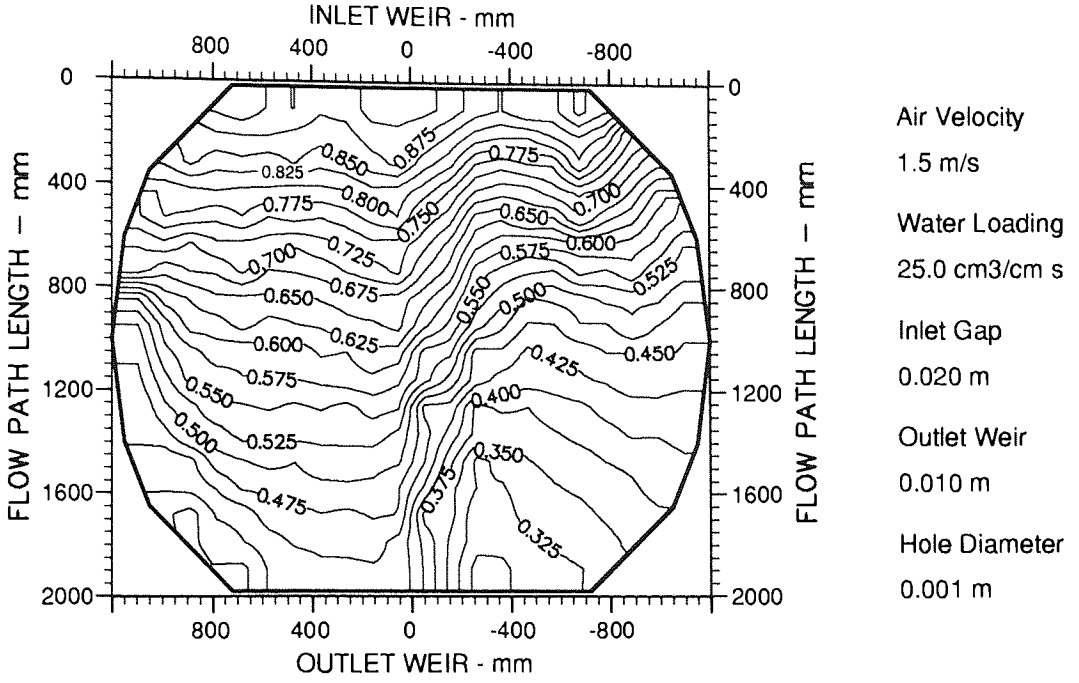

Fig. 9.5a Two-Dimensional Reduced Temperature Contours.

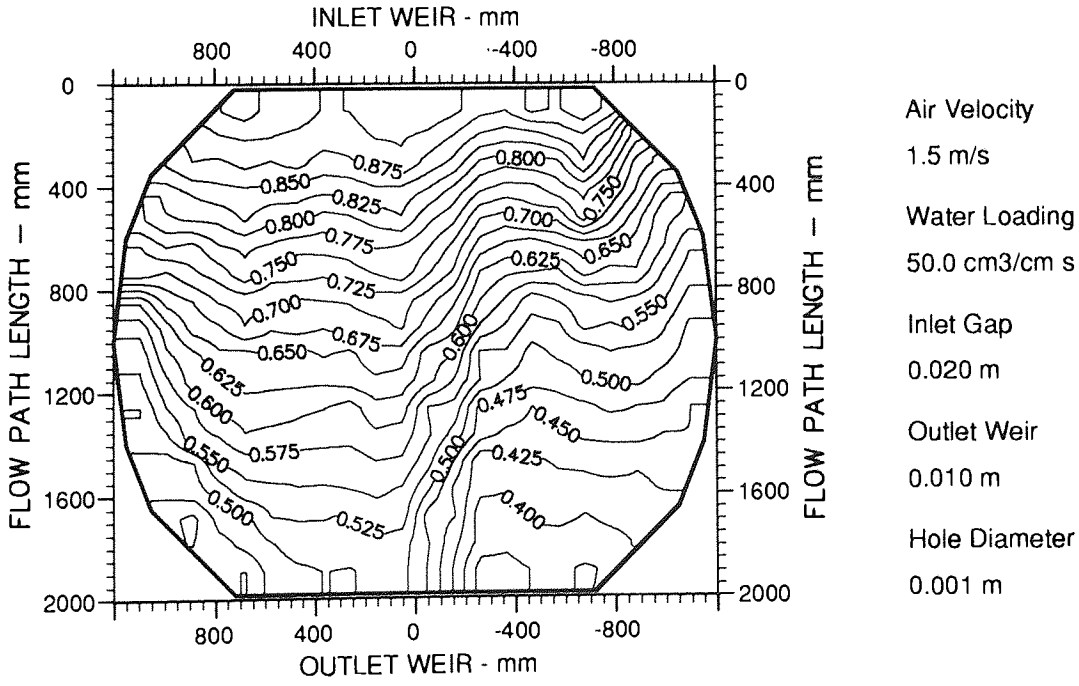

Fig. 9.5b Two-Dimensional Reduced Temperature Contours.

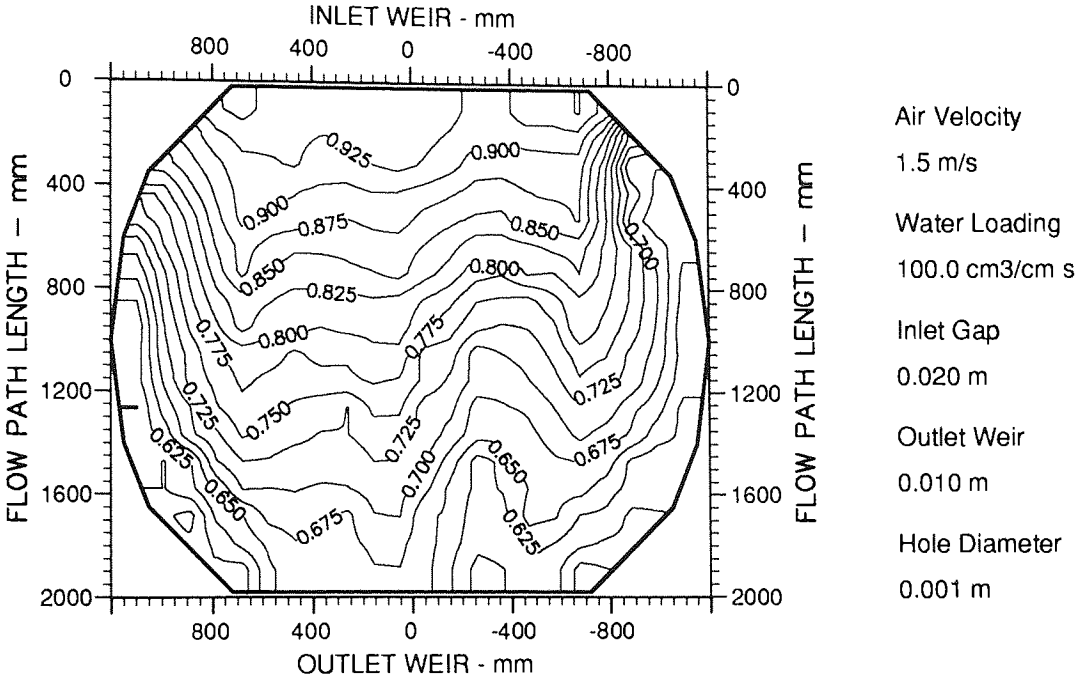

Fig. 9.5c Two-Dimensional Reduced Temperature Contours.

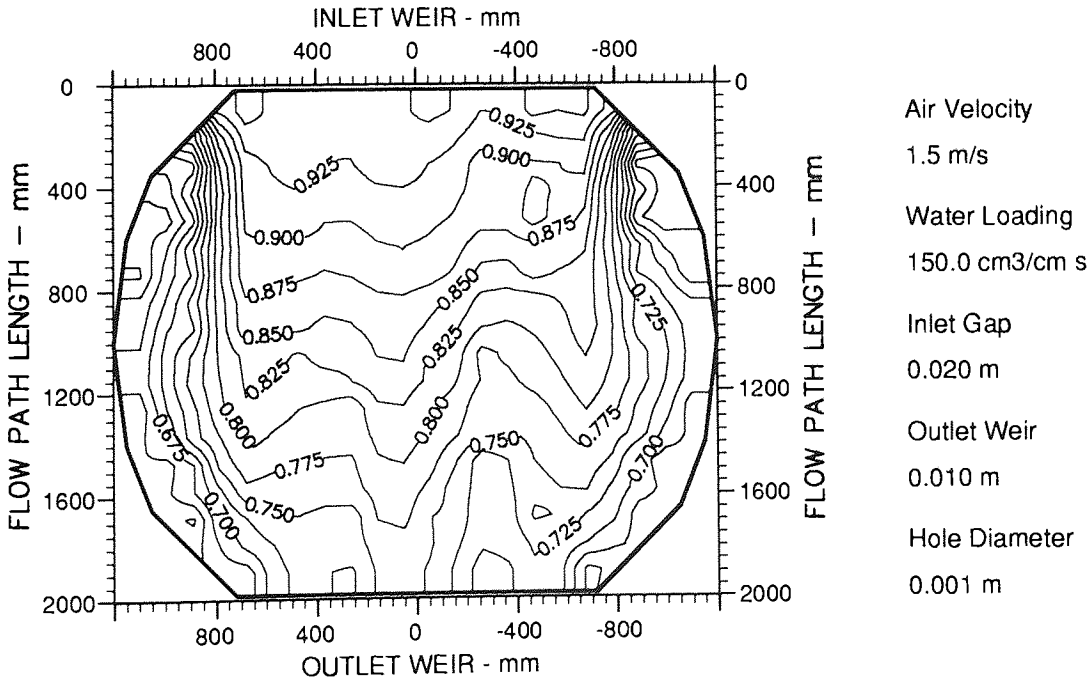

Fig. 9.5d Two-Dimensional Reduced Temperature Contours.

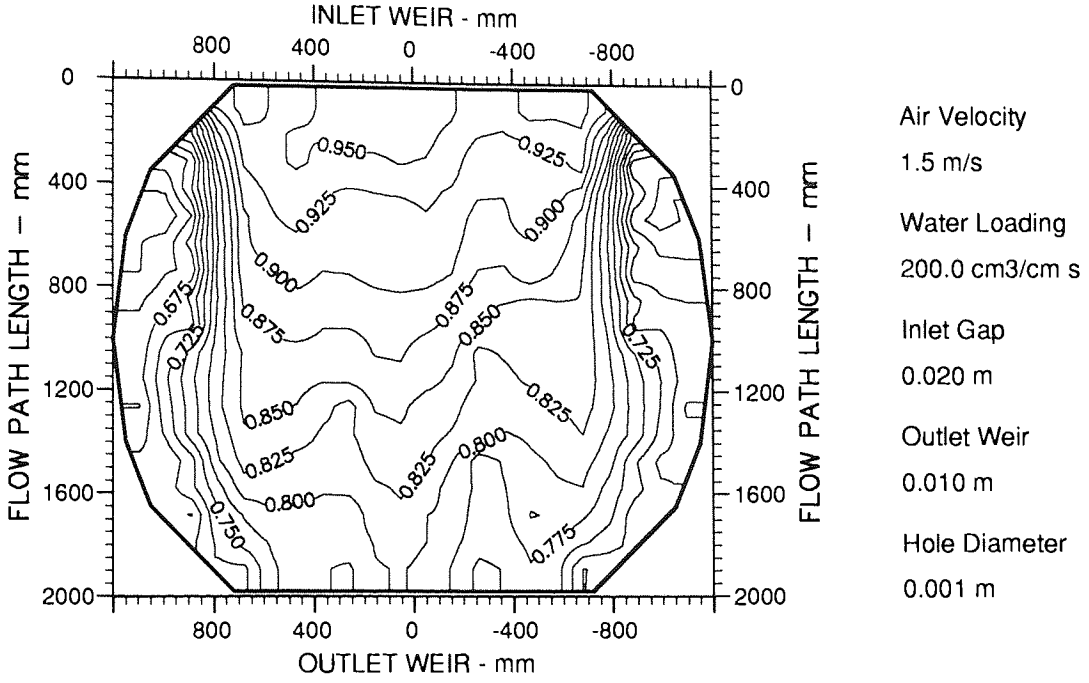

Fig. 9.5e Two-Dimensional Reduced Temperature Contours.

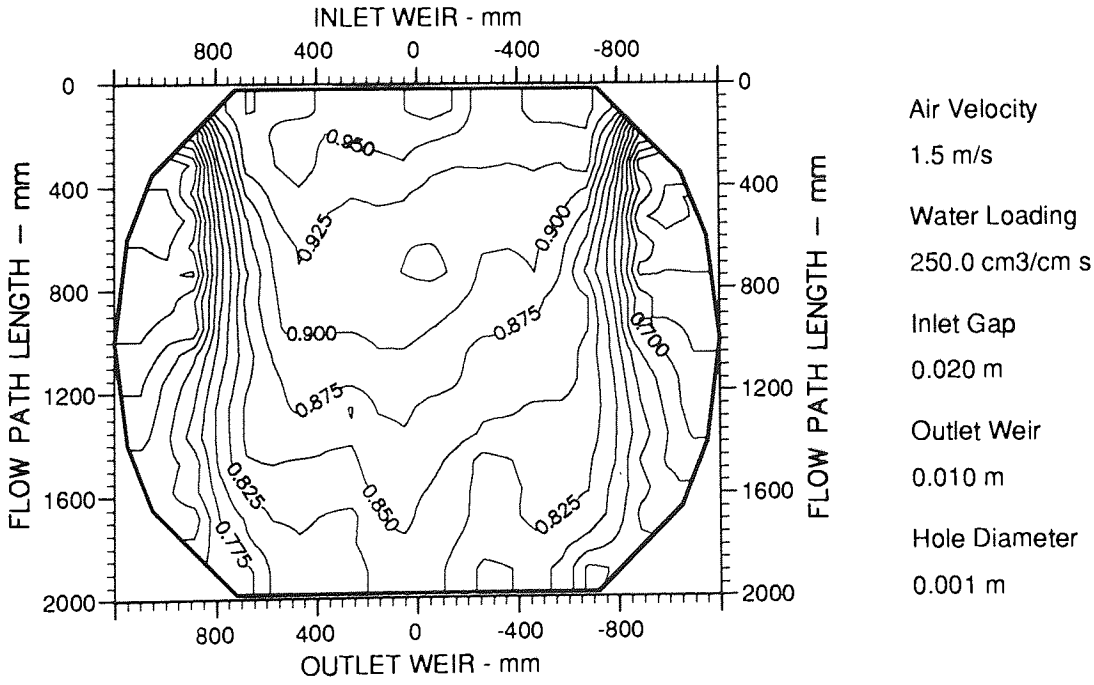

Fig. 9.5f Two-Dimensional Reduced Temperature Contours.

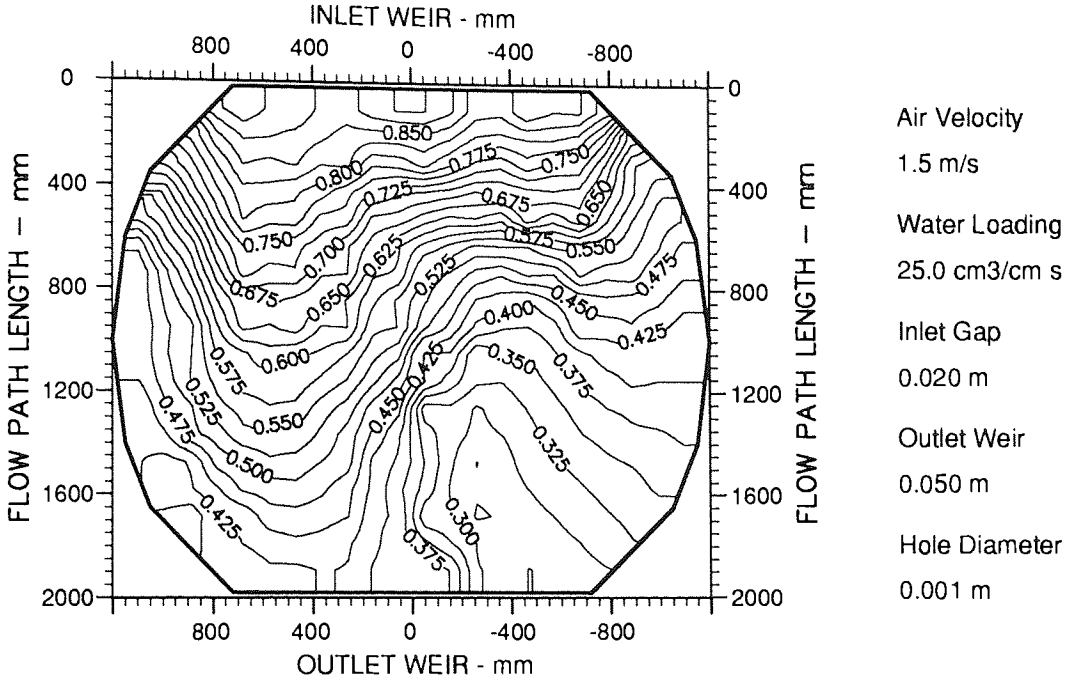

Fig. 9.6a Two-Dimensional Reduced Temperature Contours.

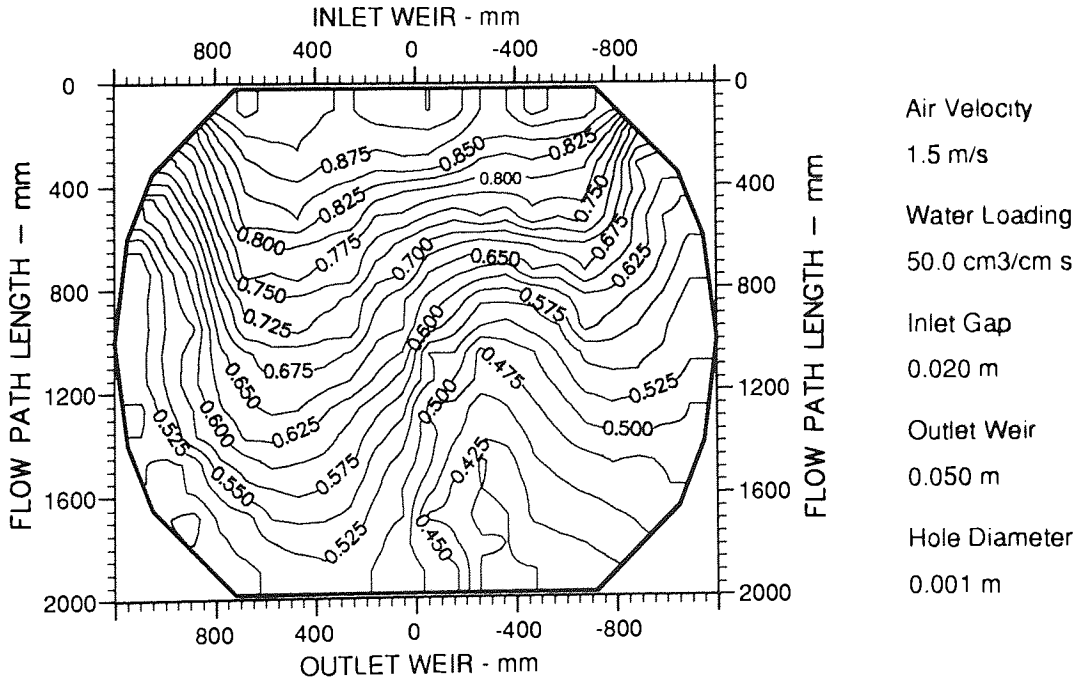

Fig. 9.6b Two-Dimensional Reduced Temperature Contours.

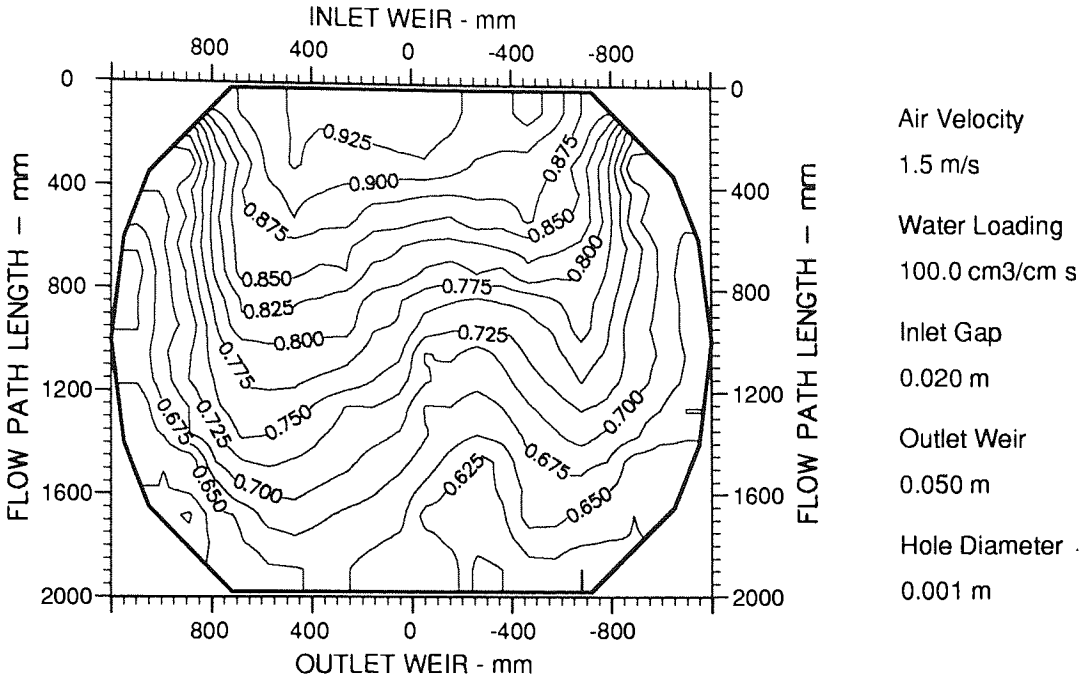

Fig. 9.6c Two-Dimensional Reduced Temperature Contours.

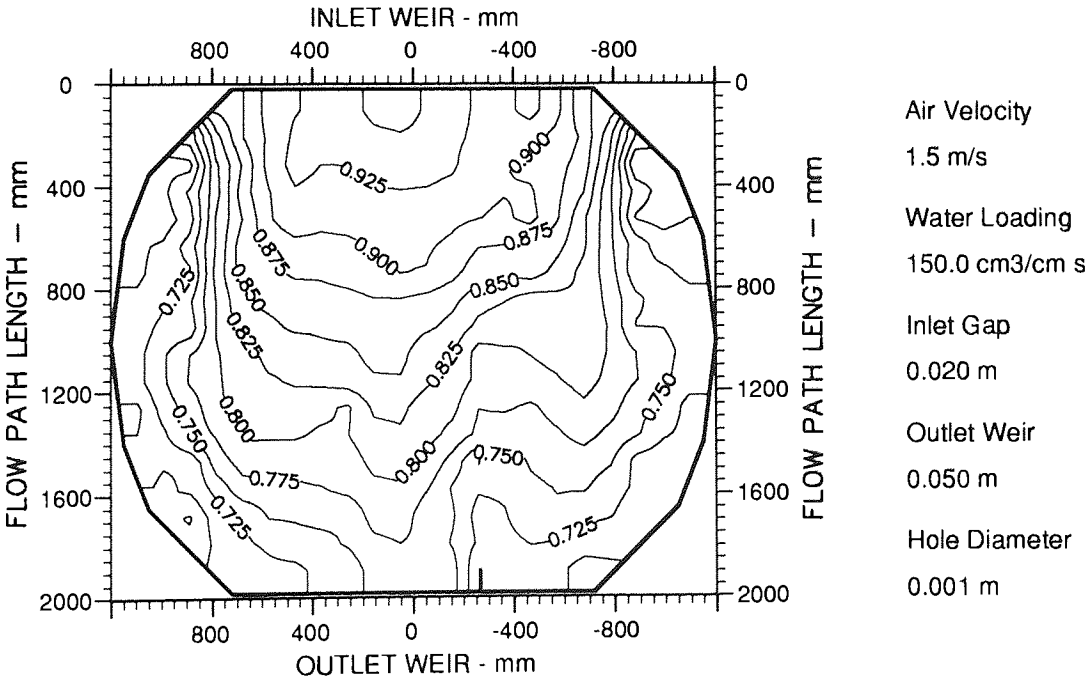

Fig. 9.6d Two-Dimensional Reduced Temperature Contours.

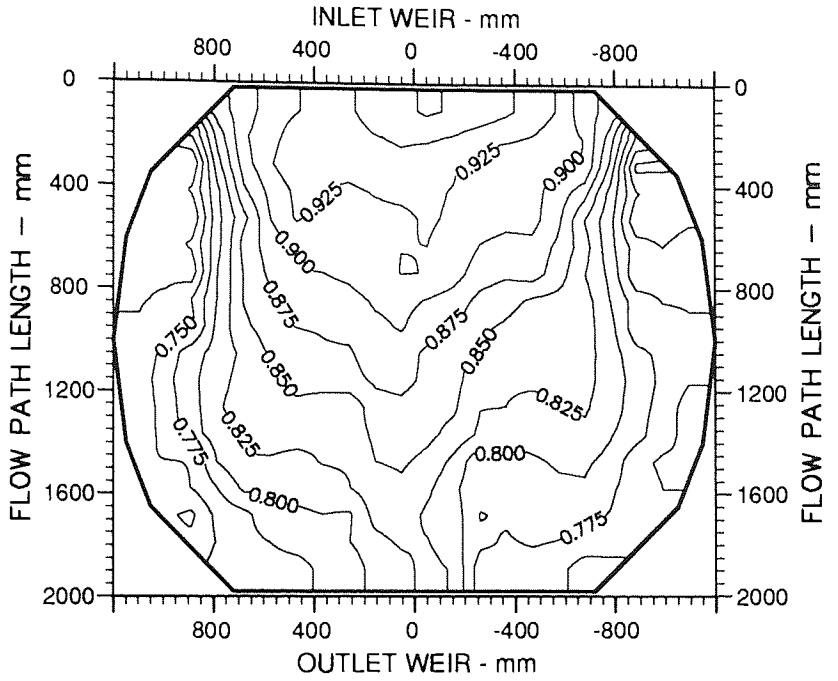

Fig. 9.6e Two-Dimensional Reduced Temperature Contours.

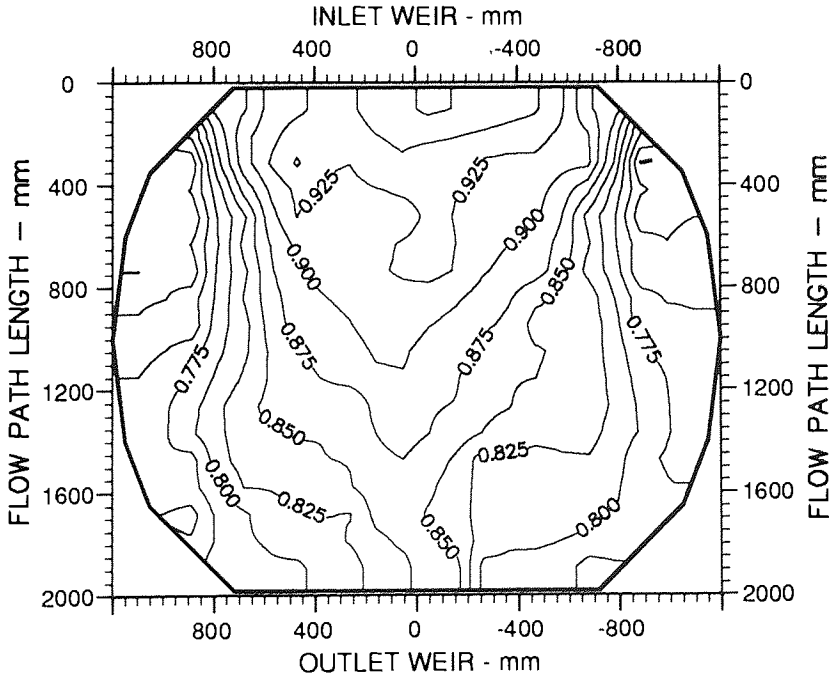

Fig. 9.6f Two-Dimensional Reduced Temperature Contours.

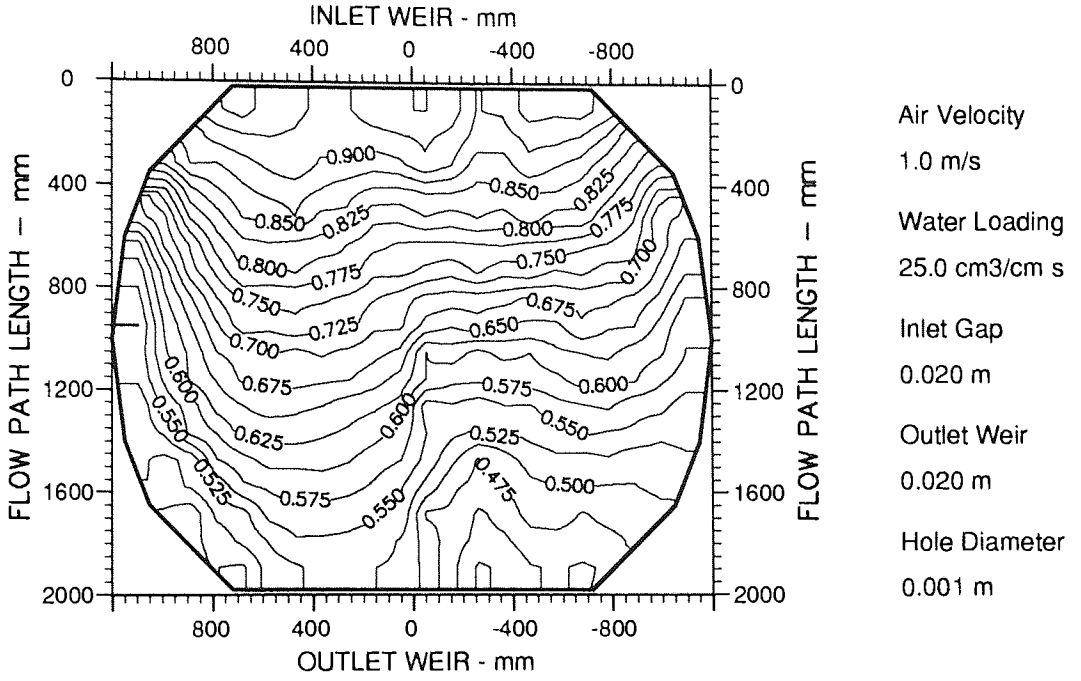

Fig. 9.7a Two-Dimensional Reduced Temperature Contours.

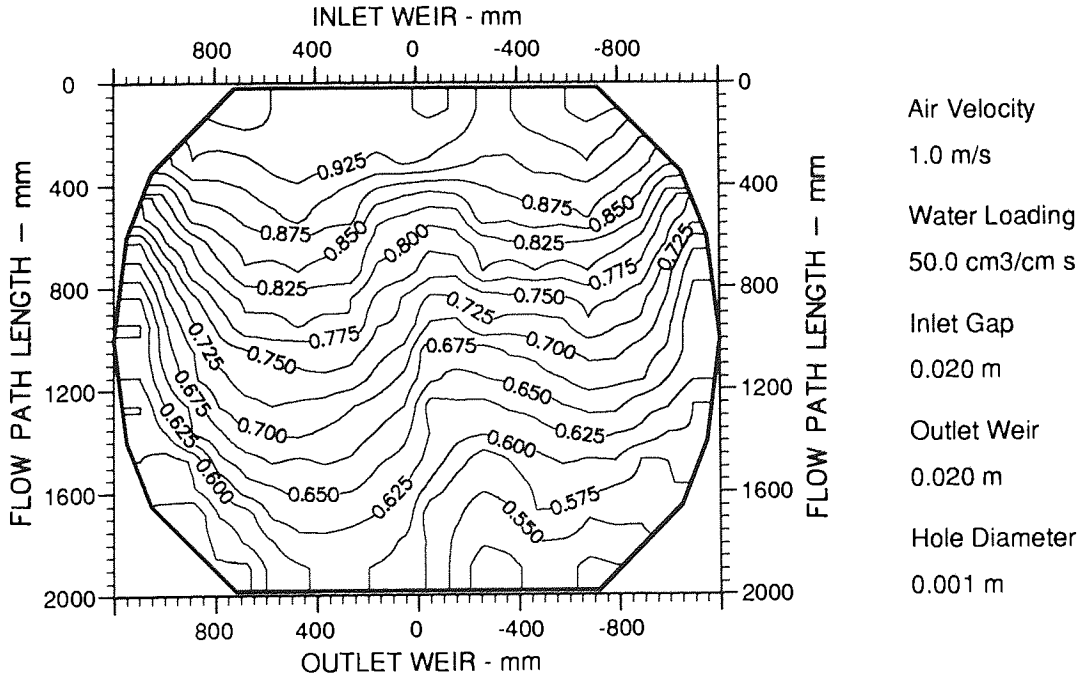

Fig. 9.7b Two-Dimensional Reduced Temperature Contours.

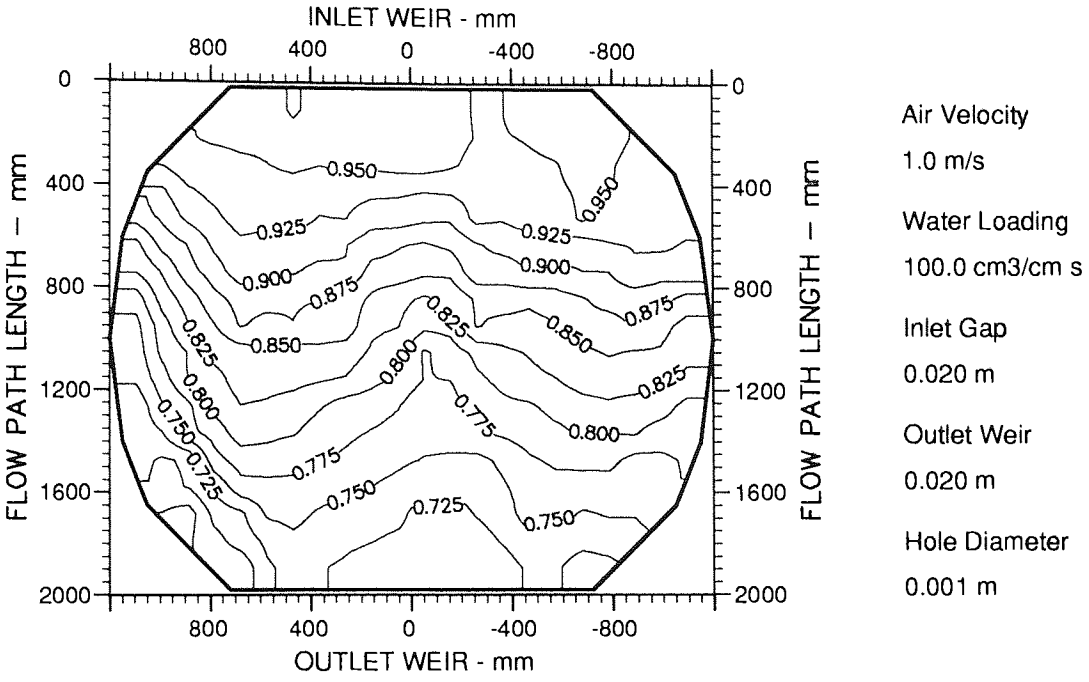

Fig. 9.7c Two-Dimensional Reduced Temperature Contours.

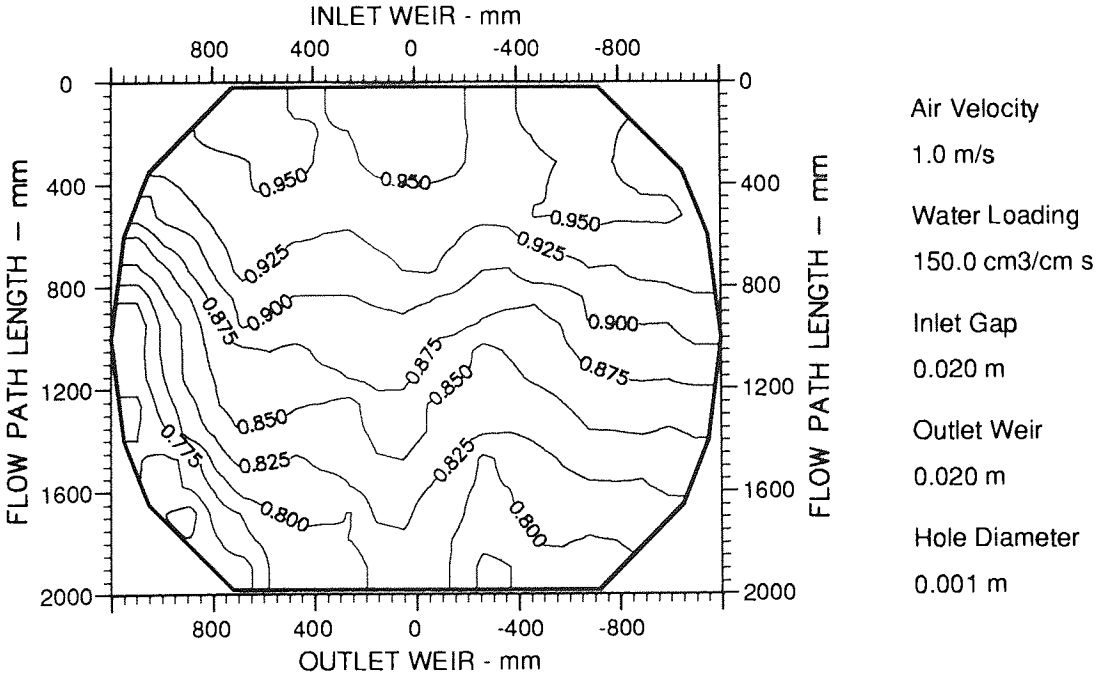

Fig. 9.7d Two-Dimensional Reduced Temperature Contours.

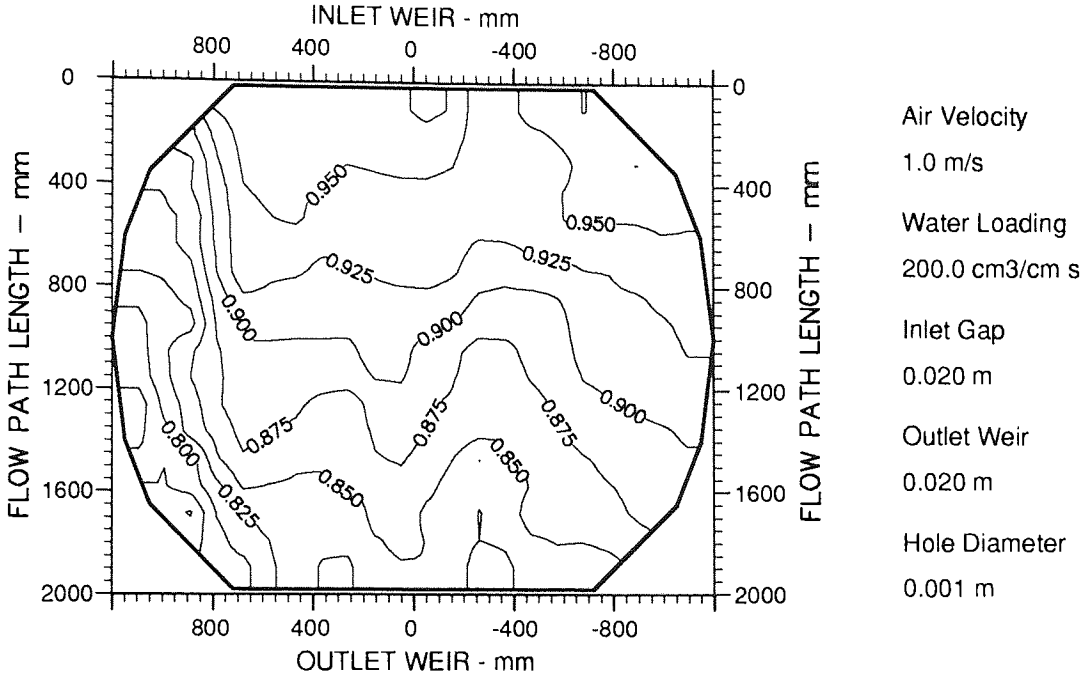

Fig. 9.7e Two-Dimensional Reduced Temperature Contours.

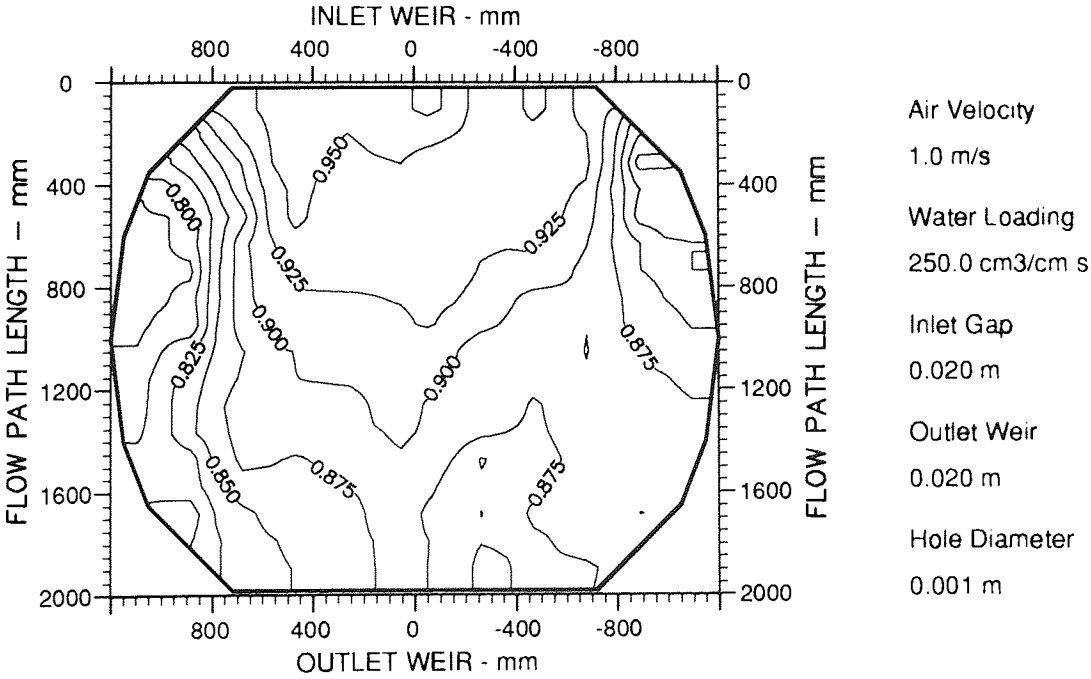

Fig. 9.7f Two-Dimensional Reduced Temperature Contours.

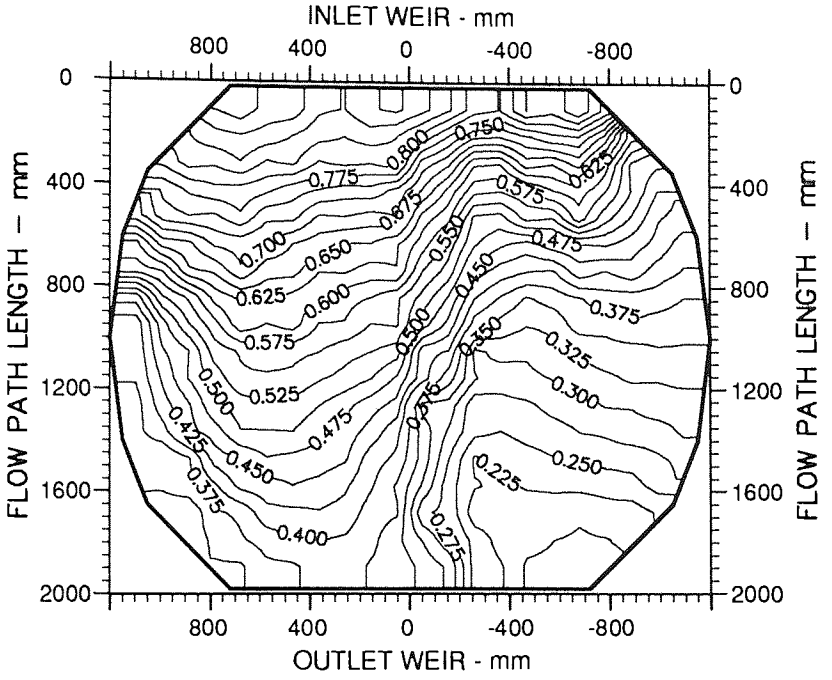

Fig. 9.8a Two-Dimensional Reduced Temperature Contours.

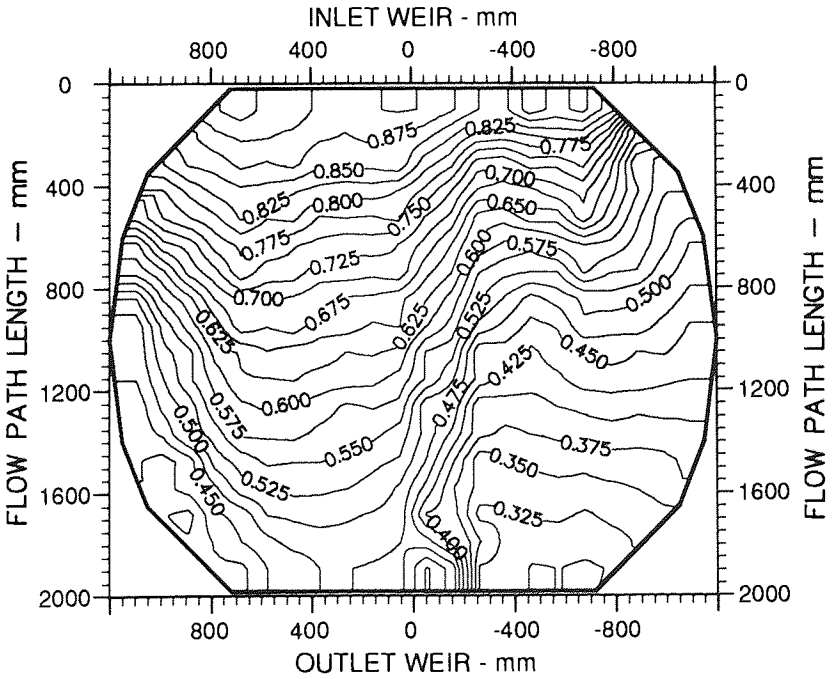

Fig. 9.8b Two-Dimensional Reduced Temperature Contours.

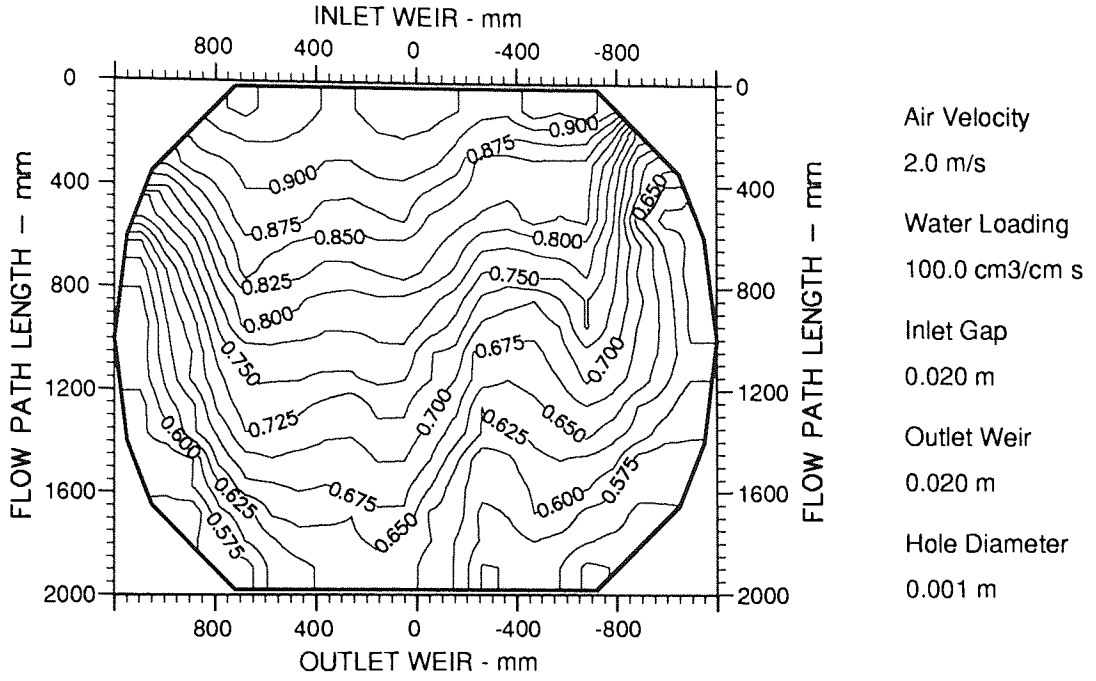

Fig. 9.8c Two-Dimensional Reduced Temperature Contours.

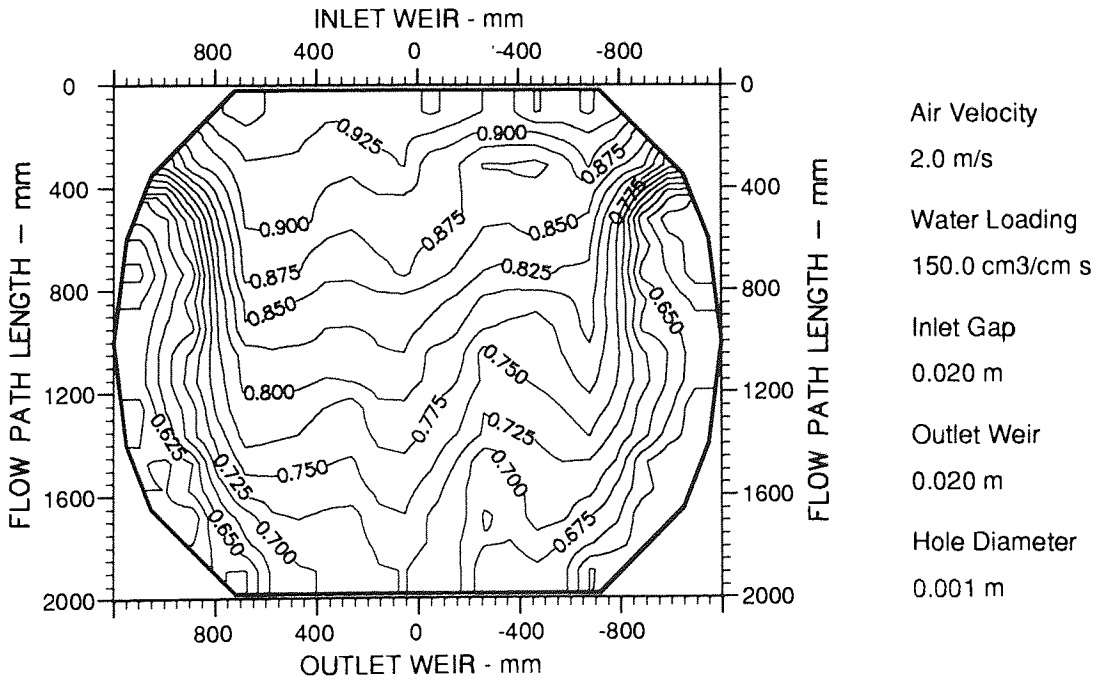

Fig. 9.8d Two-Dimensional Reduced Temperature Contours.

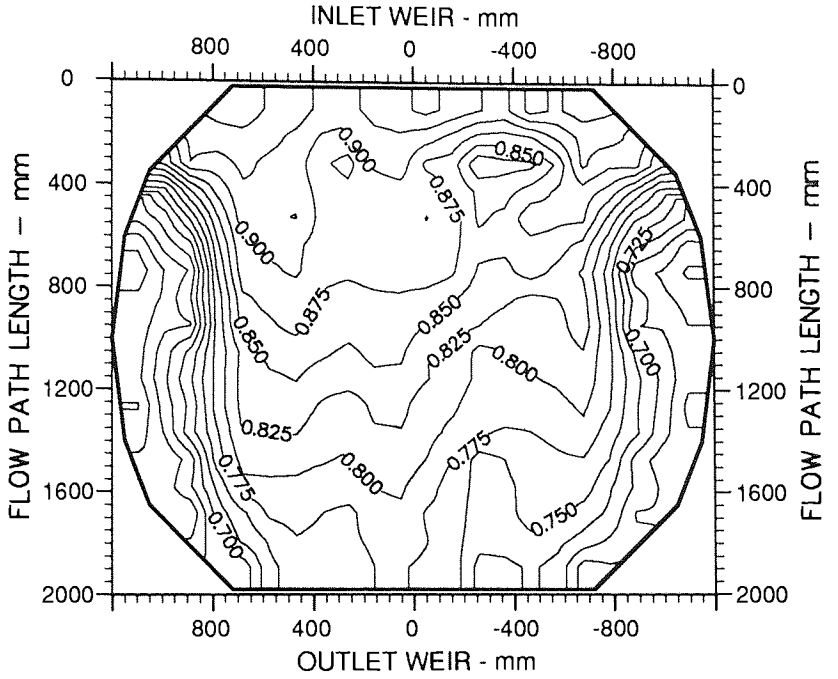

Fig. 9.8e Two-Dimensional Reduced Temperature Contours.

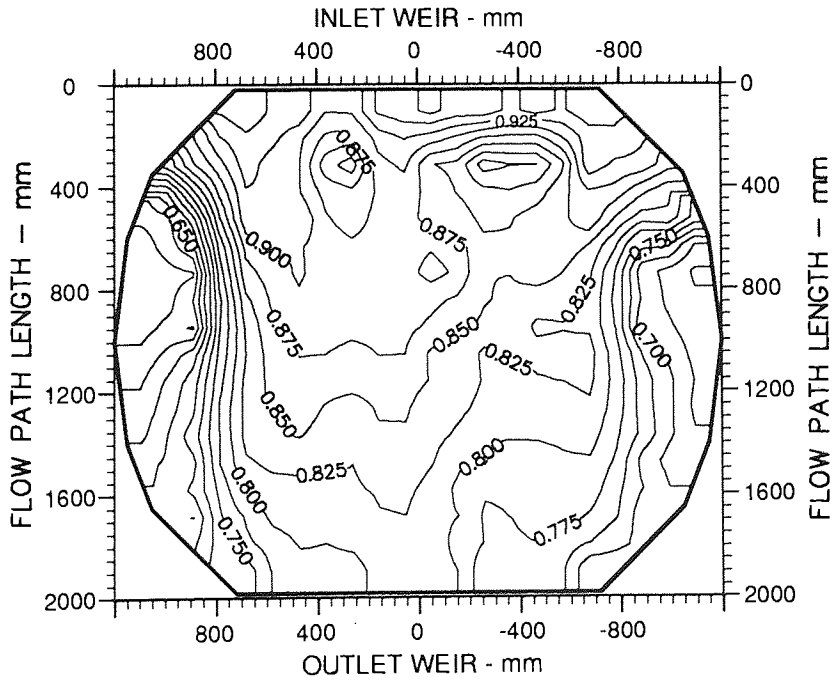

Fig. 9.8f Two-Dimensional Reduced Temperature Contours.

CHAPTER 10

10. DISCUSSION

Several experimental procedures have been used to study the liquid flow pattern and its effects on a 2.44 m diameter sieve tray. During the experimental procedures, the gaps under the inlet downcomer and the outlet weir height were changed, along with the operating variables of the air and water flowrates. The results include descriptions of how the water phase crosses the active tray, from the inlet downcomer to the outlet weir, and references were made to the phenomena of flow separation.

10.1 Separated or Non-Separated Flow

As liquid flows in a straight pipe of constant diameter, all the liquid moves in the forward direction, albeit with an imposed velocity distribution as determined by the flow regime. This is an example of non-separated flow.

As liquid flows in a straight open channel of constant width and flow depth, provided the flow is not critical at any point all the liquid moves in the forward direction, again with an imposed velocity distribution. This is another example of non-separated flow.

However, when the physical flow boundary change greatly over a short distance, such as is the case in a rapidly diverging channel, the pressure gradient at the physical flow boundary may become positive, and if the transition section extends far enough for the forward velocity component near to the boundary wall to decrease to zero then flow separation occurs. The liquid in the main flow region continues to flow in a forward direction, with an imposed velocity distribution, bounded not by the physical flow boundary of the section wall but by a separation streamline of zero velocity. The liquid between the separation streamline and the physical flow boundary now flows in the opposite direction to the main flow. This is an example of separated flow.

The essential difference between separated and non-separated flow is that in separated flow both forward and reverse velocities are exhibited in the same physical flow domain, whereas in non-separated flow only forward velocities are found.

The initial experimentation on the new 2.44 m diameter test tray was to observe how a water-only phase crosses the tray section, without the upward crossflow of air. Dye tracer studies were conducted and the results captured on video for processing. The variables in the water-only studies were the inlet gap, outlet weir and the water weir load.

Flow separation was observed in nearly all of the studies carried out. Non-separated flow was only observed in a limited number of cases, but common to the recorded cases were that the water weir load was at its lowest value, 25 cm^3/cm s, and that the outlet weir was set to 0 mm. This observation confirms the findings of Solari et al. (1982) who observed, on a 1.25 m diameter water flume, that no reverse flow was present for the condition of no outlet weir.

Associated with flow separation is the circulating region, around the separation streamline, which changed in size depending on the water weir load. The sizes of the circulating regions, expressed as a percentage of the tray area, were estimated from the video recordings and have been presented graphically in Figure 6.6. Apart from the relatively few cases of non-separated flow, the circulating regions were almost always 30% of the tray area, which was subsequently found to be the maximum value for this configuration of tray.

The flow pattern of water-only was now characterised for each combination of weir load, inlet gap and outlet weir. Next, the same characterisation procedure was repeated, but with a crossflow of air. The variables in this study were the inlet gap, outlet weir, water weir load and superficial air velocity. The technique for collecting the flow data was changed to the new experimental technique of using directional flow pointers, but the processing of the data into a measure of the circulating area, expressed as a percentage of the tray area, was identical to that for the water-only studies.

The sieve tray experiments proved interesting due to the observed differences in the size of the circulating areas, and definite trends could be seen to emerge. The sizes of the circulating regions, expressed as a percentage of the tray area, have been presented graphically in Figure 7.6. The crossflow of air has a large effect on the way in which the water phase crosses the tray section. This is demonstrated by the fact that with crossflow of air the range of circulation sizes, 0 through 30% of the tray area, is observed for water weir loads of 25 to 300 cm^3/cm s, whereas without crossflow this range of circulation sizes is observed for water weir loads of 25 to 75 cm^3/cm s. Note that the water weir loads for the case of air crossflow are dependant upon the setting of the inlet gap. The

effect of the air crossflow seems to delay the onset of separation and retard the growth of the circulating regions, once they have formed.

When investigating the water flow pattern with the air crossflow, definite trends in the size of the circulating regions were observed. Of the four variables studied, inlet gap, outlet weir, water weir load and superficial air velocity, the inlet gap and water weir load had the most dominant effects on the developed flow pattern. Obviously the superficial air velocity had a great effect when compared to the case of no crossflow, but no discernible effect was noticed from one superficial air velocity to another. However this could be due to the 1 mm hole sieve tray always operating in the bubbly regime, where liquid momentum dominates over gas momentum.

The water weir load has the effect of increasing the size of the circulating regions for increasing weir load, once separation has occurred. The rate of increase in size of the circulating regions seems to be governed by the inlet condition of the gap through which the water enters the tray. When an inlet gap of 10 mm is used the maximum size of the circulating region, 30%, is achieved for a weir load of 120 cm^3/cm s, whereas for a 20 mm inlet gap the corresponding weir load is 210 cm^3/cm s, and for a 50 mm inlet gap the condition of 30% of the tray area circulating was not achieved.

In Section 6.3.6 a proposal was put forward which stated that the chances of separation were enhanced by any factor which increased the depth of water or flow on the tray. This was based on the relative liquid velocities through the inlet gap and on the tray, and the possibility of an adverse pressure gradient being formed. Extending this idea to two-phase crossflow, the likelihood of keeping non-separated flow on a sieve tray should be enhanced by

(i) Decreasing the water flowrate.

(ii) Increasing the inlet gap.

(iii) Decreasing the outlet weir.

(iv) Increasing the superficial air velocity.

The presented experimental work confirms the effects of (i), (ii) and (iv), but the results concerning the outlet weir have been inconclusive.

10.2 Non-Separated Flow

The new experimental technique of using flow pointers to reveal the direction of the liquid flow on a sieve tray has revealed that a condition of non-separated flow occurs at a moderately low water weir load of 25 to 50 cm^3/cm s. Non-separated flow is defined as all the liquid flow moving in a direction which increases its distance from the inlet weir. This allows the liquid to flow straight across the tray from the inlet downcomer to the outlet weir or to take a more extended route via the segmental regions at the sides of the tray. The flow pointers in the centre of the tray showed the water moving in a direct path between the downcomers whereas those near to the sides of the tray first reveal the water expanding to fill the flow cross-section and then contracting between the centre of the tray and the outlet weir. Dye tracer studies have revealed that, even with non-separated flow, the residence time of the water is greater at the sides of the tray than in the centre of the tray. This observation has been noted by many workers (Bell, 1972; Porter et al., 1972; Lockett and Safekourdi, 1976; Sohlo and Kinnunen, 1977; Solari and Bell, 1978; Stichlmair et al., 1987; Yu et al., 1990), and should be expected due to the greater distance that the liquid must travel.

While non-separated flow was exhibited on the tray, measurements of the distribution of water flow over the outlet weir showed that the weir load could be described as uniform, as illustrated in Figures 8.7 to 8.10 for cases of low weir loading, although, there was a tendency for the water flow at the edges of the outlet weir to be slightly greater than that of the average flow. This observation can be explained by the extra water converging on the edge of the outlet weir from the sides of the tray.

Non-separated flow over the tray is also demonstrated by the temperature profiles that are illustrated in Figures 9.1 to 9.8 for the cases of low weir loadings, data collected during water cooling-experiments. The temperature profiles for the condition of non-separated flow show that the water temperature decreases with distance travelled from the inlet downcomer, which is in agreement with the definition of non-separated flow. However, flow pointers positioned on the tray show the existence of a liquid velocity profile, revealing that for cases of low weir loadings and larger inlet gaps the liquid flow diverged upon entering the tray. Hence water entering the tray at either end of the inlet downcomer has to travel further. This leads to an extended residence time on the tray for water passing through the side regions, which results in lower temperatures being recorded in those regions than in the centre of the tray.

There appears to be a build up of liquid in the region of slower moving water at the sides of the tray which leads to a slight increase in the liquid head around the edges of the outlet weir. This can be most clearly seen in Figures 8.3 and 8.4 when the height of the clear liquid surfaces are viewed for the low superficial air velocities of 0.7 and 0.9 m/s. The consequence of this increased liquid head was reflected in the variation of liquid flow along the outlet weir. It was concluded that during non-separated flow there was a slightly greater than the average weir load at the edges of the outlet weir.

10.3 Separated Flow

The flow pointers revealed that non-separated flow is replaced by separated flow at the water weir load of 25 to 50 cm^3/cm s. This changeover is dependant upon the setting of the gap under the inlet downcomer. When separated flow occurs, the flow pointers indicate that the aerated water channels from the inlet downcomer to some point along the flow path length before spreading out to the tray walls. The distance to which the aerated water channels has been found to be very much a function of the water weir load and the inlet gap. A circulating region is bounded by the channelling zone and the tray wall, whose size is related to the distance that the water channels.

Attention has been concentrated upon the estimation of the size of these circulating regions using the directional flow pointers. This work indicates that the size of the circulating region is a function of the water flowrate (weir load) and the inlet gap. Although the air flowrate (superficial velocity) changes the water flow pattern dramatically from that of water-only there is no conclusive evidence to link the superficial air velocity or the height of the outlet weir to the size of the circulating regions.

The temperature profiles complement the observations of the flow pointers by revealing severe liquid channelling down the centre of the tray between the two downcomers. Liquid channelling is shown on the temperature profiles as a steep temperature gradient emanating from the ends of the inlet downcomer, whereas between the downcomers the profiles reveal virtually uniform liquid flow. An example of this is given in Figure 6.2, which presents the channelling of water only, and Figures 9.1c and 9.1d, which reveal the effect of the liquid flow pattern on mass transfer for the condition of liquid-channelling. However, it is the regions at the sides of the tray which are more likely to cause the fall-off in tray performance; this is where the different hypotheses of the flow patterns disagree.

The flow pointers reveal that at a certain weir load, combined with a particular setting of the inlet gap, the phenomena of flow separation takes place, but as the weir load increases, an eddy of increasing size is formed in the segmental region of the tray. This eddy continues to grow until a maximum size is realised, which corresponds to 30% of the tray area in the case of this design of tray with a 60% weir to diameter ratio.

Similarly the water-cooling experiments show up the same trend of increasing eddies at the sides of the tray for increasing weir load. The temperature profiles can be observed to break from the edge of the inlet downcomer to a position some way down the tray before making contact with the tray wall again. At its worst the liquid channelling can divide the tray into three portions; two large eddies separated from each other by a central main flow region, not unlike the Stagnant Regions Model of Porter et al. (1972).

Reference is once again drawn to the temperature profiles illustrated in Figures 9.1 to 9.8 which show that in the circulating regions the water temperature is reduced below that leaving the tray, implying that the enthalpy change of the air passing through the circulating region will be much reduced. This has been pointed out before, and is known not to cause any problems on one single tray (Porter et al., 1972). However, if this flow pattern is dominant when several single pass trays are stacked upon each other, then a detrimental effect on the tray efficiency would be noticed (Lockett et al., 1973).

The 2.44 m diameter test tray was fitted with 60% straight chordal weirs. This weir to diameter ratio is at the lower limit of most design procedures, but was chosen to maximise the impact of differing flow patterns over the tray area. As has been mentioned, the size of the circulating regions increases with increasing water weir load, but the limiting size of the circulating regions has been found to be 30% of the active area for this configuration of tray. This percentage of the active area corresponds to liquid channelling between the two downcomers, which appears to support the Stagnant Regions Model of Porter and Lockett (1972).

The most important conclusion from these experimental results with the 1 mm diameter hole tray is that liquid channelling occurs as a result of the velocity of the entering liquid. Thus it may be possible to improve the liquid flow pattern by making a modification to the tray design which reduces the momentum of the liquid entering the froth. The experiments show that increasing the inlet gap reduce the effect of the liquid channelling and two other simple techniques which are used in trayed distillation columns are the use of a seal pan or the use of a weir at the liquid inlet. Both of these modifications will have

the effect of reducing the momentum of the liquid entering the froth. In other work not reported here, it has been found that the use of an inlet weir can reduce liquid channelling on this type of tray.

CHAPTER 11

11. CONCLUSIONS

1. A large tray test rig incorporating a 2.44 m diameter column, a 150 HP air fan and a 1.2 MW water heating facility has been constructed. This unique facility is equipped for the experimental observation of liquid flow patterns, and can also be used for the evaluation of the effect of the liquid flow pattern on mass transfer by cooling water with a cross-flow of air.

2. The water-cooling experiment, in which over 100 temperature measuring devices are placed across the tray area, has proved to be a convenient and sensitive test of the effect of the liquid flow patterns on tray mass transfer.

3. A single-pass sieve tray perforated with 1 mm diameter holes has been extensively tested. Liquid channelling associated with liquid circulation at the sides of the tray has been observed on the tray. Temperature profiles, revealled by the water cooling technique, have confirmed that the driving force for heat transfer is reduced in the circulating regions.

4. The flow patterns formed on the 1 mm diameter perforated tray have been compared with those formed by water-only flow over an unperforated tray of the same size.

5. In the water-only experiments, with the exception of extremely low weir loads, the flow separated at the ends of the inlet downcomer forming circulating regions at the sides of the tray, these regions with a small increase in weir load increased to completely fill the sides of the tray outside of the downcomers.

6. The liquid flow patterns on the 1 mm diameter hole sieve tray are similar to those observed in the water-only experiments. The effect of the air flow is to delay the onset of separation and circulation, which occurs at higher weir loads than in the water-only experiments.

7. The size of the circulating regions formed on the 1 mm diameter hole sieve tray depends on the velocity of the water entering the tray and thus on the setting of the gap beneath the inlet downcomer as well as on the weir load.

8. The new experimental technique of using directional flow pointers is a cheap and effective method of quickly determining the liquid flow pattern over sieve trays.

9. The presence of liquid channelling is often accompanied by complementary variations in the liquid hold-up over the tray area. The slower moving or stagnant regions at the sides of the tray tended to have the greatest liquid hold-up and these areas corresponded to the low temperature areas shown by the water cooling experiments.

10. For all the superficial air velocities, the calculated point efficiencies increased with increasing weir load. This occurs because liquid hold-up, and thus gas residence time in the froth, increase with increasing weir load.

Recommendations for Future Work

1. To carry out further experimental investigation into the flow patterns generated on different hole diameter sieve trays.

2. To develop a theory of open channel two-phase flow, capable of explaining the observations described in this work.

3. To use this work as a sound basis for the evaluation of any future theoretical models of mass transfer on distillation trays.

4. To try and develop new flow control devices based on a better understanding of open channel two-phase flow.

CHAPTER 12

12. REFERENCES

Austin, D. G., 1975, "Chemical Engineering Drawing Symbols", Godwin, London.

AIChE., 1958, "Bubble Tray Design Manual", AIChE., New York.

Aleksandrov, A. and Vybronov, V. G., 1971, "Investigation of the hydrodynamic pattern of liquid flow on cross-flow trays", Teor. Osnovy. Kim. Tekh., 5(2) 339.

Ali, Q. H., 1986, "Gas Distribution in Shallow Large Diameter Packed Beds", Ph.D. Thesis, Aston University, Birmingham, England.

Ani, C. C., 1986, "Flow Patterns, Performance and Scale-Up of Distillation Trays", Ph.D. Thesis, Aston University, Birmingham, England.

Bell, R. L., 1972, "Experimental determination of residence time distributions on commercial scale distillation trays using a fibre optic technique", AIChE J., 18(3) 491.

Bell, R. L., 1972, "Residence time and fluid mixing on commercial scale sieve trays", AIChE J., 18(3), 498.

Bell, R. L. and Solari, R. B., 1974, "Effect of non-uniform velocity fields and retrograde flow on distillation plate efficiency", AIChE J., 20(4), 688.

Bennet, D. L., Agrawal, R. and Cook, P. J., 1972, "New pressure drop correlation for sieve tray distillation columns", AIChE J., 29(3), 434.

Biddulph, M. W., 1975, "Multicomponent distillation simulation - distillation of air", AIChE J., 21(2), 327.

Biddulph, M. W., Kler, S. C. and Lavin, J. T., 1990, "Double-expanded metal distillation tray", US Patent 88B116.

Bruin, S. and Freize, A. D., 1974, "A simple liquid mixing model for distillation plates with stagnant zones", Trans. IChemE., 52, 75.

Bultitude, D. P., 1989, "Distillation Tray Studies", Ph.D. Thesis, Nottingham University, Birmingham, England.

Chow, V. T., 1959, "Open Channel Hydraulics", McGraw-Hill, New York.

Diener, D. A., 1967, "Calculations of effect of vapour mixing on tray efficiency", Ind. Eng. Chem. Pro. Des. Dev., 6(4), 339.

Enjugu, B. A., 1986, "Flow Patterns and Performance of Distillation Trays", Ph.D. Thesis, Aston University, Birmingham, England.

Foss, A. S., Gerster, J. A. and Pigford, R. L., 1958, "Effect of liquid mixing on the performance of bubble trays", AIChE J., 4(2), 231.

French, R. H., 1986, "Open Channel Hydraulics", McGraw-Hill, New York.

Gautreaux, M. F. and O'Connell, H. E., 1955, "Effect of length of liquid path on plate efficiency", Chem. Engng Prog., 51(5), 232.

Gerster, J. A., Hill, A. B., Hochgraf, N. N. and Robinson, D. G., 1958, "Tray efficiencies in distillation columns", Final Report, Univ. of Delaware, AIChE, New York.

Gerster, J. A., Mizushina, T., Marks, T. N. and Catanach, A. W., 1955, "Plant performance of a 13-ft.-diameter extractive-distillation column", AIChE J., 1(4), 536.

Henderson, F. M., 1966, "Open Channel Flow", McMillan, New York.

Hofhuis, P. A. M. and Zuiderweg, F. J., 1979, "Sieve trays: Dispersion density and flow regimes", IChemE Symp. Ser., n56, 2.2/1.

IUSC (Inter University Software Committee), Information Graphics Working Party, 1988, Newsletter, n2.

Kafarov, V. V., Shestopalov, V. V. and Komissarov, Y. A., 1979, "Vapour-liquid flow structure on bubbler plates", IChemE Symp. Ser., n56, 2.3/79.

Keller, G. J., 1973, "Apparatus for liquid and vapour or gas mass transfer", US Patent 3 729 179.

Kirkpatrick, R. D. and Weiler, D. W., 1978, "Liquid-gas contacting tray",

US Patent 4 101 610.

Kirschbaum, E., 1934, "Efficiency of rectification and appropriate path for liquid flow", Forsch. Gebiete Ingenieur, 5, 245.

Kirschbaum, E., 1948, "Distillation and Rectification", Chemical Publishing Co., New York, 276.

Kouri, R. J. and Sohlo, J. J., 1985, "Effect of developing liquid flow patterns on distillation plate efficiency", Chem. Eng. Res. Des., 63(2), 117.

Lavin, J. T., 1986, "Improvements in distillation trays", UK Patent 2 160 788.

Lewis, W. K., 1936, "Rectification of binary mixtures", Ind. Engng Chem., 28(4), 399.

Lim, C. T., Porter, K. E. and Lockett, M. J., 1974, "The effect of liquid channelling on two pass distillation plate efficiency", Trans. IChemE, 52, 193.

Lockett, M. J., Lim, C. T. and Porter, K. E., 1973, "The effect of liquid channelling on distillation column efficiency in the absence of vapour mixing", Trans. IChemE, 51, 61.

Lockett, M. J. and Safekourdi, A., 1976, "The effect of the liquid flow pattern on distillation plate efficiency", Chem. Engng J. 11, 111.

Monovyan, A. K. and Gaivanskii, E. A., 1980, "Investigation of operation of inclined-countercurrent contact tray", Khim. Tekhnol. Topl. Masel, n9, 15.

Matsch, L. C., 1973, "Liquid-gas contact tray", US Patent 3 759 498.

Murphree, E. V., 1925, "Rectifying Column Calculations", Ind. Engng Chem., 17(7), 747.

Porter, K. E., 1973, "Destillations oder Adsorptionskolonne",
German Patent 2 322 895.

Porter, K. E., Davies, B., Enjugu, B. A. and Ani, C. C., 1987, " Investigating the effect of the liquid flow pattern on sieve tray performance by means of the water-cooling technique", IChemE Symp. Ser., n104, 569.

Porter, K. E., O'Donnell, K. A. and Latipifour, M., 1982, "The use of water-cooling to investigate flow pattern effects on tray efficiency", IChemE Jubilee Symp. Ser., 173.

Porter, K. E. and Jenkins, J. D., 1979, "The interrelationship between industrial practice and academic researchin distillation and absorption", IChemE Symp. Ser., n56, 5.1/1.

Porter, K. E., Lockett, M. J. and Lim, C. T., 1972, "The effect of liquid channelling on distillation plate efficiency", Trans. IChemE, 50, 91.

Raper, J. A., Hai, N. T., Pinczewski, W. V. and Fell, C. J. D., 1984, "Liquid passage on sieve trays operating in the spray regime", Chem. Eng. Res. Des., 62(2), 111.

Sohlo, J. J. and Kinnunen, S., 1977, "Dispersion and flow phenomena on a sieve plate", Chem. Engng Sci., 55(2), 71.

Sohlo, J. and Kouri, R. J., 1982, "An analysis of enhansed transverse dispersion on distillation plates", Chem. Engng Sci., 37(2), 193.

Solari, R. B. and Bell, R. L., 1986, "Fluid flow patterns and velocity distribution on comercial scale sieve trays", AIChE J., 32(4), 640.

Solari, R., Saez, E., D'Apollo, I. and Bellet, A., 1982, "Velocity distribution and liquid flow patterns on industrial sieve trays", Chem. Engng Comm. 13, 369.

Stichlmair, J. and Ulbrich, S., 1987, "Liquid channelling on trays and its effect on plate efficiency", IChemE Symp. Ser., n104, 555.

Stichlmair, J. and Weisshuhn, E., 1973, "Untersuchungen zum bodenwirkungsgrad unter besonderer berucksichtigung der flussigkeitsvermischung", Chem. Ing. Tech., 45(5), 242.

Taylor, J. R., 1982, "An Introduction to Error Analysis", University Science books, Mill Valley, CA, USA.

van Winkle, M., 1967, "Distillation", McGraw-Hill, New York.

Weiler, D. W., Bonnet, F. W. and Leavitt, F. W., 1971, "Slotted sieve trays", Chem. Engng Prog., 67(9), 86.

Weiler, D. W., Delnicki, W. V. and England, B. L., 1973, "Flow hydraulics of large diameter trays", Chem. Engng Prog., 69(10), 67.

Williams, B. and Yendall, E. F., 1963, "Improvements in and relating to liquid-gas

contact tray", GB Patent 941 783.

Williams, B. and Yendall, E. F., 1968, "Apparatus for liquid-gas contacting tray", US Patent 3 417 975.

Yu, K. T., Huang, J., Li, J. L. and Song, H. H., 1990, "Two-dimensional flow and eddy diffusion on a sieve tray", Chem. Engng Sci., 45(9), 2901.

Yu, K. T., Huang, J. and Zhang, Z. T., 1982, "The residence time distributions and efficiencies of large trays", Proceedings of Joint Meeting of Chemical Engineering, Beijing, China, 2, 425.

Yu, K. T., Huang, J. and Zhang, Z. T., 1986, "Residence time profile and plate efficiency for a large tray with single-pass or two-pass liquid flow", J. Chem. Ind. Engng (China), 2, 151.

Zuiderweg, F. J., 1982, "Sieve trays - a view on the state of the art", Chem. Engng Sci., 37(10), 1441.

APPENDIX 1

Temperature Data Aquisition Program

Below is the Fortran 77 coding written to control the aquisition of the temperature data via the Biodata Microlink Interface.

```
      PROGRAM TEMPERATURE*COLLECTION
C
      LOGICAL*2  OPENGP,SENDCO,CLOSEG
      INTEGER*2  READDA,WRITED
      INTEGER*2  SIFC,UNL,UNT,LAD,TAD,SAD
C
      LOGICAL*2  NUM
      INTEGER*2  WRGE,RRGE,RGE,RTD8H,COMBUF,K
      INTEGER*2  J,I,IMON,MON,BUF(240),BUM,SECADD
      INTEGER*2  CHAN,BUFF(240),PRTINT(120),COUNT
      REAL  RES(120),TEMP(120),AVT(5),AVTE(5,120),SUM
      REAL  A,B,C,AIRV,WEIRL,DEW,DIA,WEIR,HOW,GAP,FREE
      REAL  CTEMP(20,120),ACTEMP(120)
      CHARACTER*2  ALPHA,ANS
C
      DATA  SIFC,UNL,UNT / 128,63,95 /
      DATA  LAD,TAD,SAD / 32,64,96 /
      DATA  WRGE,RRGE / 0,4 /
C
      RTD8H=15
      RGE=RRGE
      IMON=1
      DO 10 J=1,25
         WRITE (*,100)
  100    FORMAT (4X,' ')
  10  CONTINUE
      OPEN (UNIT=15,FILE='TEMP.DAT',STATUS='UNKNOWN')
      OPEN (UNIT=16,FILE='CTEMP.DAT',STATUS='UNKNOWN')
C
C*************************************************************
C     READ IN PRT CALIBRATION DATA
C*************************************************************
C
      OPEN (UNIT=13,FILE='CAL.DAT',STATUS='UNKNOWN')
      DO 11 I=1,5
         READ (13,101) AVT(I)
  101    FORMAT(26X,F6.2)
         READ (13,102) ALPHA
  102    FORMAT(4X,A2)
         DO 12 J=1,120,8
            READ (13,103) (AVTE(I,K),K=J,(J+7))
  103       FORMAT(13X,8(2X,F6.2))
  12     CONTINUE
```

```
  11  CONTINUE
      CLOSE (UNIT=13)
C
C*************************************************************
C     OPEN CONNECTION WITH DRIVERS
C*************************************************************
C
      IF (.NOT.OPENGP()) THEN
         WRITE(*,200)
  200    FORMAT(10X,'OPENING ERROR')
         STOP
      END IF
C
C*************************************************************
C     RESET ALL DEVICES CONNECTED TO BUS
C*************************************************************
C
      COMBUF=SIFC
      NUM=SENDCO(COMBUF)
      IF (.NOT.NUM) THEN
         WRITE(*,201)
  201    FORMAT(10X,'SIGNAL INTERFACE CLEAR ERROR')
         STOP
      END IF
C
C*************************************************************
C     DISENGAGE THE HSC
C*************************************************************
C
      COMBUF=LAD+7
      NUM=SENDCO(COMBUF)
      IF (.NOT.NUM) THEN
         WRITE(*,202)
  202    FORMAT(10X,'LISTEN ADDRESS ERROR -- DISENGAGE')
         STOP
      END IF
      COMBUF=SAD+0
      NUM=SENDCO(COMBUF)
      IF (.NOT.NUM) THEN
         WRITE(*,203)
  203    FORMAT(10X,'LISTEN ADDRESS ERROR -- DISENGAGE')
         STOP
      END IF
      BUF(1)=0
      BUF(2)=0
      CALL INT2BY (BUF(1),2)
      BUM=WRITED(BUF(1),2)
      IF (BUM.NE.2) THEN
         WRITE(*,204)
  204    FORMAT(10X,'DATA TRANSFER ERROR -- DISENGAGE')
         STOP
      END IF
      COMBUF=UNL
      NUM=SENDCO(COMBUF)
      IF (.NOT.NUM) THEN
         WRITE(*,205)
  205    FORMAT(10X,'UNLISTEN ERROR -- DISENGAGE')
         STOP
      END IF
C
C*************************************************************
```

```
C     SET THE RANGES OF ALL CHANNELS PLUS
C     RETURN FLAG AT THE LAST CHANNEL
C*************************************************************
C
      DO 13 SECADD=1,RTD8H
         DO 14 CHAN=0,7
            COMBUF=LAD+7
            NUM=SENDCO(COMBUF)
            IF (.NOT.NUM) THEN
               WRITE(*,206)
  206          FORMAT(10X,'LISTEN ADDRESS ERROR -- RANGES')
               STOP
            END IF
            COMBUF=SAD+SECADD
            NUM=SENDCO(COMBUF)
            IF (.NOT.NUM) THEN
               WRITE(*,207)
  207          FORMAT(10X,'LISTEN ADDRESS ERROR -- RANGES')
               STOP
            END IF
            BUF(1)=4*CHAN
            IF ((SECADD.EQ.RTD8H).AND.(CHAN.EQ.7))
               BUF(1)=BUF(1)+2
            END IF
            BUF(2)=RGE
            CALL INT2BY (BUF(1),2)
            BUM=WRITED(BUF(1),2)
            IF (BUM.NE.2) THEN
               WRITE(*,208)
  208          FORMAT(10X,'DATA TRANSFER ERROR -- RANGES')
               STOP
            END IF
            CONBUF=UNL
            NUM=SENDCO(COMBUF)
            IF (.NOT.NUM) THEN
               WRITE(*,209)
  209          FORMAT(10X,'UNLISTEN ERROR -- RANGES')
               STOP
            END IF
   14    CONTINUE
   13 CONTINUE
C
C*************************************************************
C     SET BASIC UNITS OF THE HSC AND GIVE THE
C     NUMBER OF UNIT BETWEEN EACH CHANNEL
C*************************************************************
C
      COMBUF=LAD+7
      NUM=SENDCO(COMBUF)
      IF (.NOT.NUM) THEN
         WRITE(*,210)
  210    FORMAT(10X,'LISTEN ADDRESS ERROR -- SETHSC')
         STOP
      END IF
      COMBUF=SAD+0
      NUM=SENDCO(COMBUF)
      IF (.NOT.NUM) THEN
         WRITE(*,211)
  211    FORMAT(10X,'LISTEN ADDRESS ERROR -- SETHSC')
         STOP
      END IF
```

```
      BUF(1)=4+8
      BUF(2)=1
      CALL INT2BY (BUF(1),2)
      BUM=WRITED(BUF(1),2)
      IF (BUM.NE.2) THEN
         WRITE(*,212)
 212     FORMAT(10X,'DATA TRANSFER ERROR -- SETHSC')
         STOP
      END IF
      COMBUF=UNL
      NUM=SENDCO(COMBUF)
      IF (.NOT.NUM) THEN
         WRITE(*,213)
  213    FORMAT(10X,'UNLISTEN ERROR -- SETHSC')
         STOP
      END IF
C
C*************************************************************
C     SET TALK ADDRESS TO THE FIRST RTD8H
C*************************************************************
C
  99  COMBUF=TAD+7
      NUM=SENDCO(COMBUF)
      IF (.NOT.NUM) THEN
         WRITE(*,214)
  214    FORMAT(10X,'LISTEN ADDRESS ERROR -- FIRSTRTD8H')
         STOP
      END IF
      COMBUF=SAD+1
      NUM=SENDCO(COMBUF)
      IF (.NOT.NUM) THEN
         WRITE(*,215)
  215    FORMAT(10X,'LISTEN ADDRESS ERROR -- FIRSTRTD8H')
         STOP
      END IF
C
C*************************************************************
C     ENABLE THE GET COMMAND
C*************************************************************
C
      COMBUF=8
      NUM=SENDCO(COMBUF)
      IF (.NOT.NUM) THEN
         WRITE(*,216)
  216    FORMAT(10X,'LISTEN ADDRESS ERROR -- ENABLE')
         STOP
      END IF
C
C*************************************************************
C     READ IN TWO TIMES THE NUMBER OF CHANNELS OF DATA
C     BYTES, CONVERT ALL DATA BYTES TO INTEGERS AND
C     REARRANGE DATA DUE TO THE HSC READING FROM CHANNEL
C     7 TO 0
C*************************************************************
C
      BUM=READDA(BUF(1),(RTD8H*8*2))
      IF (BUM.NE.(RTD8H*8*2)) THEN
         WRITE(*,217)
 217     FORMAT(10X,'DATA TRANSFER ERROR -- READ DATA')
         STOP
      END IF
```

```
      COMBUF=UNT
      NUM=SENDCO(COMBUF)
      IF (.NOT.NUM) THEN
         WRITE(*,218)
  218    FORMAT(10X,'UNTALK ADDRESS ERROR -- READ DATA')
         STOP
      END IF
      CALL BYT2IN (BUF(1),(RTD8H*8*2))
      DO 15 I=1,(RTD8H*8*2),16
         DO 16 J=0,14,2
            BUFF(I+J)=BUF(I+14-J)
            BUFF(I+J+1)=BUF(I+14-J+1)
  16     CONTINUE
  15  CONTINUE
C
C*************************************************************
C     CALCULATE RESISTANCES AND TEMPERATURES
C*************************************************************
C
      DO 17 I=1,((RTD8H*8*2)-1),2
         COUNT=(I+1)/2
         PRTINT(COUNT)=((BUFF(I)*256)+BUFF(I+1))
         RES(COUNT)=((PRTINT(COUNT)*0.00625)+96.0)
         TEMP(COUNT)=((RES(COUNT)-100.0)*60.0/(119.40-96.09))
  17  CONTINUE
C
C*************************************************************
C     HI LO ERROR DETECTION AND TEMPERATURE
C     CONVERSION USING CALIBRATION DATA
C*************************************************************
C
      DO 18 I=1,(RTD8H*8)
         IF (I.EQ.17) THEN
            CTEMP(IMON,I)=99.99
            GO TO 18
         ELSE IF (I.EQ.20) THEN
            CTEMP(IMON,I)=99.99
            GO TO 18
         ELSE IF (I.EQ.54) THEN
            CTEMP(IMON,I)=99.99
            GO TO 18
         ELSE IF (I.EQ.91) THEN
            CTEMP(IMON,I)=99.99
            GO TO 18
         END IF
         IF (TEMP(I).LT.-10.0) THEN
            CTEMP(IMON,I)=99.99
            GO TO 18
         ELSE IF (TEMP(I).GE.55.0) THEN
            CTEMP(IMON,I)=99.99
            GO TO 18
         END IF
         IF (TEMP(I).GT.AVT(2)) THEN
            A=AVT(1)-AVT(2)
            B=AVTE(1,I)-AVTE(2,I)
            C=TEMP(I)-AVTE(2,I)
            CTEMP(IMON,I)=AVT(2)+(C*A/B)
         ELSE IF (TEMP(I).GT.AVT(3)) THEN
            A=AVT(2)-AVT(3)
            B=AVTE(2,I)-AVTE(3,I)
            C=TEMP(I)-AVTE(3,I)
```

```
            CTEMP(IMON,I)=AVT(3)+(C*A/B)
         ELSE IF (TEMP(I).GT.AVT(4)) THEN
            A=AVT(3)-AVT(4)
            B=AVTE(3,I)-AVTE(4,I)
            C=TEMP(I)-AVTE(4,I)
            CTEMP(IMON,I)=AVT(4)+(C*A/B)
         ELSE IF (TEMP(I).LE.AVT(4)) THEN
            A=AVT(4)-AVT(5)
            B=AVTE(4,I)-AVTE(5,I)
            C=TEMP(I)-AVTE(5,I)
            CTEMP(IMON,I)=AVT(5)+(C*A/B)
         END IF
   18  CONTINUE
C
C*************************************************************
C     ROUTINE TO RETURN THE CURSOR TO
C     THE TOP LEFT OF THE SCREEN
C*************************************************************
C
      CALL HOME
C
C*************************************************************
C     OUTPUT TO RAW TEMPERATURE FILE - TEMP.DAT
C*************************************************************
C
      WRITE(15,300) TEMP(21),TEMP(19),TEMP(18),TEMP(22),
     >TEMP(113)
      WRITE(15,301) TEMP(1),TEMP(29),TEMP(51),TEMP(50),
     >TEMP(116),TEMP(115),TEMP(114),TEMP(9)
      WRITE(15,302) TEMP(5),TEMP(2),TEMP(30),TEMP(52),
     >TEMP(49),TEMP(117),TEMP(120),TEMP(88),TEMP(10),
     >TEMP(14)
      WRITE(15,303) TEMP(8),TEMP(6),TEMP(3),TEMP(31),
     >TEMP(53),TEMP(24),TEMP(118),TEMP(87),TEMP(86),
     >TEMP(11),TEMP(15),TEMP(42)
      WRITE(15,303) TEMP(25),TEMP(7),TEMP(4),TEMP(32),
     >TEMP(55),TEMP(23),TEMP(119),TEMP(85),TEMP(84),
     >TEMP(12),TEMP(16),TEMP(43)
      WRITE(15,303) (TEMP(I),I=26,28),TEMP(97),TEMP(56),
     >TEMP(109),TEMP(17),TEMP(82),TEMP(83),TEMP(13),
     >TEMP(41),TEMP(44)
      WRITE(15,303) TEMP(59),TEMP(58),TEMP(57),TEMP(98),
     >TEMP(73),TEMP(20),TEMP(112),TEMP(81),
     >(TEMP(I),I=48,45,-1)
      WRITE(15,303) TEMP(62),TEMP(61),TEMP(60),TEMP(99),
     >TEMP(76),TEMP(75),TEMP(111),TEMP(66),TEMP(68),
     >TEMP(70),TEMP(90),TEMP(89)
      WRITE(15,303) TEMP(104),TEMP(64),TEMP(63),TEMP(74),
     >TEMP(77),TEMP(78),TEMP(65),TEMP(67),TEMP(69),
     >TEMP(94),TEMP(93),TEMP(92)
      WRITE(15,302) TEMP(102),TEMP(101),TEMP(33),TEMP(80),
     >TEMP(79),TEMP(71),TEMP(72),TEMP(106),TEMP(105),
     >TEMP(107)
      WRITE(15,301) TEMP(103),TEMP(100),TEMP(34),TEMP(35),
     >TEMP(39),TEMP(40),TEMP(110),TEMP(108)
      WRITE(15,304) TEMP(38)
      WRITE(15,305) TEMP(96),TEMP(36),TEMP(37)
  300 FORMAT(43X,5(F6.2,4X))
  301 FORMAT(28X,8(F6.2,4X))
  302 FORMAT(18X,10(F6.2,4X))
  303 FORMAT(8X,12(F6.2,4X))
```

```
  304 FORMAT(63X,F6.2)
  305 FORMAT(10X,3(F6.2,4X))
C
C*************************************************************
C     OUTPUT TO CALIBRATED TEMPERATURE FILE - CTEMP.DAT
C*************************************************************
C
      WRITE(16,300) CTEMP(IMON,21),CTEMP(IMON,19),
     >CTEMP(IMON,18),CTEMP(IMON,22),CTEMP(IMON,113)
      WRITE(16,301) CTEMP(IMON,1),CTEMP(IMON,29),
     >CTEMP(IMON,51),CTEMP(IMON,50),CTEMP(IMON,116),
     >CTEMP(IMON,115),CTEMP(IMON,114),CTEMP(IMON,9)
      WRITE(16,302) CTEMP(IMON,5),CTEMP(IMON,2),
     >CTEMP(IMON,30),CTEMP(IMON,52),CTEMP(IMON,49),
     >CTEMP(IMON,117),CTEMP(IMON,120),CTEMP(IMON,88),
     >CTEMP(IMON,10),CTEMP(IMON,14)
      WRITE(16,303) CTEMP(IMON,8),CTEMP(IMON,6),
     >CTEMP(IMON,3),CTEMP(IMON,31),CTEMP(IMON,53),
     >CTEMP(IMON,24),CTEMP(IMON,118),CTEMP(IMON,87),
     >CTEMP(IMON,86),CTEMP(IMON,11),CTEMP(IMON,15),
     >CTEMP(IMON,42)
      WRITE(16,303) CTEMP(IMON,25),CTEMP(IMON,7),
     >CTEMP(IMON,4),CTEMP(IMON,32),CTEMP(IMON,55),
     >CTEMP(IMON,23),CTEMP(IMON,119),CTEMP(IMON,85),
     >CTEMP(IMON,84),CTEMP(IMON,12),CTEMP(IMON,16),
     >CTEMP(IMON,43)
      WRITE(16,303) (CTEMP(IMON,I),I=26,28),CTEMP(IMON,97),
     >CTEMP(IMON,56),CTEMP(IMON,109),CTEMP(IMON,17),
     >CTEMP(IMON,82),CTEMP(IMON,83),CTEMP(IMON,13),
     >CTEMP(IMON,41),CTEMP(IMON,44)
      WRITE(16,303) CTEMP(IMON,59),CTEMP(IMON,58),
     >CTEMP(IMON,57),CTEMP(IMON,98),CTEMP(IMON,73),
     >CTEMP(IMON,20),CTEMP(IMON,112),CTEMP(IMON,81),
     >(CTEMP(IMON,I),I=48,45,-1)
      WRITE(16,303) CTEMP(IMON,62),CTEMP(IMON,61),
     >CTEMP(IMON,60),CTEMP(IMON,99),CTEMP(IMON,76),
     >CTEMP(IMON,75),CTEMP(IMON,111),CTEMP(IMON,66),
     >CTEMP(IMON,68),CTEMP(IMON,70),CTEMP(IMON,90),
     >CTEMP(IMON,89)
      WRITE(16,303) CTEMP(IMON,104),CTEMP(IMON,64),
     >CTEMP(IMON,63),CTEMP(IMON,74),CTEMP(IMON,77),
     >CTEMP(IMON,78),CTEMP(IMON,65),CTEMP(IMON,67),
     >CTEMP(IMON,69),CTEMP(IMON,94),CTEMP(IMON,93),
     >CTEMP(IMON,92)
      WRITE(16,302) CTEMP(IMON,102),CTEMP(IMON,101),
     >CTEMP(IMON,33),CTEMP(IMON,80),CTEMP(IMON,79),
     >CTEMP(IMON,71),CTEMP(IMON,72),CTEMP(IMON,106),
     >CTEMP(IMON,105),CTEMP(IMON,107)
      WRITE(16,301) CTEMP(IMON,103),CTEMP(IMON,100),
     >CTEMP(IMON,34),CTEMP(IMON,35),CTEMP(IMON,39),
     >CTEMP(IMON,40),CTEMP(IMON,110),CTEMP(IMON,108)
      WRITE(16,304) CTEMP(IMON,38)
      WRITE(16,305) CTEMP(IMON,96),CTEMP(IMON,36),
     >CTEMP(IMON,37)
C
C*************************************************************
C     OUTPUT TO SCREEN
C*************************************************************
C
      WRITE(*,501) CTEMP(IMON,21),CTEMP(IMON,19),
     >CTEMP(IMON,18),CTEMP(IMON,22),CTEMP(IMON,113)
```

```
      WRITE(*,502) CTEMP(IMON,1),CTEMP(IMON,51),
     >CTEMP(IMON,115),CTEMP(IMON,9)
      WRITE(*,503) CTEMP(IMON,25),CTEMP(IMON,4),
     >CTEMP(IMON,55),CTEMP(IMON,85),CTEMP(IMON,12),
     >CTEMP(IMON,43)
      WRITE(*,503) CTEMP(IMON,59),CTEMP(IMON,57),
     >CTEMP(IMON,73),CTEMP(IMON,81),CTEMP(IMON,47),
     >CTEMP(IMON,45)
      WRITE(*,503) CTEMP(IMON,104),CTEMP(IMON,63),
     >CTEMP(IMON,77),CTEMP(IMON,67),CTEMP(IMON,94),
     >CTEMP(IMON,92)
      WRITE(*,502) CTEMP(IMON,103),CTEMP(IMON,34),
     >CTEMP(IMON,40),CTEMP(IMON,108)
      WRITE(*,504) CTEMP(IMON,38)
      WRITE(*,505) CTEMP(IMON,96)
  501 FORMAT (16X,5(F6.2,6X))
  502 FORMAT (22X,4(F6.2,6X))
  503 FORMAT (10X,6(F6.2,6X))
  504 FORMAT (40X,F6.2)
  505 FORMAT (10X,F6.2)
C
C*************************************************************
C     NUMBER OF SCANS
C*************************************************************
C
      MON=20
      IF (IMON.LT.MON) THEN
         IMON=IMON+1
         GO TO 99
      END IF
C
C*************************************************************
C     AVERAGING OF THE 20 SETS OF DATA
C*************************************************************
C
      DO 19 I=1,120
         SUM=0.0
         COUNT=0
         ACTEMP(I)=99.99
         DO 20 J=1,20
            IF (CTEMP(J,I).NE.99.99) THEN
               COUNT=COUNT+1
               SUM=SUM+CTEMP(J,I)
            END IF
  20     CONTINUE
         IF (COUNT.NE.0) THEN
            ACTEMP(I)=SUM/COUNT
         END IF
  19  CONTINUE
C
C*************************************************************
C     SAVE RUN AND OPERATING PARAMETERS ?
C*************************************************************
C
      WRITE (*,600)
  600 FORMAT (4X,' ')
      WRITE (*,601)
  601 FORMAT (4X,'DO YOU WISH TO RECORD THE RUN ? (Y OR N)')
      READ (*,602) ANS
  602 FORMAT (A1)
      IF ((ANS.EQ.'Y').OR.(ANS.EQ.'y')) THEN
```

```
      WRITE (*,603)
603   FORMAT (4X,'INPUT AIR VELOCITY ? (m/s)')
      READ(*,*) AIRV
      WRITE(*,604)
604   FORMAT(4X,'INPUT WEIR LOAD ? (cm3/cm.s)')
      READ(*,*) WEIRL
      WRITE(*,605)
605   FORMAT(10X,'INPUT DEW POINT ? (deg c)')
      READ(*,*) DEW
      DIA=2.440
      WEIR=1.50
      HOW=0.010
      GAP=0.010
      FREE=10.0
C
      WRITE (*,600)
      WRITE (*,600)
      WRITE (*,600)
      WRITE (*,606) AIRV
      WRITE (*,607) WEIRL
      WRITE (*,608) DEW
      WRITE (*,600)
      WRITE (*,609) DIA
      WRITE (*,610) WEIR
      WRITE (*,611) FREE
      WRITE (*,612) HOW
      WRITE (*,613) GAP
C
      WRITE (15,600)
      WRITE (15,600)
      WRITE (15,600)
      WRITE (15,606) AIRV
      WRITE (15,607) WEIRL
      WRITE (15,608) DEW
      WRITE (15,600)
      WRITE (15,609) DIA
      WRITE (15,610) WEIR
      WRITE (15,611) FREE
      WRITE (15,612) HOW
      WRITE (15,613) GAP
C
      WRITE (16,600)
      WRITE (16,600)
      WRITE (16,600)
      WRITE (16,606) AIRV
      WRITE (16,607) WEIRL
      WRITE (16,608) DEW
      WRITE (16,600)
      WRITE (16,609) DIA
      WRITE (16,610) WEIR
      WRITE (16,611) FREE
      WRITE (16,612) HOW
      WRITE (16,613) GAP
C
      OPEN (UNIT=17,FILE='ACTEMP.DAT',STATUS='UNKNOWN')
C
      WRITE (17,606) AIRV
      WRITE (17,607) WEIRL
      WRITE (17,608) DEW
      WRITE (17,600)
      WRITE (17,609) DIA
```

```
      WRITE (17,610) WEIR
      WRITE (17,611) FREE
      WRITE (17,612) HOW
      WRITE (17,613) GAP
      WRITE (17,600)
      WRITE (17,600)
      WRITE (17,600)
     WRITE(17,300) ACTEMP(21),ACTEMP(19),
    >ACTEMP(18),ACTEMP(22),ACTEMP(113)
     WRITE(17,301) ACTEMP(1),ACTEMP(29),
    >ACTEMP(51),ACTEMP(50),ACTEMP(116),
    >ACTEMP(115),ACTEMP(114),ACTEMP(9)
     WRITE(17,302) ACTEMP(5),ACTEMP(2),
    >ACTEMP(30),ACTEMP(52),ACTEMP(49),
    >ACTEMP(117),ACTEMP(120),ACTEMP(88),
    >ACTEMP(10),ACTEMP(14)
     WRITE(17,303) ACTEMP(8),ACTEMP(6),
    >ACTEMP(3),ACTEMP(31),ACTEMP(53),
    >ACTEMP(24),ACTEMP(118),ACTEMP(87),
    >ACTEMP(86),ACTEMP(11),ACTEMP(15),
    >ACTEMP(42)
     WRITE(17,303) ACTEMP(25),ACTEMP(7),
    >ACTEMP(4),ACTEMP(32),ACTEMP(55),
    >ACTEMP(23),ACTEMP(119),ACTEMP(85),
    >ACTEMP(84),ACTEMP(12),ACTEMP(16),
    >ACTEMP(43)
     WRITE(17,303) (ACTEMP(I),I=26,28),ACTEMP(97),
    >ACTEMP(56),ACTEMP(109),ACTEMP(17),
    >ACTEMP(82),ACTEMP(83),ACTEMP(13),
    >ACTEMP(41),ACTEMP(44)
     WRITE(17,303) ACTEMP(59),ACTEMP(58),
    >ACTEMP(57),ACTEMP(98),ACTEMP(73),
    >ACTEMP(20),ACTEMP(112),ACTEMP(81),
    >(ACTEMP(I),I=48,45,-1)
     WRITE(17,303) ACTEMP(62),ACTEMP(61),
    >ACTEMP(60),ACTEMP(99),ACTEMP(76),
    >ACTEMP(75),ACTEMP(111),ACTEMP(66),
    >ACTEMP(68),ACTEMP(70),ACTEMP(90),
    >ACTEMP(89)
     WRITE(17,303) ACTEMP(104),ACTEMP(64),
    >ACTEMP(63),ACTEMP(74),ACTEMP(77),
    >ACTEMP(78),ACTEMP(65),ACTEMP(67),
    >ACTEMP(69),ACTEMP(94),ACTEMP(93),
    >ACTEMP(92)
     WRITE(17,302) ACTEMP(102),ACTEMP(101),
    >ACTEMP(33),ACTEMP(80),ACTEMP(79),
    >ACTEMP(71),ACTEMP(72),ACTEMP(106),
    >ACTEMP(105),ACTEMP(107)
     WRITE(17,301) ACTEMP(103),ACTEMP(100),
    >ACTEMP(34),ACTEMP(35),ACTEMP(39),
    >ACTEMP(40),ACTEMP(110),ACTEMP(108)
     WRITE(17,304) ACTEMP(38)
     WRITE(17,305) ACTEMP(96),ACTEMP(36),ACTEMP(37)
606 FORMAT (4X,'AIR VELOCITY (m/s)      ',F3.1)
607 FORMAT (4X,'WEIR LOAD (cm3/cm.s)    ',F4.0)
608 FORMAT (4X,'DEW POINT (deg c)       ',F4.1)
609 FORMAT (4X,'COLUMN DIAMETER (m)     ',F5.3)
610 FORMAT (4X,'WEIR LENGTH (m)         ',F5.3)
611 FORMAT (4X,'FREE AREA (%)           ',F4.1)
612 FORMAT (4X,'OUTLET WEIR HEIGHT (m) ',F5.3)
613 FORMAT (4X,'INLET WEIR GAP (m)      ',F5.3)
```

```
      END IF
      CLOSE (UNIT=15)
      CLOSE (UNIT=16)
      CLOSE (UNIT=17)
C
C*************************************************************
C     CLOSE CONNECTION WITH DRIVERS
C*************************************************************
C
      IF (.NOT.CLOSEG()) THEN
         WRITE(*,219)
  219    FORMAT(10X,'CLOSING ERROR')
         STOP
      END IF
C
C*************************************************************
C     STOP AND END
C*************************************************************
C
      STOP
      END
C
C*************************************************************
C     SUBROUTINE USED TO RETURN THE CURSOR
C     TO THE TOP LEFT OF THE SCREEN
C*************************************************************
C
      SUBROUTINE HOME
      CHARACTER*4  STRING
      STRING='\x1B[;H'C
      PRINT*,STRING
      RETURN
      END
```

APPENDIX 2

Temperaure Plotting Program

Below is contained the Fortran 77 coding written to generate the temperature contours and surfaces. The coding calls on routines from the UNIRAS suite of software.

```
      PROGRAM TEMPERATURE
      INTEGER  I,J,K,NUM,LENY(6),LENX(7),IPLANE(3),LENGTH(6)
      REAL  AIRV,WEIRL,DEW,DIA,WEIR,HOW,GAP,FREE,TDOWN
      REAL  TEMPIN(5),TEMP(108),AIR(3),X(108),Y(108)
      REAL  XPOS(108),YPOS(108),TPOS(108),TR(108),ZCL(39)
      REAL  ZEST(24,20),XEDGE(17),YEDGE(17)
      CHARACTER*2  ALPHA
      CHARACTER*4  LABY(6),LABX(7)
      CHARACTER*21  TEXT(6)
C
      PARAMETER(JMEMFX=10000,JMEMSZ=JMEMFX+400)
      COMMON /UNIMEM/ IDUM1,MEMMAX,IDUM2,ITEM(JMEMSZ)
      MEMMAX=JMEMFX
C
      DATA  ZCL / 0.025,0.050,0.075,0.100,0.125,0.150,0.175
     $,0.200,0.225,0.250,0.275,0.300,0.325,0.350,0.375,0.400
     $,0.425,0.450,0.475,0.500,0.525,0.550,0.575,0.600,0.625
     $,0.650,0.675,0.700,0.725,0.750,0.775,0.800,0.825,0.850
     $,0.875,0.900,0.925,0.950,0.975 /
      DATA  LENY /6*-1/
      DATA  LENX /7*-1/
      DATA  LABY /'2000','1600','1200','800','400','0'/
      DATA  LABX /' ','800','400',' 0','-400','-800',' '/
      DATA  IPLANE /1,1,1/,LENGTH /0,16,0,21,0,16/
      DATA  TEXT /' ','WEIR LENGTH - mm',' '
     #,'FLOW PATH LENGTH - mm',' ','REDUCED TEMP - '/
C
C*************************************************************
C     COLUMN WALL DATA
C*************************************************************
C
      XEDGE(1)=999.999
      XEDGE(2)=-1200.0
      XEDGE(3)=-1150.0
      XEDGE(4)=-1050.0
      XEDGE(5)=-720.0
      XEDGE(6)=720.0
      XEDGE(7)=1050.0
      XEDGE(8)=1150.0
      XEDGE(9)=1200.0
      XEDGE(10)=1150.0
      XEDGE(11)=1050.0
      XEDGE(12)=720.0
```

```
      XEDGE(13)=-720.0
      XEDGE(14)=-1050.0
      XEDGE(15)=-1150.0
      XEDGE(16)=-1200.0
      XEDGE(17)=999.999
C
      YEDGE(1)=999.999
      YEDGE(2)=0.0
      YEDGE(3)=-400.0
      YEDGE(4)=-650.0
      YEDGE(5)=-980.0
      YEDGE(6)=-980.0
      YEDGE(7)=-650.0
      YEDGE(8)=-400.0
      YEDGE(9)=0.0
      YEDGE(10)=400.0
      YEDGE(11)=650.0
      YEDGE(12)=980.0
      YEDGE(13)=980.0
      YEDGE(14)=650.0
      YEDGE(15)=400.0
      YEDGE(16)=0.0
      YEDGE(17)=999.999
C
C*************************************************************
C     PRT POSITIONS ON TRAY AND INLET DOWNCOMER
C*************************************************************
C
      DO 42 I=1,8
         X(I)=(-700+((I-1)*200))
         Y(I)=900
  42  CONTINUE
C
      DO 43 I=9,18
         X(I)=(-900+((I-9)*200))
         Y(I)=700
  43  CONTINUE
C
      DO 44 I=19,30
         X(I)=(-1100+((I-19)*200))
         Y(I)=500
  44  CONTINUE
C
      X(19)=(X(19)+100)
      X(30)=(X(30)-100)
C
      DO 45 I=31,42
         X(I)=(-1100+((I-31)*200))
         Y(I)=300
  45  CONTINUE
C
      DO 46 I=43,54
         X(I)=(-1100+((I-43)*200))
         Y(I)=100
  46  CONTINUE
C
      X(43)=(X(43)-50)
      X(54)=(X(54)+50)
C
      DO 47 I=55,66
         X(I)=(-1100+((I-55)*200))
```

```
         Y(I)=(-100)
   47  CONTINUE
C
       X(55)=(X(55)-50)
       X(66)=(X(66)+50)
C
       DO 48 I=67,78
          X(I)=(-1100+((I-67)*200))
          Y(I)=(-300)
   48  CONTINUE
C
       DO 49 I=79,90
          X(I)=(-1100+((I-79)*200))
          Y(I)=(-500)
   49  CONTINUE
C
       X(79)=(X(79)+100)
       X(90)=(X(90)-100)
C
       DO 50 I=91,100
          X(I)=(-900+((I-91)*200))
          Y(I)=(-700)
   50  CONTINUE
C
       DO 51 I=101,108
          X(I)=(-700+((I-101)*200))
          Y(I)=(-900)
   51  CONTINUE
C
C*************************************************************
C      READING IN TEMPERATURE DATA
C*************************************************************
C
       READ (14,300) AIRV
       READ (14,301) WEIRL
       READ (14,302) DEW
       READ (14,303) ALPHA
       READ (14,304) DIA
       READ (14,305) WEIR
       READ (14,306) FREE
       READ (14,307) HOW
       READ (14,308) GAP
       READ (14,303) ALPHA
       READ (14,303) ALPHA
       READ (14,303) ALPHA
       READ (14,309) (TEMPIN(I),I=1,5)
       READ (14,310) (TEMP(I),I=1,8)
       READ (14,311) (TEMP(I),I=9,18)
       READ (14,312) (TEMP(I),I=19,30)
       READ (14,312) (TEMP(I),I=31,42)
       READ (14,312) (TEMP(I),I=43,54)
       READ (14,312) (TEMP(I),I=55,66)
       READ (14,312) (TEMP(I),I=67,78)
       READ (14,312) (TEMP(I),I=79,90)
       READ (14,311) (TEMP(I),I=91,100)
       READ (14,310) (TEMP(I),I=101,108)
       READ (14,313) TDOWN
       READ (14,314) (AIR(I),I=1,3)
  300 FORMAT (27X,F3.1)
  301 FORMAT (27X,F4.0)
  302 FORMAT (27X,F4.1)
```

```
  303 FORMAT (4X,A2)
  304 FORMAT (27X,F5.3)
  305 FORMAT (27X,F5.3)
  306 FORMAT (27X,F4.1)
  307 FORMAT (27X,F5.3)
  308 FORMAT (27X,F5.3)
  309 FORMAT (43X,5(F6.2,4X))
  310 FORMAT (28X,8(F6.2,4X))
  311 FORMAT (18X,10(F6.2,4X))
  312 FORMAT (8X,12(F6.2,4X))
  313 FORMAT (63X,F6.2)
  314 FORMAT (10X,3(F6.2,4X))
C
C*************************************************************
C     SETTING UP IRREGULAR ARRAYS
C*************************************************************
C
      TEMP(3)=99.99
      NUM=0
      DO 12 I=1,108
         IF (TEMP(I).NE.99.99) THEN
            NUM=NUM+1
            XPOS(NUM)=X(I)
            YPOS(NUM)=Y(I)
            TPOS(NUM)=TEMP(I)
         END IF
  12  CONTINUE
C
C*************************************************************
C     AVERAGING INLET WATER TEMPERATURE
C*************************************************************
C
      WINT=DEW
      DO 13 I=1,5
         IF (TEMPIN(I).NE.99.99) THEN
            IF (TEMPIN(I).GT.WINT) THEN
               WINT=TEMPIN(I)
            END IF
         END IF
  13  CONTINUE
C
C*************************************************************
C     WET BULB TEMPERATURE
C*************************************************************
C
      TWB=DEW
C
C*************************************************************
C     SETTING UP REDUCED TEMPERATURES
C*************************************************************
C
      DO 14 I=1,NUM
         TR(I)=(TPOS(I)-TWB)/(WINT-TWB)
  14  CONTINUE
C
C*************************************************************
C     ROUTINES TO COMMENCE PLOTTING
C*************************************************************
C
      CALL GROUTE ('S HPOSTA4;E')
      CALL GOPEN
```

```
      CALL RORIEN (2)
      CALL GLIMIT (-1200.0,1200.0,-1000.0,1000.0,0.0,1.0)
      CALL RUNDEF (999.999,9999)
      CALL GFAULT (XEDGE,YEDGE,17,1)
      CALL GINTPF (XPOS,YPOS,TR,NUM,ZEST,24,20)
      HFAC=118.0
      CALL GVPORT (50.0,(42.0+HFAC),80.0,80.0)
      CALL GWBOX (1.2,1.0,0.0)
      CALL RCLASS (ZCL,39,0)
      CALL GSMTH (-1)
      CALL GCONAA (-60,60)
      CALL GCONA (1.7,3,30.0,3)
      CALL GCNR2V (ZEST,24,20)
      CALL GSCALE
      CALL GWICOL (0.4,1)
      CALL GVECT (XEDGE,YEDGE,17)
      CALL GSCAMM
      CALL RTXJUS (0,6)
      CALL RTXHEI (2.5)
      CALL RTX (-1,'Air Velocity',155.0,(105.0+HFAC))
      CALL RTXN (AIRV,1,155.0,(99.0+HFAC))
      CALL RTXC (-1,' m/s')
      CALL RTX (-1,'Water Loading',155.0,(91.0+HFAC))
      CALL RTX (-1,'Inlet Gap',155.0,(77.0+HFAC))
      CALL RTXN (GAP,3,155.0,(71.0+HFAC))
      CALL RTXC (-1,' m')
      CALL RTX (-1,'Outlet Weir',155.0,(63.0+HFAC))
      CALL RTXN (HOW,3,155.0,(57.0+HFAC))
      CALL RTXC (-1,' m')
      CALL RTX (-1,'Hole Diameter',155.0,(49.0+HFAC))
      CALL RTX (-1,'0.001 m',155.0,(43.0+HFAC))
      CALL RTXNBO (8,'T')
      CALL RTXN (WEIRL,1,155.0,(85.0+HFAC))
      CALL RTXC (-1,' cm3/cm.s')
C
      CALL GSCALE
      CALL RUXLOP (1)
      CALL RUXSTI (7)
      CALL RUXDIS (1,1,9999)
      CALL RUXDIS (2,1,9999)
      CALL RUXDIS (3,1,9999)
      CALL RUXDIS (4,1,9999)
      CALL RUXDIS (6,1,9999)
      CALL RUXDIS (7,0,9999)
      CALL RUXDIS (8,0,9999)
      CALL RUXTEX (6,-1,'FLOW PATH LENGTH - mm'
     #,999.999,999.999,2.4)
      CALL RUXIS (2,-1200.0,2.3,1,LENY,LABY,6)
      CALL RUXTEA (4,9999,9999,999.999,9999,9999,-90.0)
      CALL RUXTEX (6,-1,'FLOW PATH LENGTH - mm'
     #,999.999,999.999,2.4)
      CALL RUXIS (2,1200.0,2.3,2,LENY,LABY,6)
      CALL RUXTEA (4,9999,9999,999.999,9999,9999,0.0)
      CALL RUXTEX (6,-1,'OUTLET WEIR - mm'
     #,999.999,999.999,2.5)
      CALL RUXIS (1,-1000.0,2.3,1,LENX,LABX,7)
      CALL RUXTEX (6,-1,'INLET WEIR - mm'
     #,999.999,999.999,2.5)
      CALL RUXIS (1,1000.0,2.3,2,LENX,LABX,7)
C
C*************************************************************
```

```
C      COLUMN WALL DATA
C*************************************************************
C
       XEDGE(1)=999.999
       XEDGE(2)=-1200.0
       XEDGE(3)=-1150.0
       XEDGE(4)=-1050.0
       XEDGE(5)=-720.0
       XEDGE(6)=720.0
       XEDGE(7)=1050.0
       XEDGE(8)=1150.0
       XEDGE(9)=1200.0
       XEDGE(10)=1150.0
       XEDGE(11)=1050.0
       XEDGE(12)=720.0
       XEDGE(13)=-720.0
       XEDGE(14)=-1050.0
       XEDGE(15)=-1150.0
       XEDGE(16)=-1200.0
       XEDGE(17)=999.999
C
       YEDGE(1)=999.999
       YEDGE(2)=1000.0
       YEDGE(3)=600.0
       YEDGE(4)=350.0
       YEDGE(5)=0.0
       YEDGE(6)=0.0
       YEDGE(7)=350.0
       YEDGE(8)=600.0
       YEDGE(9)=1000.0
       YEDGE(10)=1400.0
       YEDGE(11)=1650.0
       YEDGE(12)=2000.0
       YEDGE(13)=2000.0
       YEDGE(14)=1650.0
       YEDGE(15)=1400.0
       YEDGE(16)=1000.0
       YEDGE(17)=999.999
C
C*************************************************************
C      PRT POSITIONS ON TRAY AND INLET DOWNCOMER
C*************************************************************
C
       DO 62 I=1,8
          X(I)=(-700+((I-1)*200))
          Y(I)=100
  62   CONTINUE
C
       DO 63 I=9,18
          X(I)=(-900+((I-9)*200))
          Y(I)=300
  63   CONTINUE
C
       DO 64 I=19,30
          X(I)=(-1100+((I-19)*200))
          Y(I)=500
  64   CONTINUE
C
       X(19)=(X(19)+100)
       X(30)=(X(30)-100)
C
```

```
      DO 65 I=31,42
         X(I)=(-1100+((I-31)*200))
         Y(I)=700
   65 CONTINUE
C
      DO 66 I=43,54
         X(I)=(-1100+((I-43)*200))
         Y(I)=900
   66 CONTINUE
C
      X(43)=(X(43)-50)
      X(54)=(X(54)+50)
C
      DO 67 I=55,66
         X(I)=(-1100+((I-55)*200))
         Y(I)=1100
   67 CONTINUE
C
      X(55)=(X(55)-50)
      X(66)=(X(66)+50)
C
      DO 68 I=67,78
         X(I)=(-1100+((I-67)*200))
         Y(I)=1300
   68 CONTINUE
C
      DO 69 I=79,90
         X(I)=(-1100+((I-79)*200))
         Y(I)=1500
   69 CONTINUE
C
      X(79)=(X(79)+100)
      X(90)=(X(90)-100)
C
      DO 70 I=91,100
         X(I)=(-900+((I-91)*200))
         Y(I)=1700
   70 CONTINUE
C
      DO 71 I=101,108
         X(I)=(-700+((I-101)*200))
         Y(I)=1900
   71 CONTINUE
C
C*************************************************************
C     READING IN TEMPERATURE DATA
C*************************************************************
C
      READ (15,300) AIRV
      READ (15,301) WEIRL
      READ (15,302) DEW
      READ (15,303) ALPHA
      READ (15,304) DIA
      READ (15,305) WEIR
      READ (15,306) FREE
      READ (15,307) HOW
      READ (15,308) GAP
      READ (15,303) ALPHA
      READ (15,303) ALPHA
      READ (15,303) ALPHA
      READ (15,309) (TEMPIN(I),I=1,5)
```

```
      READ (15,310) (TEMP(I),I=1,8)
      READ (15,311) (TEMP(I),I=9,18)
      READ (15,312) (TEMP(I),I=19,30)
      READ (15,312) (TEMP(I),I=31,42)
      READ (15,312) (TEMP(I),I=43,54)
      READ (15,312) (TEMP(I),I=55,66)
      READ (15,312) (TEMP(I),I=67,78)
      READ (15,312) (TEMP(I),I=79,90)
      READ (15,311) (TEMP(I),I=91,100)
      READ (15,310) (TEMP(I),I=101,108)
      READ (15,313) TDOWN
      READ (15,314) (AIR(I),I=1,3)
C
C*************************************************************
C     SETTING UP IRREGULAR ARRAYS
C*************************************************************
C
      TEMP(3)=99.99
      NUM=0
      DO 20 I=1,108
         IF (TEMP(I).NE.99.99) THEN
            NUM=NUM+1
            XPOS(NUM)=X(I)
            YPOS(NUM)=Y(I)
            TPOS(NUM)=TEMP(I)
         END IF
  20  CONTINUE
C
C*************************************************************
C     AVERAGING INLET WATER TEMPERATURE
C*************************************************************
C
      WINT=DEW
      DO 21 I=1,5
         IF (TEMPIN(I).NE.99.99) THEN
            IF (TEMPIN(I).GT.WINT) THEN
               WINT=TEMPIN(I)
            END IF
         END IF
  21  CONTINUE
C
C*************************************************************
C     WET BULB TEMPERATURE
C*************************************************************
C
      TWB=DEW
C
C*************************************************************
C     SETTING UP REDUCED TEMPERATURES
C*************************************************************
C
      DO 22 I=1,NUM
         TR(I)=(TPOS(I)-TWB)/(WINT-TWB)
  22  CONTINUE
C
C*************************************************************
C     ROUTINES TO COMMENCE PLOTTING
C*************************************************************
C
      CALL GRESET
      CALL GLIMIT (-1200.0,1200.0,0.0,2000.0,0.0,1.0)
```

```
CALL RUNDEF (999.999,9999)
HFAC=0.0
CALL GVPORT (50.0,(42.0+HFAC),80.0,80.0)
CALL GWBOX (1.0,1.0,0.5)
CALL GEYE (6.0,4.0,7.0)
CALL GSCALE
CALL GVPROJ(2)
CALL RAXDIS (3,1,9999)
CALL RAXDIS (7,1,9999)
CALL RAXDIS (6,1,9999)
CALL RAXLFO (0,0,1,0)
CALL RAXBTI (9999,999.999,999.999,200.0)
CALL RAXSTI (3)
CALL RAXDIS (4,1,3)
CALL RAXIS3 (1,3.0,IPLANE,LENGTH,TEXT)
CALL RAXDIS (4,1,0)
CALL RAXIS3 (2,3.0,IPLANE,LENGTH,TEXT)
CALL RAXBTI (9999,999.999,999.999,0.1)
CALL RAXSTI (1)
CALL RAXIS3 (3,3.0,IPLANE,LENGTH,TEXT)
CALL GFAULT (XEDGE,YEDGE,17,1)
CALL GINTPF (X,Y,TR,NUM,ZEST,24,20)
CALL GSMTH (-1)
CALL GCONWI (0.0,1)
CALL GCNR3V (ZEST,24,20)
CALL GRESET
CALL GSCAMM
CALL RTXJUS (0,6)
CALL RTXHEI (2.5)
CALL RTX (-1,'Air Velocity',155.0,(109.0+HFAC))
CALL RTXN (AIRV,1,155.0,(103.0+HFAC))
CALL RTXC (-1,' m/s')
CALL RTX (-1,'Water Loading',155.0,(95.0+HFAC))
CALL RTX (-1,'Inlet Gap',155.0,(81.0+HFAC))
CALL RTXN (GAP,3,155.0,(75.0+HFAC))
CALL RTX (-1,'Outlet Weir',155.0,(67.0+HFAC))
CALL RTXN (HOW,3,155.0,(61.0+HFAC))
CALL RTX (-1,'Hole Diameter',155.0,(53.0+HFAC))
CALL RTX (-1,'0.001 m',155.0,(47.0+HFAC))
CALL RTXNBO (8,'T')
CALL RTXN (WEIRL,1,155.0,(89.0+HFAC))
CALL RTXC (-1,' cm3/cm.s')
CALL GCLOSE
END
```

APPENDIX 3

Height Of Clear Liquid Measurements

Below are the values of the height of clear liquid (cm), measured over the 2.44 m diameter tray for the conditions as found in Chapter 8.

Superficial Air Velocity 0.7 m/s

Water Weir 25 $cm^3/cm\ s$

	2.9			2.4		3.0		3.5	
	2.8		1.6				2.2	3.4	
2.7				1.6		2.4			3.4
	1.7		1.1				2.2	3.1	
	2.9			1.9		1.9		2.0	
1.7			2.2				1.8		2.2
	2.1			1.9		1.7		1.6	
	1.3		1.4				1.5	1.2	

Superficial Air Velocity 0.7 m/s

Water Weir 35 $cm^3/cm\ s$

	3.1			2.6		3.5		3.7	
	2.9		2.1				2.3	3.8	
3.1				1.9		2.6			3.8
	2.8		1.2				2.5	3.5	
	3.2			2.0		2.3		2.9	
1.7			2.3				2.1		2.7
	2.2			1.9		2.0		1.8	
	1.3		1.3				1.5	1.4	

Superficial Air Velocity 0.7 m/s

Water Weir 55 $cm^3/cm\ s$

	3.3			2.1		3.7		4.1	
	3.2		2.1				2.8	4.1	
3.3				2.1		3.0			4.0
	2.1		1.4				2.7	3.6	
	3.5			2.5		2.2		3.5	
2.5			2.5				2.1		3.1
	2.6			2.0		2.0		2.1	
	1.5		1.7				1.7	1.4	

Superficial Air Velocity 0.7 m/s

Water Weir 75 $cm^3/cm\ s$

	3.5		2.3		2.8		4.1		
	3.2	2.3				3.0	3.5		
3.3			2.2		3.2			4.2	
	3.2	1.7				2.9	3.9		
	3.6		2.8		2.8		3.8		
2.2		2.7				2.7		3.9	
	2.6		2.3		2.3		3.1		
	1.8	1.7				2.0	3.1		

Superficial Air Velocity 0.7 m/s

Water Weir 110 $cm^3/cm\ s$

	3.9		1.8		2.1		4.4		
	3.6	2.9				3.4	4.5		
3.7			2.6		3.4			3.8	
	3.1	2.0				3.1	3.8		
	3.9		3.5		3.2		4.3		
3.8		3.0				2.9		4.4	
	4.1		2.6		2.6		4.1		
	2.8	2.0				2.1	3.7		

Superficial Air Velocity 0.9 m/s

Water Weir 25 $cm^3/cm\ s$

	3.1		2.1		3.1		3.7		
	2.3	2.1				2.4	3.4		
2.0			2.1		2.4			3.5	
	2.1	2.2				2.5	2.2		
	2.0		2.2		2.4		2.1		
2.0		2.1				2.0		2.0	
	1.9		2.0		1.9		1.8		
	1.9	1.7				1.7	1.7		

Superficial Air Velocity 0.9 m/s

Water Weir 35 $cm^3/cm\ s$

	3.3		2.5		3.3		3.9		
	2.9	2.3				2.5	3.7		
2.5			2.2		2.6				3.5
	2.3	2.2				2.4	2.6		
	2.2		2.4		2.3		2.2		
2.3		2.2				2.0			2.2
	2.2		2.2		2.0		2.0		
	2.1	1.9				1.9	1.7		

Superficial Air Velocity 0.9 m/s

Water Weir 55 $cm^3/cm\ s$

	3.4		2.8		3.6		4.0		
	2.9	2.6				2.5	3.9		
2.4			2.4		2.7				3.9
	2.5	2.4				2.6	2.3		
	2.1		2.5		2.6		3.4		
2.3		2.5				2.1			3.2
	2.2		2.3		2.1		2.0		
	2.1	1.9				1.9	1.9		

Superficial Air Velocity 0.9 m/s

Water Weir 75 $cm^3/cm\ s$

	3.4		2.8		2.8		4.3		
	2.8	2.8				3.0	4.0		
2.5			2.7		3.1				4.2
	2.7	2.6				2.8	4.3		
	2.6		2.9		2.8		3.1		
2.6		2.6				2.3			3.5
	2.5		2.5		2.1		2.5		
	2.4	2.1				1.9	2.0		

Superficial Air Velocity 0.9 m/s

Water Weir 110 $cm^3/cm\ s$

	3.3		2.0	2.2		4.6			
	3.0	3.0			3.0	4.2			
2.9			2.8	3.4			3.6		
	2.9	2.6			2.8	3.7			
	2.7		2.8	3.1		4.1			
2.9		2.7			2.7		4.4		
	2.7		2.6	2.4		3.5			
	2.4	2.2			2.0	3.9			

Superficial Air Velocity 1.2 m/s

Water Weir 25 $cm^3/cm\ s$

	1.3		1.5	1.6		1.6			
	1.7	1.4			1.4	1.7			
1.6			1.4	1.4			1.4		
	1.5	1.3			1.3	1.5			
	1.8		1.4	1.4		1.6			
1.7		1.2			1.2		1.4		
	1.4		1.0	1.0		1.1			
	1.1	1.0			1.1	1.2			

Superficial Air Velocity 1.2 m/s

Water Weir 35 $cm^3/cm\ s$

	1.6		1.8	1.9		1.7			
	1.8	1.7			1.5	1.7			
1.9			1.5	1.6			1.9		
	1.9	1.4			1.3	1.8			
	1.9		1.8	1.6		1.7			
1.9		1.5			1.4		1.5		
	1.4		1.3	1.2		1.5			
	1.2	1.2			1.3	1.2			

Superficial Air Velocity 1.2 m/s

Water Weir 55 $cm^3/cm\ s$

	1.6			1.9		1.8		
	2.0		1.7				1.8	2.0
1.9				1.7		1.8		2.0
	1.9		1.6				1.7	1.9
	2.1			1.7		1.6		1.7
2.1			1.5				1.5	1.7
	1.5			1.4		1.4		1.6
	1.2		1.2				1.3	1.4

Superficial Air Velocity 1.2 m/s

Water Weir 75 $cm^3/cm\ s$

	1.8			1.7		1.6		2.2
	2.1		2.0				1.8	2.2
2.2				1.9		2.0		2.2
	2.1		1.9				1.6	2.1
	2.4			1.8		2.0		2.0
2.3			1.7				1.8	2.0
	1.7			1.5		1.3		1.7
	1.3		1.3				1.1	1.5

Superficial Air Velocity 1.2 m/s

Water Weir 110 $cm^3/cm\ s$

	1.9			1.0		1.1		2.2
	2.5		2.5				2.2	2.4
2.7				2.2		2.2		2.3
	2.3		2.1				2.0	2.2
	2.7			2.1		2.2		2.4
2.8			1.9				2.0	2.4
	2.2			1.8		1.6		2.1
	1.8		1.5				1.4	1.8

Superficial Air Velocity 1.5 m/s

Water Weir 25 $cm^3/cm\ s$

	1.2			1.3		1.3		1.1
	1.2		1.3				1.0	1.6
1.3				1.2		1.3		1.5
	1.3		1.2				1.2	1.3
	1.5			1.1		1.4		1.1
1.2			1.0				1.2	1.2
	1.2			0.9		1.0		1.1
	1.0		0.9				1.3	1.1

Superficial Air Velocity 1.5 m/s

Water Weir 35 $cm^3/cm\ s$

	1.0			1.4		1.3		1.2
	1.3		1.4				1.4	2.0
1.3				1.6		1.5		1.9
	1.5		1.5				1.4	1.4
	1.6			1.3		1.4		1.3
1.5			1.1				1.3	1.3
	1.3			0.9		1.2		1.1
	1.1		1.1				1.4	1.1

Superficial Air Velocity 1.5 m/s

Water Weir 55 $cm^3/cm\ s$

	1.1			1.7		1.3		1.9
	1.5		1.5				1.6	1.8
1.6				1.7		1.5		1.9
	1.5		1.6				1.5	1.6
	1.6			1.5		1.5		1.5
1.5			1.3				1.5	1.4
	1.6			1.0		1.2		1.4
	1.1		1.1				1.4	1.1

Superficial Air Velocity 1.5 m/s

Water Weir 75 $cm^3/cm\ s$

	1.2			1.2		1.2		0.9	
	1.6		1.8				1.6	1.9	
1.7				1.8		1.6			2.0
	1.7		1.7				1.7	1.7	
	1.8			1.5		1.6		1.6	
1.6			1.3				1.5		1.5
	1.4			1.1		1.2		1.3	
	1.3		1.1				1.3	1.1	

Superficial Air Velocity 1.5 m/s

Water Weir 110 $cm^3/cm\ s$

	1.4			0.9		0.8		1.2	
	1.8		1.9				1.8	2.3	
1.9				2.0		1.7			2.0
	1.9		1.9				1.8	1.8	
	2.2			1.6		1.8		2.1	
2.0			1.5				1.8		2.0
	1.8			1.2		1.5		1.9	
	1.6		1.3				1.4	1.4	

APPENDIX 4

Flow Over Outlet Weir Measurements

When the liquid flow over the outlet weir was investigated, the depth of water in eight comparment boxes was recorded - the outlet weir being divided into eight equal lengths. Below are the recorded depths of water (cm) in the compartments for the range of air and water flowrates.

Air (m/s)	Water (cm^3/cm s)	Compartment Number							
		1	2	3	4	5	6	7	8
0.7	25	16	7	7	7	6	6	5	10
	35	28	15	13	9	8	9	10	18
	55	29	18	13	11	8	9	10	18
	75	31	20	25	19	13	19	27	23
	110	31	38	41	30	25	34	39	32
0.9	25	16	8	7	7	6	7	6	9
	35	27	15	11	9	8	8	8	16
	55	29	17	14	10	8	9	9	19
	75	32	21	24	19	13	21	27	23
	110	34	37	39	33	26	31	41	29
1.2	25	13	8	8	8	7	7	6	7
	35	28	17	12	12	8	9	8	13
	55	31	20	17	11	9	10	9	18
	75	34	23	25	19	13	19	26	25
	110	36	38	38	33	24	32	38	29
1.5	25	15	9	9	9	7	8	7	7
	35	28	20	15	11	9	9	8	12
	55	32	21	20	12	10	10	10	16
	75	34	25	27	20	13	17	24	25
	110	40	41	42	33	24	32	37	30

APPENDIX 5

Temperature Data Measured During Water Cooling Experiments

All the calibrated, averaged temperature data from the water cooling experiments are contained on a 3.5", 1.2Mbyte diskette found in the rear cover of the thesis. The diskette was formatted using MSDOS version 3.3.

On insertion into a suitable disk drive, several sub-directories are viewed, for example,

G10W0	G10W10	G10W20	G10W50
G20W0	G20W10	G20W20	G20W50
G50W0	G50W10	G50W20	G50W50

The sub-directory naming convention is as follows,

G Relates to the gap under the inlet downcomer.

20 The first number relates to the size of the gap under the inlet downcomer in mm.

G Relates to the outlet weir height.

20 The second number relates to the height of the outlet weir in mm.

On moving down a level, into a sub-directory, the temperature data files are viewed, for example,

ACTEMP1.DAT	ACTEMP7.DAT	ACTEMP13.DAT
ACTEMP2.DAT	ACTEMP8.DAT	ACTEMP14.DAT
ACTEMP3.DAT	ACTEMP9.DAT	ACTEMP15.DAT
ACTEMP4.DAT	ACTEMP10.DAT	ACTEMP16.DAT
ACTEMP5.DAT	ACTEMP11.DAT	ACTEMP17.DAT
ACTEMP6.DAT	ACTEMP12.DAT	ACTEMP18.DAT

The data files shown in column one contain temperature data for the air superficial velocity of 1.0 m/s, those shown in column two for 1.5 m/s and those shown in column three for 2.0 m/s.

The data files shown in row one contain temperature data for the water weir load of 25 cm^3/cm s, those shown in row two for 50 cm^3/cm s, row three 100 cm^3/cm s, row four 150 cm^3/cm s, row five 200 cm^3/cm s and row six 250 cm^3/cm s.

On using a suitable editor, or a 132 character screen, the individual files can then be viewed, an example of which is shown in figure 5.4 along with an explanatory note concerning the temperature data. The positions of the temperature measuring devices are also provided in Chapter 5.

Note: All the temperature data contained on the diskette were measured on a 1mm hole diameter sieve tray.

APPENDIX 6

Efficiency Calculation Program

Below the Fortran 77 coding, written to calculate the point and tray efficiencies from the recorded temperature data as held in Appendix 5, is presented.

```
      PROGRAM EFFICIENCY
C
      INTEGER*2  I,J,K,NUM
      REAL  PAIR,PWATER,PI,CP,AIRV,WEIRL,DEW,DIA,WEIR
      REAL  FREE,HOW,GAP,TEMPIN(5),TEMP(108),AIR(4),TDOWN
      REAL  T(108),SUM,TIN,TOUT,DRY,MG,ML,HUMIN,HIN,HOUT
      REAL  HUMEQ,HOUTEQ,EMV,HUM(108),H(108),EOG,RATIO
      CHARACTER*2  ALPHA
C
      PAIR=1.22
      PWATER=1000.0
      PI=3.141593
      CP=4.18
C
C*************************************************************
C     READING IN TEMPERATURE DATA
C*************************************************************
C
         READ (14,300) AIRV
         READ (14,301) WEIRL
         READ (14,302) DEW
         READ (14,303) ALPHA
         READ (14,304) DIA
         READ (14,305) WEIR
         READ (14,306) FREE
         READ (14,307) HOW
         READ (14,308) GAP
         READ (14,303) ALPHA
         READ (14,303) ALPHA
         READ (14,303) ALPHA
         READ (14,309) (TEMPIN(I),I=1,5)
         READ (14,310) (TEMP(I),I=1,8)
         READ (14,311) (TEMP(I),I=9,18)
         READ (14,312) (TEMP(I),I=19,30)
         READ (14,312) (TEMP(I),I=31,42)
         READ (14,312) (TEMP(I),I=43,54)
         READ (14,312) (TEMP(I),I=55,66)
         READ (14,312) (TEMP(I),I=67,78)
         READ (14,312) (TEMP(I),I=79,90)
         READ (14,311) (TEMP(I),I=91,100)
         READ (14,310) (TEMP(I),I=101,108)
         READ (14,313) TDOWN
         READ (14,314) (AIR(I),I=1,3)
```

```
  300     FORMAT (27X,F3.1)
  301     FORMAT (27X,F4.0)
  302     FORMAT (27X,F4.1)
  303     FORMAT (4X,A2)
  304     FORMAT (27X,F5.3)
  305     FORMAT (27X,F5.3)
  306     FORMAT (27X,F4.1)
  307     FORMAT (27X,F5.3)
  308     FORMAT (27X,F5.3)
  309     FORMAT (43X,5(F6.2,4X))
  310     FORMAT (28X,8(F6.2,4X))
  311     FORMAT (18X,10(F6.2,4X))
  312     FORMAT (8X,12(F6.2,4X))
  313     FORMAT (63X,F6.2)
  314     FORMAT (10X,3(F6.2,4X))
C
C*************************************************************
C     SCREENING OUT NULL TEMPERATURE VALUES
C*************************************************************
C
      NUM=0
      DO 10 I=1,108
         IF (TEMP(I).NE.99.99) THEN
            NUM=NUM+1
            T(NUM)=TEMP(I)
         END IF
  10  CONTINUE
C
C*************************************************************
C     AVERAGING INLET AND OUTLET MEASURED TEMPERATURES
C*************************************************************
C
      J=0
      SUM=0.0
      DO 11 I=1,5
         IF (TEMPIN(I).NE.99.99) THEN
            J=J+1
            SUM=SUM+TEMPIN(I)
            END IF
  11  CONTINUE
      TIN=SUM/J
      PRINT*,'TIN = ',TIN
C
      J=0
      SUM=0.0
      DO 12 I=101,108
         IF (TEMP(I).NE.99.99) THEN
            J=J+1
            SUM=SUM+TEMP(I)
         END IF
  12  CONTINUE
      TOUT=SUM/J
      PRINT*,'TOUT = ',TOUT
      PRINT*,'TDOWN = ',TDOWN
      IF (TDOWN.NE.99.99) THEN
         IF (TDOWN.GT.TOUT) THEN
            TOUT=TDOWN
         END IF
      END IF
C
      J=0
```

```
      SUM=0.0
      DO 13 I=1,3
         IF (AIR(I).NE.99.99) THEN
            J=J+1
            SUM=SUM+AIR(I)
         END IF
   13 CONTINUE
      DRY=SUM/J
      PRINT*,'DRY = ',DRY
      PRINT*,'DEW =',DEW
C
C*************************************************************
C     CALCULATING MASS FLOWRATES - KG/S
C*************************************************************
C
      MG=PAIR*AIRV*PI*(DIA**2)/4
      PRINT*,'MG = ',MG
      ML=PWATER*WEIRL*WEIR/10000.0
      PRINT*,'ML = ',ML
C
C*************************************************************
C     CALCULATING INLET AIR HUMIDITY AND ENTHALPY
C*************************************************************
C
      CALL PSYCHRO (DRY,DEW,HUMIN,HIN)
      PRINT*,'HUMIN =',HUMIN
      PRINT*,'HIN = ',HIN
C
C*************************************************************
C     OVERALL HEAT BALANCE TO GIVE HOUT
C*************************************************************
C
      HOUT=((ML*CP/MG)*(TIN-TOUT))+HIN
      PRINT*,'HEAT LOST FROM WATER =',(ML*CP*(TIN-TOUT))
      PRINT*,'HOUTAV = ',HOUT
C
C*************************************************************
C     CALCULATING TRAY EFFICIENCY
C*************************************************************
C
      PRINT*,'TOUT =',TOUT
      CALL PSYCHRO (TOUT,TOUT,HUMEQ,HOUTEQ)
      PRINT*,'HUMEQ =',HUMEQ
      PRINT*,'HOUTEQ = ',HOUTEQ
      EMV=(HOUT-HIN)/(HOUTEQ-HIN)
      PRINT*,'EMV =',EMV
C
C*************************************************************
C     CALCULATING POINT EFFICIENCY
C*************************************************************
C
      SUM=0.0
      DO 14 I=1,NUM
         CALL PSYCHRO (T(I),T(I),HUM(I),H(I))
         SUM=SUM+H(I)
   14 CONTINUE
      EOG=(ML*CP/MG)*(TIN-TOUT)*NUM/(SUM-(NUM*HIN))
      PRINT*,'EOG =',EOG
C
C*************************************************************
C     CALCULATING EMV/EOG
```

```
C*************************************************************
C
      RATIO=EMV/EOG
      PRINT*,'RATIO =',RATIO
      END
C
C*************************************************************
C     ROUTINE TO CALCULATE AIR HUMIDITY AND ENTHALPY
C*************************************************************
C
      SUBROUTINE PSYCHRO (TDB,TWB,HUM,ENTH)
      REAL  A,B,C,D,E,F,G,Z1,Z2,Z3,Z4,Z5
      REAL  TD1,TD2,M1,M2,C1,C2,C3,Y1,Y2
      REAL  LO,TWB,TDB,P0,PSS,HUM,ENTH
      A=-2948.997118
      B=-2.1836674
      C=-0.000150474
      D=-0.0303738468
      E=0.00042873
      F=4.76955
      G=25.83220018
      TD1=273.15
      TD2=273.16
      P0=101.325
      M1=18.01534
      M2=28.9645
      C1=0.000666
      C2=1.00568
      C3=1.84598
      LO=2500.84
      Z1=A/(TWB+TD1)
      Z2=B*LOG(TWB+TD1)
      Z3=C*(10**(D*(TWB-0.01)))
      Z4=E*(10**(F*(1.0-(TD2/(TWB+TD1)))))
      Z5=G
      PSS=10**(Z1+Z2+Z3+Z4+Z5)
      Y1=P0*C1*(TDB-TWB)
      HUM=(M1/M2)*(PSS-(1000.0*Y1))/((1000.0*P0)-PSS+(1000.0*Y1))
      ENTH=(C2*TDB)+(HUM*(LO+(C3*TDB)))
      RETURN
      END
```